LIBRARY
DEC 19 1956
PURDUE

JOURNAL OF THE AERONAUTICAL SCIENCES

VOLUME 23 DECEMBER, 1956 NUMBER 12

CONTENTS

In Memoriam—Lester Durand Gardner ..... FRONTISPIECE

Recent Developments in the Theory of Wing-Body Wave Drag ..... HARVARD LOMAX AND MAX. A. HEASLET 1061

Spectral Theory of Buffeting and Gust Response: Unification and Extension ..... H. S. RIBNER 1075

Some Integrated Volume Properties in Linearized Flow and Their Connection with Drag Reduction at Supersonic Speeds ..... Z. O. BLEVISS 1078

Influence of Aerodynamic Heating on the Effective Torsional Stiffness of Thin Wings ..... BERNARD BUDIANSKY AND J. MAYERS 1081

The Tip Correction for Wind-Tunnel Tests of Propellers ..... THEODORE R. GOODMAN 1094

Normal Forces on Flat Plates in Low-Density Supersonic Flow ..... D. M. TELLEP AND L. TALBOT 1099

Piston Theory—A New Aerodynamic Tool for the Aeroelastician ..... HOLT ASHLEY AND GARABED ZARTARIAN 1109

Readers' Forum 1119

Index to Volume 23 1131

Published by
INSTITUTE OF THE AERONAUTICAL SCIENCES, INC.

JOURNAL OF THE AERONAUTICAL SCIENCES

Editor: W. R. SEARS

Director, Graduate School of Aeronautical Engineering, Cornell University

Associate Editor: ROBERT R. DEXTER *Managing Editor:* RITA J. TURINO

Editorial Assistant: CAROLINE TAYLOR

Editorial Committee

Aerodynamics and Fluid Mechanics

Holt Ashley
H. Julian Allen
Dean R. Chapman
Francis H. Clauser
Hugh L. Dryden
John C. Evvard
Antonio Ferri
Alexander Flax
Wallace D. Hayes
R. T. Jones
Carl Kaplan
H. W. Liepmann
C. C. Lin
H. F. Ludloff
Harold Luskin
Clark B. Millikan
C. D. Perkins
H. J. E. Reid
George S. Schairer
G. B. Schubauer
John Stack
Theodore Theodorsen
Arthur N. Tifford
Th. von Kármán

Flight Testing

R. R. Gilruth
Melvin N. Gough
W. L. Howland
W. F. Milliken, Jr.

Rotating Wing Aircraft

F. B. Gustafson
K. H. Hohenemser
Bartram Kelley
R. B. Maloy
Ralph McClarren
R. H. Miller
R. H. Prewitt
Igor I. Sikorsky

Structures

John E. Duberg
N. J. Hoff
Samuel Levy
J. F. McBrearty
W. Ramberg
E. E. Sechler
F. R. Shanley
C. R. Strang
S. Timoshenko

Meteorology

C. F. Brooks
D. M. Little
F. W. Reichelderfer
K. C. Spengler

Vibration and Flutter

Lee Arnold
M. A. Biot
R. L. Bisplinghoff
Harold A. Cheilek
I. E. Garrick
Martin Goland

Aircraft Design

W. E. Beall
E. H. Heinemann
Hall L. Hibbard
Richard Hutton
C. L. Johnson
A. A. Kartveli
E. G. Stout
F. K. Teichmann

Electronics

Welcome W. Bender
K. C. Black
M. V. Kiebert, Jr.
David S. Little
S. B. Rogers
Paul Rosenberg
L. M. Sherer

Physiologic Problems

H. G. Armstrong
Louis H. Bauer
Robert J. Benford
W. Randolph Lovelace, II
Ross A. MacFarland

Flight Propulsion

William Bollay
George W. Brady
R. P. Kroon
Frank E. Marble
Abe Silverstein
Martin Summerfield
E. S. Taylor

Instruments

Alan G. Binnie
Charles H. Colvin
Frank R. Cook
C. S. Draper
S. G. Eskin
C. F. Savage
R. C. Sylvander

SUBSCRIPTION RATES

JOURNAL OF THE AERONAUTICAL SCIENCES, Published Monthly.—United States and Possessions: 1 Year, $15.00; Single Copies, $1.50. Foreign Countries Including Canada (American Currency Rates): 1 Year, $16.00; Single Copies, $1.50.

AERONAUTICAL ENGINEERING REVIEW, Published Monthly.—United States and Possessions: 1 Year, $3.00; Single Copies, $0.50. Foreign Countries Including Canada (American Currency Rates): 1 Year, $3.50; Single Copies, $0.50.

Notices of change of address should be sent to the Institute at least 30 days prior to actual change of address.

Manuscripts for publication, proofs, and all correspondence should be addressed to the Editorial Office of the JOURNAL.

Correspondence regarding subscriptions may be addressed to the Editorial Office of the JOURNAL OF THE AERONAUTICAL SCIENCES, 2 East 64th Street, New York 21, N.Y., or to the Publication Office, 20th and Northampton Sts., Easton, Pa.

© *Copyright, 1956, by the Institute of the Aeronautical Sciences, Inc.*

Entered as Second Class Matter at the Post Office, Easton, Pa., May 1, 1937. Acceptance for mailing at a special rate of Postage provided for in the Act of August 24, 1912. Authorized April 29, 1937.

LESTER DURAND GARDNER—Founder, Institute of the Aeronautical Sciences; Fellow, Institute of the Aeronautical Sciences, and Honorary Fellow, The Royal Aeronautical Society of Great Britain; Daniel Guggenheim Medalist; Publisher; Soldier; Public Servant; Delegate at Large in the promotion of aviation throughout the world.

In Memoriam

We of the Institute owe an incalculable debt to Lester Gardner. His was the vision to see the need for a strong and active association of aeronautical scientists and engineers at a time when air power and air transportation were selling at a discount. He realized the potential value of such a society to the national defense—a concept that needed no argument a short decade later.

For L.D.G., vision was but the prelude to action. Never one to "let George do it," he plunged into any project that intrigued him with a fervor that left his colleagues and associates gasping.

And so it was when he took the Institute under his wing. From the moment of its founding in 1932 to the day he went on inactive duty in 1946, he poured out his boundless energy, day and night, in season and out, to make the Institute the foremost organization of its kind and, through it, to keep America in the forefront of aviation development.

And so—to Lester Gardner—Hail and Farewell!

Now that he has gone, we can do no less than rededicate ourselves to the objectives to which he devoted all the years of his life.

Aviation is vastly more complicated, vastly more important today than was even imagined in the Institute's early years. All the more reason, therefore, that we should make the best possible use of this vital force that Lester Gardner nurtured, brought to fruition, and left in our hands.

The Members, Officers, and Staff of the Institute can pay their best tribute to the Founder by keeping the organization strong and alive to every opportunity to advance the arts and science of aeronautics. Through its channels, we must do what we can to make and to keep this country strong in the air—for peace or for war.

Lester Durand Gardner 1876–1956

Lester Durand Gardner, who founded the Institute of the Aeronautical Sciences in 1932, died November 23 in New York after an illness of several weeks. Burial was at Arlington National Cemetery on November 27.

Lester Gardner was an indefatigable worker for aviation. One of his last efforts in its behalf was a campaign last year to raise funds to establish the Jerome C. Hunsaker Chair at Massachusetts Institute of Technology. The drive raised $500,000. In 1954, M.I.T. had established the Lester Durand Gardner Scholarship Fund of $50,000.

It was only last summer that the National Aeronautic Association conferred upon him the title "Elder Statesman of Aviation"—the last of many honors bestowed on "Major Gardner," as he was known to thousands here and abroad. He was the third American to be made an Honorary Fellow of the 86-year-old Royal Aeronautical Society of Great Britain.

In 1944, Polytechnic Institute of Brooklyn gave him its honorary degree of Doctor of Laws. He was the recipient of the Daniel Guggenheim Medal for Aeronautics in 1947. He also was a Fellow of the Institute of the Aeronautical Sciences, honorary member of the Wings Club and The Aviation Country Club, and member of the University Club, New York, the Army and Navy Club in Washington, the Society of Automotive Engineers, American Society of Mechanical Engineers, American Legion, the Society of Colonial Wars, and Sons of the American Revolution.

He served in the Army Air Service in World War I, leaving it after the Armistice with the rank of Major.

He was educated in the Detroit public schools and was graduated from M.I.T. in 1898 with a Bachelor of Science degree. Following a year of administrative law at Columbia University, he became interested in publishing and was successively on the staffs of *The New York Times*, *The New York Herald Tribune*, *The Sun*, and *Everybody's* and *Colliers* magazines.

In 1915, he became president of the Gardner-Moffat Company, which later became the Gardner Publishing Company, publishers of *Aviation* magazine and *The Rubber Age*. The former was sold to McGraw-Hill, who continued its publication for many years before changing its name to *Aviation Week*. It was as publisher of *Aviation* that Major Gardner helped aviation through many of its growing pains.

Always interested in scientific developments, Major Gardner entered the field of radioactivity and use of radium, uranium, and thorium. He took out several patents. Following a visit to the Curies in Paris, he imported the first radium to be used for therapeutics in this country.

In 1915 he attended the first reserve officers training camp at Plattsburg, after which he and Philip J. Roosevelt published *American Defense*, a magazine that did much to arouse both official and public opinion in support of United States defense needs. While in active service in 1917–1918, he organized 89 aero squadrons for overseas service.

Major Gardner served on numerous aviation committees and official delegations appointed to further the development of aviation. He was president of the Aeronautical Chamber of Commerce of America in 1928. He also was a former president of the Technology Club of New York.

In 1932, with the help of other aviation leaders, he founded the Institute of the Aeronautical Sciences, with original headquarters at Rockefeller Center. The Institute soon became one of the greatest scientific organizations in the world, and its activities were directed by Major Gardner until his retirement in 1946.

Major Gardner also founded the Aeronautical Archives of the IAS, which contains one of the world's principal aeronautical collections. He was the first Archives president.

JOURNAL OF THE AERONAUTICAL SCIENCES

VOLUME 23 DECEMBER, 1956 NUMBER 12

Recent Developments in the Theory of Wing-Body Wave Drag

HARVARD LOMAX* AND MAX. A. HEASLET*

Ames Aeronautical Laboratory, NACA

SUMMARY

The theoretical study of wave drag on airplanes flying at supersonic speeds is re-examined in the light of the recent discovery of the transonic area rule. A supersonic area rule is presented together with a discussion of its range of applicability. In regions where the supersonic area rule is seriously in error other methods, based on linearized theory, for calculating the wing-body interference effects are outlined. In addition, some recent results based on the nonlinear small-perturbation equation for transonic flow are briefly discussed. Comparisons between theory and experiment are given.

SYMBOLS

a, b	= minor and major axes, respectively, of elliptic wing plan form (See Fig. 11)
$a_n(x)$, $b_n(x)$, $A_n(x)$, $B_n(x)$	= functions giving strengths of nth order multipole distributions [See Eqs. (30) and (31)]
$\overline{A}_n, \overline{B}_n$	= coefficients in Fourier expansion of $S'_w(x, \theta)$ [See Eqs. (8) and (9)]
$\overline{\overline{A}}_n, \overline{\overline{B}}_n$	= coefficients in Fourier expansion of $S'(x, \theta) - [\beta l(x, \theta)/2q]$ [See Eq. (38)]
C_L, C_D	= lift and drag coefficients, respectively
D	= drag
$L_2(\theta) + L_1(\theta)$	= streamwise distance between oblique planes bounding airplane for given θ
L_w, L_B	= lift on the wing and body, respectively
$l(x, \theta)$	= projection in θ direction of resultant force on oblique section
$l_c(x)$	= lift on body integrated from nose to station x
M	= free-stream Mach Number
Δp	= difference in pressure on opposed sides of wing
q	= free-stream dynamic pressure, $(1/2)\rho_0 U_0^2$
$S(x, \theta)$	= airplane area in oblique plane given by Eq. (3)
$S_f(x)$	= fuselage area in plane normal to free-stream direction
$S_w(x, \theta)$	= wing area in oblique plane
t	= maximum wing thickness
U_0	= free-stream velocity
V_w, V_B	= volume of wing and body, respectively
x, y, z	= Cartesian coordinates, x parallel to free-stream direction
x, r, θ	= cylindrical coordinates, x parallel to free-stream direction
β	= $\sqrt{M^2 - 1}$
γ	= ratio of specific heats
$\lambda_u(x, y)$	= slope of wing upper surface
$\Delta\lambda(x, y, z)$	= difference in slope on opposed sides of wing
ρ_0	= free-stream density
$\varphi(x, y, z)$	= perturbation velocity potential
ω	= semiapex angle of circular cone

Presented at the Aerodynamics–I Session, Twenty-Fourth Annual Meeting, IAS, New York, January 23–26, 1956.

* Aeronautical Research Scientist.

INTRODUCTION

When WHITCOMB demonstrated that a reasonably slender airplane and a body of revolution with the same longitudinal distribution of cross-sectional area (normal to the free stream) could have similar wave drags at transonic speeds, a new impetus was given to the study of interfering wings and bodies. Such studies proceeded, of course, along both experimental and theoretical lines. The purpose of this paper is to present some of the theoretical methods used and some results of their applications.

In particular, we shall limit ourselves to analyses restricted by the assumption that the disturbance velocities induced by the airplane are small relative to U_0, the flight velocity. If the axes are fixed in the body, the x axis parallel to the free-stream, and φ is the perturbation velocity potential, the inviscid fluid theory for supersonic flow can then be based on the linear differential equation

$$\beta^2\varphi_{xx} - \varphi_{yy} - \varphi_{zz} = 0 \qquad (1)$$

where $\beta^2 = M^2 - 1$, M being the free-stream Mach Number. Our discussion of the recent results based on this equation will, for the most part, be limited to analyses heretofore classified.

As M approaches 1, Eq. (1) is, except for very special cases, an inadequate idealization of the flow field and a general analysis must be based on the nonlinear equation

$$\beta^2\varphi_{xx} - \varphi_{yy} - \varphi_{zz} = -[M^2(\gamma + 1)/U_0]\varphi_x\varphi_{xx} \quad (2a)$$

or, for the particular case of sonic flight speed,

$$\varphi_{yy} + \varphi_{zz} = [(\gamma + 1)/U_0]\varphi_x\varphi_{xx} \quad (2b)$$

Analysis Based on the Wave Equation

Preliminary Remarks

To begin with, a certain familiarity with solutions to problems involving wings and bodies in flow fields governed by the wave equation is assumed. For example, we recall that sources, doublets, and higher order singularities, when properly distributed, can simulate the potential flow about such wings and bodies. Equally pertinent to our subsequent discussion is the division commonly made of the total drag into the separate parts commonly referred to as the viscous, vortex, and wave drags. In practical applications, of course, all three types of drags must be considered simultaneously. Nevertheless, in the succeeding discussion the viscous drag will be ignored, so that the expression "optimum combination" will refer to that combination having, under given restraints, the lowest value of vortex drag plus wave drag. Further, by imagining the airplane to be enclosed by an infinitely long circular cylinder parallel to the free stream, we adopt the usual definition of vortex and wave drags as the forces in the free-stream direction given by the flux of momentum across the ends and sides of the cylinder, respectively, as the distance from the airplane to the surface of the cylinder tends to infinity. The condition for minimum vortex drag is the same for both subsonic and supersonic flow and, as shown by Munk,[1] depends upon the horizontal and vertical distribution of vorticity streaming behind the airplane. The condition for a lower limit to the wave drag will be presented later.

Finally, in the following, considerable use is made of a theorem presented by Hayes[2] in 1946. Let r be the radius of the cylinder, mentioned above, across which the momentum flux is to be measured. Then Hayes' theorem states:

(a) To the lowest order in $1/r$, as r tends to infinity, and at a fixed azimuth angle θ, the magnitude of the perturbation velocity potential φ in the vicinity of the cylinder's surface is invariant to a finite translation of sources (or any other singular solution to the wave equation) along the plane

$$x_1 = x + \beta y_1 \cos\theta + \beta z_1 \sin\theta \quad (3)$$

where x is any reference distance along the axis of the cylinder.

The Supersonic Area Rule

The very simplicity of the concept suggested by the words "area rule" suggests a universality that is hard to resist. Hence, shortly after the transonic area rule was discovered, a supersonic area rule was presented by both Jones[3] and Whitcomb. The development of this rule as given by Jones, and later as discussed by Ward,[4] stems from a classical result (see reference 5, p. 60) which, for our purposes, can be paraphrased as follows:

(b) In linearized theory the potential flow about an airplane can be simulated by a distribution of simple sources on the airplane's surface provided that none of the thin wing-like members carry a local loading.

(c) Within the group of airplanes given by theorem (b) there is a smaller family whose local source strength is proportional (within the accuracy of linearized theory) to the local airplane surface slope in the streamwise direction.*

To construct the supersonic area rule for this limited family of airplanes is simple enough. First consider a line θ = constant along our enclosing control surface. Along this line the momentum flux caused by an airplane of the prescribed group is, by theorem (a), the same as that which would occur along the line if all the singularities simulating the airplane were moved to the axis of the control surface along the oblique planes given by Eq. (3). By theorem (b), these singularities are simple sources only. Using theorem (c), one can show the strength of the equivalent source on the cylinder's axis is proportional to the gradient of the normal (to the free stream) projection of the area intersected by the oblique planes. But Kármán[6] has derived the equation for the wave drag of a line of sources. Using his result and averaging the drag of the equivalent source lines for all θ, we get for drag D, divided by free-stream dynamic pressure q, the expression

$$\frac{D}{q} = -\frac{1}{4\pi^2}\int_0^{2\pi} d\theta \int_{-L_0(\theta)}^{L_1(\theta)} dx_1 \int_{-L_0(\theta)}^{L_1(\theta)} dx_2 \times S''(x_1, \theta)S''(x_2, \theta)\ln|x_1 - x_2| \quad (4)$$

where $S(x, \theta)$ is the normal projection of the oblique section area (see Fig. 1), $S''(x, \theta) = (\partial^2/\partial x^2)S(x, \theta)$, and the interval $-L_0(\theta) \leq x \leq L_1(\theta)$ is the airplane length relative to the oblique planes determined by a fixed Mach Number and θ. Eq. (4) applies to all airplanes which satisfy conditions (b) and (c) and which further satisfy the condition that both $S(x, \theta)$ and $S'(x, \theta)$ be continuous.

Eq. (4) provides an abundance of practical information for those cases to which it does apply. To illustrate this, let us consider a thin wing centrally mounted on a body of revolution at zero angle of attack, and let the x axis coincide with the centerline of the body. Since, according to condition (c), the wing must be thin and the body slender, in finding $S(x, \theta)$ the variation with z_1 can be neglected when the oblique plane [Eq. (3)] cuts the wing, and the variation with both z_1 and y_1 can be neglected when the oblique plane cuts the body as illustrated in Fig. 2. This permits the term $S(x, \theta)$ to be separated into two parts,

* It is the latter family that Ward and Jones consider. By ordering the source strength in terms of thickness ratio, Ward argues that the physical meaning of condition (c) is to limit the subset to slender bodies and their nonlifting wings or their combination.

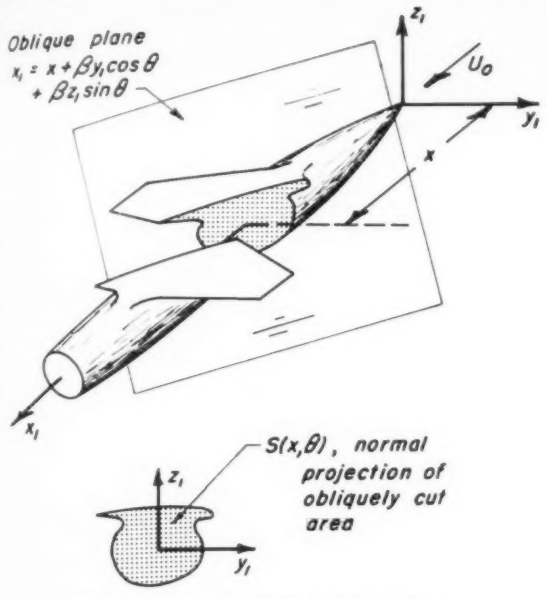

FIG. 1. Airplane section in oblique plane.

$$S(x, \theta) = S_f(x) + S_w(x, \theta) \tag{5}$$

where $S_f(x)$ is the cross-sectional fuselage area normal to the free stream and, therefore, independent of θ, and $S_w(x, \theta)$ is the normal projection of the wing area cut by the plane $x_1 = x + \beta y_1 \cos\theta$. In terms of $\lambda_u(x, y)$, the slope of the wing's upper surface, $S'_w(x, \theta)$ is given by the equation

$$S'_w(x, \theta) = 2 \int_{\text{wing}} \lambda_u(x + \beta y_1 \cos\theta, y_1) dy_1 \tag{6}$$

where the limits of integration are determined by the intersection of the oblique plane with the exposed portions of the wing.

The next step in simplifying our results is to expand $S'_w(x, \theta)$ in a Fourier series (by symmetry only cos $n\theta$ terms are needed, where n is even); thus, if

$$S'(x, \theta) = S_f(x) + \frac{1}{U_0} \bar{A}_0(x) + \frac{1}{U_0} \sum_2^\infty \bar{A}_n(x) \cos n\theta \tag{7}$$

then

$$\frac{1}{U_0} \bar{A}_0(x) = \frac{1}{2\pi} \int_0^{2\pi} S'_w(x, \theta) d\theta \tag{8}$$

$$\frac{1}{U_0} \bar{A}_n(x) = \frac{1}{\pi} \int_0^{2\pi} S'_w(x, \theta) \cos n\theta \, d\theta \tag{9}$$

and by Eq. (4) the drag becomes

$$\frac{D}{q} = -\frac{1}{2\pi U_0^2} \int_{-L_0}^{L_1} dx_1 \int_{-L_0}^{L_1} dx_2 [U_0 S''_f(x_1) + \bar{A}'_0(x_1)] [U_0 S''_f(x_2) + \bar{A}'_0(x_2)] \ln |x_1 - x_2| + \frac{1}{q} \sum_2^\infty D_n \tag{10}$$

where

$$\frac{D_n}{q} = -\frac{1}{4\pi U_0^2} \int_{-L_0}^{L_1} dx_1 \int_{-L_0}^{L_1} dx_2 \times \bar{A}'_n(x_1) \bar{A}'_n(x_2) \ln |x_1 - x_2| \tag{11}$$

From Eqs. (8) through (11) the following conclusions can be drawn. The fuselage area $S_f(x)$ has no effect on the $\bar{A}_n$ and D_n terms, so the drag of all the higher harmonics is a function of the wing design only. The complete effect of wing-body interference, therefore, appears in the sum of $\bar{A}_0(x)$ and the fuselage area distribution determined by planes normal to the free stream.

Next let us consider some simple examples of how low wave drag fuselage designs can be calculated on the basis of the above results when the wing and Mach Number are fixed. The simplest case is to find the optimum modification to a cylinder on which a given wing is to be mounted, as shown in Fig. 3. This modification is given by

$$S'_f(x) = -\frac{1}{2\pi} \int_0^{2\pi} S'_w(x, \theta) d\theta \tag{12}$$

One can show that the volume removed from the cyl-

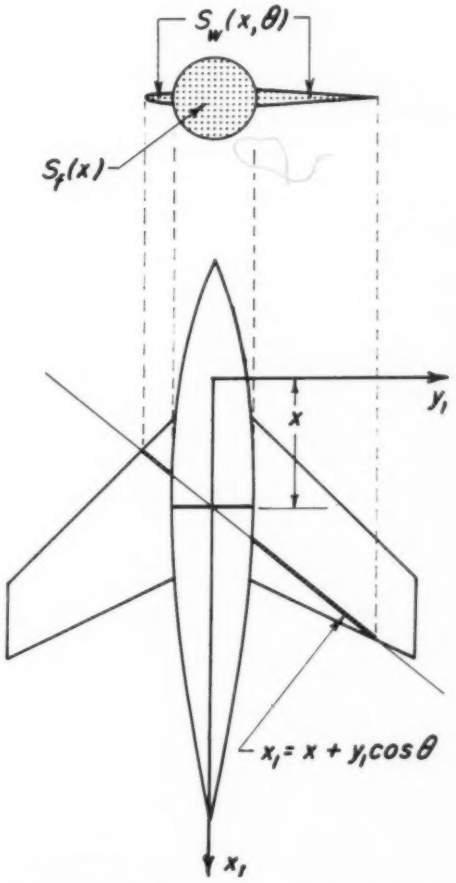

FIG. 2. Simplified evaluation of $S(x, \theta)$ for planar wing and slender fuselage.

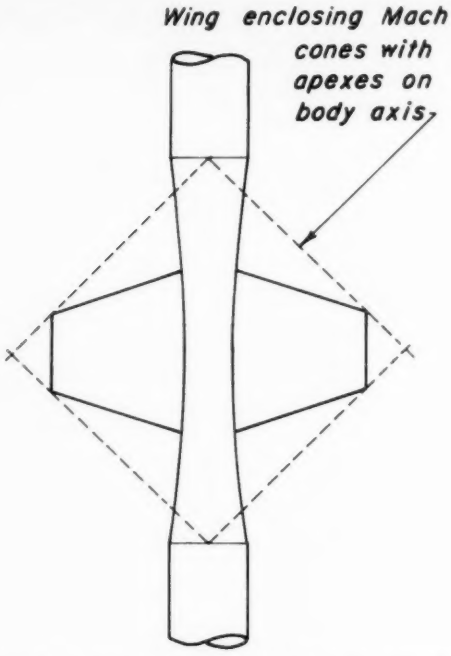

FIG. 3. Wing and optimum modification to straight-sided cylinder.

inder by such a modification is identical to the volume of the exposed wing and that the drag of the combination is equal to the drag of the (exposed) wing alone minus the drag of the modified cylinder alone.

If, instead of an infinite cylinder, a closed body is combined with a given wing, the optimum body shape is, in general, more difficult to find, although the problem often reduces to a simple reinterpretation of the result for an optimum slender body of revolution having the same geometric restraints. For example, consider the following problem:

Given the (nonlifting) wing, body length, and total volume (sufficiently large) of the combination, what is the area distribution of the body which yields a minimum wave drag if the apexes of the Mach fore and after cones enclosing the wing lie within the body?

The solution in this case is obtained by mounting the given wing panels on a Sears-Haack body (by definition, the closed slender body which has a minimum drag for a fixed volume and length) and then modifying this body by taking out of it the wing volume in accordance with Eq. (12). This follows from the above; first, since the wing is given, the term $\frac{1}{q}\sum_{2}^{\infty} D_n$ in Eq. (10) is fixed, and with the modification given by Eq. (12) the initial term in the right member of Eq. (10) is simply the drag of the body alone; second, since the wing plus the modification have no net volume, the total volume remains unchanged. Notice that the location of the wing along the body is immaterial provided the required indentation can be assimilated by the fuselage.

Returning to our theoretical considerations, we can combine Eq. (6) with Eqs. (8) and (9) and, by means of a simple transformation of coordinates, write Eq. (12) in the form

$$S'_f(x) = -\frac{1}{\pi}\iint_\sigma \frac{\lambda_u(\xi,\eta)d\xi d\eta}{\sqrt{\beta^2\eta^2 - (x-\xi)^2}} \tag{13}$$

and the value of $A_n(x)$ in the form, for $n > 0$,

$$\bar{A}_n(x) = \frac{2U_0}{\pi}\iint_\sigma \frac{\lambda_u(\xi,\eta)\cos\left\{n\cos^{-1}\left[(x-\xi)/\beta\eta\right]\right\}d\xi d\eta}{\sqrt{\beta^2\eta^2 - (x-\xi)^2}} \tag{14}$$

where σ is the region defined in Fig. 4.

Eq. (13) has an interesting interpretation. It tells us that the optimum fuselage area change (under the prescribed assumptions) is determined by integrating sources over the portion of the wing in the "region of silence." In other words, $S'_f(x)$ is determined by a planar source distribution that cannot disturb the flow field at the point x, 0 in either forward or reverse flow.

Another point to be made concerns the problem of finding the optimum wing thickness for a given plan form. This is resolved by determining the thickness that gives the lowest value of $\sum_{2}^{\infty} D_n$ in Eq. (10)—that is, by minimizing (under the pertinent restraints) the higher harmonics $\bar{A}_n(x)$ independent of the value of $\bar{A}_0(x)$ which is absorbed into the fuselage analysis.

In the above, some simple illustrations were given for finding minimum wave-drag combinations under certain geometric conditions and at a fixed free-stream Mach Number. It is also possible to consider a range of Mach Numbers at once. Define the wing area cuts, made at a given Mach Number, by

$$\bar{S}(x, M) = \frac{1}{2\pi}\int_0^{2\pi} S_w(x,\theta)d\theta \tag{15}$$

Then, using Eqs. (8), (10), and (15), and simple variational procedures, one can show that

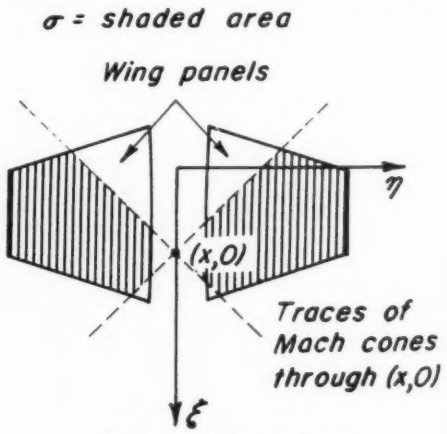

FIG. 4. Definition of area σ.

$$S'_f(x) = -\frac{1}{n}\sum_{i=1}^{n} \bar{S}'(x, M_i) \tag{16}$$

gives the minimum value to the sum of the drag coefficients at $M = M_1, M_2, M_3, \ldots, M_n$. If a certain weighting is assigned to each of the drags, as would, for example, be the case if the airplane were required to accelerate to a given Mach Number in a minimum time, the best fuselage area distribution can still be readily determined. In fact, if, for a fixed wing, $\int_{M_a}^{M_b} f(M)C_D(M)dM$ is to be minimized, the solution for the distortion of a cylinder is simply

$$S'_f(x) = -\frac{1}{M_b - M_a}\int_{M_a}^{M_b} f(M)\bar{S}'(x, M)dM \tag{17}$$

Notice that $\bar{S}(x, M)$ is an average of the obliquely cut wing areas, and $S'_f(x)$, as determined by Eq. (16) or (17), is obtained by further averaging with respect to the Mach Number.

Regions in Which Supersonic Area Rule Fails

The power of the supersonic area rule is evident from the simple and direct geometric interpretations that could be given in each of the above cases. Unfortunately, however, there are many combinations of wings and bodies to which the rule does not apply. Equally unfortunate is the fact that the boundaries of its validity or the errors incurred by its use in specific cases are not always easy to assess. We are particularly concerned here with those situations for which the perturbation velocities in the flow field are small enough for linearized theory to apply but for which the requirements given in (b) and (c) above are not satisfied.

Combinations of wings and bodies which cannot be simulated by simple sources alone, in accordance with (b), are easy to construct. Any thin wing cambered with respect to the local stream so as to support local loading is a member of such a class, and in extreme cases the wave drag can be zero although the oblique area distributions can be any of an infinite set. Combinations of this type were pointed out by Busemann and Ferrari many years ago. For example, the wave drag, as given by linearized theory, of a particular form of the Busemann biplane is shown by the solid line in Fig. 5. Notice that the total drag is a minimum (zero) whenever $\beta h/c$ is a simple fraction of the form $1/2, 1/4, \ldots, 1/2n, \ldots$ and is a local maximum whenever $\beta h/c$ equals $1, 1/3, 1/5, \ldots, 1/(2n + 1), \ldots$. Further, the local maximums all lie on the straight line connecting (1, 1) with the origin. Compare these results with those given by the supersonic area rule and one sees the latter sometimes overestimates and sometimes underestimates the correct value of the drag.

Examples of objects that can be simulated by simple sources only but which are still of such a shape that their wave drags are not adequately predicted by the supersonic area rule because they violate condition (c) can also be given. Consider a rectangular or triangular wing mounted centrally on a flat sided fuselage for which β times the height h of the side is greater than the root chord, both wing and fuselage being at zero angle of attack. Assuming the fuselage area does not change in size or shape in the free-stream direction we find that the drag of the combination as given by the supersonic area rule is the same as the wave drag of the exposed half wing alone. But the correct linearized value is half that of a complete wing formed by the exposed half panel and its reflection in the plane of the wing-body juncture. The ratio of the two drags is shown in Fig. 6 and the magnitude of the difference is clearly appreciable.

Another example along the same lines is provided by some results published by Nielsen[7] who studied the wing-body combination shown in Fig. 7. For the particular case shown a sonic-edged sweptback wing mounted on a circular cylinder the wave drag given by the supersonic area rule is about 1.35 times that given by linear theory.

Finally an interesting inversion to the relation shown in Fig. 5 between the drags given by linearized theory and the supersonic area rule for the Busemann biplane is provided by a tube having its surface corrugated in the form of a sine wave. Thus if the radius is given by

$$R = r_0 + \delta \sin (2\pi x_1/l) \tag{18}$$

the obliquely cut area (assuming control-surface theory and neglecting terms of the order δ^2 compared to δ) can be shown to be independent of θ by reason of radial symmetry and can be written

$$S(x, \theta) = 2\pi r_0 \delta J_0(2\pi\beta r_0/l) \sin (2\pi x/l) \tag{19}$$

where $J_0(z)$ is the Bessel function of the first kind. According to Eq. (4), the wave drag of one "corrugation length" (determined by finding the average of a large number of them) is

$$D/q = 8\pi^5(r_0^2\delta^2/l^2)J_0^2(2\pi\beta r_0/l) \tag{20}$$

and the comparison between this and the correct linearized value, as given by von Kármán,[8] is shown in Fig. 8. Notice the difference between these results and those shown in Fig. 5. In the one case, the approximation given by the supersonic area rule gives zero values for the wave drag when the correct values are not zero, and, in the other case, the reverse is true.

Drag in Terms of Obliquely Cut Areas and Forces

The preceding examples illustrate the fact that many types of wings and bodies and their combinations lie outside the class restricted by (b) and (c) above. It is interesting to examine these types still using Hayes' theorem but applying it to a field containing singularities that can simulate any object for which linearized theory is applicable. A simple way of carrying out this objective is to combine Hayes' theorem with Green's theorem which relates surface distributions of sources and doublets to surface slopes and loadings. Thus, one finds[9] for the wave drag

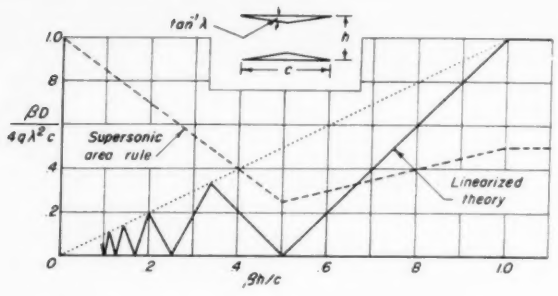

FIG. 5. Wave drag variation for a Busemann biplane.

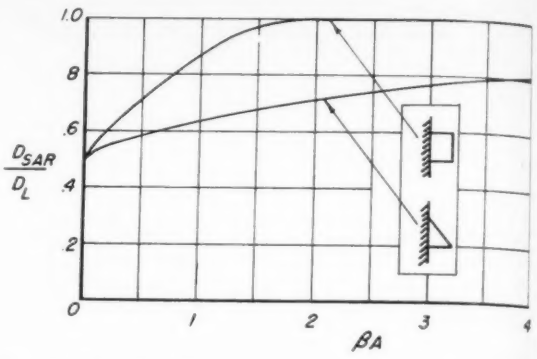

FIG. 6. Comparison between wave drags given by linearized theory and supersonic area rule for planar wings.

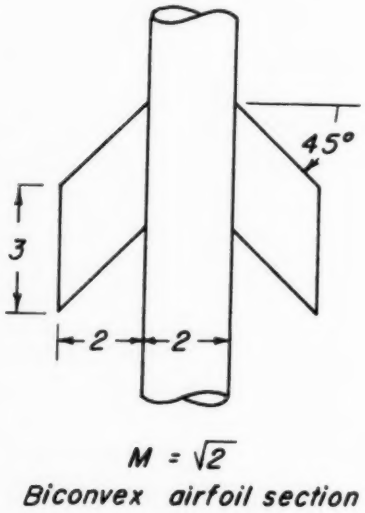

FIG. 7. Dimensions of wing studied in reference 7.

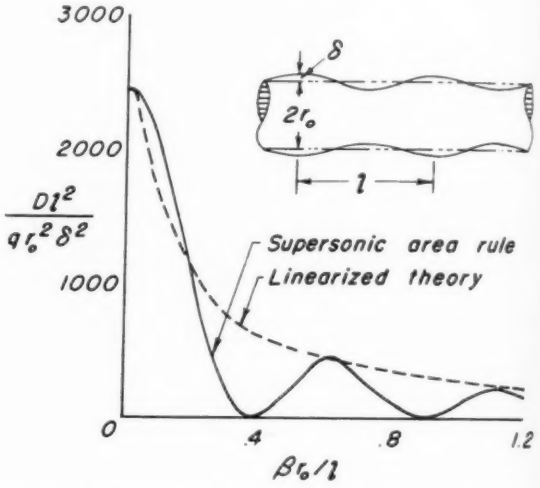

FIG. 8. Comparison between wave drags given by linearized theory and the supersonic area rule for a corrugated cylinder.

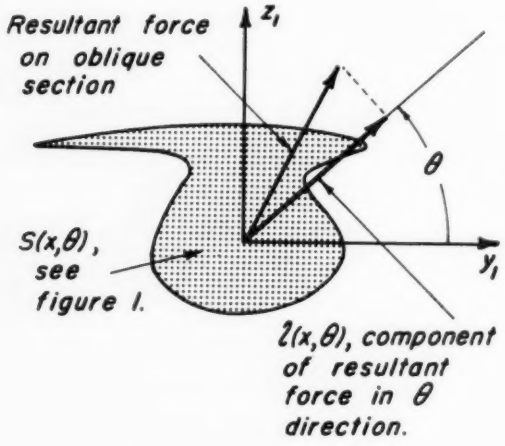

FIG. 9. Definition of $l(x, \theta)$.

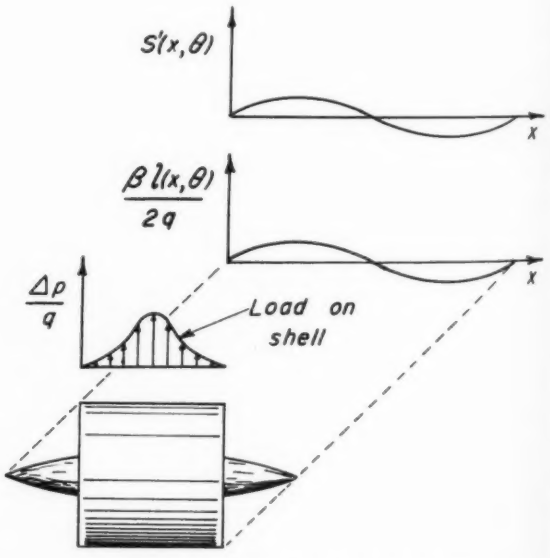

FIG. 10. Shrouded body with zero wave drag.

$$\frac{D}{q} = -\frac{1}{4\pi^2}\int_0^{2\pi} d\theta \int_{-L_0(\theta)}^{L_1(\theta)} dx_1 \int_{-L_0\theta}^{L_1\theta} dx_2 \times \left[S''(x_1, \theta) - \frac{\beta l'(x_1, \theta)}{2q}\right]\left[S''(x_2, \theta) - \frac{\beta l'(x_2, \theta)}{2q}\right] \times \ln|x_1 - x_2| \quad (21)$$

where $l(x, \theta)$ is the component of force pointing in the θ direction on the oblique section defining $S(x, \theta)$ (see Fig. 9).

The similarity between Eq. (4)—the equation giving the drag according to the supersonic area rule—and Eq. (21) is immediately apparent. In fact, the manner in which the term $\beta l/2q$ couples with the term $S'(x, \theta)$ gives the error made in using the supersonic area rule. Clearly this error is small when the Mach Number is near 1 or when the force coefficient l/q is small relative to the area gradient $S'(x, \theta)$.

An immediate application of Eq. (21) is its use in the calculation of zero wave drag, nonlifting, shrouded bodies of revolution. For example, consider a body of revolution surrounded by a thin circularly cylindrical tube—of negligible thickness, though this is not essential—such as is shown in Fig. 10. Specify any radially symmetric loading on the tube's surface. This fixes a value of $\beta l/2q$ which is independent of θ due to symmetry. Construct a body having an area variation in normal cuts (for simplicity, we are considering only those cases for which the difference in cross-sectional area between an oblique and normal cut is small) identical to this variation of $\beta l/2q$, and place this body inside a straight sided cylinder. The loading induced on the cylinder will be just that value of $\beta l/2q$ originally assumed and, by Eq. (21) the combination will have a negligible wave drag. The existence of such a body was first mentioned by Ferrari.[10] Graham, Beane, and Licher[11] have published a construction similar to the one given here.

Another application of Eq. (21), first pointed out by R. T. Jones, is its use in determining a lower bound to the wave drag for a given total lift. Let $2\Lambda(\theta)$ be the distance in the x direction between the two oblique planes bounding the airplane—i.e., $L_0(\theta) + L_1(\theta)$ in our previous notation. Then, in terms of the Fourier expansion,

$$S'(x, \theta) - \frac{\beta l(x, \theta)}{2q} = \sum_1^\infty C_n(\theta) \sin n\psi \quad (22)$$

where

$$\cos \psi = x/\Lambda(\theta) \quad (23)$$

The drag can be written

$$\frac{D}{q} = \frac{1}{8}\sum_1^\infty n \int_0^{2\pi} C_n^2(\theta)\, d\theta \quad (24)$$

Notice that $C_1(\theta)$ can be interpreted in terms of S_0, the base area (for simplicity in concept consider the body to be followed by a semi-infinite cylinder having the same shape as the base), and L, the total lift. Thus,

$$C_1(\theta) = [2/\pi\Lambda(\theta)]\,[S_0 - (\beta L \sin\theta/2q)] \quad (25)$$

and the C_n's for the higher n's depend on the moments of area and lift.

Now fix the total lift and assume the area and loading is distributed in such a way that $\sum_2^\infty C_n^2(\theta) = 0$. The drag of such an arrangement is given by

$$\frac{D}{q} = \frac{1}{2\pi^2}\int_0^{2\pi}\left(S_0 - \frac{\beta L \sin\theta}{2q}\right)^2 \frac{d\theta}{\Lambda^2(\theta)} \quad (26)$$

If $1/\Lambda^2(\theta)$ is expanded in a Fourier series, so that

$$\frac{1}{\Lambda^2(\theta)} = \sum_0^\infty (\beta_n \cos n\theta + \alpha_n \sin n\theta) \quad (27)$$

one can show that the minimum wave drag occurs when

$$S_0 = (\beta L/2q)\,(\alpha_1/\beta_0) \quad (28)$$

and is given by

$$(D/q)_{min} = (1/2\pi)\,(\beta L/2q)^2 \times [\beta_0 - (\beta_2/2) - (\alpha_1^2/2\beta_0)] \quad (29)$$

Notice that a combination with vertical symmetry ($\alpha_1 = 0$) or with a value of $\Lambda(\theta)$ that is the same for all θ has the lowest wave drag for the given conditions if the base area is zero.

Method of Multipoles

One general solution to the wave equation (see, for instance, reference 5, p. 527) consists of an infinite set of basic singular solutions referred to as multipoles These basic singularities can be distributed along a line and, by appropriate weighting, can be made to simulate any potential field exterior to a certain cylinder along whose axis they lie. The expression for the perturbation velocity potential for a distribution of nth order multipoles, starting at $-L_0$ and continuing along the x axis, can be written (for a discussion related to problems of the type concerning us here see reference 12)

$$\varphi(x, r, \theta) = -\frac{r^n}{2\pi}\left(\frac{1}{r}\frac{\partial}{\partial r}\right)^n \int_{-L_0}^{x-\beta r} \frac{[a_n(x_1)\cos n\theta + b_n(x_1)\sin n\theta]}{\sqrt{(x - x_1)^2 - \beta^2 r^2}}\, dx_1 \quad (30a)$$

or, alternatively,

$$\varphi(x, r, \theta) = -\frac{1}{2\pi}\int_{-L_0}^{x-\beta r} \frac{[A_n(x_1)\cos n\theta + B_n(x_1)\sin n\theta]\cosh\{n\cosh^{-1}[(x-x_1)/\beta r]\}}{\sqrt{(x - x_1)^2 - \beta^2 r^2}} \times dx_1 \quad (30b)$$

$$\left.\begin{aligned} A_n(x) &= (-\beta)^n\,(\partial^n/\partial x^n)a_n(x) = (-\beta)^n a_n^{(n)}(x) \\ B_n(x) &= (-\beta)^n b_n^{(n)}(x) \end{aligned}\right\} \quad (31)$$

The drag caused by these multipoles is simply

$$D = 2D_0 + \sum_1^n (D_{A_n} + D_{B_n}) \quad (32)$$

where D_{A_n} and D_{B_n} are given by Eq (11), the $\bar{A}_n'(x)$ being replaced by $A_n'(x)$ and $B_n'(x)$, respectively.

Vertically Symmetric Combinations—In this part let us consider a wing-body combination symmetrical about a horizontal plane ($z = 0$) and at zero angle of attack. Placing the line of multipoles along the axis of the body they are to represent, we see the drag of the wing and multipole line is given by Eq. (32) wherein D_{Bn} is zero (by symmetry) and D_{An} is now given by Eq. (11) except that the terms $\overline{A_n}'(x)$ are replaced by $\overline{A_n}'(x) + A_n'(x)$. This leads at once to the possibility of zero wave drag if

$$\frac{1}{U_0} A_0(x) = -\frac{1}{2\pi} \int_0^{2\pi} S'_w(x, \theta) d\theta \qquad (33a)$$

$$\frac{1}{U_0} A_n(x) = -\frac{1}{\pi} \int_0^{2\pi} S'_w(x, \theta) \cos n\theta d\theta \qquad (33b)$$

which defines the optimum strengths of the multipoles so placed.

In order to illustrate the amount of drag that one can associate with the various multipoles throughout a Mach Number and aspect ratio range, the nonlifting elliptic wing with a biconvex section shown in Fig. 11 was analyzed. The wave drag of this wing was first calculated by R. T. Jones[13] and is given by the equation

$$C_D = (4/\beta)\,(t/2a)^2 \left\{ [1 + 2(a/b\beta)^2] \div [1 + (a/b\beta)^2]^{3/2} \right\} \qquad (34)$$

The reduction in wave drag (details of the calculations appear in reference 12) as the wing is combined with the first three (non-zero) optimum multipole distributions is also shown in Fig. 11. Notice that for values of the Mach Number near unity most of the drag is destroyed by a line of sources only, but as the Mach Number increases, the higher order multipoles play an increasingly important role.

The principal difficulty in applying this method to physical problems is to find the shape of the fuselage corresponding to the multipole distributions. We shall consider here only those cases for which the wing source sheet and the line of multipoles simulate the entire flow field exterior to the airplane surface. For such cases, the possibility of zero wave drag, mentioned above, is a fiction if the body is to have finite length. This follows, since any sources added to those given by Eqs. (33) must increase the drag; yet sources must be added if the body is to close and be real since the initial magnitudes of $A_0(x)$ are negative for a real wing. Generalizations as to what the numbers and strengths of the multipoles can be in the presence of some basic source distribution or starting streamtube to insure the simulation of real shapes are difficult to develop. As an illustration, consider the variation with r of the radial velocity φ_r (the induced velocity principally affecting the body shape) induced by a multipole line. For small values of r, φ_r varies as $1/r^{n+1}$, whereas for large values of r (staying always behind the foremost Mach cone), it varies as $1/\sqrt{r}$. For instance, the magnitude of the first crest of the wave in φ_r (shown in Fig. 12) is produced by the multipole distribution

$$a_2(x) = c_2[1 - (x/L_0)^2]^3\,(x/L_0)$$

where $2L_0$ is the total multipole length. Clearly, the existence of a stream surface representing a real shape will depend on its distance from the multipole line as the induced velocity field begins to take effect as well as on the strength of that field, but a more specific statement would require detailed information regarding a particular case.

An example in which slender-body theory—i.e., φ_{nr} and $\varphi_{n\theta} \sim 1/r^{n+1}$—was used to calculate the body shape at $M = 1.4$ is given in reference 12. An elliptic wing having an aspect ratio equal to 3 and a biconvex airfoil section with maximum thickness ratio of 5 per cent was combined with a body having a maximum diameter about 1/5 of the wing span. For this case, it was found that the full strength of the a_0 term could be used, but only a portion of the a_2 term. An experiment (details of which are described in the reference) was carried out to test two combinations; one, the wing described mounted on a basic body (combination of a Sears-Haack body and a Kármán ogive) and the other, essentially the same wing mounted on a body modified according to the stream surface induced by the wing source sheet, the basic body source line, $a_0(x)$ and the best possible variation of $a_2(x)$, under the condition that the fuselage remain real. The results for the experimental drag rise are shown in Fig. 13. Less wave drag was attained throughout the Mach Number range shown by modifying the body even though the modified body had more volume. Notice that the agreement between experiment and theory is especially good as to the actual drag reduction at the design Mach Number.

If, in the region affected by the multipoles, the body does not distort greatly from a known surface, the distortions can be calculated by using a control-surface method in which the induced velocities are evaluated on a given surface and assumed to remain unchanged in the flow field on either side. The advantage of a control-surface method for the calculation of body shapes lies principally in the fact that the distortion fields are linear so that body modifications induced by the various orders of multipoles can simply be superimposed. It is disadvantageous in that accuracy falls off rapidly as the modified body surface approaches the body axis.

Nielsen[7] using a circularly cylindrical control surface has presented calculations of a body shape for the combination shown in Fig. 7. Nielsen found that the axially symmetric body distortion reduced the wave drag 22 per cent below that for the wings mounted on the undistorted cylinder, and the distortion caused by the next higher harmonic caused a further reduction of 42 per cent. At the wing-body juncture (the region of highest indentation) the maximum body indentation required for the full use of the higher harmonic was found to be six times that required for the lower.

In applying the method of multipoles as described above, one should always remember that only for a limited number of bodies can the entire exterior flow field be simulated by a set of multipoles along a single

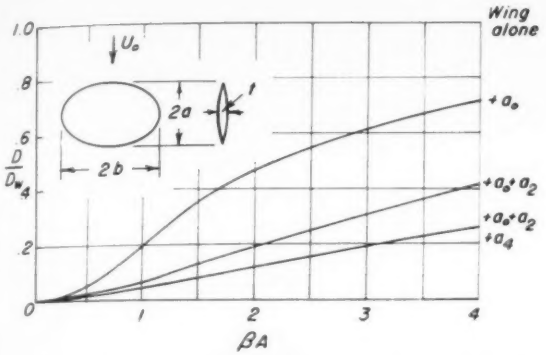

FIG. 11. Reductions in wave drag caused by combining first three non-zero optimum multipole distributions with elliptic wing.

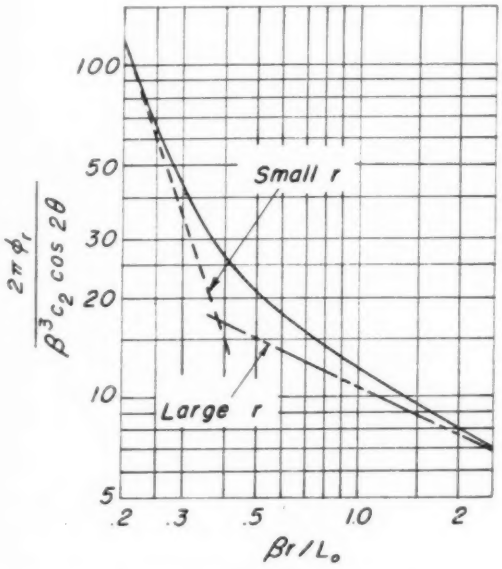

FIG. 12. Variation with radial distance of magnitude of first crest of wave in φ_r.

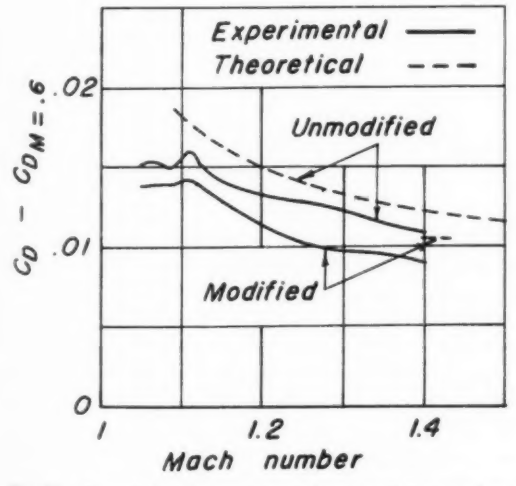

FIG. 13. Comparison between experiment and theory of wave drag for an elliptic wing combined with a basic body and one modified by zero and second-order multipole distributions.

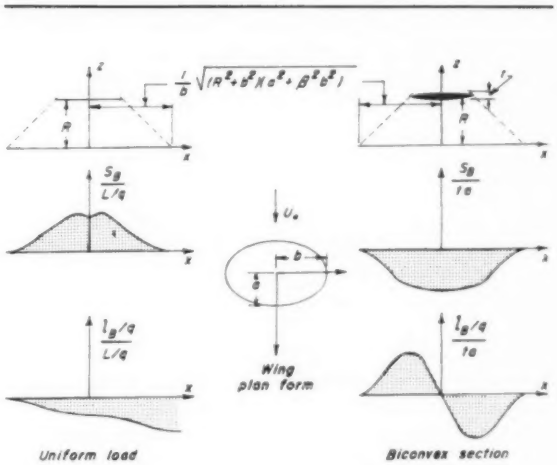

FIG. 14. Optimum area and lift variations on slender body beneath elliptic wing.

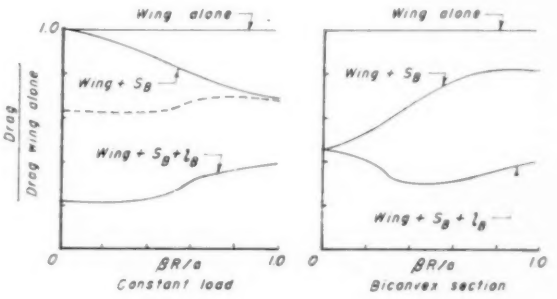

FIG. 15. Reduction in wave drag caused by combining bodies described by Fig. 14 with elliptic wing for which $\beta A = 2$.

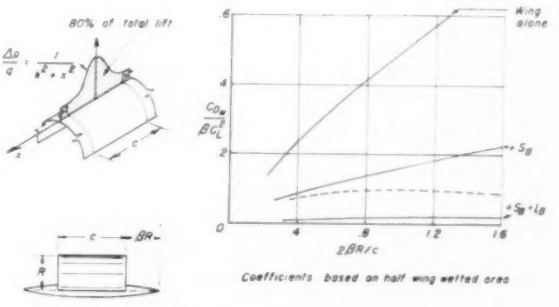

FIG. 16. Drag estimates for partially shrouded body.

line and, in general, the optimum fuselage to go with a given wing cannot be expected to lie within this limited set. Hence, the optimum multipole distribution associated with a nonlifting wing gives, when used directly to calculate the body shape, a fuselage better than, say, a straight-sided cylinder, but it probably does not yield the solution to the physical problem of finding the fuselage which combines with a given wing to produce the lowest drag for the combination.

Asymmetry and Lift—Next let us consider a wing-body combination for which the wing is thin and nowhere inclined at a large angle with respect to the free stream but otherwise of arbitrary thickness, camber, and disposition in x_1, y_1, z_1 space. For convenience, place the x_1 axis along the center line of the body and let $\Delta\lambda(x_1, y_1, z_1)$ be the difference between the streamwise slope on the opposed sides of the wing and $\Delta p(x_1, y_1, z_1)$ be the difference between the pressures across the same surface. Now cut the wing with the oblique plane, Eq. (3), and obtain the projections in a y_1, z_1 plane of the oblique section so formed. One can then show that

$$\frac{l(x, \theta)}{q} = \sin\theta \int_{wing} \frac{1}{q} \Delta p(x + \beta y_1 \cos\theta + \beta z_1 \sin\theta, y_1, z_1) dy_1 + \cos\theta \int_{wing} \frac{1}{q} \times \Delta p(x + \beta y_1 \cos\theta + \beta z_1 \sin\theta, y_1, z_1) dz_1 \quad (35)$$

and

$$S'(x, \theta) = \int_{wing} \Delta\lambda(x + \beta y_1 \cos\theta + \beta z_1 \sin\theta, y_1, z_1)\, ds_1 \quad (36)$$

where ds_1 is an element of arc in the y_1, z_1 plane. Finally, let us generalize the expansion given by Eq. (7) to include the asymmetry and lift. Thus,

$$S'(x, \theta) - \frac{\beta l(x, \theta)}{2q} = \sum_0^\infty [\bar{\bar{A}}_n(x) \cos n\theta + \bar{\bar{B}}_n(x) \sin n\theta] \quad (37)$$

where

$$\frac{1}{U_0} \bar{\bar{A}}_0(x) = \frac{1}{2\pi} \int_0^{2\pi} \left[S'(x, \theta) - \frac{\beta l(x, \theta)}{2q} \right] d\theta \quad (38)$$

etc.

If multipoles are placed along the x axis and used to simulate the body shape, it follows, just as before, that, from the point of view of lowering the wave drag, their optimum distributions denoted by A_n and B_n are given by the negatives of $\bar{\bar{A}}_n$ and $\bar{\bar{B}}_n$, respectively. In particular, let us study A_0 and B_1, since, if we assume slender-body theory applies for the calculation of the body shape, these give the total body volume and lift. For simplicity, consider only closed bodies; then, if V_B and L_B are the volume and lift on the body,

$$V_B = -\frac{1}{U_0} \int_{-L_0}^{L_1} x A_0(x)\, dx \quad (39)$$

$$\frac{\beta L_B}{2q} = -\frac{1}{U_0} \int_{-L_0}^{L_1} B_1(x) dx \quad (40)$$

Place Eqs. (35), (36), and the negatives of Eq. (38) in Eqs. (39) and (40), reverse the order of integration, and one can show

$$V_B = -V_w + \frac{\beta^2}{4} \iint_{wing} \left[z \frac{\Delta p}{q} dy dx + y \frac{\Delta p}{q} dz dx \right] \quad (41)$$

$$L_B = -L_w \quad (42)$$

where V_w and L_w are the volume of the wing and the lift on the wing, respectively.

Notice, from Eq. (41), that a lifting wing about the body creates an optimum multipole distribution which will have, by itself, positive volume—that is, a real body can be constructed that will destroy all the equivalent source distribution caused by the wing so located.

Two examples illustrating some of the above concepts have been worked out. In the first, a uniformly loaded elliptic wing having a biconvex section was moved above the body axis as shown in Fig. 14. Typical variations of body area and integrated loading [$l_e(x)$ represents the lift integrated from the nose to station x] given by the optimum multipole distributions are also shown in the Figure.

The effects on the wave drag of combining bodies having these area and load distributions with their wings are shown by the solid lines in Fig. 15. These results are simply a generalization of those presented earlier in Fig. 11.

If the full value of $B_1(x)$ generated under the lifting wing were used to simulate the body shape, the total lift of the wing-body combination would be zero [see Eq. (42)]. Hence, if the airplane is to carry a fixed total lift, this distribution should be modified by the condition that the body carry no net lift. With such a restraint the wave drag can only be reduced to the dashed line shown in the Figure, provided only $A_0(x)$ and $B_1(x)$ are used to generate the body shape. The difference between the dashed and solid line is given by Eq. (26) if S_0 is zero.

For the second example, an infinitely long semicircular cylinder, without thickness but with the loading

$$\Delta p/q = 1/(k^2 + x^2)$$

was analyzed. In order to use this model to estimate the performance of a practical combination, the infinite wing was assumed to approximate a finite wing with the chord required to carry 80 per cent of the total lift. Further, a body with a length equal to that of the optimum multipoles which the finite wing would generate was assumed to have the same relative effects on the wave drag when combined with its wing as the infinite body would with the infinite wing. Fig. 16 shows the drag of the wing alone and the wing plus the various multipole distributions. For C_D, the total drag was used, for C_L, 80 per cent of the total lift.

Both coefficients were based on half the wing wetted area.

Again the dashed line in the Figure represents the level to which the drag can be reduced by combining a wing with a body generated by $a_0(x)$ and the optimum distribution of $b_1(x)$ under the condition that the body carry no total lift. Although the wing has no thickness and no supporting strut was included, the study shows that a very large portion of the wave drag due to both lift and thickness can be eliminated by the arrangement chosen.

A comparison of the partially shrouded body with two flat-plate wings is given in Fig. 17. Shown are the sum of the total vortex drag and total wave drag of a body and semicylindrical wing (without thickness) together with drags of triangular and rectangular flat plates. To actually achieve the results shown for the semicylindrical wing and body, the wing should be cambered so that the vortex drag is a minimum and so the variation of lift required on the body is as small as possible. This accomplished, which does not seem unreasonable in light of the results shown in Fig. 16, the comparisons are fair since all coefficients are based on the wing wetted areas. Note, the partially enshrouded wing-body combination has almost as low a value of $C_D/\beta C_L^2$ as the triangular plate even though it is carrying a considerable amount of volume. For example, a 40,000-lb. airplane flying at a Mach Number equal to 2 at 50,000 ft., with an aspect ratio 2 wing, would carry an optimum volume equal to about 700 cu. ft. This volume is sufficient to fill a Sears-Haack body 45 ft. long with a maximum diameter equal to 6 ft.

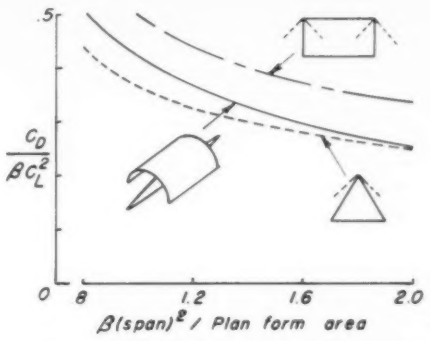

FIG. 17. Sum of wave and vortex drags for shrouded body and two flat-plate wings.

The Limiting Case $M \to 1$

After the original transonic area rule had been discovered, many pointed out that it was already contained in the existing body of linearized theory. This was, in fact, true, but the significance of the linearized results in this respect had been ignored or overlooked by everyone. However, this should not prevent us from now reinspecting the linearized theory and seeking to find from it what further information we can about the flow in the transonic vicinity.

Naturally, linearized theory as it applied to near sonic flow fields was not disregarded without reason, the reason being simply that the solutions to most boundary value problems contained whole regions filled with infinite perturbation velocities, a condition which clearly violates the assumptions basic to the theory. A few special cases were known which avoided this difficulty (as pointed out, for example, in reference 14). Thus, lifting surfaces without thickness as well as infinite sweptback wings with constant airfoil section and chord have flow fields in which the perturbation velocities are small compared to a sonic free-stream velocity. Recognized as necessary for the existence of such flows was the condition that there be no net source strength in planes normal to the free stream. But an infinite streamwise cylinder having the same constant cross-sectional area before and behind a wing and an indentation in the wing vicinity, such that the sum of the wing and body cross-sectional areas equals the same constant, also satisfies this criterion, and perhaps in this sense the area rule is best described by linearized theory. To apply this result to practical flows the additional assumption (and a very strong one, but one that experiment now justifies) must be made—that any area variation added to the stream surface comprising the wing and fore and aft cylinders to distort or close it yields a drag at near sonic speeds peculiar to that area variation only.

With these concepts in mind, linearized theory can be used to estimate the actual pressure distribution over the central portion of a thin wing and slender body combination in which the body has been modified according to the transonic area rule. Such calculations have been carried out by Byrd.[15]

Further, results such as Eq. (21) can be examined for the case when $\beta \approx 0$ in an attempt to find simple extensions to the area rule. Investigations along this line have been carried out by Baldwin.[16] Studying just the zero lift case, Baldwin expanded Eq. (4) in powers of β and found, at Mach Numbers near 1, the drag depends upon the longitudinal distribution of both the area and moments of area about the body axis. Theoretically, this "moment of area" rule yields the same value of the wave drag as the area rule at $M = 1$ and, in addition, decreases the subsequent rise in drag as the Mach Number increases.

Experimental verification of the usefulness of the moment of area rule is shown in Fig. 18. The drag

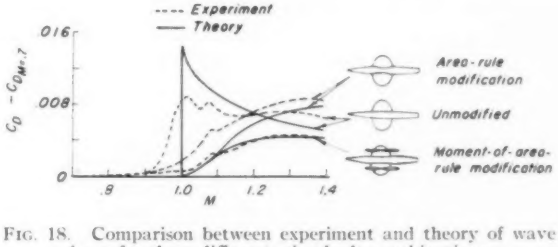

FIG. 18. Comparison between experiment and theory of wave drags for three different wing-body combinations.

rise above $M = 0.7$ is shown* for three configurations, all having the same total volume. One has a simple undistorted body (combination of Sears-Haack and Kármán ogive shapes). The other two have been modified, but both have the same area distribution. By carrying some volume out on the wing panels in the form of pods, one of these has a better moment of area distribution and the resulting decrease in wave drag is evident.

Nonlinear Transonic Theory

Although, as has been pointed out, linearized theory can be used to study a few very special types of boundary value problems at sonic speeds, solutions to transonic small-perturbation problems in general should be be based on Eq. (2a) or (2b). The nonlinear character of these equations makes the analysis of any but the simplest kind of problem exceedingly difficult. However, some progress has been made which has led to a few rather general conclusions.

The following discussion of the analytical results based on the nonlinear Eq. (2b) is closely related to the well-developed theory of slender wing-body combinations furnished by Jones[17] and Ward.[18] Therefore, we shall first review briefly the pertinent portions of slender-body theory and then describe its generalization to the nonlinear case.

First, we recall that the perturbation potential for the flow field in the vicinity of a slender configuration is given by the relation

$$\varphi(x, y, z) = \varphi_2(x; y, z) + f(x) \tag{43}$$

where φ_2 is the two-dimensional harmonic potential satisfying the boundary conditions in transverse or crossflow planes. The function $f(x)$ represents an additive effect that is determined completely by the longitudinal distribution of cross-sectional area and this can be calculated from knowledge of the flow about an equivalent body of revolution at zero angle of attack. For supersonic flow, $f(x)$ is given explicitly by the relation

$$f(x) = -\frac{U_0}{2\pi}\frac{\partial}{\partial x}\int_0^x S'(x_1)\ln\frac{2(x - x_1)}{\beta}\,dx_1 \tag{44}$$

where the body nose is at $x = 0$ and $S'(x)$ is the gradient of cross-sectional area $S(x)$. Implicit in the theory is the fact that $S'(x)$ has no discontinuities along the body and that its magnitude is small where body length L is the reference dimension. Furthermore, $S'(0) = 0$, but no further restrictions are placed on $S'(L)$, the gradient of $S(x)$ at the tail.

If D denotes the drag of an arbitrary wing-body configuration and D_B denotes the drag of the equivalent body of revolution, the two values of drag may then be related as follows

$$D = D_B - \frac{\rho_0}{2}\left[\int_C \varphi_2\frac{\partial\varphi_2}{\partial n}\,ds - \int_{C_B}\varphi_{2B}\frac{\partial\varphi_{2B}}{\partial n}\,ds\right] \tag{45}$$

In Eq. (45), ρ_0 is free-stream density and φ_2 and φ_{2B} are the crossflow potentials associated with the wing-body configuration and the body of revolution, respectively. The curvilinear integrals extend around the contours of the two configurations in the plane of the tail. As written, Eq. (45) contains contributions to both the vortex drag and the wave drag, but it is not difficult to evaluate the vortex drag separately and to show that it is proportional to the square of the angle of attack and is represented by the same expression at all Mach Numbers.

The wave drag of the equivalent body of revolution is given by

$$D_B = (1/2)\rho_0 U_0^2\Big(-(1/2\pi)\int\int S''(x_1)S''(x_2)\ln|x_1 - x_2|\,dx_1dx_2 + [S'(L)/\pi]\int S''(x_1)\ln(L - x_1)dx_1 - \{[S'(L)]^2/2\pi\}\ln[\beta\sqrt{S(L)/2\sqrt{\pi}}]\Big) \tag{46}$$

We observe here a dependence on Mach Number for bodies having finite angles at the base, and, in fact, the theory predicts excessive values of drag as Mach Number approaches 1. On the other hand, when the class of bodies is such that $S'(L) = 0$, the drag becomes independent of Mach Number and remains finite throughout the Mach Number range. Although, as has been mentioned, the predictions at sonic speed are certainly suspect by virtue of the infinite pressures, the theory appears to be telling us that only for certain classes of shapes does a slender wing-body combination and its equivalent body of revolution have the same wave drag. We shall now see that this conclusion is supported by the more exact transonic theory.

In a discussion as to what extent nonlinear theory modifies the results of the slender-body analysis just outlined, the papers of Oswatitsch,[19, 20] and Harder and Klunker[21] should be consulted. The following remarks are, however, drawn largely from a forthcoming paper by Heaslet and Spreiter.

In order to achieve some success with the nonlinear equation of flow, we restrict our attention to a comparison of wings alone and bodies alone. For sufficiently slender configurations it is found possible to derive from Eq. (2b) results directly analogous to those based on slender-body theory, provided the angle of attack of the wing is kept small relative to the thickness-chord ratio of the wing. Under these conditions it can be shown that the formal expression of Eq. (43) remains the same and that the perturbation potential in the vicinity of the wing is given by

$$\varphi(x, y, z) = \varphi_2(x; y, z) + g(x) \tag{47}$$

where $g(x)$ is determined by the longitudinal distribution of cross-sectional area and, thus, can be calculated from a knowledge of the flow field about a body of revolution at the same Mach Number and at zero angle of attack. In the case of slender-body theory the

* In each case the theoretical or experimental value of the body alone wave drag has been subtracted out.

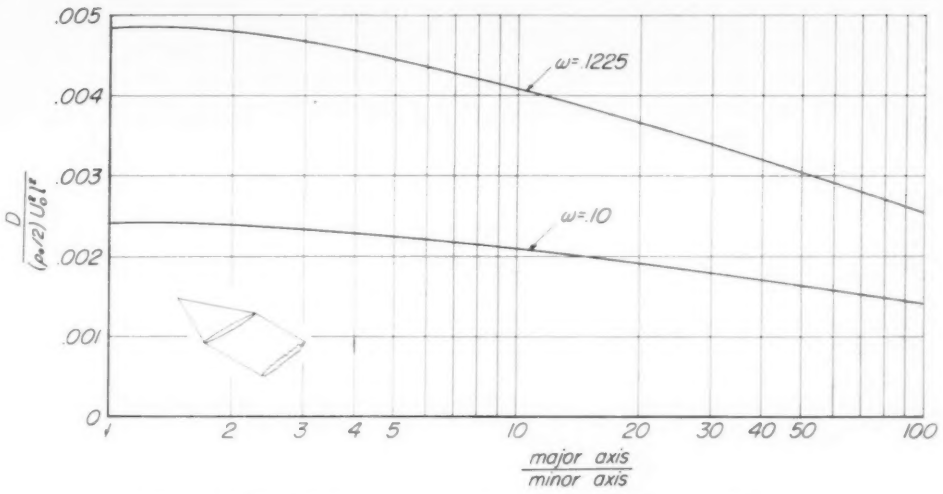

FIG. 19. Theoretical wave drag at $M = 1$ of elliptic cone-cylinders.

function $f(x)$ could be written in terms of airplane geometry—e.g., Eq. (44)—but in the nonlinear case no explicit result for $g(x)$ has been determined. However, one can show that Eq. (45) still applies in the nonlinear case where D_B is now the drag of the equivalent body of revolution at sonic speed. This result corroborates slender-body theory in stating that in certain cases the drag of a configuration and its equivalent body of revolution are the same but that this is only true when certain end conditions are satisfied.

Although the function of $g(x)$ in Eq. (47) cannot be given explicitly, it can be evaluated in certain specific cases. For example, the solution given for the circular cone-cylinder by Yoshihara[22] does furnish sufficient information to calculate $g(x)$ for one particular variation of area. Such calculations have actually been carried out for the case of slender elliptic cone-cylinders. The end conditions in these cases are such that the integrals of Eq. (45) do not vanish, and the results show that the drag of various cone-cylinders having the same longitudinal distribution of cross-section area, but different cross-section shapes, may differ substantially. The magnitude of the effect is illustrated in Fig. 19, which shows the variation of drag with ratio of major to minor axis of the elliptic cross section for two families of cone-cylinders. The cross-section area of all members of one family is the same as that of a circular cone with semiapex angle ω equal to 0.10 radian, whereas that of the other family is the same as a circular cone with ω equal to 0.1225 radian. It can be seen that, within a single family, the drag is a maximum for the circular cone-cylinder and diminishes continuously as the cone becomes thinner and wider. For the two families shown, the drag of wing-like members (aspect ratio about 2) is about 3/4 that of the circular cone-cylinder.

Since solutions for sonic flow around three-dimensional shapes other than cone-cylinders have not yet been obtained, the remainder of the discussions will be confined to cases in which experimental information is known for two or more wings or bodies having the same, or affinely related, longitudinal distribution of cross-section area. Probably the most extensive set of data of this type is that given in references 23 and 24 for a large family of affinely related wings of rectangular plan form having NACA 63AOXX sections. Since the results for $M = 1$ can be presented most concisely by using the variables suggested by the transonic similarity rules, the experimental results for the zero-lift pressure drag at $M = 1$ are given in Fig. 20 by plotting $C_D/\tau^{5/3}$ as a function of $A\tau^{1/3}$ where A is the wing aspect ratio and τ, the wing thickness ratio. As can be seen, the results define a single curve which approaches a straight line through the origin for low aspect ratio wings and a horizontal line for high aspect ratio wings.

Now, if it is assumed that the effects of the violation of the theoretical requirements that occurs at the round nose of the unswept leading edge of each wing of the present family can be disregarded, and that Eqs. (47) and (45) can be applied, it can be shown that all wings having a given longitudinal distribution of cross-section area have the same drag as stated by the transonic area rule. Combination of this fact with the transonic similarity rules[25] yields the result that $C_D/\tau^{5/3}$ is linearly proportional to $A\tau^{1/3}$. Examination of the data of Fig. 20 shows that the experimental results display this trend for wings of $A\tau^{1/3}$ less than about unity. This limit to the range of applicability of the area rule is undoubtedly different for wings having plan forms that are nonrectangular, but lack of data precludes making corresponding comparisons for other plan forms at the present time.

REFERENCES

[1] Munk, Max, M., *The Minimum Induced Drag of Aerofoils*, NACA Rep. 121, 1921.

[2] Hayes, Wallace D., *Linearized Supersonic Flow*, North American Aviation Report AL-222, June 18, 1947.

[3] Jones, Robert T., *Theory of Wing-Body Drag at Supersonic Speeds*, NACA RM A53H18a, 1953.

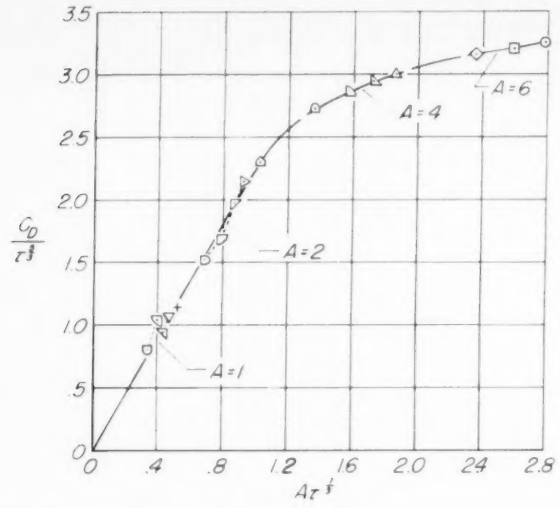

FIG. 20. Experimental values of zero-lift wave drag at $M = 1$ for a family of rectangular wings having NACA 63AOXX sections.

[4] Ward, G. N., *The Drag of Source Distributions in Linearized Supersonic Flow*, Cranfield College of Aeronautics Rep. No. 88, February, 1955.

[5] Lamb, Horace, *Hydrodynamics*, Sixth Edition, Dover Publications, Inc., 1945.

[6] von Kármán, Theodore, and Moore, Norton B., *The Resistance of Slender Bodies Moving with Supersonic Velocities with Special Reference to Projectiles*, Trans. A.S.M.E. Vol. 54, pp. 303–310, December 15, 1932.

[7] Nielsen, Jack N., *General Theory of Wave-Drag Reduction for Combinations Employing Quasi-Cylindrical Bodies with an Application to Swept-Wing and Body Combinations*, NACA RM A55B07, 1955.

[8] von Kármán, Th., *The Problems of Resistance in Compressible Fluids*, Estratto dagli atti del V Convegno della "Fondazione Alessandro Volta" Tema: Le alte velocitá in aviazione. Roma, 30 Settembre–6 Ottobre, 1935 XIII. Roma Reale Accademia D'Italia, 1936–XIV.

[9] Lomax, Harvard, *The Wave Drag of Arbitrary Configurations Linearized Flow as Determined by Areas and Forces in Oblique Planes*, NACA RM A55A18, 1955.

[10] Ferrari, C., *Campi di corrente impersonora attorno a solid di rivoluzione*, L'Aerotecnica, Vol. XVII, fasc. 6, pp. 507–518, June, 1937. (Also available as Brown Univ. Graduate Div. of Applied Math. Trans. 3965a.)

[11] Graham, E. W., Beane, B. J., and Licher, R. M., *The Drag of Non-Planar Thickness Distributions in Supersonic Flow*, Douglas Aircraft Co., Inc., Santa Monica, Rep. SM-18280, May, 1954.

[12] Lomax, Harvard, and Heaslet, Max. A., *A Special Method for Finding Body Distortions That Reduce the Wave Drag of Wing and Body Combinations at Supersonic Speeds*, NACA RM A55B16, 1955.

[13] Jones, Robert T., *Theoretical Determination of the Minimum Drag of Airfoils at Supersonic Speeds*, Journal of the Aeronautical Sciences, Vol. 19, No. 12, pp. 813–822, December, 1952.

[14] Heaslet, Max. A., Lomax, Harvard, and Spreiter, John R., *Linearized Compressible-Flow Theory for Sonic Flight Speeds*, NACA Rep. 956, 1950.

[15] Byrd, Paul F., *Theoretical Pressure Distributions for Some Slender Wing-Body Combinations at Zero Lift*, NACA RM A54J07, 1955.

[16] Baldwin, Barrett S., Jr., and Dickey, Robert R., *Application of Wing-Body Theory to Drag Reductions at Low Supersonic Speeds*, NACA RM A54J19, 1955.

[17] Jones, Robert T., *Properties of Low-Aspect-Ratio Pointed Wings at Speeds Below and Above the Speed of Sound*, NACA Rep. 835, 1946.

[18] Ward, G. N., *Supersonic Flow Past Slender Pointed Bodies*, Quart. J. Mech. and Appl. Math., Vol. 2, Pt. 1, pp. 75–97, 1949.

[19] Oswatitsch, K., *Die theoretischen arbeiten über schallnahe strömungs am flugtechnischen Institut der Kungl. Tekniska Högskolan, Stockholm*, Proc. Eighth Inst. Int. Cong. on Theo. and Appl. Mech. pp. 261–262, 1953.

[20] Oswatitsch, K., *Ein aquivalenzsatz für nichtangestellte flügel kleiner Spannweite in schallnaher strömung*, Zeitschrift für flugwissenschaften, 3 Jahrgang heft 2, pp. 29–46, February, 1955.

[21] Harder, Keith C., and Klunker, E. B., *On Slender-Body Theory at Transonic Speeds*, NACA RM L54A29a, 1954.

[22] Yoshihara, Hideo, *On the Flow Over a Cone-Cylinder Body at Mach Number One*, WADC Tech. Rep. 52–295, November, 1952.

[23] Nelson, Warren H., and McDevitt, John B., *The Transonic Characteristics of 22 Rectangular, Symmetrical Wing Models of Varying Aspect Ratio and Thickness*, NACA TN 3501, 1955.

[24] McDevitt, John B., *A Correlation by Means of Transonic Similarity Rules of Experimentally Determined Characteristics of a Series of Symmetrical and Cambered Wings of Rectangular Plan Form*, NACA Rep. 1253, 1955.

[25] Spreiter, John R., *On the Range of Applicability of the Transonic Area Rule*, NACA RM A54F28, 1954.

Symposium on Digital Computing in the Aircraft Industry

New York University, Jan. 31–Feb. 1, 1957

A joint symposium, sponsored by New York University, Mathematics Department, Research Division; International Business Machines Corp.; Society for Industrial and Applied Mathematics; and the Institute of the Aeronautical Sciences, Inc., will be held at the Gould Student Center, N.Y.U. College of Engineering Campus, University Heights, N.Y. This symposium will cover applications of the digital calculator in Aerodynamics; Dynamics; Structures; Statistics and Probability; Operations Research; Logistics; and Nuclear, Design, and General Computations.

Please contact one of the following individuals if you wish to attend: Arnold S. Wolf, IBM Corp., 590 Madison Ave., New York 22, or Dr. Max Woodbury, N.Y.U., Research Division, 401 W. 205 St., New York.

Spectral Theory of Buffeting and Gust Response: Unification and Extension

H. S. RIBNER*
University of Toronto

SUMMARY

The statistical approach to the dynamic response of aircraft in turbulent air is generalized and extended. The basic element is the response of the airplane to flight through an inclined sinusoidal upwash pattern in (a) three, (b) two, or (c)—without inclination—one dimension. Case (a) is general; in case (b) the airplane is idealized as a lifting surface or a lifting line; in case (c), as a lifting point. Earlier results of Liepmann are recovered in the cases of a lifting line and a lifting point. An extension of the case of a lifting line is made for the sweptback lifting line, and an extension of the case of a lifting point to provide rolling moments due to spanwise upwash gradients. The general case (a) and the lifting surface in case (b) are new.

SYMBOLS

a	=	tangent of sweep angle (lifting line)
i	=	$\sqrt{-1}$
$\boldsymbol{k}$	=	wave number vector (k_1, k_2, k_3)
dL	=	amplitude of single-wave lift response
L	=	resultant gust lift response
U	=	flight speed
t	=	time
dW	=	amplitude of single-wave upwash
w	=	resultant gust upwash
x, y, z	=	coordinates relative to stationary axes
x', y', z'	=	coordinates relative to axes attached to moving airplane
Γ	=	transfer function describing airplane single-wave response
ψ	=	gust spectrum function

Subscripts (on scalar symbols)

1 = gust idealized as one-dimensional
2 = gust idealized as two-dimensional
Primes denote spectral quantities associated with $\partial w/\partial y$

INTRODUCTION

THE PURPOSE of this note is first, to provide a general formulation for flight through turbulent air in three dimensions—one that will include and extend the basic relations pioneered by Liepmann[1] for one dimension and extended by him[2] and by Diederich[3] to two dimensions—and second, to introduce for all three cases a unified spectral approach, adapted from certain problems in turbulence.[4, 5] The spectral formalism is derived in the main from reference 5, but the origins (cited therein and in reference 4) go back much farther.

Received February 28, 1956.

* Research Associate and Assistant Professor, Institute of Aerophysics.

THREE-DIMENSIONAL GUST RESPONSE

Lifting Airplane

The approach is based on the concept that turbulent gusts and wakes may be represented as a superposition or spectrum of plane sinusoidal waves of shearing motion of all orientations and wave lengths; this is the physical interpretation of a Fourier integral—e.g., see reference 5. Considering the upwash component alone, an elementary spectrum component may be written

$$dW e^{i(k_1 x + k_2 y + k_3 z)} \tag{1}$$

This is a plane wave pattern of arbitrary orientation in space: the planes of constant upwash are normal to the vector $\boldsymbol{k} = k_1, k_2, k_3$. The upwash varies sinusoidally in the direction of $\boldsymbol{k}$ with wave number $k = \sqrt{k_1^2 + k_2^2 + k_3^2}$ (wave length $= 2\pi/k$).

The incremental lift response of an airplane flying through this inclined wavy upwash field is of the form

$$dL e^{ik_1 x} \tag{2}$$

when the airplane is assumed to move along the $-x$ axis; x is the coordinate of a reference point in the airplane. Eqs. (1) and (2) refer to stationary axes; relative to axes (x', y', z') moving with the airplane, Eq. (2) implies a sinusoidal time variation of lift via $x = x' - Ut$.

Evaluation of the lift response [Eq. (2)] serves to determine a three-dimensional "transfer function" $\Gamma(\boldsymbol{k})$ defined by

$$dL = \Gamma(\boldsymbol{k})\, dW \tag{3}$$

The transfer function plays a central role in gust response.

The spatial mean square upwash in the spectrum wave (more exactly, group of waves in band dk_1, dk_2, dk_3) is $|dW|^2$; if the gust turbulence is homogeneous (spatially uniform, on the average) this may be written $\psi(\boldsymbol{k})dk_1dk_2dk_3$ where $\psi(\boldsymbol{k})$ is a "spectral density" of mean square upwash. (The statistical relations herein are exact for homogeneous turbulence and approximate for atmospheric turbulence and wakes.) The corresponding mean square lift increment is $|dL|^2$. Thus upon summing over all of the waves that constitute the turbulent gust pattern, there results

mean square upwash:

$$\overline{w^2} = \Sigma |dW|^2 = \int\int\int \psi(\boldsymbol{k}) dk_1 dk_2 dk_3 \tag{4}$$

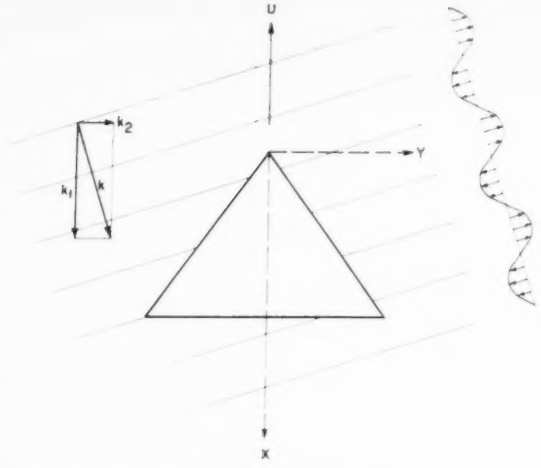

FIG. 1. The basic aerodynamic problem for gust response—flight through a yawed sinusoidal upwash pattern. A closely related problem is flight through a yawed sharp-edged gust.

mean square lift:

$$\overline{L^2} = \Sigma \left| dL \right|^2 = \int\int\int \left| \Gamma(\boldsymbol{k}) \right|^2 \psi(\boldsymbol{k}) dk_1 dk_2 dk_3 \quad (5)$$

where the integrals go from $-\infty$ to ∞ in k_1, k_2, k_3.

The first of these expressions relates the mean square upwash in the turbulent field to its spectral density in three dimensions, $\psi(\boldsymbol{k})$. The second evaluates the mean square lift increment in terms of the spectral density and transfer function. The two together relate the mean square incremental lift to the mean square upwash velocity in the gust pattern. A prerequisite is knowledge of the gust spectral density—e.g., see reference 2—and the airplane transfer function.

Eqs. (1) to (5) describe the lift response of a complete airplane flying through a random gust upwash pattern in space. This is the most general formulation of the gust-response problem in the engineering sense. (The negligible contributions of u and v fluctuations to lift are excluded.) The price of this generality is the difficulty in calculating the transfer function $\Gamma(k_1, k_2, k_3)$. The difficulty may be reduced progressively, along with the generality, by idealizing the airplane as (1) a lifting surface, (2) a lifting line,[2, 3] or (3) a lifting point.[1]

Two-Dimensional Gust Response

Lifting Surface

As a lifting surface the airplane is assumed to be sensitive only to the pattern of upwash in the (x, y) plane; the vertical (z) variation, of wave length $2\pi/k_3$, is taken to have no effect on response. Thus k_3 may be integrated out in the equations with a consequent reduction to two dimensions, the (x, y) plane. The results are

elementary wave:

$$dW_2 e^{i(k_1 x + k_2 y)} \quad (6)$$

lift response:

$$dL_2 e^{ik_1 x} \quad (7)$$

transfer relation:

$$dL_2 = \Gamma(k_1, k_2) dW_2 \quad (8)$$

spectral density:

$$\psi_2(k_1, k_2) = \int \psi(\boldsymbol{k}) dk_3 \quad (9)$$

mean square upwash:

$$\overline{w^2} = \Sigma \left| dW_2 \right|^2 = \int\int \psi_2(k_1, k_2) dk_1 dk_2 \quad (10)$$

mean square lift:

$$\overline{L^2} = \Sigma \left| dL_2 \right|^2 = \int\int \left| \Gamma(k_1, k_2) \right|^2 \psi_2 dk_1 dk_2 \quad (11)$$

The upwash pattern in the elementary two-dimensional wave [Eq. (6)] when plotted as a relief map has the appearance of a corrugated sheet. The corrugations are yawed relative to the spanwise (y) direction by an angle arctan $(-k_2/k_1)$ (the x axis has been taken as directed downstream). The basic aerodynamic problem is thus the calculation of the lift response [Eq. (7)] of the lifting surface flying through a *yawed* sinusoidal gust [Eq. (6)]. (See Fig. 1.) This suffices to determine the two-dimensional transfer function $\Gamma(k_1, k_2)$ by Eq. (8). The calculation must be performed for all values of k_1 and k_2.

Alternatively, the basic problem may be taken as the lift response $\Delta L(k_2/k_1, \xi)$ for flight through a *yawed* sharp-edged gust: an extension of the notion of "indicial response." Here $\tan^{-1}(-k_2/k_1)$ is the angle of yaw of the gust leading edge, and ξ is the distance of penetration of the reference point into the gust, measured along the $-x$ axis. The lift response for the sinusoidal gust of Eq. (6) can be obtained therefrom by means of Duhamel's integral—e.g., see reference 6.

Lifting Line

If the airplane is still further idealized as a lifting line the instantaneous chordwise variation of upwash is neglected. Under this assumption Liepmann[2] and Diederich[3] have formulated the transfer function for a wing without sweep in terms of a simple strip theory for wing response. Under the lifting line assumption Eqs. (6) to (8) lead directly to the same result [Eq. (14) of reference 2]. Moreover, the result is easily generalized to swept wings: it is found that k_2 in Eq. (14) of reference 2 need only be replaced by $k_2 \pm ak_1$, where a is the tangent of the sweep angle of the reference line, and the plus and minus signs are applied respectively to the right- and left-hand wing panels. The derivation is given in the Appendix. It is of interest that $k_2 \pm ak_1$ vanishes when the wave yaw matches the wing-panel sweep.

One-Dimensional Gust Response

Lifting Point

The limiting simplification represents the airplane as a lifting point moving along a line. This point sees

only the upwash pattern along the x axis; the spanwise (y) variation, of wave length $2\pi/k_2$, is taken to have no effect on lift. As was done with k_3, k_2 may be integrated out in the equations with a consequent reduction to one dimension: the x axis. The results are

elementary wave:

$$dW_1 e^{ik_1 x} \tag{12}$$

lift response:

$$dL_1 e^{ik_1 x} \tag{13}$$

transfer relation:

$$dL_1 = \Gamma(k_1) dW_1 \tag{14}$$

spectral density:

$$\psi_1(k_1) = \int \psi_2(k_1, k_2) dk_2 \tag{15}$$

or

$$\psi_1(k_1) = \int\int \psi(\boldsymbol{k}) dk_2 dk_3 \tag{16}$$

mean square upwash:

$$\overline{w^2} = \Sigma |dW_1|^2 = \int \psi_1(k_1) dk_1 \tag{17}$$

mean square lift:

$$L^2 = \Sigma |dL_1|^2 = \int |\Gamma(k_1)|^2 \psi_1 dk_1 \tag{18}$$

Rolling Moments

Spanwise upwash gradients would seem, at first thought, foreign to the one-dimensional idealization of the last paragraph. However, they may be injected in first approximation by replacing the upwash field by the first two terms of its Taylor expansion in y:

$$w(x, y) \simeq w(x, 0) + y(\partial w/\partial y)_{(x,0)}$$

Eqs. (12) to (18) refer to the first term. A similar set of equations corresponding to the second term are (where the prime does not signify a derivative):

elementary wave:

$$(\partial w/\partial y)_{(x,0)} = dW_1' e^{ik_1 x} \tag{19}$$

rolling moment response:

$$dl_1 e^{ik_1 x} \tag{20}$$

transfer relation:

$$dl_1 = \Gamma'(k_1) dW_1' \tag{21}$$

spectral density:

$$\psi_1'(k_1) = \int k_2^2 \psi_2(k_1, k_2) dk_2 \tag{22}$$

or

$$\psi_1'(k_1) = \int\int k_2^2 \psi(\boldsymbol{k}) dk_2 dk_3 \tag{23}$$

mean square $\partial w/\partial y$:

$$\overline{\left(\frac{\partial w}{\partial y}\right)^2} = \Sigma |dW_1'|^2 = \int \psi_1'(k_1) dk_1 \tag{24}$$

mean square rolling moment:

$$\overline{l^2} = \Sigma |dl_1|^2 = \int |\Gamma'(k_1)|^2 \psi_1' dk_1 \tag{25}$$

The effects of vertical (z) gradients may be evaluated similarly, with k_3 replacing k_2 as the factor of ψ in the analogs of Eqs. (22) and (23).

Concluding Remarks

The present formalism may be enlarged to include all three components u, v, w of gust velocity, the corresponding forces, moments, and deflections developed by the airplane, and, finally, the dynamics of the resulting airplane motion, with considerations of aeroelasticity. The analyses of references 3 and 7 point the way.

Appendix—Transfer Function of Sweptback Lifting Line

Let $h(\tau, y)$ be the increment of wing lift at time τ following unit impulsive angle of attack at time 0 over a chordwise strip of width dy at y. Then, if the angle of attack variation along the reference line in the wing is $w(t, y)/U$, the corresponding wing lift is[2]

$$\text{lift} = \frac{1}{U} \int_{-b/2}^{b/2} dy \int_{-\infty}^{\infty} h(\tau, y)\, w(t - \tau, y) d\tau \tag{26}$$

Now consider flight with velocity U through the stationary sinusoidal wave, [Eq. (6)], such that the airplane moves a distance ξ in the $-x$ direction in a time τ; then time and distance are related by $\tau = \xi/U$. At time t the upwash distribution along the swept reference line in the right-hand wing panel may be written

$$w(t, y) = dW_2 e^{ik_1(\bar{x} + ay) + ik_2 y}$$

where $x = \bar{x} + ay$ defines the sweptback line in terms of $(\bar{x}, 0)$, the coordinates of the apex. At the earlier time $t - \tau$ the line is a distance ξ farther downstream, whence

$$w(t - \tau, y) = dW_2 e^{ik_1(\bar{x} + \xi + ay) + ik_2 y}$$

This relation may be generalized to apply to both wing panels and inserted in Eq. (26), the lift may be written $dL_2 e^{ik_1 x}$, and the ratio $dL_2/dW_2 \equiv \Gamma(k_1, k_2)$ formed, with the result

$$\Gamma(k_1, k_2) = \frac{1}{U^2} \int_{-b/2}^{b/2} dy \int_{-\infty}^{\infty} h\left(\frac{\xi}{U}, y\right) e^{ik_1 \xi + i(k_2 \pm ak_1)y} d\xi \tag{27}$$

wherein the plus sign in the exponent refers to the right-hand wing panel, the minus sign to the left-hand wing panel. When the tangent a of the angle of sweepback is zero, Eq. (27) reduces to Eq. (14) of reference 2.

References

[1] Liepmann, H. W., *On The Application of Statistical Concepts to the Buffeting Problem*, Journal of the Aeronautical Sciences, Vol. 19, No. 12, p. 793, December, 1952.

[2] Liepmann, H. W., *Extension of the Statistical Approach to Buffeting and Gust Response of Wings of Finite Span*, Journal of the Aeronautical Sciences, Vol. 22, No. 3, p. 197, March, 1955.

[3] Diederich, Franklin W., *The Dynamic Response of a Large Airplane to Continuous Random Atmospheric Disturbances*,

(*Continued on page 1118*)

Some Integrated Volume Properties in Linearized Flow and Their Connection with Drag Reduction at Supersonic Speeds

Z. O. BLEVISS*

Douglas Aircraft Company, Inc.

SUMMARY

In some recent linearized studies of the drag of generalized (nonplanar) aircraft configurations in supersonic flow the bodies (aircraft configurations) were represented by singularities (elements of lift, side-force, and volume). This paper studies one aspect of the problem of relating the singularity distribution to the body geometry—namely, the relationship between the total singularity strength and the total body volume.

The "body" studied here is the region between a cylindrical mean surface and the stream surface that coincides with it at upstream infinity, the mean surface being parallel to the free stream and having an arbitrary closed cross section. It is shown that (a) in the absence of transverse forces the total body volume is equal to the total strength of the volume elements within the mean surface, (b) the body volume due to transverse forces may be obtained from an integration of the potential in the Trefftz plane, and (c) for certain mean surface cross-sectional shapes and positions the body volume due to given transverse forces is equal in magnitude to the fuselage volume required along a given axis to produce the minimum wave drag.

INTRODUCTION

IN REFERENCES 1 and 2 the drag of generalized (nonplanar) aircraft configurations in supersonic flow was studied using linearized theory. It was assumed there that the body (aircraft configuration) could be represented by singularities (elements of lift, side-force, and volume). It is obviously necessary to relate the distribution of the singularities to the geometry of the body. One aspect of this problem will be studied here —namely, the relation of the total volume of the body to the total strength of the singularities.

DISCUSSION

In principle, a body shape may be constructed from the singularities as follows. Take a cylindrical mean surface with generators in the free-stream direction; in cross section the mean surface is closed and of arbitrary shape. Consider the stream surface which at upstream infinity coincides with the mean surface. The "body" will be the region between the mean surface and its associated stream surface between upstream and downstream infinity. The volume will be counted as positive when the stream surface is outside the mean surface and negative in the opposite case. The stream surface should be computed from *linearized* theory. This means that if v_n is the normal velocity (outwash) at the point P on the mean surface and α is the slope (local angle of attack) of the stream surface at a point Q such that PQ is normal to the mean surface, then $\alpha U_\infty = v_n$, where U_∞ is the free-stream velocity. The body shape will thus depend on the mean surface chosen. It will in general be hollow. However, it will not be hollow in the two limiting cases most generally encountered: (a) in the linearized theory of slender bodies the singularities are located along a line, and the mean surface is a circular cylinder whose radius tends to zero; (b) in the theory of thin planar wings the singularities are distributed over a plane, and the mean surface also shrinks to a plane in the limit. For convenience, the bodies obtained in these limiting cases will be called "local bodies."

The volume element[1, 2] is a source-sink dipole with its axis in the free-stream direction. Any distribution of volume elements is, of course, equivalent to a distribution of sources and sinks.

The purpose of this paper is to prove the following statements. (1) The volume of a body is equal to the total strength of all volume elements inside the mean surface, provided no other singularities are present. (2) The volume of the body is the same for all mean surfaces containing the same volume elements, provided no other singularities are present. [Note that this follows immediately from statement (1).] (3) The contribution of other singularities—i.e., transverse-force elements—to the volume can be evaluated from the potential in the Trefftz plane according to Eq. (5). The significance of this contribution will be illustrated later.

Before proceeding with the proof of statements (1) and (3) it is important to note that since the body shape is constructed from a *linearized* mean surface as described above, the volume is additive in the singularities. Hence it is sufficient to consider any simple distribution of singularities in the proof. It is convenient to consider the volume elements distributed along a streamwise line, but the distribution of transverse-force elements may be general. Then, in the proof, the volume elements may be replaced by a local body of revolution, according to the well-known slender-body relation between source-strength and cross-sectional area. Higher order singularities, such as quad-

Received December 13, 1955.

* Aerodynamics Research Engineer.

The author would like to acknowledge many helpful discussions with E. W. Graham, P. A. Lagerstrom, and M. E. Graham.

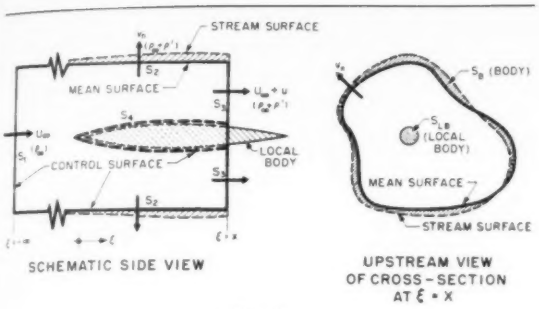

FIG. 1.

rupoles, etc., do not contribute to the volume and will be ignored. The results obtained in the following proof will be more general than statements (1) and (3).

Consider the control surface and local body of revolution shown in Fig. 1. The control surface has the following components: S_2 is the mean cylindrical surface (with arbitrary cross-sectional shape) extending from $\xi = -\infty$ to $\xi = x$; S_1 is normal to the free-stream direction at $\xi = -\infty$ and is equal to the cross-sectional area of the mean surface; S_3 is normal to the free-stream direction at $\xi = x$ and is equal to $S_1 - S_{LB}$, where S_{LB} is the cross-sectional area of the local body at $\xi = x$; S_4 closes the control surface following the surface of the body.

For steady flow, the conservation of mass requires that the mass flux out of S_2 and S_3 be equal to the mass flux into S_1—i.e.,

$$\iint_{S_2} (\rho_\infty + \rho')(U_\infty + u)dS + \iint_{S_2} (\rho_\infty + \rho')v_n dS = \rho_\infty U_\infty S_1 \quad (1)$$

where ρ' is the density perturbation, u is the velocity perturbation in the free-stream direction, v_n is the velocity (perturbation) at and normal to the mean surface, and the subscript ∞ denotes free-stream conditions. Eq. (1) is general. In *subsonic and supersonic* linearized flow the perturbations are small and the products of perturbation quantities may be neglected. Eq. (1) then reduces to

$$\rho_\infty \iint_{S_2} v_n dS = \rho_\infty U_\infty S_{LB}(x) - \iint_{S_3(x)} (\rho_\infty u + U_\infty \rho')dS \quad (2)$$

where the dependence on x of certain quantities is explicitly exhibited for clarity. Using the fact that $U_\infty \rho' = -\rho_\infty M_\infty{}^2 u$, where M_∞ is the free-stream Mach Number, Eq. (2) may be written

$$\iint_{S_2} \frac{v_n}{U_\infty} dS = S_{LB}(x) + \frac{(M_\infty{}^2 - 1)}{U_\infty} \iint_{S_3(x)} udS \quad (3)$$

The integral over S_2 can be interpreted as the cross-sectional area S_B of the body at $\xi = x$ (see Fig. 1). Briefly, this can be seen as follows. At any point on S_2, v_n/U_∞ is the slope of the stream surface in the plane containing v_n and U_∞. Integrating this slope along a generator of S_2 from $\xi = -\infty$ to $\xi = x$ yields the body thickness at $\xi = x$. Integrating this thickness around the mean surface cross-sectional contour gives $S_B(x)$ and Eq. (3) becomes

$$S_B(x) = S_{LB}(x) + \frac{(M_\infty{}^2 - 1)}{U_\infty} \iint_{S_3(x)} udS \quad (4)$$

where the sign convention for S_B is the same as for v_n (see Fig. 1).

The volume of the body from $\xi = -\infty$ to $\xi = x$ is

$$V_B(x) = \int_{-\infty}^{x} S_B(\xi)d\xi$$

Interchanging the S and ξ integrations and noting that

$$\int_{-\infty}^{x} ud\xi = \phi(x)$$

where ϕ is the perturbation velocity potential, there results*

$$V_B(x) = V_{LB}(x) + \frac{(M_\infty{}^2 - 1)}{U_\infty} \iint_{S_3(x)} \phi dS \quad (5)$$

V_{LB} is the volume of the local body up to $\xi = x$. The sign convention for V_B is the same as for v_n.

The case of particular interest in this paper is $x = +\infty$. Then, in Eq. (5), $V_B(\infty)$ is the body volume between upstream and downstream infinity, $V_{LB}(\infty)$ is the volume of all local bodies (or the sum of all volume elements) contained within the mean surface, and the last term is the integral of ϕ in the Trefftz plane over the area enclosed by the mean surface contour.

If the flow field is created by volume elements alone—i.e., there are no transverse forces—$\phi = 0$ in the Trefftz plane and $V_B = V_{LB}$. This proves statements (1) and (2).

Assume now that, in addition, transverse-force elements are present. In general, $\phi \neq 0$ in the Trefftz plane and the integral in Eq. (5) is not zero. Then the last term in Eq. (5) represents the contribution of the transverse forces to the body volume. This proves statement (3). This contribution depends on the mean surface chosen and may be negative. In particular, it should be noted that the contribution approaches zero as the area S_3 approaches zero. Thus, transverse forces do not contribute to local body volumes.

To illustrate the above remarks consider the axially symmetrical supersonic flow about a fuselage at zero angle of attack surrounded by a ring wing (see references 1 and 2). Let the ring wing have zero thickness, infinitesimal chord Δc, and uniform outward radial loading per unit length around the wing

* In this interchange of integrations care must be exercised whenever the ξ integration intersects the body upstream of $\xi = x$. This leads to an additional term in Eq. (5) which may be neglected in the linear theory. However, for nonslender bodies in incompressible flow ($M_\infty = 0$) Eq. (4) applies when S_4 is far enough from the body, and, in general, the additional term in Eq. (5) must be retained. For this case the additional term is equal to the "volume of additional apparent mass" when S_3 is downstream of the body.

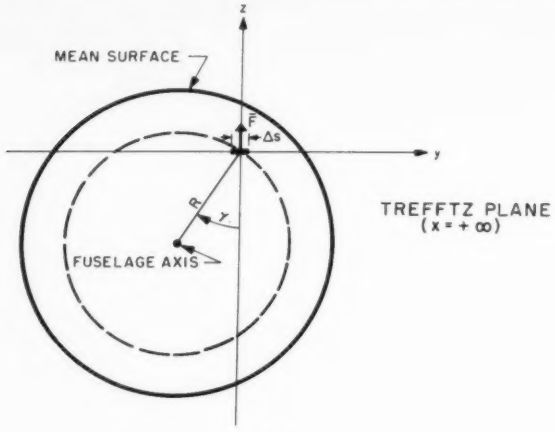

FIG. 2.

$$F = C_F(1/2)\rho_\infty U_\infty{}^2 \Delta c$$

The potential distribution in the Trefftz plane is

$$\phi = \begin{cases} 0 & \text{outside the ring} \\ -F/\rho_\infty U_\infty = -(1/2)C_F U_\infty \Delta c & \text{inside the ring} \end{cases}$$

Consider any mean surface enclosing the ring wing. The contribution of the fuselage to V_B is the fuselage volume V_F. The ring wing contributes a volume

$$V_{RW} = -(1/2)C_F(M_\infty{}^2 - 1)\pi R^2 \Delta c$$

where R is the radius of the wing. The total body volume is

$$V_B = V_F + V_{RW}$$

A necessary condition for zero wave drag is $V_B = 0$. A necessary and sufficient condition is that the body volume be zero identically at all points of the mean surface—i.e., v_n is zero at every point of the mean surface. Since the ring wing contributes negative volume it is clear that V_B can be made zero for a given wing loading F by adjusting V_F. Furthermore, the fuselage volume can be distributed along the axis of symmetry in such a way that $V_B(x) = 0$ for all x. Using the axial symmetry, this means that the body volume is zero identically at all points of the mean surface and, hence, the wave drag is zero. Since there is no trailing vortex system, the total drag is also zero. This is the "Ferrari ring wing plus central fuselage." It is the three-dimensional counterpart of the Busemann biplane.

In the general case, the physical significance of the volume contributed by transverse forces is not known. However, for certain cases in *supersonic* flow a physical significance can be attached to this volume. The above example is a particularly simple case that illustrates most of the essential points. It is seen that, if this volume is negative, a fuselage may be introduced to produce favorable interference with the transverse forces and, hence, to reduce the wave drag. The fuselage volume required for minimum (not necessarily zero) wave drag is equal in magnitude to this volume. This fuselage volume must be properly distributed to attain the minimum.

In the more general case of a given transverse-force element interfering with a fuselage that lies along a given axis, the correct result for the fuselage volume required for minimum wave drag is obtained from Eq. (5) if a particular mean surface is used. Very briefly, the result is obtained as follows. Consider a lifting element (force in $+z$ direction) with infinitesimal chord Δc and span Δs carrying a load

$$\bar{F} = C_F(1/2)\rho_\infty U_\infty{}^2 \Delta c \Delta s$$

Choose a mean surface with circular cross section that encloses the lifting element and whose axis of revolution coincides with the given fuselage axis. The geometry in the Trefftz plane is shown in Fig. 2. The potential distribution in the Trefftz plane corresponds to the two-dimensional incompressible flow due to a dipole (see, for example, reference 2) and is given by

$$\phi = (1/4\pi)C_F U_\infty \Delta c \Delta s[z/(y^2 + z^2)]$$

To obtain the body volume due to the lifting element, ϕ must be integrated over the circular region enclosed by the mean surface. It can be shown[3] that the integral is zero for the annular region between the mean surface and the concentric circle (dashed in Fig. 2) that passes through the dipole. The integral of ϕ over the area enclosed by the dashed circle can be readily obtained by using the mean value theorem of potential theory,[4] which for this case can be stated as follows: if ϕ has no singularities within the dashed circle the average value of ϕ over the area enclosed by the circle is equal to ϕ at the center of the circle. Then the integral of ϕ over the area enclosed by the circular mean surface is the value of ϕ at the fuselage axis multiplied by πR^2, and the body volume due to the lifting element is {with $z/(y^2 + z^2) = -[(\cos \gamma)/R]$}

$$V_{LE} = [(M_\infty{}^2 - 1)/4]C_F \Delta c \Delta s R \cos \gamma$$

Setting the total body volume equal to zero—i.e., $V_B = V_F + V_{LE} = 0$—the required fuselage volume is $V_F = -V_{LE}$. This is the result given in references 5, 6, and 7 for the fuselage volume required for minimum wave drag. It should be noted that, since the flow field is not axially symmetrical about the fuselage axis, the minimum wave drag cannot be zero; hence, the body volume is not identically zero at all points of the mean surface. The significance of the body volumes due to the lift element for mean surfaces with other cross-sectional shapes is not yet clear. A more complete discussion of these results is given in reference 3.

REFERENCES

[1] Graham, E. W., Beane, B. J., and Licher, R. M., *The Drag of Non-Planar Thickness Distributions in Supersonic Flow*, The Aeronautical Quarterly, Vol. VI, pp. 99–113, May, 1955.

[2] Graham, E. W., Lagerstrom, P. A., Licher, R. M., and Beane, B. J., *A Theoretical Investigation of the Drag of Generalized Aircraft Configurations in Supersonic Flow*, Douglas Aircraft Company, Inc. Report No. SM-19181, July, 1955.

(*Continued on page 1098*)

Influence of Aerodynamic Heating on the Effective Torsional Stiffness of Thin Wings

BERNARD BUDIANSKY* AND J. MAYERS**

Langley Aeronautical Laboratory, NACA

SUMMARY

Analysis is made of the loss of torsional stiffness that may be incurred by thin wings subjected to axial stresses induced by aerodynamic heating. Theoretical results are presented for the effective torsional stiffness of solid wings of symmetrical double-wedge cross section accelerated to supersonic speeds. It is demonstrated that serious losses of torsional stiffness may occur in such wings; the influence of various parameters such as Mach Number, acceleration, and thickness ratio are discussed.

SYMBOLS

A	= cross-sectional area
B	= quantity defined by Eq. (17)
E	= Young's modulus
G	= shear modulus
$H(z)$	= function defined by Eq. (23)
I_p	= mass polar moment of inertia per unit length
J	= torsional stiffness constant
M	= Mach Number
N_{Pr}	= Prandtl Number
$P(\lambda, \lambda_f)$	= function defined by Eqs. (22)
R	= Reynolds Number
T	= temperature
T_t	= total torque on cross section
T_σ	= torque on cross section due to axial stresses
$T_{St.\ V.}$	= torque on cross section due to St. Venant shear stresses
W_c	= complementary energy density
a	= velocity of sound
b	= span
c	= chord
c_m	= specific heat of wing material
d	= maximum thickness of wing
g	= acceleration due to gravity
h	= heat-transfer coefficient
h_f	= heat-transfer coefficient based on final flight velocity M_f
k	= parameter defined by Eq. (B-17)
k_a	= thermal conductivity of air
$m(\lambda_f)$	= function defined by Eq. (27)
$p(\lambda)$	= function defined by Eq. (B-22)
r	= radial distance from center of twist to point in cross section
s	= λ/λ_f
t	= wing thickness
t_s	= skin thickness of hollow wing
x, y	= rectangular coordinates
z	= dummy variable
Λ	= function of time parameter λ defined by Eq. (9)
α	= coefficient of thermal expansion
β	= nondimensional chordwise coordinate, $2x/c$ (h constant along the chord)
γ	= ratio of specific heats
γ_{xy}	= shear strain in xy-plane
ϵ_y	= spanwise strain
η	= nondimensional spanwise coordinate, $2y/b$
η_r	= temperature-recovery factor
θ	= temperature parameter, $[T - T_{aw}^{(0)}]/[T_{aw}^{(f)} - T_{aw}^{(0)}]$ or $(T - T_\infty)/[T_{aw}^{(f)} - T_\infty]$ if $T_{aw}^{(0)} = T_\infty$
λ	= time parameter
λ_f	= value of time parameter when $M = M_f$
ν	= kinematic viscosity
ξ	= nondimensional chordwise coordinate, x/c (h variable along the chord)
ρ_m	= mass density of wing material
$\sigma_x, \sigma_y, \sigma_z$	= normal stresses
τ	= time
τ_f	= time at which M_f is attained
τ_{xy}	= shear stress in xy-plane
φ	= angle of twist
ψ	= complementary energy
ω	= frequency

Subscripts

ave	= average
aw	= adiabatic wall
eff	= effective
el	= elementary
f	= final flight condition
max	= maximum
min	= minimum
0	= initial flight condition
∞	= free stream

Superscripts

0	= initial flight condition
f	= final flight condition

Presented at the Thermal Stress Analysis Session, Twenty-Fourth Annual Meeting, IAS, New York, January 23–26, 1956.

* Formerly, Head, Structural Mechanics Branch. Now, Associate Professor of Structural Mechanics, Division of Engineering and Applied Physics, Harvard University.

** Aeronautical Research Scientist.

INTRODUCTION

AN EFFECT of aerodynamic heating that has received little attention is the apparent change in the structural stiffness of aircraft components that can be caused by thermal stress. In the present paper attention is centered on the loss of torsional stiffness that may be incurred by thin wings subjected to thermally induced axial stresses. The physical mechanism underlying this type of stiffness loss is reviewed, and theoretical results are presented for the effective torsional stiffness of solid wings of double-wedge cross section accelerated to supersonic speeds. Details of the analyses are given in appendixes.

EFFECTIVE TORSIONAL STIFFNESS

It is well known that the torsional behavior of beams having thin cross sections can be strongly affected by axial stress. For example, the torsional buckling of bars is attributed to the action of axial compressive

stress in effectively reducing torsional stiffness.[1] In an entirely analogous fashion, the presence of axial thermal stress in a thin beam can produce an apparent change in its torsional stiffness.

The torsional effect of axial stress can be calculated simply. Fig. 1(a) shows a longitudinal element of a beam, with axial stress of magnitude σ_y at some point P located a distance r from the axis of twist AA. If the beam is twisted, the fiber PQ, originally parallel to the axis AA, assumes the new position P′Q′ shown in Fig. 1(b). It may be reasoned intuitively that the stress σ_y "follows the fiber" and hence assumes the direction P′Q′ when the beam is twisted. There is then a component $\sigma_y r(d\varphi/dy)$ of the axial stress that is perpendicular to the axis of twist. The total torque on the cross section due to the initial axial stress over the entire cross section is then

$$T_\sigma = \int_A \sigma_y r^2 (d\varphi/dy) dA \tag{1}$$

This torque due to the axial stresses must be added to the torque due to the St. Venant shear stresses

$$T_{\text{St. V.}} = GJ(d\varphi/dy) \tag{2}$$

to yield the total external torque on the cross section

$$T_t = \left[GJ + \int_A \sigma_y r^2 dA\right](d\varphi/dy) \tag{3}$$

The quantity in the brackets is the effective torsional stiffness of the beam; thus,

$$GJ_{eff}/GJ = 1 + \left[\int_A \sigma_y r^2 dA/GJ\right] \tag{4}$$

The same result has been derived by Goodier,[2] without recourse to the intuitive approach, on the basis of general equations of nonlinear elasticity.

When the axial stresses σ_y on a free-end beam (such as a wing or stabilizer) are due to temperature, they are necessarily self-equilibrating; that is, the net thrust and bending moment due to σ_y must vanish. Consequently, as can be easily verified, the magnitude of the torque [see Eq. (1)] due to such thermal stresses is independent of the axis of twist, as is the St. Venant torque [see Eq. (2)]. It may be worthy of mention that, within the framework of elementary beam theory, self-equilibrated axial stresses have no influence on bending stiffness.

It can be seen from Eq. (4) that a distribution of thermal stress σ_y that is compressive (negative) in the vicinity of the leading and trailing edges of a wing would cause a decrease in the torsional stiffness. As will be shown, such distributions of thermal stress are produced by the aerodynamic heating encountered in accelerated flight.

Solid Double-Wedge Wings

On the basis of various simplifying assumptions, the temperatures, stresses, and torsional stiffness changes in solid wing sections of symmetrical double-wedge profile [see Fig. 2(a)] undergoing various flight histories are calculated in Appendix A. Before the detailed presentation of final results of some generality, numerical results for a particular example will be shown in order to exhibit the essential features of the problem.

Illustrative Example

Consider a double-wedge airfoil of solid stainless steel instantaneously accelerated from Mach Number zero to Mach Number 3 at 50,000 ft. altitude. The chord is 36 in. and the midchord thickness—3 per cent of the chord—is 1.08 in. On the assumption that the initial temperature of the wing is the stratospheric free-stream temperature of −67°F., the temperature variation along the chord is shown in Fig. 3(a) for several values of time τ following the acquisition of Mach Number 3. In the calculations, the temperatures were assumed constant through the thickness, and heat conduction along the chord was neglected. The symmetry of the temperature distribution about the midchord is a consequence of the additional assumption of a constant heat-transfer coefficient in the boundary layer along the chord. The variation of temperature along the chord is simply a consequence of the fact that the massive midchord region takes longer to heat up than the thinner leading and trailing edge regions. An elementary calculation of the axial stresses resulting from the temperatures in Fig. 3(a) yields the distributions shown in Fig. 3(b) for the corresponding instants of time. Eventually, for very long times, the temperature in the wing would become uniform at the adiabatic wall temperature of 569°F., and, correspondingly, all thermal stresses would vanish. But at the intermediate times shown it is seen that compressive stresses occur near the leading and trailing edges, with equilibrating tensile stresses around the midchord. At each instant, then, the torsional stiffness is reduced according to Eq. (4), with the resultant time variation of effective stiffness shown by the intermediate curve in Fig. 4. Thus, about 1.25 min. after the sudden acquisition of Mach Number 3, the wing section sustains its maximum loss of torsional stiffness having effectively only 22.5 per cent of its original stiffness left. As flight at Mach 3 continues, the stiffness gradually increases, tending toward its original value as temperatures become uniform and thermal stresses vanish. It should be mentioned that the shear modulus G has been assumed invariant with temperature; any reduction of G with temperature would, of course, lower the torsional stiffness further.

Also shown in Fig. 4 are the variations with time of GJ_{eff}/GJ for instantaneous accelerations to Mach Numbers 2 and 4. The indicated reduction to zero stiffness after about 35 minutes of flight at Mach Number 4 may be interpreted as torsional buckling. According to Fig. 4, the wing at Mach Number 4 would unbuckle at time $\tau = 2.38$ min. and then gradually regain its torsional stiffness.

Since instantaneous acquisition of velocity is physically impossible, it is of interest to determine how the results would be modified by the imposition of more

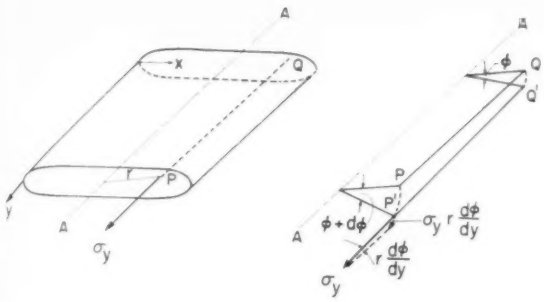

FIG. 1. Torsional effect of axial stress in a beam. (a) *left.* Longitudinal element. (b) *right.* Torque-producing component of axial stress.

FIG. 2. Wing cross sections considered in analyses. (a) *left.* Solid double-wedge section. (b) *center.* Solid constant-thickness section. (c) *right.* Hollow double-wedge section.

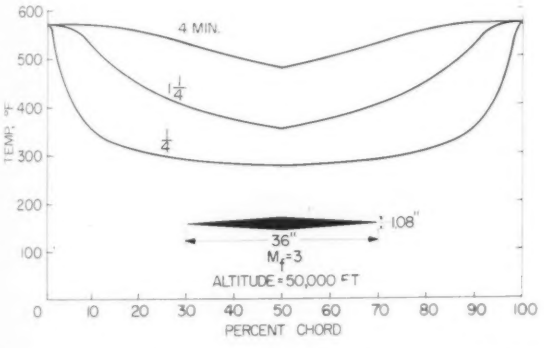

FIG. 3(a). History of temperature distributions for a solid steel double-wedge wing after sudden acquisition of velocity.

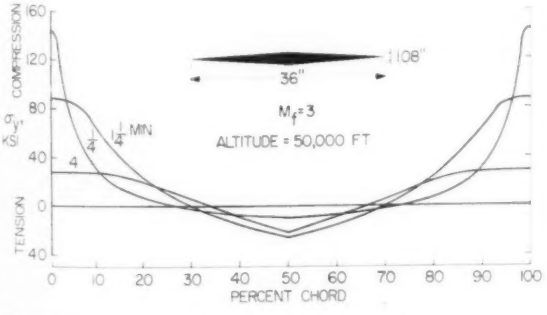

FIG. 3(b). History of thermal stress distributions for a solid steel double-wedge wing after sudden acquisition of velocity.

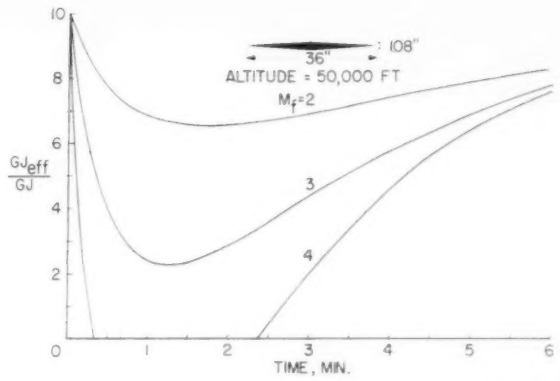

FIG. 4. Effective torsional stiffness history of a solid steel double-wedge wing after sudden acquisition of velocity.

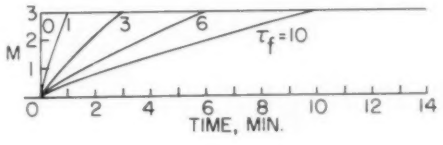

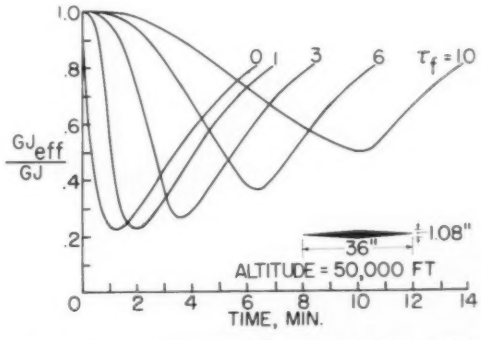

FIG. 5. Influence of acceleration rate on the effective torsional stiffness of a solid steel double-wedge wing. (a) *top.* Flight histories. (b) *bottom.* Effective torsional stiffness histories.

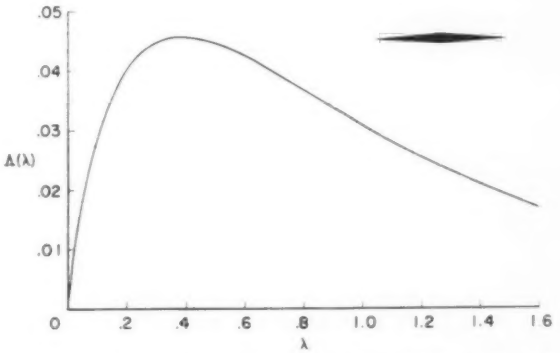

FIG. 6. Variation of $\Lambda(\lambda)$ [function defined by Eq. (9)] with time parameter λ.

realistic flight conditions. Fig. 5(a) shows a family of five flight histories: the instantaneous acquisition of Mach 3 already considered, and accelerated flights that reach Mach 3 in 1, 3, 6, and 10 min., respectively. The calculated variation with time of GJ_{eff}/GJ for each flight history is shown in Fig. 5(b). It is of significance that, at least for the particular wing considered, the maximum loss of stiffness for moderately rapid accelerations is only slightly less than that calculated for instantaneous acceleration; even for the very sluggish acceleration that takes 10 min. to get up to speed a stiffness loss of over 50 per cent would be incurred.

The next section presents the general results on which the preceding examples were based, and also discusses the assumptions with which the results were derived.

General Results and Discussion

Instantaneous Acceleration

The following initial and flight conditions are specified:

(1) For time $\tau < 0$, the wing flies at Mach Number M_0.

(2) The initial wing temperature at $\tau = 0$ is $T_{aw}^{(0)}$, the adiabatic wall temperature corresponding to M_0; in general, adiabatic wall temperature is given by

$$T_{aw} = T_\infty\{1 + [\eta_r(\gamma - 1)M^2/2]\} \tag{5}$$

where T_∞ is the free-stream temperature.

(3) At time $\tau = 0$, the wing suddenly acquires a speed of Mach Number M_f.

(4) The free-stream temperature T_∞ is assumed constant throughout the flight; this condition may be considered to correspond to flight with any altitude variation in the isothermal stratosphere between 35,000 and 105,000 ft., or to constant altitude flight.

The temperatures in the wing cross section are calculated for time $\tau > 0$ on the basis of the following assumptions:

(1) The heat-transfer coefficient h which governs the flow of heat from the boundary layer to the wing is constant along the chord, but may vary with time (as the altitude changes, for example).

(2) Temperatures are assumed constant through the wing thickness at each chordwise station.

(3) Heat conduction along the chord, as well as spanwise heat conduction, is neglected.

(4) Radiation effects are neglected.

Finally, the axial stresses on the cross section are calculated on the basis of the elementary theory that assumes plane sections remain plane, with no lateral restraint, and torsional stiffness changes are computed according to Eq. (4). All material properties, such as elastic moduli and coefficient of thermal expansion, are assumed invariant with temperature, and all deformations are assumed to be elastic.

It is shown in Appendix A that, for $\tau > 0$, the temperatures, stresses, and effective torsional stiffness are then governed by the following equations:

$$\frac{T - T_{aw}^{(0)}}{T_{aw}^{(f)} - T_{aw}^{(0)}} = 1 - e^{-[\lambda/(2x/c)]} \qquad 0 \le x \le c/2 \tag{6a}$$

$$= 1 - e^{-[\lambda/2[1-(x/c)]]} \qquad c/2 \le x \le c \tag{6b}$$

$$\frac{\sigma_y}{E\alpha[T_{aw}^{(f)} - T_{aw}^{(0)}]} = e^{-[\lambda/(2x/c)]} - (1 - \lambda)e^{-\lambda} + \lambda^2 Ei(-\lambda) \qquad 0 \le x \le c/2 \tag{7a}$$

$$= e^{-[\lambda/2[1-(x/c)]]} - (1 - \lambda)e^{-\lambda} + \lambda^2 Ei(-\lambda) \qquad c/2 \le x \le c \tag{7b}$$

$$GJ_{eff}/GJ = 1 - (E\alpha/G) \times \{[T_{aw}^{(f)} - T_{aw}^{(0)}]/(d/c)^2\}\Lambda(\lambda) \tag{8}$$

where

$$\Lambda(\lambda) = (1/8)[e^{-\lambda}(4\lambda + 7\lambda^2 + \lambda^3) + Ei(-\lambda)(10\lambda^2 + 8\lambda^3 + \lambda^4)] \tag{9}$$

and λ is a time parameter defined by

$$\lambda = \frac{2}{\rho_m c_m d}\int_0^\tau h(\tau)d\tau \tag{10}$$

$$= \frac{2h_f\tau}{\rho_m c_m d} \qquad \text{for constant} \quad h = h_f \tag{10a}$$

In Eqs. (7) and (9) $Ei(-\lambda)$ is the exponential integral function defined by

$$Ei(-\lambda) = -\int_\lambda^\infty (e^{-z}/z)dz$$

and tabulated in reference 3.

An alternative form of the result [Eq. (8)] for the effective torsional stiffness is obtained by the use of Eq. (5) for the adiabatic wall temperature; thus,

$$(GJ_{eff}/GJ) = 1 - (E\alpha/G)T_\infty\{[M_f^2 - M_0^2]/(d/c)^2\} \times [\eta_r(\gamma - 1)/2]\Lambda(\lambda) \tag{11}$$

A plot of $\Lambda(\lambda)$ versus λ is shown in Fig. 6; the maximum value of $\Lambda(\lambda)$ occurs for $\lambda = 0.386$ and is equal to 0.0456. Since λ is a monotonically increasing function of time, this maximum value of Λ must be attained at some time during the flight. Consequently, the minimum value of GJ_{eff}/GJ, from Eq. (8), is

$$(GJ_{eff}/GJ)_{min} = 1 - (0.0456)(E\alpha/G) \times \{[T_{aw}^{(f)} - T_{aw}^{(0)}]/(d/c)^2\} \tag{12}$$

or, from Eq. (11) with $\eta_r = 0.9$ and $\gamma = 1.4$,

$$(GJ_{eff}/GJ)_{min} = 1 - (0.00821)(E\alpha/G)T_\infty \times \{[M_f^2 - M_0^2]/(d/c)^2\} \tag{13}$$

From Eq. (13) it is seen that the maximum per cent reduction in torsional stiffness is dependent on parameters that may be characterized as pertaining to (a) material, $E\alpha/G$; (b) geometry, d/c; (c) altitude, T_∞; and (d) velocity, $M_f^2 - M_0^2$.

It is important to note that the result for $(GJ_{eff}/GJ)_{min}$ is not dependent on the magnitude of the heat-transfer coefficient. This fact is actually a conse-

quence of the assumed infinite acceleration, but it is significant nonetheless, since, as will be shown, the results for infinite acceleration remain nearly valid in many cases of moderately rapid acceleration.

It may be remarked that if interest centers on acceleration from a subsonic speed to a moderately high supersonic speed, little error is introduced by setting $M = 0$. (For example, if M_0 is actually 1/2, then M_f^2 differs from $M_f^2 - M_0^2$ by less than 7, 3, and 2 per cent for $M_f = 2$, 3, and 4, respectively.) On the basis of Eq. (13), with $M_0 = 0$, Fig. 7 shows how $(GJ_{eff}/GJ)_{min}$ varies with the thickness ratio d/c, at several values of M_f, for the case of stainless steel wings ($E\alpha/G = 24.2 \times 10^{-6}$/°F.) and stratospheric flight ($T_\infty = 393$°F. absolute). The Figure shows how susceptibility to loss of torsional stiffness increases sharply with decreasing thickness ratio. The effect of varying material is indicated in Fig. 8, wherein $(GJ_{eff}/GJ)_{min}$ is shown, for $M_f = 3$, for titanium ($E\alpha/G = 11.4 \times 10^{-6}$/°F.) and aluminum ($E\alpha/G = 33.4 \times 10^{-6}$/°F.) as well as for steel. (These assumed values of $E\alpha/G$, incidentally, are only to be regarded as reasonable estimates for illustrative purposes; in any particular design problem, a careful choice of the value of $E\alpha/G$ appropriate to the temperature range involved should, of course, be made.)

A useful representation of Eq. (13) is afforded by Fig. 9, which shows (for steel wings in the stratosphere and $M_0 = 0$) plots of d/c against M_f for several values of $(GJ_{eff}/GJ)_{min}$. This Figure indicates the limitations on thickness ratios at any Mach Number; for example, a steel double-wedge wing cannot have a thickness ratio less than about 3½ per cent if it is to retain more than half its original torsional stiffness after instantaneous acceleration to Mach 3 in the stratosphere.

The results previously shown in Figs. 3 and 4 for the illustrative example of a 3-ft. chord, 3 per cent thick steel airfoil at 50,000 ft. altitude were obtained from Eqs. (6), (7), and (11); in order to show the results in terms of time in minutes, it was necessary to assign specific values to the quantities involved in the time parameter λ given by Eq. (10a). The major uncertainty in evaluating λ lies in the specification of the heat-transfer coefficient h_f. For the illustrative purposes of the present report, the simple empirical formula for the case of a turbulent boundary layer (see, for example, reference 4)

$$h = [(0.030)k_a/x]R_x^{4/5}N_{Pr}^{1/3} \tag{14}$$

was used as a basis for specifying h. Since the present calculation requires a value of h constant along the chord, rather than the variable h given by Eq. (14), the value given by Eq. (14) at the midchord, $x = c/2$, was chosen. Thus,

$$h_f = \frac{(0.030)k_a(M_f a)^{4/5}N_{Pr}^{1/3}}{(c/2)^{1/5}(\nu)^{4/5}} \tag{15}$$

The time τ in terms of the time parameter λ then becomes, from Eqs. (10a) and (15),

$$\tau = [(d/c)c^{6/5}(\rho_m c_m)/BM_f^{4/5}]\lambda \tag{16}$$

where $$B = (0.0689)k_a(a/\nu)^{4/5}N_{Pr}^{1/3} \tag{17}$$

For the assumed altitude of 50,000 ft., the following values were assigned to the parameters in Eq. (17):

$a = 971$ ft./sec.
$\nu = 8.18 \times 10^{-4}$ sq.ft./sec.
$k_a = 3.16 \times 10^{-6}$ B.t.u./ft.-sec.-°F.
$N_{Pr}^{1/3} = 0.9$

The value of $(\rho_m c_m)$ for stainless steel was taken as 59.1 B.t.u./ft.³-°F.

It should be remarked that recent boundary-layer studies indicate that Eq. (14) for h may be seriously in error at supersonic speeds (see, for example, reference 5). However, as has already been mentioned, the magnitude of h does not influence the minimum value of GJ_{eff}/GJ where instantaneous acceleration is assumed; only the time at which the minimum occurs is effected by h. The magnitude of h does influence $(GJ_{eff}/GJ)_{min}$ for the case of finite acceleration, but, as will be shown in the next section, the magnitude of this influence may be quite small for moderately rapid accelerations.

Finite Acceleration

Appendix A also contains a derivation of the temperatures, stresses, and torsional stiffness changes of a solid double-wedge wing subjected to the following initial and flight conditions:

(1) For time $\tau < 0$, the wing has zero velocity.

(2) The initial wing temperature is T_∞, the free-stream temperature.

(3) For time $0 < \tau < \tau_f$ the wing flies at *constant altitude* with the Mach Number variation

$$M = M_f(\tau/\tau_f)^{5/6} \tag{18}$$

Here M_f is the final and largest flight Mach Number, and τ_f is the time at which it is attained.

(4) For time $\tau > \tau_f$, the wing continues to fly at constant altitude at Mach Number M_f.

The simplifying assumptions outlined in the last section continue to apply; but one new assumption is needed, namely the variation with time of the heat-transfer coefficient during the accelerated portion of the flight. Eq. (15) was used as a basis for this assumed variation; thus, while the Mach Number is changing,

$$h = h_f(M/M_f)^{4/5} \tag{19}$$

where h_f is the value of h corresponding to M_f. From Eqs. (18) and (19),

$$h = h_f(\tau/\tau_f)^{2/3} \tag{20}$$

during the accelerated portion of the flight.

The final results for the effective torsional stiffness are

$$GJ_{eff}/GJ = 1 - (E\alpha/G) \times \{[T_{av}^{(f)} - T_\infty]/(d/c)^2\} P(\lambda, \lambda_f) \tag{21}$$

where

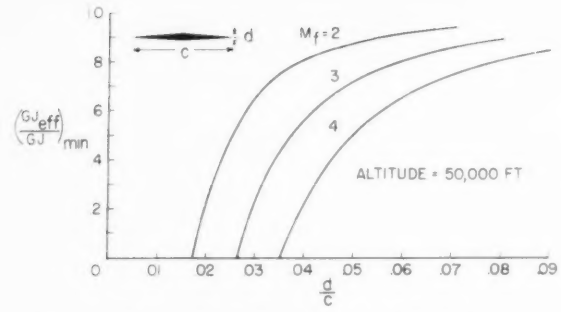

FIG. 7. Effect of Mach Number and airfoil thickness ratio on the minimum effective torsional stiffness of instantaneously accelerated solid steel double-wedge wings.

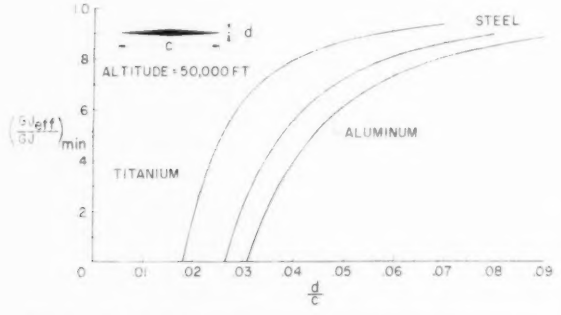

FIG. 8. Effect of material variation and airfoil thickness ratio on the minimum effective torsional stiffness of solid double-wedge wings instantaneously accelerated to $M_f = 3$.

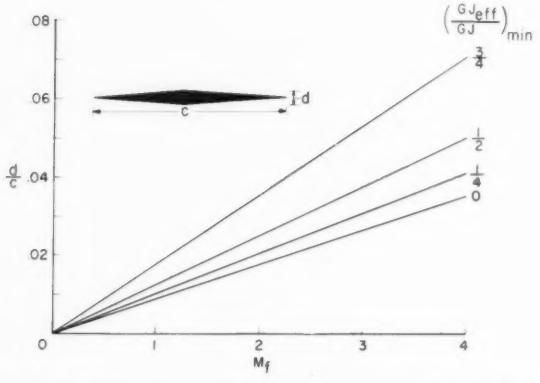

FIG. 9. Combination of airfoil thickness ratio and Mach Number that give various maximum reductions of torsional stiffness for solid steel double-wedge wings undergoing instantaneous acquisition of velocity in the stratosphere.

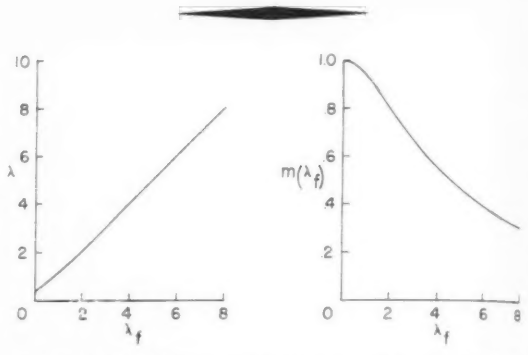

FIG. 10. Effect of finite acceleration on maximum reduction of torsional stiffness for solid double-wedge wings. (a) *left*. Values of λ that maximize $P(\lambda, \lambda_f)$ [see Eq. (22b)]. (b) *right*. Ratio of $(\Delta GJ_{eff})_{max}$ due to finite acceleration to $(\Delta GJ_{eff})_{max}$ due to infinite acceleration given by Eq. (27).

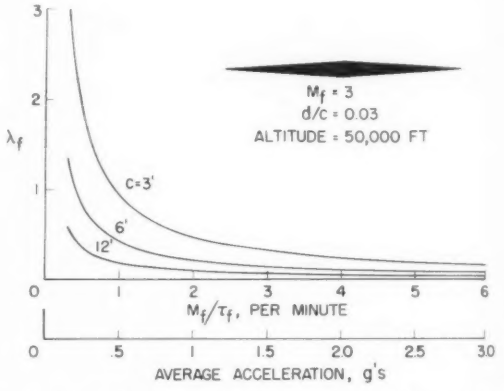

FIG. 11. Variation of λ_f with average acceleration and airfoil chord length for solid steel double-wedge wings.

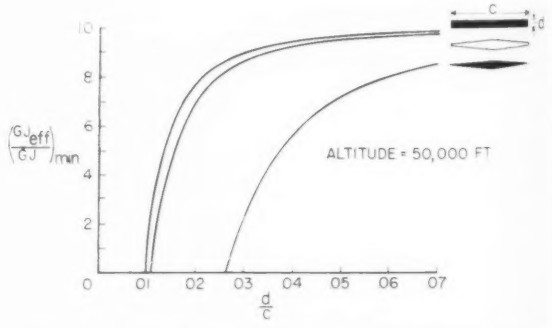

FIG. 12. Effect of airfoil configuration and thickness ratio on the minimum effective torsional stiffness of steel wings instantaneously accelerated to $M_f = 3$.

$$P(\lambda, \lambda_f) = \frac{8 + H[(3/5)\lambda_f^{-2/3}\lambda^{5/3}]}{72\lambda_f} \qquad (0 \leq \lambda \leq \lambda_f) \quad (22a)$$

$$= \frac{H[\lambda - (2/5)\lambda_f] - H(\lambda - \lambda_f)}{72\lambda_f} \qquad (\lambda \geq \lambda_f) \quad (22b)$$

$$H(z) = e^{-z}(-8 - 8z + 26z^2 + 27z^3 + 3z^4) + Ei(-z)(50z^3 + 30z^4 + 3z^5) \quad (23)$$

Here, as in the previous section, λ is the time parameter defined by Eq. (10a)—i.e.,

$$\lambda = 2h_f\tau/\rho_m c_m d \qquad (10a)$$

and λ_f, the value of the time parameter at which Mach Number M_f is attained, is

$$\lambda_f = 2h_f\tau_f/\rho_m c_m d \qquad (24)$$

It should be true that as $\lambda_f \to 0$, the results for effective stiffness reduce to those for instantaneous acceleration, with $M_0 = 0$ (or $T_{aw}^{(0)} = T_\infty$). That this is indeed so follows from the fact that, as can be readily verified, the first derivative of H is

$$H'(z) = 120\Lambda(z)$$

Consequently, for $\lambda = \lambda_f$,

$$\lim_{\lambda_f \to 0} P(\lambda, \lambda_f) = [-(2/5)H'(\lambda) + H'(\lambda)]/72 = \Lambda(\lambda) \qquad (25)$$

Thus, for $\lambda_f \to 0$

$$GJ_{eff}/GJ = 1 - (E\alpha/G)\{[T_{aw}^{(f)} - T_\infty]/(d/c)^2\}\Lambda(\lambda) \qquad (26)$$

which is precisely the result given by Eq. (8) with $T_{aw}^{(0)} = T_\infty$.

The effect of various rates of finite acceleration to a given Mach Number M_f on the minimum value of GJ_{eff}/GJ that occurs can now be determined. The larger λ_f, the longer is the time to reach M_f, and hence the slower is the acceleration. It is found that, for any λ_f, the largest value of $P(\lambda, \lambda_f)$ always occurs for a value of λ greater than λ_f; in other words, the minimum effective torsional stiffness always occurs after the steady portion of the flight begins. Fig. 10(a) shows the variation with λ_f of the values of λ which yield the maximum value of $P(\lambda, \lambda_f)$, as given by Eq. (22b). It is seen that as λ_f increases, the maximizing values of λ occur closer and closer to λ_f. Fig. 10(b) shows how the ratio

$$m(\lambda_f) = [P(\lambda, \lambda_f)]_{max}/[P(\lambda, 0)]_{max} \qquad (27)$$

varies with λ_f; here, of course, $[P(\lambda, 0)]_{max}$ is the same as $[\Lambda(\lambda)]_{max} = 0.0456$. For a given wing, altitude, and maximum Mach Number M_f, the ordinate in Fig. 10(b) is equal to the ratio of the maximum torsional stiffness change due to a finite acceleration to the change due to instantaneous acceleration. Consequently, if λ_f is known, Fig. 10(b) can be used to assess the effect of finite acceleration on the results previously found for the minimum effective stiffness for the case of instantaneous acceleration. Thus, from Eqs. (12) and (13) for instantaneous acceleration,

$$(GJ_{eff}/GJ)_{min} = 1 - m(\lambda_f)[0.0456][E\alpha/G] \times \{[T_{aw}^{(f)} - T_\infty]/(d/c)^2\} \quad (28a)$$

or

$$(GJ_{eff}/GJ)_{min} = 1 - m(\lambda_f)[0.00821][E\alpha/G][T_\infty M_f^2/(d/c)^2] \quad (28b)$$

The curves of Fig. 5 for the illustrative example were obtained from Eq. (21), and showed that, for this example, moderately rapid accelerations produced maximum stiffness losses only slightly less than those incurred by instantaneous acceleration. The general expression Eq. (28a) and Eq. (28b), and Fig. 10(b), indicate that, in general, the relieving effects of finite acceleration are quite small if λ_f is about one or less. With the use of Eq. (15) for h_f, it is found that in terms of the average acceleration M_f/τ_f in Mach Numbers per unit time,

$$\lambda_f = [BM_f^{9/5}/(d/c)c^{6/5}\rho_m c_m]/(M_f/\tau_f) \qquad (29)$$

where B depends on altitude, and is given by Eq. (17). Fig. 11 shows curves of λ_f against M_f/τ_f in Mach Numbers per minute, for an altitude of 50,000 ft., $d/c = 0.03$, and $M_f = 3$. The material is stainless steel, with $\rho_m c_m = 59.1$ B.t.u./ft.^{3}-°F.; separate curves are shown for chord lengths of 3, 6, and 12 ft. The corresponding values of λ_f for other thickness ratios, Mach Numbers, chord length, and materials may be readily found by scaling according to Eq. (29). (The value of $(\rho_m c_m)$ for both aluminum and titanium is about 36.6 B.t.u./ft.^{3}-°F.) An auxiliary abscissa in Fig. 11 shows average acceleration in g's.

Inspection of Fig. 11 reveals that for a very wide range of parameters the values of λ_f are quite small, so that the corresponding values of $m(\lambda_f)$ are close to unity. Consequently, the results for infinite acceleration have practical validity in many cases of finite acceleration. Of course, when accelerations are so slow as to modify the instantaneous acceleration results appreciably, the stiffness effects can be estimated quantitatively by the use of Fig. 10(b) for $m(\lambda_f)$.

Another important conclusion that may be drawn from Figs. 10(b) and 11 is that inaccuracies in the estimate of the heat-transfer coefficient are not likely to be serious insofar as the effect on torsional stiffness is concerned. Since, as Eq. (24) shows, λ_f is proportional to h_f, a change in h_f by even a factor of two or three is unimportant if λ_f is well within the range where the instantaneous acceleration results are nearly valid.

These considerations concerning the *magnitude* of the assumed value of h_f are without reference to the errors introduced by the assumed constancy of h along the chord. The next section attempts to shed light on the nature of the modifications of the results that are introduced by permitting h to vary in the chordwise direction.

Effect of Heat-Transfer Coefficient Variable Along the Chord

The constant-thickness wing of rectangular cross section shown in Fig. 2(b) would not suffer any loss of torsional stiffness if, as was assumed for the double-wedge, the heat-transfer coefficient were constant along the chord; the wing temperature would simply rise uniformly and no thermal stresses would develop. Consequently, it may be instructive to consider the effect on the constant-thickness wing of a variable heat-transfer coefficient; in this way, an idea can be gained of the errors involved in the preceding calculations for the double-wedge wing which ignored the chordwise variation of h.

From the approximate Eq. (14) for the heat-transfer coefficient of a turbulent boundary layer, it follows that h varies inversely as the fifth root of the distance from the leading edge; thus,

$$h(x) = h(c)/(x/c)^{1/5} \tag{30}$$

Consequently, in accelerated flight, the wing temperature in a constant-thickness wing would be largest at the leading edge and decrease continuously toward the trailing edge. In Appendix A, the temperatures, stresses, and stiffness changes are calculated for an instantaneously accelerated constant-thickness wing; except for the use of Eq. (30) for h, all of the conditions and assumptions used for the double-wedge wing were applied. The final result for the minimum effective stiffness is

$$(GJ_{eff}/GJ)_{min} = 1 - (0.00606)(E\alpha/G)\{[T_{aw}^{(f)} - T_{aw}^{(2)}]/(d/c)^{0}\} \tag{31a}$$

or

$$(GJ_{eff}/GJ)_{min} = 1 - (0.00109)(E\alpha/G)[T_{\infty}(M_f^2 - M_0^2)/(d/c)^2] \tag{31b}$$

In Fig. 12, the results of Eq. (31) are shown for constant-thickness stainless steel wings, with $M_0 = 0$ and $M_f = 3$, and are compared with those found for the double-wedge wing on the basis of a constant h. It is apparent that the stiffness loss of the constant-thickness wing is quite substantially less than that of the double-wedge wing. It is reasonable, therefore, to expect that the results found for the double-wedge wing with constant h would be modified only slightly if the variation of h along the chord were taken into account. This expectation is all the more plausible when it is realized that the peak influence of a variable h need not coincide in time with the occurrence of the maximum stiffness loss found on the basis of a constant h.

As a matter of auxiliary interest, the results found for the solid constant-thickness wing are applicable with only a slight modification to a hollow wing of constant skin thickness, with no internal structure. For the hollow double-wedge wing shown in Fig. 2(c)

$$(GJ_{eff}/GJ)_{min} = 1 - (0.00808)(E\alpha/G) \times \{[T_{aw}^{(f)} - T_{aw}^{(0)}]/(d/c)^2\} \tag{32a}$$

or

$$(GJ_{eff}/GJ)_{min} = 1 - (0.00145)(E\alpha/G)T_{\infty} \times [(M_f^2 - M_0^2)/(d/c)^2] \tag{32b}$$

and, again for stainless steel wings in the stratosphere, with $M_0 = 0$, and $M_f = 3$, the results for the hollow wing are shown in Fig. 12. For the hollow wing of constant-skin thickness, as for the solid constant-thickness wing, no stiffness loss would be found if the heat-transfer coefficient were made constant along the chord. It should be remarked, however, that these results for the pure hollow wing may be somewhat academic, since the addition of internal structures such as shear web, would change the results appreciably. Depending on the precise distribution of web material, the multiweb wing would probably suffer stiffness losses substantially greater than those shown for the pure hollow wing.

Free-End Effect

The assumption that plane sections remain plane, used in the calculation of thermal stresses, is strictly valid only far from a free end. At a free end, of course, no axial stresses can exist, and the effect of the free end is felt for some distance inboard from the tip. Thus, the effective torsional stiffness remains at its original value at the tip, and is actually variable along the span, approaching the values calculated in the preceding sections with increasing distance from the free end.

In Appendix B an approximate calculation is made of the spanwise variation of the effective torsional stiffness of instantaneously accelerated, double-wedge wings of constant chord and finite span (see Fig. 13). In addition, the change in the first natural torsional frequency of the wings considered as free-free beams is calculated approximately; the change in frequency—or, more precisely, the change in the frequency squared—constitutes a measure of the integrated effect of the torsional stiffness changes along the span. The results of the calculation are presented in Fig. 14, which shows, as a function of the aspect ratio b/c, the ratio of the maximum change in frequency squared to that calculated on the basis of the constant effective stiffness given by the elementary theory [see Eq. (8)]. It is evident from this figure that insofar as the overall effects of torsional stiffness changes are concerned little error is incurred in the use of the elementary thermal stress theory for reasonable aspect ratios; even for a value of wing aspect ratio as low as 1.5, the error is only slightly greater than 10 per cent.

Effect of Initial Twist

All of the foregoing results for effective torsional stiffness are based on the assumption that the wing is initially "perfect"—that is, untwisted—and hence remains untwisted while it experiences thermal stress. A wing with some initial twist would undergo additional twist as a result of the thermal stress distributions considered; indeed, as the condition for thermal buckling of the perfect wing is approached, this additional twist would become substantial (though not infinite, because of nonlinear large deflection effects). It follows from

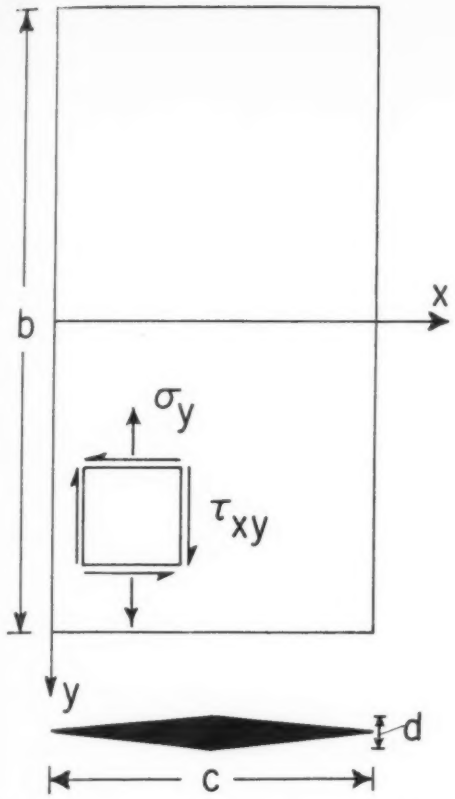

FIG. 13. Wing geometry and coordinate system for finite-span wing considered in Appendix B.

the theory of twisted beams[6] that for a sufficiently large final twist, the effective torsional stiffness would be considerably higher than that of a perfect wing subjected to the same thermal stress.* On the other hand, the magnitude of such a final twist would probably be undesirable from both structural and aerodynamic considerations. In summary, then, the behavior of a pretwisted wing would be qualitatively as follows: for moderate initial twist, the effective torsional stiffness of a thermally stressed wing should be approximately the same as that calculated for a perfect wing as long as the condition for thermal buckling of the perfect wing is not approached; when the thermal buckling condition *is* approached, the pretwisted wing would probably suffer excessive deformation, even though its final torsional stiffness would not be as low as that predicted for the perfect wing.

These considerations are consistent with the tests and calculations of Vosteen and Fuller[7] who dealt with a flat cantilever plate subjected to thermal stress distributions similar to those considered herein. The thickness ratio was quite low (1/80), aggravating the effects of initial displacements, as evidenced by the fact that appreciable distortion occurred during heating, with a consequent large deviation of measured torsional frequencies from those predicted by an analysis in terms of flat plate theory analogous to the beam theory of the present paper.

* This observation was originally made to the authors by Joseph N. Kotanchik of the NACA.

CONCLUDING REMARKS

The results exhibited show that serious losses in effective torsional stiffness can be produced in thin solid wings by the thermal stresses that arise during and after accelerated flight to supersonic speeds. The thermal stresses in solid wings are mainly attributable to chordwise mass variations; consequently, solid wings having thickness distributions more uniform than the double-wedge profiles considered in this paper may be expected to suffer smaller losses of stiffness. Similar losses of stiffness can occur in built-up wings, wherein the origin of thermal stress resides primarily in temperature differences between internal and external elements. Stiffness losses for built-up wings would probably be less serious than for solid wings; but, in any case, the magnitudes of the torsional stiffness changes of any shape of wing cross section can be estimated by means of the simple formula

$$\int_A \sigma_y r^2 dA$$

once the thermal stresses σ_y on the cross section are known.

APPENDIX A—ANALYTICAL CALCULATIONS

Let it be assumed that, at station x along the chord of a thin solid wing of arbitrary cross section, an element $(t dx)$ retains the heat transmitted to it from the boundary layer at the upper and lower surfaces. Then, with the additional assumption that the temperature of the element is uniform through its thickness, the heat balance equation governing the temperature T is

$$2h[T_{aw} - T] = \rho_m c_m t(\partial T/\partial \tau) \qquad \text{(A-1)}$$

where, in general, the heat-transfer coefficient h is variable in both space and time. The adiabatic wall temperature T_{aw} is taken as

$$T_{aw} = T_\infty\{1 + [\eta_r(\gamma - 1)/2]M^2\} \qquad \text{(A-2)}$$

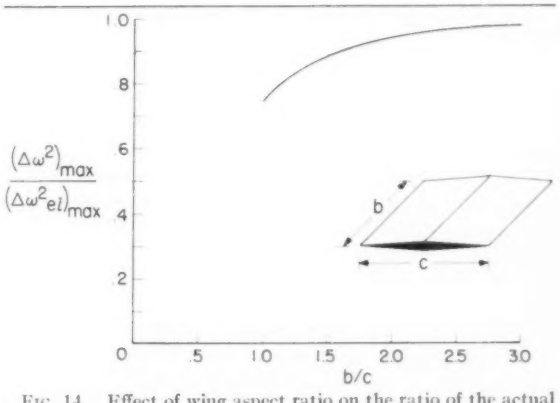

FIG. 14. Effect of wing aspect ratio on the ratio of the actual change in first torsional frequency squared to that based on elementary theory (effect of free end neglected) for solid double-wedge wings considered as free-free beams. $(E/G = 2.54.)$

where M and T_∞ are the free-stream Mach Number and temperature, respectively. In the ensuing calculations, T_∞ is assumed constant throughout the various flight histories to be considered.

Instantaneous Acceleration

Let the Mach Number history of the wing be

$$\begin{aligned} M &= M_0 \quad \text{for} \quad \tau < 0 \\ &= M_f \quad \text{for} \quad \tau \geqq 0 \end{aligned}$$

and let the wing temperature at time $\tau = 0$ be $T_{aw}^{(0)}$, the adiabatic wall temperature corresponding to $M = M_0$. Then, for $\tau > 0$, Eq. (A-1) may be written as

$$[(T_{aw}^{(f)} - T_{aw}^{(0)}) - (T - T_{aw}^{(0)})] = (\rho_m c_m d/2h)(t/d)[\partial(T - T_{aw}^{(0)})/\partial\tau] \qquad \text{(A-3)}$$

where d is the maximum airfoil thickness and $T_{aw}^{(f)}$ corresponds to $M = M_f$. Write

$$\theta = [T - T_{aw}^{(0)}]/[T_{aw}^{(f)} - T_{aw}^{(0)}]$$

$$\lambda = (2/\rho_m c_m d)\int_0^\tau h d\tau$$

Then Eq. (A-3) becomes

$$1 - \theta = (t/d)(\partial\theta/\partial\lambda) \qquad \text{(A-4)}$$

The solution of Eq. (A-4), with the initial condition $\theta = 0$ at $\lambda = 0$, is

$$\theta = 1 - e^{-[\lambda/(t/d)]} \qquad \text{(A-5)}$$

This result for the temperature history is for thin solid wings of arbitrary cross section and with arbitrary variation of h along the chord. Thermal stresses and torsional stiffness changes will be calculated for two special cases.

Solid Double-Wedge Section; h Constant Along the Chord

For the symmetrical double-wedge airfoil shown in Fig. 2(a)

$$\begin{aligned} t/d &= 2x/c \qquad (x \leqq c/2) \\ &= 2[1 - (x/c)] \qquad (x \geqq c/2) \end{aligned}$$

Hence,

$$\left.\begin{aligned} \theta &= 1 - e^{-(\lambda/\beta)} \qquad 0 \leqq \beta \leqq 1 \\ &= 1 - e^{-[\lambda/2(1-(\beta/2))]} \qquad 1 \leqq \beta \leqq 2 \end{aligned}\right\} \qquad \text{(A-6)}$$

where $\beta = 2x/c$. If h is assumed uniform along the chord, then λ is independent of x (or β). For the symmetrical temperature distribution given by Eq. (A-6), the assumption that plane sections remain plane requires that the longitudinal strain distribution ϵ_y be constant over the cross section. Then, by Hooke's law,

$$\epsilon_y = \text{constant} = (\sigma_y/E) + \alpha(T - T_{aw}^{(0)}) \qquad \text{(A-7)}$$

where any effect on ϵ_y of stresses σ_x and σ_z in the plane of the cross section is neglected. Application of the equilibrium condition of zero thrust

$$\int_0^c t\sigma_y dx = 0$$

or

$$(\sigma_y)_{ave} = 0$$

permits the evaluation of the constant in Eq. (A-7), with the following result for the stress:

$$\sigma_y = E\alpha[(T - T_{aw}^{(0)})_{ave} - (T - T_{aw}^{(0)})]$$

or

$$\sigma_y/E\alpha(T_{aw}^{(f)} - T_{aw}^{(0)}) = \theta_{ave} - \theta \qquad \text{(A-8)}$$

where

$$\theta_{ave} = \int_0^1 \beta\theta(\beta)d\beta \Big/ \int_0^1 \beta d\beta = 2\int_0^1 \beta\theta(\beta)d\beta$$

Evaluation of Eq. (A-8) with the use of Eq. (A-6) for θ provides the results for the stresses given by Eqs. (7a) and (7b)—i.e.,

$$\frac{\sigma_y}{E\alpha[T_{aw}^{(f)} - T_{aw}^{(0)}]} = e^{-[\lambda/(2x/c)]} - (1 - \lambda)e^{-\lambda} + \lambda^2 Ei(-\lambda) \qquad 0 \leqq x \leqq c/2$$

$$= e^{\lambda/2[1-(x/c)]} - (1 - \lambda)e^{-\lambda} + \lambda^2 Ei(-\lambda) \qquad c/2 \leqq x \leqq c$$

The effective torsional stiffness given by Eq. (4) is evaluated by approximating the radial distance r from the midchord by $|(c/2) - x|$; then, for the symmetrical stress distribution under consideration,

$$GJ_{eff} = GJ + 2\int_0^{c/2} [(c/2) - x]^2 t\sigma_y dx$$

or, with

$$t = (2x/c)d = \beta d$$

$$GJ_{eff} = GJ + (c^3 d/4)\int_0^1 \beta(1 - \beta)^2\sigma_y d\beta$$

With the original torsional stiffness GJ approximated by

$$GJ = (G/3)\int_0^c t^3 dx$$

or

$$GJ = (1/12)Gcd^3$$

$$GJ_{eff}/GJ = 1 + (3/G)(c/d)^2\int_0^1 \beta(1 - \beta)^2\sigma_y d\beta \qquad \text{(A-9)}$$

Evaluation of the integral in Eq. (A-9), with σ_y given by Eq. (7), provides the result for GJ_{eff}/GJ given by Eq. (8)—i.e.,

$$GJ_{eff}/GJ = 1 - (E\alpha/G) \times \{[T_{aw}^{(f)} - T_{aw}^{(0)}]/(d/c)^2\}\Lambda(\lambda) \qquad \text{(8)}$$

where

$$\Lambda(\lambda) = (1/8)[e^{-\lambda}(4\lambda + 7\lambda^2 + \lambda^3) + Ei(-\lambda)(10\lambda^2 + 8\lambda^3 + \lambda^4)] \qquad \text{(9)}$$

Constant-Thickness Section; h Variable Along the Chord

With the thickness t constant ($= d$) and the variation along the chord of the heat-transfer coefficient governed by the equation

$$h(x) = h(c)/(x/c)^{1/5} \tag{30}$$

the temperature history at each chordwise station x is described by

$$\theta = 1 - e^{-[\lambda/(x/c)^{1/5}]}$$

where the time parameter λ is now defined as

$$\lambda = (2/\rho_m c_m d)\int_0^\tau h(c, \tau)d\tau$$

The temperature is not symmetrical about the midchord and the assumption that plane sections remain plane permits the possibility of rotation as well as translation of the cross section. Hence,

$$\epsilon_y = a_0 + a_1 x$$

where a_0 and a_1 are constants. Setting

$$\epsilon_y = a_0 + a_1 x = (\sigma_y/E) + \alpha[T - T_{aw}{}^0]$$

and imposing the condition of zero thrust

$$t\int_0^c \sigma_y dx = 0$$

and of zero moment

$$t\int_0^c x\sigma_y dx = 0$$

permits the evaluation of the constants a_0 and a_1. With the introduction of the notation $\xi = x/c$, the stresses then turn out to be given by

$$\sigma_y/E\alpha[T_{aw}{}^{(f)} - T_{aw}{}^{(0)}] = 4\int_0^1 \theta d\xi - 6\int_0^1 \xi\theta d\xi - 6\xi\left[\int_0^1 \theta d\xi - 2\int_0^1 \xi\theta d\xi\right] - \theta$$

where $\theta = 1 - e^{-(\lambda/\xi^{1/5})}$

Then,

$$\sigma_y/E\alpha(T_{aw}{}^{(f)} - T_{aw}{}^{(0)}) = [-4A(\lambda) + 6B(\lambda)] + 6\xi[A(\lambda) - 2B(\lambda)] + e^{-(\lambda/\xi^{1/5})} \tag{A-10}$$

where $A(\lambda) = \int_0^1 e^{-(\lambda/\xi^{1/5})}\,d\xi$

$$B(\lambda) = \int_0^1 \xi e^{-(\lambda/\xi^{1/5})}\,d\xi$$

The quantities $A(\lambda)$ and $B(\lambda)$ can be evaluated by means of successive integration by parts to give

$$A(\lambda) = (e^{-\lambda}/24)[24 - 6\lambda + 2\lambda^2 - \lambda^3 + \lambda^4] + (\lambda^5/24)Ei(-\lambda)$$

$$B(\lambda) = (-\lambda^5/30240)A(\lambda) + (e^{-\lambda}z/6048) \times [3024 - 336\lambda + 42\lambda^2 - 6\lambda^2 + \lambda^4]$$

With $GJ = (G/3)ct^3$, and r^2dA taken as $t[x - (c/2)]^2 \times dx$, the expression for the effective stiffness [Eq. (4)] becomes

$$GJ_{eff}/GJ = 1 + \left\{3\int_0^1 [\xi - (1/2)]^2\sigma_y d\xi/G(d/c)^2\right\} \tag{A-11}$$

Substitution of Eq. (A-10) for σ_y, and evaluation of the integral yields

$$GJ_{eff}/GJ = 1 - (E\alpha/G) \times [(T_{aw}{}^{(f)} - T_{aw}{}^{(0)})/(d/c)^2]Q(\lambda) \tag{A-12}$$

where $Q(\lambda) = -(1/2)A(\lambda) + 3B(\lambda) - 3C(\lambda)$

$$C(\lambda) = \int_0^1 \xi^2 e^{-(\lambda/\xi^{1/5})}d\xi = \frac{\lambda^5}{360360}B(\lambda) + \frac{e^{-\lambda}}{72072}[24024 - 1716\lambda + 132\lambda^2 - 11\lambda^3 + \lambda^4]$$

The maximum value of $Q(\lambda)$ occurs at $\lambda = 0.60$ and is equal to 0.00606, from which Eqs. (31) for $(GJ_{eff}/GJ)_{min}$ follow.

The result quoted in the body for $(GJ_{eff}/GJ)_{min}$ of a hollow double-wedge wing of depth d and constant skin thickness follows from the observation that Eq. (A-10) remains valid for the hollow wing if λ is redefined as

$$\frac{1}{\rho_m c_m t_s}\int_0^\tau h(c)d\tau$$

where t_s is the skin thickness. The torsional stiffness of the hollow wing is approximately

$$GJ = (G/2)t_s cd^2$$

so that, with $r^2dA = 2t_s[x - (c/2)]^2dx$ in the formula for effective stiffness,

$$GJ_{eff}/GJ = 1 + \left\{4\int_0^1 [\xi - (1/2)]^2\sigma_y d\xi/G(d/c)^2\right\} \tag{A-13}$$

Comparison with Eq. (A-11) shows that the maximum relative stiffness change for the hollow wing is 4/3 times that of the solid wing, whence Eq. (32) of the text follows.

Finite Acceleration

The solid symmetrical double-wedge wing is now considered to accelerate at constant altitude from Mach Number zero to Mach Number M_f according to the relation

$$M = M_f(\tau/\tau_f)^{5/6} \tag{18}$$

For $\tau > \tau_f$, the Mach Number remains constant at the value of M_f. On the basis of Eq. (15) for the heat-transfer coefficient,

$$h = h_f(M/M_f)^{4/5} \tag{19}$$

where h_f is the value of h corresponding to M_f, and, as before, is constant along the chord. Hence, from Eqs. (18) and (A-14)

$$h = h_f(\tau/\tau_f)^{2/3} \qquad 0 \leqq \tau \leqq \tau_f$$
$$= h_f \qquad \tau \geqq \tau_f$$

The initial wing temperature is assumed equal to the free-stream temperature T_∞.

For the double-wedge wing, with $0 < x < c/2$, the heat balance Eq. (A-1) may be written

$$\partial(T - T_\infty)/\partial\tau = [(2h/\rho_m c_m d)/(2x/c)] \times [(T_{aw} - T_\infty) - (T - T_\infty)] \quad \text{(A-14)}$$

But, from Eq. (A-2),

$$T_{aw} - T_\infty = (T_{aw}^{(f)} - T_\infty)(M/M_f)^2$$

Hence, by Eq. (18),

$$\begin{aligned} T_{aw} - T_\infty &= (T_{aw}^{(f)} - T_\infty)(\tau/\tau_f)^{5/3} && 0 \leqq \tau \leqq \tau_f \\ &= T_{aw}^{(f)} - T_\infty && \tau \geqq \tau_f \end{aligned}$$

Now, let

$$\lambda = 2h_f\tau/\rho_m c_m d$$

$$\lambda_f = 2h_f\tau_f/\rho_m c_m d$$

$$s = \lambda/\lambda_f$$

$$\theta = (T - T_\infty)/[T_{aw}^{(f)} - T_\infty]$$

Then, for $0 \leqq x \leqq c/2$, the formulation in nondimensional terms of the differential equation governing the temperature history becomes

$$\left.\begin{aligned} \partial\theta/\partial s &= [\lambda_f/(2x/c)][s^{7/3} - s^{2/3}\theta] && 0 \leqq s \leqq 1 \\ \partial\theta/\partial s &= [\lambda_f/(2x/c)][1 - \theta] && s \geqq 1 \end{aligned}\right\} \quad \text{(A-15)}$$

The solution of Eq. (A-15) satisfying the initial condition $\theta(0) = 0$ is

$$\left.\begin{aligned} \theta &= s^{5/3} - \frac{5}{3}\frac{\beta}{\lambda_f}(1 - e^{-(3/5)(\lambda_f s^{5/2}/\beta)}) && 0 \leqq s \leqq 1 \\ &= 1 - \frac{5}{3}\frac{\beta}{\lambda_f}[e^{-(\lambda_f/\beta)(s-1)} - e^{-(\lambda_f/\beta)[s-(2/5)]}] && s \geqq 1 \end{aligned}\right\} \quad \text{(A-16)}$$

where $\beta = 2x/c$. The values of θ for $x \geqq c/2$, by symmetry, are given by Eq. (A-16) with β replaced by $2[1 - (\beta/2)]$.

From Eq. (A-8), with $T_{aw}^{(0)}$ replaced by T_∞, the thermal stresses are given by

$$\sigma_y/E\alpha(T_{aw}^{(f)} - T_\infty) = \theta_{ave} - \theta \quad \text{(A-17)}$$

where, as before,

$$\theta_{ave} = 2\int_0^1 \beta\theta(\beta)d\beta$$

Then, from Eq. (A-9),

$$\frac{GJ_{eff}}{GJ} = 1 + \frac{3E\alpha}{G}\frac{(T_{aw}^{(f)} - T_\infty)}{(d/c)^2} \times \int_0^1 \beta(1 - \beta)^2[\theta_{ave} - \theta(\beta)]d\beta \quad \text{(A-18)}$$

The use of Eq. (A-16) for θ in the evaluation of Eq. (A-18) provides the results for GJ_{eff}/GJ given by Eqs. (21), (22a), and (22b).

Appendix B—Free-End Effect on Thermal Stress and Torsional Stiffness

The constant-chord double-wedge wing of finite span b shown in Fig. 13 is considered to be instantaneously accelerated from $M = M_0$ to $M = M_f$, and to undergo, at each spanwise station, the temperature history given by Eq. (6). An approximate calculation will be made of the accompanying thermal stress distribution in the wing, with cognizance of the fact that at the wing tips, $y = \pm(b/2)$, the axial stress σ_y must vanish.

For the sake of simplicity, the analysis is based on the "sheet-stringer" type of approximate elasticity theory common in aircraft structural analysis. That is, the effects of normal chordwise stresses on distortion are entirely ignored; only the axial stress σ_y and the shear stress τ_{xy}, both assumed constant through the thickness, are considered pertinent, and obey the equation of equilibrium

$$t(\partial\sigma_y/\partial y) + (\partial/\partial x)(t\tau_{xy}) = 0 \quad \text{(B-1)}$$

The strain-temperature-stress relations are assumed to be

$$\epsilon_y = (1/E)\sigma_y + \alpha[T - T_{aw}^{(0)}] \quad \text{(B-2)}$$

$$\gamma_{xy} = (1/G)\tau_{xy} \quad \text{(B-3)}$$

The associated complementary energy density is

$$W_c = (\sigma_y^2/2E) + \alpha[T - T_{aw}^{(0)}]\sigma_y + (\tau_{xy}^2/2G) \quad \text{(B-4)}$$

since

$$\epsilon_y = \partial W_c/\partial\sigma_y$$

$$\gamma_{xy} = \partial W_c/\partial\tau_{xy}$$

A solution for the stresses σ_y and τ_{xy} may be found by minimizing the total complementary energy of the wing, with the only stress states admitted to competition in the minimization process those that satisfy the equilibrium Eq. (B-1) and the boundary conditions

$$\sigma_y[x, \pm(b/2)] = 0 \quad \text{(B-5)}$$

By symmetry, attention may be restricted to one quadrant of the wing, say $0 \leqq x \leqq c/2$ and $0 \leqq y \leqq b/2$. With the introduction of the nondimensional variables $\beta = 2x/c$, $\eta = 2y/b$, the equilibrium Eq. (B-1) may be written, for $0 \leqq x \leqq c/2$, with $t = \beta d$, as

$$(c/b)(\partial\sigma_y/\partial\eta) \times (1/\beta)[\partial(\beta\tau_{xy})/\partial\beta] = 0 \quad \text{(B-6)}$$

An approximate solution will be found by assuming that

$$\sigma_y = (\sigma_y)_{el}g(\eta) \quad \text{(B-7)}$$

where $(\sigma_y)_{el}$ is the elementary stress distribution given by Eq. (7), and $g(\eta)$ is a function that describes how the magnitude of this distribution varies along the span. From Eq. (B-5),

$$g(1) = 0 \quad \text{(B-8)}$$

From Eq. (B-7), then,

$$\frac{\sigma_y}{E\alpha[T_{aw}^{(f)} - T_{aw}^{(0)}]} = p(\beta)g(\eta) \quad \text{(B-9)}$$

where

$$p(\beta) = e^{-(\lambda/\beta)} - (1 - \lambda)e^{-\lambda} + \lambda^2 Ei(-\lambda) \quad \text{(B-10)}$$

From the equilibrium Eq. (B-6),

$$\frac{\beta\tau_{xy}}{E\alpha[T_{aw}^{(f)} - T_{aw}^{(0)}]} = -\left(\frac{c}{b}\right) g'(\eta) \int_0^\beta \beta p(\beta)d\beta + e(\eta) \quad \text{(B-11)}$$

But $\tau_{xy} = 0$ at the midchord, $\beta = 1$; also, it must be true that

$$\int_0^1 \beta p(\beta)d\beta = 0$$

by virtue of the fact that $(\sigma_y)_{el}$ produces no net thrust. Hence, $e(\eta) = 0$, and, carrying out the integration in Eq. (B-11) yields

$$\frac{\tau_{xy}}{E\alpha[T_{aw}^{(f)} - T_{aw}^{(0)}]} = \left(\frac{c}{b}\right) q(\beta)g'(\eta) \quad \text{(B-12)}$$

where

$$q(\beta) = -(1/2)\{e^{-(\lambda/\beta)}(\beta - \lambda) - \{\lambda^2 Ei[-(\lambda/\beta)]/\beta\}^1 - \beta\{1 - \lambda]e^{-\lambda} - \lambda^2 Ei(-\lambda)\}\} \quad \text{(B-13)}$$

The complementary energy in one quadrant of the wing is

$$\psi = \int_0^{b/2} \int_0^{c/2} tW_c dxdy = \frac{bcd}{4} \int_0^1 \int_0^1 \beta W_c d\beta d\eta$$

With the use of the temperature relationship

$$\frac{T - T_{aw}^{(0)}}{T_{aw}^{(f)} - T_{aw}^{(0)}} = 1 - e^{-(\lambda/\beta)}$$

and Eq. (6), as well as the expressions (B-9) and (B-12) for the stresses, the energy may be written in nondimensional form as

$$F = \frac{8\psi}{bcdE\alpha^2[T_{aw}^{(f)} - T_{aw}^{(0)}]^2} = \int_0^1 \int_0^1 \left\{[p(\beta)g(\eta)]^2 + 2(1 - e^{-(\lambda/\beta)})p(\beta)g(\eta) + \frac{E}{G}\left(\frac{c}{b}\right)^2 [q(\beta)g'(\eta)]^2\right\} \beta d\beta d\eta$$

After integration with respect to β,

$$F = \int_0^1 \{c_1(\lambda)[\{g(\eta)\}^2 - 2g(\eta)] + (1/4)(E/G)(c/b)^2 c_2(\lambda)[g'(\eta)]^2\} d\eta$$

where

$$c_1(\lambda) = [(1/2) - \lambda]e^{-2\lambda} - 2\lambda^2 Ei(-2\lambda) - (1/2)[(1 - \lambda)e^{-\lambda} - \lambda^2 Ei(-\lambda)]^2 \quad \text{(B-14)}$$

$$c_2(\lambda) = \int_0^1 \{\beta[(\beta - \lambda)e^{-(\lambda/\beta)} - \lambda^2 Ei[-(\lambda/\beta)]/\beta - \beta(1 - \lambda)e^{-\lambda} + \beta\lambda^2 Ei(-\lambda)]^2\} d\beta \quad \text{(B-15)}$$

[Numerical integration appears necessary in the evaluation of $c_2(\lambda)$.]

The unknown function $g(n)$ is now determined from the condition that it minimize F. Application of the calculus of variations yields the Euler equation

$$g'' - k^2 g = -k^2 \quad \text{(B-16)}$$

where

$$k^2 = 4[c_1(\lambda)/c_2(\lambda)](G/E)(b/c)^2 \quad \text{(B-17)}$$

and the natural boundary condition

$$g'(0) = 0 \quad \text{(B-18)}$$

Eq. (B-18) merely states that $\tau_{xy} = 0$ at $\eta = 0$ as it should by symmetry. The solution of (B-16) that satisfies the boundary conditions (B-8) and (B-18) is

$$g(\eta) = 1 - (\cosh k\eta / \cosh k) \quad \text{(B-19)}$$

The factor $g(n)$, which modifies the stresses σ_y according to Eq. (B-9), may also be used directly as a modifying factor on the reduction of torsional stiffness. Consequently, applying the factor $g(n)$ to the second term in Eq. (8) gives

$$GJ_{eff}/GJ = 1 - (E\alpha/G) \times \{[T_{aw}^{(f)} - T_{aw}^{(0)}]/(d/c)^2\}^1 \Lambda(\lambda)g(\eta, \lambda) \quad \text{(B-20)}$$

where g has been shown as a function of λ as well as n to emphasize its dependence on time through the quantity k defined by Eq. (B-17). From Eq. (B-20) it follows that the reduction in stiffness is zero at the wing tip, where $g = 0$; at the midspan, the end effect changes the stiffness reduction from that previously calculated without end effect by the factor $1 - (1/\cosh k)$, and for k large, this factor is very nearly unity. For the limiting case of infinite aspect ratio, Eq. (B-20) reduces to the result found by the elementary theory. A measure of the overall importance of the changes in stiffness will be found by calculating approximately the change in the square of the first torsional frequency of the wing considered as a free-free beam. On the basis of the assumed vibration mode shape

$$\varphi = \varphi_1 \sin(\pi y/b)$$

the frequency ω may be estimated by a simple Rayleigh solution that equates the maximum potential energy

$$(1/2) \int_{-b/2}^{b/2} GJ_{eff}(d\varphi/dy)^2 dy$$

to the maximum kinetic energy

$$(1/2)\omega^2 \int_{-b/2}^{b/2} I_p \varphi^2 dy$$

The result for ω^2 is

$$\omega^2 = \pi^2[GJ/I_p b^2] \times (1 - \{E\alpha[T_{aw}^{(f)} - T_{aw}^{(0)}]/(d/c)^2\}^1 \Lambda(\lambda)p(\lambda)) \quad \text{(B-21)}$$

where

$$p(\lambda) = 1 - [\pi^2/k(\pi^2 + k^2)] \tanh k \quad \text{(B-22)}$$

For the unheated wing, the frequency squared is

$$\omega_0^2 = \pi^2[GJ/I_p b^2]$$

so that $\Delta\omega^2$, the change in ω^2, is

$$\Delta\omega^2 = -\omega_0^2[E\alpha(T_{aw}^{(f)} - T_{aw}^{(0)})/(d/c)^2] \times \Lambda(\lambda)p(\lambda) \quad \text{(B-23)}$$

When the elementary stress distribution is considered to act all along the span, the result for $\Delta\omega^2$ is given by

(*Continued on page 1108*)

The Tip Correction for Wind-Tunnel Tests of Propellers

THEODORE R. GOODMAN*
Cornell Aeronautical Laboratory, Inc.

Introduction

THE DIAMETER of propellers of current interest may be as large as 19 ft., and for VTOL applications even larger. It is clear, therefore, that with present-day facilities it is impossible to test such propellers in a wind tunnel whose cross-sectional area is large compared with the cross-sectional area of the propeller disc. The tunnel walls will be near the propeller tips, and, as a consequence, the local flow near the tips will be altered. Whereas this effect was present for smaller propellers as well, it was of negligible importance, and the bulk of the wind-tunnel wall interference could be computed as a simple blockage correction. With a "large" model in a "small" tunnel, the altered flow at the tips can cause an additional correction of the same order of magnitude as the blockage correction.

The primary reason for testing full-scale models is the difficulty of designing models with dynamic similarity at high speeds. Nevertheless, as a first step in computing the tunnel-tip correction, a low-speed (incompressible) analysis will be performed. Furthermore, it will be assumed that the propeller is lightly loaded and consists of a large number of blades. The per cent error introduced by these approximations is certainly less important in computing interference corrections (which themselves are presumed small) than they would be in computing the aerodynamic characteristics of the propeller itself. Suppose, for instance, that the interference correction is 10 per cent, and the error in the correction is 20 per cent, then the error in the corrected data will be only 2 per cent.

The analysis which follows is accompanied by graphs for the computation of corrections in thrust and efficiency for two-, three-, and four-bladed propellers as a function of advance ratio and ratio of propeller radius to tunnel radius. The theory might possibly be extended to the analysis of shrouded propellers and ducted fans.

The Propeller of Highest Efficiency

In order to make the analysis which follows perfectly clear, a preliminary glimpse will be taken at the propeller of highest efficiency. This analysis is based on blade element theory and assumes a lightly loaded propeller with a large number of blades. The analysis appears in Chapter VII of Glauert's article in Durand[1] and is reproduced here almost verbatim from that source.

Define

B = number of blades
K = local circulation
R = blade radius
ρ = air density
Ω = angular velocity of propeller
ω = angular velocity of the air behind propeller disc
r = radial distance along blade
T = thrust
Q = torque
V = forward speed
u = axial velocity at propeller disc
x = $\Omega r/V$

The expressions for the elements of thrust and torque on a blade element are obtained from cascade theory (see reference 1, Chapter V)

$$dT/dr = BK\rho[\Omega - (\omega/2)]\Omega \tag{1}$$

$$dQ/dr = BK\rho ur \tag{2}$$

also

$$BK = 2\pi\omega r^2 \tag{3}$$

and an alternative expression for the thrust is obtained from a consideration of the axial momentum as

$$dT/dr = 4\pi r\rho u(u - V) \tag{4}$$

By equating the two expressions for the element of thrust, it appears that the axial and rotational velocities are related by the equation

$$u(u - V) = (1/2)[\Omega - (\omega/2)]\omega r^2 \tag{5}$$

and, finally, the loss of energy due to the reaction of the blade elements under consideration is

$$dE/dr = \Omega(dQ/dr) - V(dT/dr) \tag{6}$$

Passing now to the approximation of a lightly loaded propeller, Eq. (5) may be taken to be

$$V(u - V) = (1/2)\Omega\omega r^2 \tag{7}$$

or, by virtue of Eq. (3),

$$u = V + (BK\Omega/4\pi V)$$

and Eq. (1) for the element of thrust becomes approximately

$$dT/dr = BK\rho\Omega r \tag{8}$$

Also, by virtue of Eqs. (3) and (7), Eq. (6) for the loss

Received December 28, 1955.

* Formerly, with the Aerodynamic Research Department. Now, with Allied Research Associates, Inc.

The author is indebted to the students and staff of the Aeronautical Engineering Department of Cornell University who offered a suggestion which led to a simplification of the analysis.

of energy becomes

$$\left.\begin{aligned} dE/dr &= BK\rho[(BK\Omega^2/4\pi V) + (BKV/4\pi\Omega^2)]r \\ &= (B^2K^2\rho\Omega/4\pi)[(\Omega r/V) + (V/\Omega r)] \end{aligned}\right\} \quad (9)$$

Writing

$$\gamma = BK\Omega/2\pi V^2 \quad (10)$$

These last two expressions become

$$\left.\begin{aligned} V(dT/dr) &= (2\pi\rho V^4/\Omega)\gamma x \\ dE/dr &= (2\pi\rho V^4\gamma^2/\Omega)[(1 + x^2)/2x] \end{aligned}\right\} \quad (11)$$

The optimum condition is now derived from the condition that the ratio of the increments of VT and E, due to an arbitrary small increase of γ at any radius, must be independent of the radial coordinate x (see reference 1, Chapter VII). The condition is, therefore,

$$[\gamma(1 + x^2)]/x = Ax$$

where A is a constant, and this condition reduces immediately to

$$BK\Omega/2\pi V^2 = \gamma = [Ax^2/(1 + x^2)] \quad (12)$$

This completes the quotation from Durand with regard to the propeller of highest efficiency. In Chapter VII, Section 4 of his article, Glauert presents an approximate method originally given by Prandtl for accounting for a finite number of blades by considering the radial flow near the blade tips. The author has reworked the Prandtl solution taking into account the presence of a nearby wall. The distribution of thrust near the tip is markedly affected if the tip is close to the wall, and the correction to thrust and efficiency, which it is necessary to apply to raw wind-tunnel data, may, under certain circumstances, be considerable.

The Propeller Tip Near a Wall

The model of the propeller will be taken to be identical to the Prandtl model. The system of vortex sheets is replaced by a series of parallel lines at a regular gap and extending indefinitely to the left, as

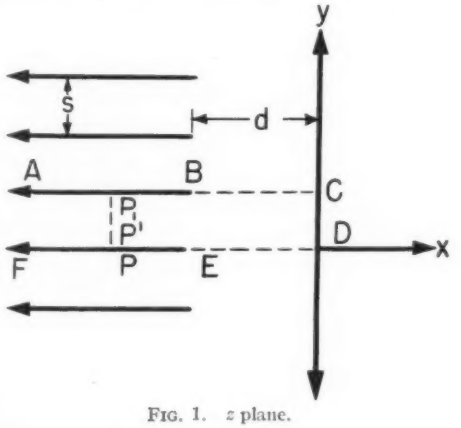

Fig. 1. z plane.

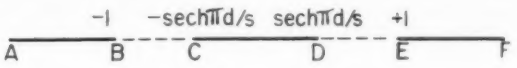

Fig. 2. ζ plane.

in Fig. 1. The gap represents the normal distance at the boundary of the slipstream between the successive vortex sheets, and hence

$$s = (2\pi R/B)\sin\phi_1 = (2\pi R/B)(\lambda/\sqrt{1 + \lambda^2}) \quad (13)$$

where ϕ_1 is the angle of the screw surface at the boundary of the slipstream, defined by the equation

$$\tan\phi_1 = V/\Omega R = \lambda$$

At a distance to the right of the boundary of the slipstream is a vertical wall infinite in extent. The distance d is thereby seen to represent the difference between the tunnel radius and the radius of the propeller disc.

The flow around the edges of the vortex sheets of the slipstream in the presence of a wall may then be estimated approximately from the flow around the edges of the system of semi-infinite parallel lines as shown in Fig. 1, when the system of blades moves downward at right angles to the lines with uniform velocity. From considerations of symmetry, it is seen that the lines BC and ED are equipotential lines, and hence the entire solution, which is periodic in nature, can be synthesized by considering merely the polygon ABCDEF in the $z(= x + iy)$ plane. By using the Schwarz-Christophel theorem, the inside of this polygon can be mapped on to the upper half of the ζ plane. This plane is shown in Fig. 2, and the mapping function is given below.

$$\zeta = (\{\cosh[\pi(d - z)/s]\}/[\cosh(\pi d/s)]) \quad (14)$$

In the ζ plane, the complex velocity admits square root singularities at the points B C D E, and, at the same time, the velocity at infinity must be finite. If w represents the complex potential, then the solution must be of the form

$$dw/d\zeta = (b\zeta + c)/\sqrt{(\zeta^2 - 1)[\mathrm{sech}^2(\pi d/s) - \zeta^2]} \quad (15)$$

where b and c are constants.

Since $dw/dz = (dw/d\zeta)(d\zeta/dz)$ the complex velocity in the z plane may be obtained with the aid of Eq. (14), and also by using Eq. (14) the result may be expressed in terms of z. The resulting equation is

$$\frac{dw}{dz} = \frac{b\cosh[\pi(d - z)/s] + c}{\sqrt{\cosh^2[\pi(d - z)/s] - \cosh^2(\pi d/s)}} \quad (16)$$

As $Re\ z \to \infty$, $dw/dz \to 0$. If this condition is applied, then the result is that $b = 0$, and, Eq. (16) reduces to

$$dw/dz = c/\sqrt{\cosh^2[\pi(d - z)/s] - \cosh^2(\pi d/s)} \quad (17)$$

In order that the solid lines as indicated in Fig. 1 be streamlines, and the dotted lines be equipotential lines, the constant c must be a pure real number. The

circulation fall-off near the tip is obtained by integrating the tangential component of velocity, u, from P to E, and then from E to P′. For this purpose set $z = x$ and integrate Eq. (17) from $-a$ to 0. The factor 2 takes into account both the upper and lower surfaces.

$$F = 2c \int_{-a}^{0} \frac{dx}{\sqrt{\cosh^2[\pi(d-x)/s] - \cosh^2(\pi d/s)}} \tag{18}$$

This integral can be evaluated by the substitution $\cosh[\pi(d-x)/s] = \theta$. The result is

$$F = (2sc/\pi)\cosh(\pi d/s) cd^{-1} \times \left([\cosh(\pi d/s)]/\left\{\cosh\left[\pi(d+a)/s\right]\right\}_0^1\right) \tag{19}$$

where Glaisher's notation for the Jacobian elliptic function has been used, and the modulus is sech $(\pi d/s)$.

When a becomes infinite there is no fall-off, and F must be unity. This condition determines c. Using the identity $cd^{-1}q = K - sn^{-1}q$, where K is the complete elliptic integral of the first kind, and also using the fact that $sn^{-1}(0) = 0$, there is obtained for c

$$c = \pi/2\, sK \cosh(\pi d/s) \tag{20}$$

whence

$$F = (1/K) cd^{-1}\left([\cosh(\pi d/s)]/\left\{\cosh[\pi(d+a)/s]\right\}_0^1\right) \tag{21}$$

In this formula a denotes the distance of the section under consideration from the edge of the lines, and must be replaced by $(R - r)$ in applying the result to the system of vortex sheets of the slipstream. Write, therefore, in accordance with Eq. (13),

$$f = \pi a/s = [B(R-r)\sqrt{1+\lambda^2}]/(2R\lambda) \tag{22}$$

$$g = \pi d/s = (Bd\sqrt{1+\lambda^2})/(2R\lambda) \tag{23}$$

$$F = 1/K\, cd^{-1}\left\{(\cosh g)/[\cosh(f+g)]\right\}_0^1 \tag{24}$$

The quantity F represents a reduction factor which must be applied to the circulation about the blade element at any station due to the proximity of that station to the tip. If this correction is applied, then by virtue of Eq. (12) the optimum distribution of circulation along the blades becomes

$$\gamma = Ax^2F/(1+x^2) \tag{25}$$

where F is given by Eq. (24) and f may be expressed as

$$f = [B(1-\lambda x)\sqrt{1+\lambda^2}]/2\lambda \tag{26}$$

The relationship between F and f is given in Fig. 3 for various values of g. Since the quantity g is directly proportional to d, it is seen that $g = \infty$ corresponds to the case of no wall at all, and the smaller the value of g, the nearer the wall is to the tips. The distributions shown in Fig. 3 indicate that the presence of the wall tends to make the tips less effective as tips, i.e., the circulation at any station is larger when there is a wall present than when there is not. This behavior might have been anticipated; because of the constraint of the wall, less air is able to flow *around* the propeller disc and more air must flow *through* it. The gain in thrust caused by the presence of the wall is purchased at a price, however; since the distribution of thrust is such that the propeller operates at highest efficiency in free air, the presence of the wind-tunnel walls necessitates a loss of propulsive efficiency.

It will be assumed that the thrust distribution on all propellers can be represented by the ideal optimum distribution as given in the preceding section modified in accordance with the tip correction as computed in this section. This assumption can be justified on two grounds. First, any particular propeller will be designed so that the thrust distribution will tend to be optimum as a principle of good design. Hence, the optimum distribution cannot be extraordinarily far from the actual distribution for any particular propeller. Second, it is presumed that the computed correction to measured data as obtained in the wind tunnel is small in order that conditions in the wind tunnel approximate free air conditions. If this is so, a rough approximation to the wind-tunnel wall corrections is sufficient for practical purposes; any small errors in the corrections are of higher order in the data.

The Correction to the Thrust

The ultimate purpose of the present study is to determine quantitatively the difference in behavior of a propeller in a wind tunnel from that of a propeller in free air. The quantity F for the propeller in free air can be obtained by allowing d(or g) to approach infinity. The result of this limiting process coincides with the result given by Glauert. Denote the value of F for $g \to \infty$ as F_∞; then, by virtue of Eq. (24),

$$F_\infty = (2/\pi)\cos^{-1} e^{-f} \tag{27}$$

If reference is made to the first of Eqs. (11), then, with the aid of Eq. (25), the thrust of the propeller in the wind tunnel is given by

$$T = \int_0^{1/\lambda} \frac{2\pi\rho l^4 A x^3 F}{\Omega^2(1+x^2)}\, dx \tag{28}$$

The equation which corresponds to the propeller in free air is identical to this, except that F is replaced by F_∞. The difference between the thrust in the tunnel and the thrust in free air divided by the thrust in free air gives the per cent increase in thrust due to the presence of the walls. Let $t = \lambda x$, and then, if use is made of the identity $cd^{-1}q = K - sn^{-1}q$ the result is

$$\frac{\delta T}{T} = \frac{\displaystyle\int_0^1 \frac{t^3 dt}{\gamma^2 + t^2}\left\{\sin^{-1} e^{-\mu(1-t)} - \frac{\pi}{2K} sn^{-1}\left[\frac{\cosh g}{\cosh(\mu - \mu t + g)}\right]\right\}}{\displaystyle\int_0^1 \frac{t^3 dt}{\lambda^2 + t^2}\cos^{-1} e^{-\mu(1-x)}} \tag{29}$$

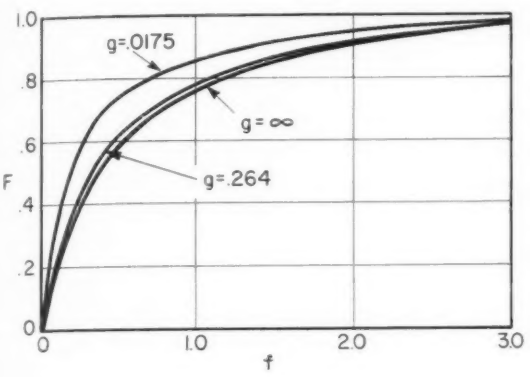

FIG. 3.

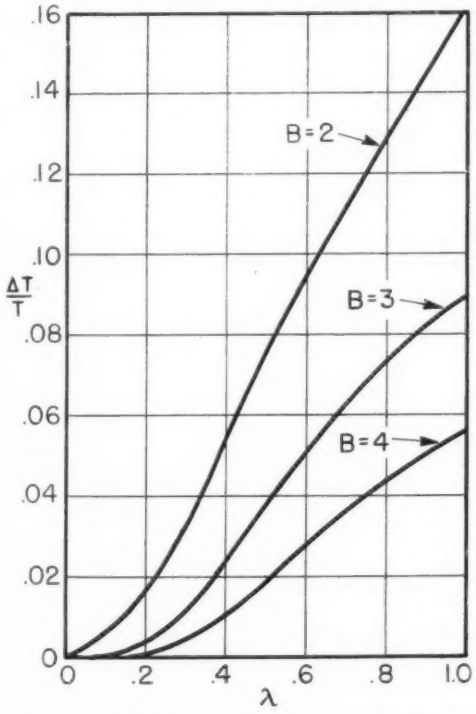

FIG. 5. Per cent of incremental thrust for a B bladed propeller vs. ratio of forward speed to tip speed for a ratio of propeller radius to tunnel radius of 0.93.

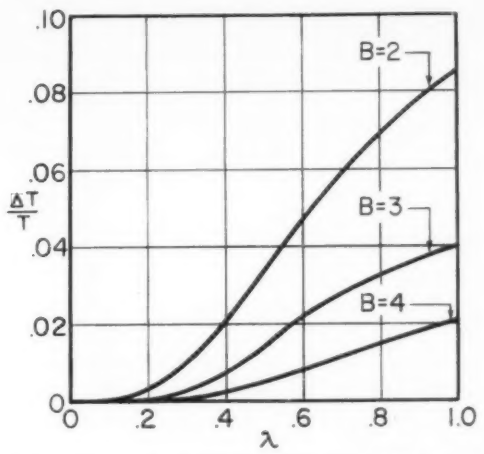

FIG. 4. Per cent of incremental thrust for a B bladed propeller vs. ratio of forward speed to tip speed for a ratio of propeller radius to tunnel radius of 0.87.

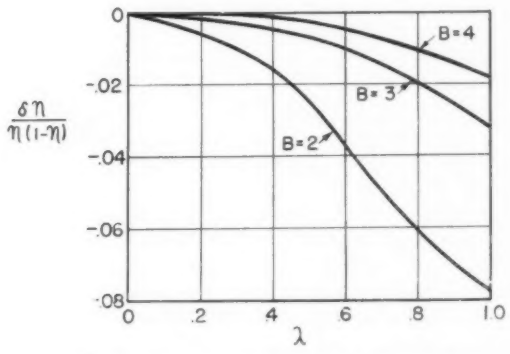

FIG. 6. Efficiency drop for a B bladed propeller vs. ratio of forward speed to tip speed for a ratio of propeller radius to tunnel radius of 0.87.

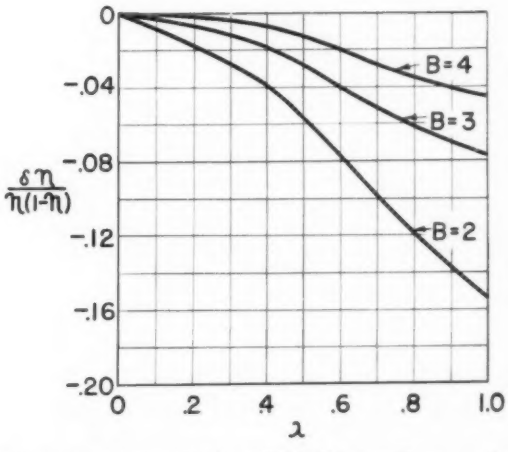

FIG. 7. Efficiency drop for a B bladed propeller vs. ratio of forward speed to tip speed for a ratio of propeller radius to tunnel radius of 0.93.

where $$\mu = B\sqrt{1 + \lambda^2}/2\lambda \tag{30}$$

These integrals have been evaluated by Simpson's rule using the Smithsonian Elliptic Functions Tables.[2] In Figs. 4 and 5 is shown a plot of $\delta T/T$ vs. λ for a 2-, 3-, and 4-bladed propeller, in one case when the ratio of disc radius to tunnel radius is 0.87, and in the other when this ratio is 0.93. It is readily ascertained that the per cent increase in thrust due to the proximity of the tips to the wall may be larger than tolerable experimental error.

The Correction to the Propulsive Efficiency

The propulsive efficiency is defined to be

$$\eta = VT/\Omega Q \tag{31}$$

The energy (see Eq. 6) is

$$E = \Omega Q - VT \tag{32}$$

In view of Eqs. (11), it is convenient to express the efficiency in terms of the thrust and energy

$$\eta = VT/(E + VT) \tag{33}$$

A small change in T or E will cause a corresponding change in η. Denote this change by δ. The operator δ will be interpreted to mean the small difference between a quantity in the tunnel and in free air. By logarithmic differentiation it is found that

$$\begin{aligned}\delta\eta/\eta &= (\delta T/T) - [(\delta E + V\delta T)/(E + VT)] \\ &= (\delta T/T) - (\delta E/E)[E/(E + VT)] - \\ &\qquad (\delta T/T)[VT/(E + VT)] \\ &= (\delta T/T) - (1 - \eta)(\delta E/E) - \eta(\delta T/T) \qquad (34)\end{aligned}$$

or $$\delta\eta/[\eta(1 - \eta)] = (\delta T/T) - (\delta E/E) \tag{35}$$

The quantity $\delta T/T$ has already been determined in Eq. (29). By using the second of Eqs. (11) coupled with Eq. (25), the energy may be found. Once again, the difference is taken between the value in the tunnel, and that in free air, and divided by the value in free air. The result is

$$\delta E/E = \int_0^1 \frac{t^3 dt}{\lambda^2 + t^2}\{F^2 - F_\infty{}^2\} \Big/ \int_0^1 \frac{t^3 dt\, F_\infty{}^2}{\lambda^2 + t^2} \tag{36}$$

where F and F_∞ are given by Eqs. (24) and (27), respectively, and if f is expressed in terms of t the result is $f = B(1 - t)\sqrt{1 + \lambda^2}/2\lambda$. Once again the integrals have been performed by Simpson's rule. The results have been applied to Eq. (35) and graphs for the efficiency correction have been plotted in Figs. 6 and 7.

Conclusions

When a full-scale propeller is tested in a wind tunnel whose cross section is about the same size as the propeller disc, it is necessary, in addition to the blockage correction, to apply a wall-tip correction. The effect of the walls is (1) to increase the thrust, and (2) to decrease the propulsive efficiency.

The two corrections have been obtained quantitatively in an approximate manner for incompressible flow.

References

[1] Durand, W. F. (Ed.), *Aerodynamic Theory*, Glauert, H., "Airplane Propellers," Vol. IV, Division L, Chapter VII, Section 4, pp. 169-360, Julius Springer, Berlin, 1935.

[2] Spenceley, G. W., and Spenceley, R. M., *Smithsonian Elliptic Functions Tables*, Smithsonian Institution, Washington, D.C., November, 1947.

Some Integrated Volume Properties in Linearized Flow...

(*Continued from page 1080*)

[3] Bleviss, Z. O., *Some Integrated Volume Properties in Linearized Flow and Their Connection with Drag Reduction at Supersonic Speeds*, Douglas Aircraft Company, Inc. Report No. SM-19469, February, 1956.

[4] Courant, R., and Hilbert, D., *Methoden der Mathematischen Physik*, Vol. II, Julius Springer, Berlin, 1937.

[5] Graham, E. W., "*Examples of Wave Drag Calculation by Application of Fourier Analysis About a Streamwise Axis*, Douglas Aircraft Company, Inc. Report No. SM-19529, January, 1956.

[6] Graham, M. E., *Application of Drag Reduction Methods to Supersonic Biplanes*, Douglas Aircraft Company, Inc., Report No. SM-19258, September, 1955.

[7] Lomax, Harvard, and Heaslet, Max. A., *Recent Developments in the Theory of Wing-Body Wave Drag*, presented at the 24th Annual Meeting, IAS, New York, January 23–26, 1956, Preprint No. 617.

Normal Forces on Flat Plates in Low-Density Supersonic Flow†

D. M. TELLEP* AND L. TALBOT**

University of California

SUMMARY

Normal forces on rectangular flat plates in supersonic, rarefied flow were measured over the range $200 < Re < 2{,}400$ and $3.7 < M < 4.1$ at angles of attack up to eight degrees. In addition, the effect of aspect ratio on normal forces was determined with a series of models having an aspect ratio range from 1.0 to 2.0.

The results were compared to linearized inviscid theory and indicated normal forces which were 33 per cent to 77 per cent greater than values predicted by theory, the experimental normal forces decreasing with increasing Reynolds Number. The decrease in normal force with decreasing aspect ratios was found to be from 3 to 7 per cent greater in magnitude than predicted by inviscid theory and substantially independent of Reynolds Number over the range tested.

Weak interaction theory was used to derive a simple expression for the normal force and was found to predict the order of magnitude of the increased normal force as well as the trend of the normal force with Reynolds Number.

SYMBOLS

A	= platform area of plate, sq.in.
b	= span of plate, in.
C	= constant in linear viscosity temperature relation defined by Eq. (8)
C_N	= normal force coefficient
C_{N_α}	= normal force curve slope, per radian
C_p	= pressure coefficient
D	= drag force
d_b	= variable in weak interaction theory, defined by Eq. (9)
J	= slip parameter, $(2/3)(\sqrt{Re}/M)$
L	= chord of plate, in.
M	= Mach Number
N	= net normal force, grams
N_g	= gross normal force, grams
N_t	= tare force, grams
p	= static pressure
p_t	= stagnation pressure
q	= dynamic pressure
Re	= Reynolds Number based on chord of plate
$Re/\text{in.}$	= free-stream Reynolds Number based on 1-in. characteristic length
S	= constant in Sutherland formula, see Eq. (8)
t	= thickness of plate, in.
T	= free-stream temperature, °Rankine, or tangential force
T_t	= stagnation temperature, °Rankine
T_w	= temperature of plate surface, °Rankine
V	= velocity, ft./sec.
W	= pan force, grams
x	= distance along plate, measured from leading edge, in.
α	= angle of attack, radians
$\alpha°$	= angle of attack, degrees
γ	= ratio of specific heats
μ	= absolute viscosity, lb.sec./ft.²
ν	= kinematic viscosity, ft.²/sec.
ρ	= density, lb.sec./ft.⁴
σ	= Prandtl Number
$\bar{\chi}$	= interaction parameter, $M^3\sqrt{C}/\sqrt{Vx/\nu}$

Subscripts

∞	= conditions outside the boundary layer far downstream from the leading edge
u	= refers to upper surface of the plate
l	= refers to lower surface of the plate
0	= free-stream conditions

INTRODUCTION

RECENT INTEREST in high-altitude high-speed flight has given rise to considerable interest in the aerodynamic characteristics of bodies of simple geometries in flows where rarefaction and interaction effects exist. Aside from the obvious practical importance of obtaining aerodynamic data in flow regimes where these effects are present, there also exists a need for information and details to aid in understanding the fundamental nature of such flows. Theories accounting for the effects of rarefaction and interaction are largely in the early stages, so that empirical information is required to assess the accuracy of these theories.

The purpose of this report is to describe the experimental procedures and results of a wind-tunnel study of normal forces on rectangular flat plates in supersonic rarefied flows. The scope of this study was limited to a preliminary investigation of the effect of low Reynolds Number on the normal force and normal force aspect ratio correction for plates at small angles of attack.

To provide a physical reference for the results contained herein it may be remarked that the experimental flow conditions duplicate the fluid dynamic (but not thermal) flight condition of a plate with a 10 ft. chord flying at a Mach Number of four at altitudes of 57–68 miles.

Theoretical Considerations

The force normal to an airfoil in an inviscid flow may be readily obtained providing the pressure distribution over the surface is known. With a flat plate the problem is somewhat simplified because of the absence of surface curvature, and in this case an integration of

Received December 6, 1955.

† This work was sponsored by the Office of Naval Research and the Office of Scientific Research. Reproduction in whole or in part is permitted for any purpose of the United States Government.

* Now Research Scientist, Lockheed Missile Systems Division, Van Nuys, Calif. The work reported here is in part taken from the author's M.S. thesis in Mechanical Engineering, University of California, Berkeley.

** Assistant Professor of Mechanical Engineering, Berkeley.

the pressure acting on the surface of the plate yields the normal force directly.

Busemann[1] obtained, for the isentropic approximation to the solution for the pressure coefficient C_p on a plane surface inclined at an angle α to a uniform supersonic stream,

$$C_p = \frac{2\alpha}{\sqrt{M^2 - 1}} + \frac{\{[(\gamma - 1)/2]M^4 - 2M^2 + 2\}}{(M^2 - 1)^2}\alpha^2 + \ldots \quad (1)$$

where $C_p = (p - p_0)/(1/2)\rho_0 V_0^2$.

The normal force, N, acting on a flat plate of chord L and width b, may be written as the integral of the pressure difference between the upper and lower surfaces

$$N = -b\int_0^L (p_u - p_l)\, dx \quad (2)$$

where the subscripts u and l refer to the upper and lower surfaces, respectively, and x is the coordinate distance measured from the leading edge. Using the definitions of the normal force coefficient and the pressure coefficient, Eq. (2) may be written as

$$C_N = -\int_0^L (C_{p_u} - C_{p_l}) d(x/L) \quad (3)$$

where C_N = normal force coefficient = $N/(1/2)\rho_0 V_0^2 bL$

C_{p_u} = pressure coefficient on upper surface

C_{p_l} = pressure coefficient on lower surface

By retaining only terms of order α in Eq. (1) and substituting in Eq. (3), the normal force coefficient for a two-dimensional flat plate in an inviscid supersonic flow may be written as

$$C_N = 4\alpha/\sqrt{M^2 - 1} \quad (4)$$

This is the familiar result of linearized theory.

The above expression for the normal force coefficient may be modified to account for finite plate size. In reference 2 it is shown that the normal force developed in the areas that lie within the tip Mach cones is half that developed over the rest of the plate. Accounting for this fact, the normal force coefficient for a finite aspect ratio plate in an inviscid supersonic flow may be written as

$$C_N = 4\alpha/\sqrt{M^2 - 1}\,[1 - (0.5/AR\sqrt{M^2 - 1})] \quad (5)$$

where AR = aspect ratio = b/L.

Experiments have demonstrated that the inviscid theory is not adequate for hypersonic flow. In high Mach Number low Reynolds Number flows the boundary layer becomes quite thick due to the high stagnation temperature - static temperature ratio and the viscous nature of the flow. The thicker boundary layer results in a zone of interaction between the leading-edge shock wave and the boundary layer. The pressures in this zone are considerably different from those predicted by the inviscid theory. In addition to the zone of shock-wave - boundary-layer interaction, the boundary-layer growth causes significant changes in the pressures in the inviscid external flow field downstream of the shock wave. The influences from the inviscid external flow in turn feed back into the boundary layer to affect its rate of growth, so that the results of these mutual influences are very complex. The problem requires a simultaneous solution of the boundary-layer and external inviscid flow equations.

The boundary-layer - external flow interaction has been studied by Lees and Probstein,[6,16] Maslen,[7] Mack,[8] Kuo,[10] and others. Lees and Probstein were interested primarily in the interaction effect, whereas Maslen and Mack considered the effect of slip on the boundary layer. Maslen showed that with use of the conventional boundary-layer equations and slip boundary conditions there was no first-order *slip* correction to the pressure distribution along the plate, and he obtained a pressure interaction correction (due to the displacement effect of the boundary layer) which agrees with the first-order correction of Lees and Probstein, who used the no-slip boundary conditions. On the other hand, Mack used an Oseen-type slip boundary layer in his analysis, the same as has been used with some success by Schaaf and Sherman[9] to predict the effect of rarefaction on the skin friction. Mack found a correction to the normal force which falls rapidly to zero as the Mach Number becomes large.

The theory which will be used here for comparison with the experimental results is the first order "weak interaction" result of Lees and Probstein, which is meant to apply *far* from the leading edge of a two-dimensional flat plate in supersonic flow. Their result, which is a limiting case derived within the framework of boundary-layer theory for large Mach Numbers, is that the induced pressure due to boundary-layer growth can be expressed to first order as

$$p_w = p_\infty(1 + \gamma d_b \bar{\chi}_\infty) \quad (6)$$

where p_w is the actual pressure at the plate surface and p_∞ is the pressure at the plate surface, as determined from the inviscid flow equations, at a point far downstream where the flow deflection is the same as the surface deflection. The term $\bar{\chi}_\infty$ is the interaction parameter defined by

$$\bar{\chi}_\infty = M_\infty^3\sqrt{C}/\sqrt{V_\infty x/\nu_\infty} \quad (7)$$

where ν_∞ = kinematic viscosity. The subscript ∞ denotes values outside the boundary layer, which are obtained from inviscid flow relations. The term C, which is the constant in the linear viscosity-temperature relationship, is defined by

$$C = \sqrt{\frac{T_w}{T_\infty}}\left(\frac{T_\infty + S}{T_w + S}\right) \quad (8)$$

Here, T_w = surface temperature, °Rankine
T_∞ = temperature of fluid stream outside boundary layer, °Rankine
S = constant in Sutherland viscosity-temperature relations, (216° Rankine)

The term d_b of Eq. 6 is, for Prandtl Number $\sigma = 0.725$,

$$d_b = 0.968\,[(T_w/T_\infty)/M_\infty^2] + 0.145(\gamma - 1) \quad (9)$$

and for the laminar boundary layer on an insulated plate,

$$T_w/T_\infty = 1 + [(\gamma - 1)/2]M_\infty^2\sqrt{\sigma} \quad (10)$$

The normal force is then given by

$$N = p_{\infty_l} b \int_0^L (1 + \gamma d_{b_l}\bar{\chi}_{\infty_l})\,dx - p_{\infty_u} b \int_0^L (1 + \gamma d_{b_u}\bar{\chi}_{\infty_u})\,dx \quad (11)$$

or

$$N = bL(p_{\infty_l} - p_{\infty_u}) + 2\sqrt{L}\,b\gamma \times [(p_{\infty_l} d_{b_l} M_{\infty_l}{}^3/\sqrt{V_{\infty_l}/\nu_{\infty_l} C_l}) - (p_{\infty_u} d_{b_u} M_{\infty_u}{}^3/\sqrt{V_{\infty_u}/\nu_{\infty_u} C_u})] \quad (12)$$

The inviscid conditions on the upper and lower surfaces, indicated by subscripts u and l, are evaluated either from linearized theory or, more exactly, the oblique shock and Prandtl-Meyer relations. For small angles of attack the two methods yield essentially the same results.

Dividing through Eq. 12 by the product of dynamic pressure and the area gives for the normal force coefficient

$$C_N = [(p_{\infty_l} - p_{\infty_u})/q_0] + (2\gamma/q_0)(p_{\infty_l} d_{b_l}\bar{\chi}_{\infty_l} - p_{\infty_u} d_{b_u}\bar{\chi}_{\infty_u}) \quad (13)$$

The first term in the above expression is the result given by inviscid theory. The term in the parenthesis is positive for a positive angle of attack, and thus it is seen that the weak interaction theory predicts an increase in the normal force over inviscid theory. Calculations made on the basis of the above theory showed that the normal force varied linearly with angle of attack for angles up to 5 degrees.

It will be recalled that the weak interaction theory is meant to apply far from the leading edge. Here, however, it has been applied to the entire plate surface, and it is natural to ask what the errors involved in this procedure are. One consequence is easily demonstrated. The zeroth order skin friction, in the absence of interaction effects, varies as $1/\sqrt{x}$. Weak interaction theory predicts a correction to the skin friction which likewise varies as $1/\sqrt{x}$, and, thus, the first order interaction-corrected skin friction is nonintegrable. The weak interaction theory, if carried right up to the leading edge, gives infinite forces in all directions except the normal one, since only the induced pressure is integrable. The same holds true for Maslen's results. The difficulty stems from the nonuniformity in the expansion at $x = 0$. It is possible that the integration of the induced pressure right up to the leading edge, as was done here, does not introduce a serious error because the contribution to the normal force from the region near $x = 0$ is small, but it is clear that the procedure cannot be justified rigorously.

As yet, a satisfactory theory for the region near the leading edge is not available. The Lees-Probstein "strong interaction" theory,[16] which was developed for large values of $M^3/\sqrt{Re}$, does give finite values for all the forces at $x = 0$. However, the strong interaction theory does not join on to the weak interaction theory, and it does not seem warranted to force the two theories into agreement by an arbitrary fairing procedure in order to obtain an induced pressure variation which will be associated with an integrable skin friction.

Previous Experimental Work

The inviscid linearized theory was checked by Ferri.[11] He measured the lift on various airfoils at $Re \approx 10^6$, and found that linearized theory slightly overestimated the lift curve slope.

The first attempts at checking the weak interaction theory were made by Bogdonoff and Hammitt[5] in the Princeton helium hypersonic wind tunnel at Mach Numbers up to 15. Their initial conclusion was that the experimental data on induced pressure correlated well with the parameter $M^3/\sqrt{Re}$, but their measured pressures were considerably greater (by 2–3 times) than those predicted by weak interaction theory. However, it has since been discovered that this discrepancy was due mainly to leading-edge effects. It is now clear that the inviscid pressure field generated at a blunt leading edge in hypersonic flow strongly influences the pressures on the surface of a plate for a considerable distance downstream.[14–19] Kendall[3] measured the induced pressures on plates with sharp leading edges at $M \approx 5.8$ in air, and found that these pressures were linear in $M^3/\sqrt{Re}$, and only 15 per cent higher than predicted by weak interaction theory, up to a value of $M^3/\sqrt{Re} = 3.2$.

The effect of leading-edge bluntness is now the subject of considerable investigation. Bogdonoff and Hammitt[14] have reported more helium data for blunt-edged flat plates which they correlated with the semi-empirical equation for induced pressure

$$\Delta p/p_\infty = 0.016M^3\sqrt{t/x}\{1 + 40\sqrt{C/Re_t}\}$$

where $\Delta p = p_w - p_\infty$ is the pressure increase over the inviscid value, t the leading-edge thickness, and Re_t the Reynolds Number based on leading-edge thickness. The correlation is formed by linear superposition of the weak interaction induced pressure result and an empirical equation for the inviscid leading-edge pressures. At a Mach Number of 12 in helium, which is typical of the data reported in reference 5, the inviscid induced pressure equals the viscous induced pressure at a value $Re_t = 400$; for greater Re_t the inviscid pressure is the larger. The Hammitt-Bogdonoff experiments of reference 5 corresponded to values of $Re_t \approx 1{,}000$ or

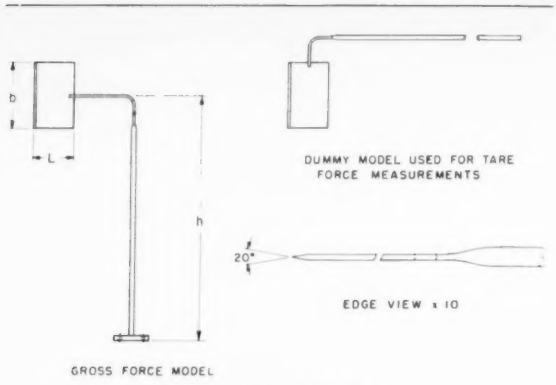

FIG. 1. Model details.

greater; whereas Kendall's data were mainly in the range of Re_t less than 50; it is easy to see why Hammitt and Bogdonoff found induced pressures considerably larger than predicted by weak interaction theory.

For the experiments reported in the present paper, the values of Re_t were of the order of 1–4. Leading-edge thickness effects may therefore be expected to be negligible.

DESCRIPTION OF EXPERIMENT

Test Facilities

The experiments were performed in the No. 4 Low Density Wind Tunnel of the University of California Low Pressures Project at the Engineering Field Station in Richmond, Calif. It is an open jet, continuous flow, non-return type wind tunnel driven by a five-stage steam ejector vacuum pump system.

An axially symmetric nozzle, designated No. 8, was used for the present experiments. The design of this nozzle is presented in reference 12, and calibrations are given in references 12 and 4. The nozzle has an exit diameter of 4.31 in. At flow rates from 5 to 26 lbs. of air per hour, it has a Mach number range from 3.7 to 4.1 and a Reynolds Number range of about 920 to 3,600 per in. The maximum nonuniformity of the Mach Number in the test section is about ±0.5 per cent. The Mach Number variation is due to the change of the nozzle boundary-layer thickness with Reynolds Number and, hence, Mach and Reynolds Number cannot be varied independently in the nozzle. Table 1 presents the characteristics of this nozzle.

Models

The models used in the experiments were designed to serve two distinct purposes. One set was designed to provide normal force data over a range of Reynolds Numbers and are designated Models No. 1 and No. 2. The other set of models, four in number, were designed to provide data on the effect of aspect ratio variations, and will be referred to as "aspect ratio" models; they are designated models A, B, C, and D. The aspect ratio models also provided normal force data over a limited range of Reynolds Numbers. The model dimensions are given in Table 2. It may be remarked that despite the low aspect ratios used, the Mach Number was sufficiently high so that the Mach cones from the opposite wing tips did not intersect upstream of the trailing edge.

TABLE 1
Nozzle Characteristics
No. 8 Nozzle (Mach 4)

Flow Rate, Lb./Hr.	Mach No.	Static Pressure, Microns Hg	T, °R.	Reynolds No. per in.	Isentropic Core Dia., in.
5.2	3.70	50	143	920	1.3
10.3	3.91	74	132	1,620	1.9
14	3.98	90	128	2,130	2.3
20	4.05	112	125	2,800	2.4
26	4.13	134	121	3,560	2.7

TABLE 2
Model Dimensions

Model	Span, in.	Chord, in.	Aspect Ratio
1	0.400	0.253	1.58
2	1.105	0.690	1.60
A	0.501	0.499	1.00
B	0.604	0.490	1.23
C	0.804	0.500	1.61
D	1.002	0.501	2.00

The plates were made of phosphor-bronze stock, 0.009 in. thick, and the leading edges were sharpened symmetrically to a 20° included angle. One surface of each plate was highly polished to provide a reflecting surface for the light beam used with the optical system for measuring the angle of attack. The models were sting-supported at their trailing edges, as shown in Fig. 1, and were positioned in a vertical plane in the air stream. The relation between the model and nozzle is best seen in Fig. 2. Fig. 2 also shows the sting shield used with the models. The vertical portion of the sting passed freely through the sting shield and transmitted forces to the balance housed inside the aluminum enclosure shown.

Balance Apparatus

The balance used for measuring the extremely small forces was a specially designed microbalance developed by R. N. Latz. The balance and its design are described in detail in reference 13, and only its general features will be described here.

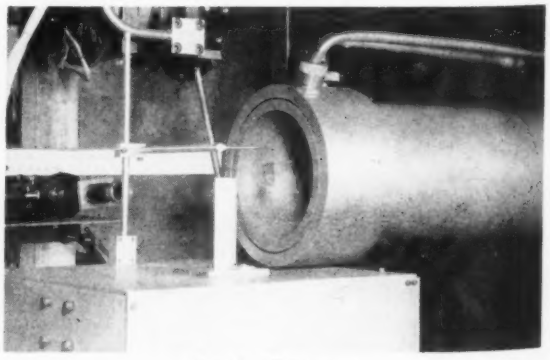

FIG. 2. Test setup.

The balance in its present form is a single component, beam-type balance with all operations remotely controlled. A schematic diagram of the balance is shown in Fig. 3. A flexure pivot is used as the pivot unit of the balance. The pivot consists of two jaws joined by means of two pairs of crossed wires. The upper jaw is fastened rigidly to the base of the balance, and the lower jaw is free to rotate with respect to the upper jaw. A shaft is mounted on the lower jaw and passes through clearance holes in the base and upper jaw to receive the model. A beam is also fastened to the lower pivot jaw to provide means for force and displacement measurements. The flexure pivot has practically a zero restoring moment and eliminates the hysteresis and wear problems associated with knife-edge pivots.

Helical quartz springs are used as the force measuring element on the balance. They are relatively insensitive to temperature variations and can be selected to provide the desired sensitivity and force range.

The spring extension can be measured on a mechanical counter mounted on the balance itself or by a counter outside the tunnel operated through a selsyn linkage system. The least count on the counters corresponds to 0.001 in. spring extension.

The null indicating system of the balance is a linear variable differential transformer (*LVDT*) which provides an electrical output whenever the balance is not at the null, or force-measuring, position. In the schematic sketch the null-indicating elements are indicated on the left arm of the beam. A counterclockwise rotation of the beam causes the core of the *LVDT* to move out of the transformer shell. This displacement of the core induces currents in the circuit of the unit which are indicated on a galvanometer. The sensitivity of the unit enables the balance arm to be positioned easily to within 0.001° of its null position.

The balance, together with its associated equipment, is shown in Fig. 4. The first element of the group (reading from left to right), is the vacuum tube voltmeter which measures the output of the audio oscillator, the second element pictured. The output of the audio oscillator is fed to the *LVDT*. The third element is the microammeter which measures the output of the *LVDT*. The fourth element shown is the control unit for the balance which includes switches to actuate the spring extension mechanism and the angle of attack system, together with mechanical computers to register spring extensions and angles of attack.

Angle of Attack Mechanism

The angle of attack mechanism is also shown in Fig. 4. It consisted of a turntable mounted on a commercial speed reduction unit with a 400:1 reduction ratio. Through gearing and a selsyn linkage system the angular position of the balance could be read remotely (on a mechanical counter) to within 0.09°.

To provide an independent measurement of the angle of attack of the plates, and to check for deflections from a set angle due to aerodynamic forces, an optical system was installed in the tunnel. It may be seen in the background of Fig. 2. It consisted of a light source and a curved galvanometer scale. The beam of light from the source was reflected by the polished surface of the plate to form an image on the galvanometer scale. With this system the angles could be measured to within 0.03°.

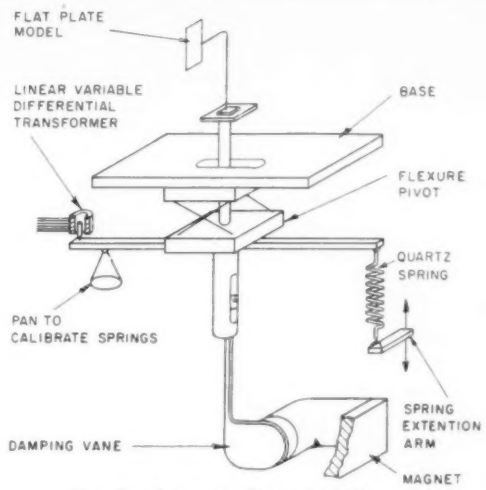

FIG. 3. Schematic diagram of balance.

Description of Tests

Prior to any set of tests on a particular plate it was necessary to establish zero incidence. Since the plates were symmetrical, the condition of zero incidence was established by adjusting the incidence until zero normal force was obtained under flow conditions.

The desired flow conditions were established roughly by a rotameter reading. Finer adjustments were made by reading the stagnation manometer. The supersonic jet was then balanced, to free it from expansion waves or shock waves at the exit plane of the nozzle, by introducing secondary air in the downstream manifold until the nozzle wall tap pressure agreed with the chamber pressure as measured on a pressure ring located around the nozzle exit.

Tare Corrections

Since the plates were supported by stings of finite size, a portion of the normal force measured each time was due to a tare force contribution from the sting. To evaluate the tare force contribution, tare force models which were intended to be identical in every respect to the lift and aspect ratio models were fabricated. These tare force models, however, were provided with a support rod which attached to the tip rather than the trailing edge as in the case of the gross force models. Details of the differences between tare force model support rods and gross force model support rods are presented in Fig. 1.

Fig. 2 shows the arrangements used for the gross force and tare force systems respectively as well as the relationship of the models to the nozzle. It may be

noted that the dummy sting in the tare force installation does not experience the same flow that the real sting does during gross force measurement because the presence of the model support rod in the tare force installation alters the flow to an unknown degree. However, the magnitudes of the gross forces and tare forces are such that a 10 per cent error in the tare force causes only 1 per cent error in the net force, so that small inaccuracies in the tare force measurements may be tolerated.

Experimental Accuracy

On the basis of the variations in the various nozzle calibrations and the accuracy with which pressures could be measured, the maximum possible errors in the Mach Numbers and Reynolds Numbers are estimated to be ±1 per cent and ±3 per cent, respectively. The values of $M^3/\sqrt{Re}$ are accurate to within ±3.4 per cent.

The estimated maximum and minimum errors in the gross normal forces and tare forces for the various models are given in Table 3.

The maximum errors correspond to conditions for which the flow rate and angle of attack are a minimum. Minimum errors correspond to conditions of maximum flow rate and maximum angle.

The normal force coefficients depend on the difference between the gross forces and the tare forces, the free-stream static pressure and the free-stream Mach Number. Accounting for the functional relationship that exists between these variables and the probable error in each of the variables, it is found that the minimum probable error in the normal force coefficients is ±3 per cent. The maximum probable errors for models No. 1 and No. 2 are ±3.6 per cent and ±4.0 per cent, respectively. For model A the maximum error in the normal force coefficient is about ±6 per cent.

A least squares analysis of the normal force coefficient variation with angle of attack leads to the following estimates for the maximum probable errors in the values of the normal force curve slope, assuming that the normal force varies linearly with α:

Model	Max. Error, per cent
1	±1.7
2	±1.9
A	±2.0

Results of Experiments

Examples of the basic data are shown in Fig. 5, which gives the variation of normal force coefficient with angle of attack and Reynolds Number, and in Fig. 6, which shows the tare force measurements on model No. 2.

The major results of the experimental work are presented in Figs. 7, 8, 9, 11, and in Table 4. The comparisons of the experimental results to linearized theory (Fig. 7) use the theory in the form

Table 3

Model	Gross Forces — Max. Error (±), Per cent	Gross Forces — Min. Error (±), Per cent	Tare Forces — Max. Error (±), Per cent	Tare Forces — Min. Error (±), Per cent
1	1.4	0.2	4.0	0.7
2	1.7	0.3	2.1	0.3
A	4.1	0.5	2.5	0.8
B	3.2	0.4	2.5	0.8
C	2.2	0.3	2.5	0.7
D	1.8	0.2	2.5	0.6

$$\left(\frac{dC_N}{d\alpha}\right)_{LT} = (C_{N\alpha})_{LT} = \frac{4\alpha}{\sqrt{M^2-1}}\left(1 - \frac{0.5}{AR\sqrt{M^2-1}}\right)$$

$$= (C_{N\alpha})_{LT_\infty}\left(1 - \frac{0.5}{AR\sqrt{M^2-1}}\right)$$

where the subscripts are defined as

LT = linearized theory for finite aspect ratio
LT_∞ = linearized theory for infinite aspect ratio

The comparison of the experimental results with the weak interaction theory (see Fig. 8) also uses linearized theory as a standard of reference. For this comparison the ratios

$$(C_{N\alpha})_{EXPT}/(C_{N\alpha})_{LT} \quad \text{and} \quad (C_{N\alpha})_{WI_\infty}/(C_{N\alpha})_{LT_\infty}$$

were used. In the second ratio the subscript WI_∞ denotes the two-dimensional or infinite aspect ratio case according to weak interaction theory.

The values of C_{N_α} for all the models and flow conditions are tabulated in Table 4.

Discussion of Results

Normal Force Data

The most interesting result of the experiments was the fact that the experimentally determined normal

Table 4
Reduced Data

Model	Re	M	$M^3/\sqrt{Re}$	$C_{N\alpha}$
1	228	3.69	3.32	0.0317
	380	3.88	2.30	0.0280
	531	3.98	2.73	0.0261
	683	4.04	2.53	0.0249
	860	4.11	2.37	0.0243
2	633	3.70	2.01	0.0260
	1,100	3.90	1.79	0.0242
	1,403	3.97	1.66	0.0232
	1,900	4.05	1.52	0.0219
	2,412	4.12	1.43	0.0214
A	447	3.69	2.37	0.0276
	803	3.90	2.09	0.0244
	1,390	4.05	1.78	0.0224
	1,751	4.12	1.67	0.0222
B	471	3.72	2.36	0.0305
	784	3.90	2.12	0.0257
	1,355	4.05	1.80	0.0242
	1,705	4.12	1.70	0.0238
C	444	3.67	2.35	0.0302
	797	3.90	2.10	0.0267
	1,336	4.04	1.80	0.0249
	1,747	4.12	1.67	0.0238
D	478	3.71	2.34	0.0309
	797	3.90	2.10	0.0271
	1,389	4.05	1.78	0.0252
	1,765	4.12	1.67	0.0237

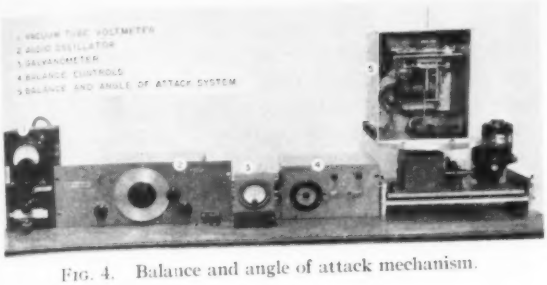

FIG. 4. Balance and angle of attack mechanism.

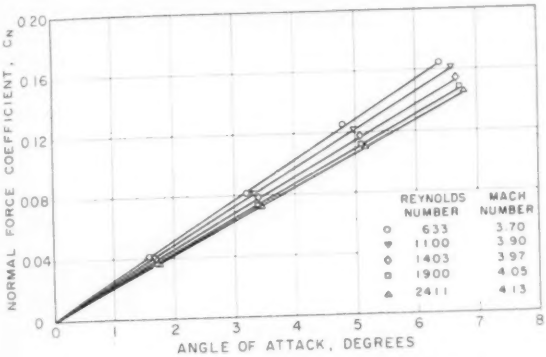

FIG. 5. Normal force coefficient vs. angle of attack.

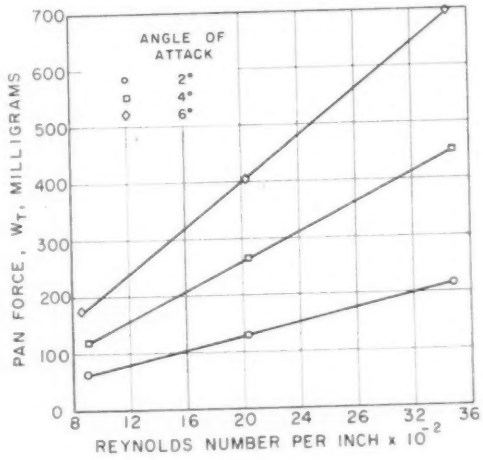

FIG. 6. Tare forces, model No. 2.

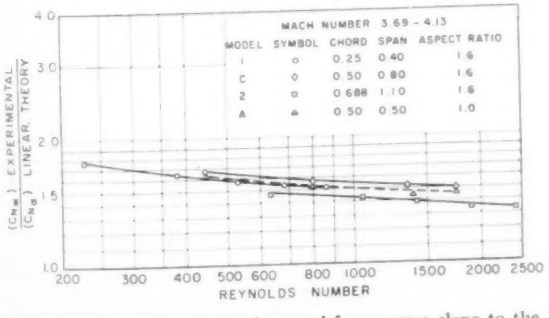

FIG. 7. Ratio of experimental normal force curve slope to theoretical normal force curve slope vs. Reynolds Number.

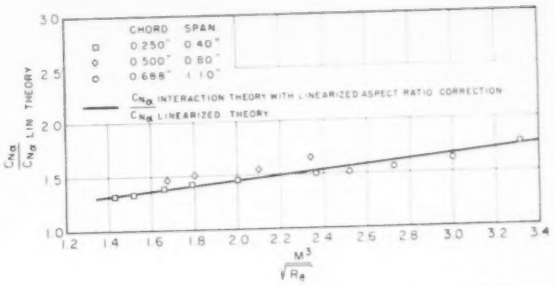

FIG. 8. Comparison between experiment and Lees-Probstein weak interaction theory.

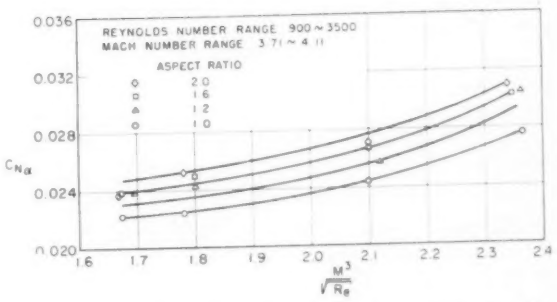

FIG. 9. Effect of aspect ratio on normal force curve slope for various values of the hypersonic interaction parameter.

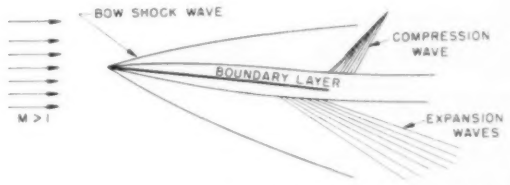

FIG. 10. Sketch of the elements in the flow field around a flat plate at a small angle in a supersonic stream.

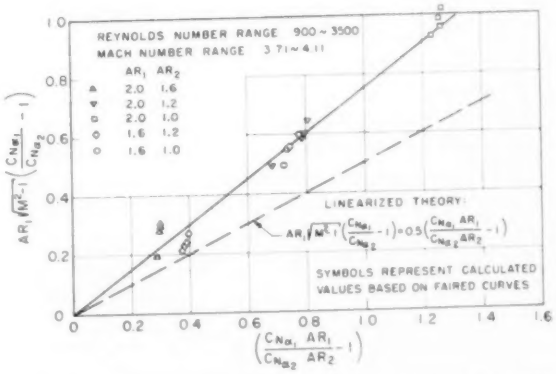

FIG. 11. Comparison of experimental and theoretical aspect ratio effect.

force curve slopes were substantially greater than predicted by linearized theory. Fig. 7 shows the variation with Reynolds Number of the ratio between experimental and theoretical normal force curve slopes, $(C_{N\alpha})_{EXPT}/(C_{N\alpha})_{LT}$.

The ratio between experimental and theoretical normal force curve slopes decreases from 1.77 at a Reynolds Number of 228 to about 1.33 at a Reynolds Number of 2,412. It should be noted that on Fig. 7 the Mach Numbers for models with different chord lengths are somewhat different for a given Reynolds Number. However, the greatest difference between the Mach Numbers at a given Reynolds Number is only about 2 per cent.

Solid curves are plotted in Fig. 7 for the data of models No. 1, No. 2, and C, which had aspect ratios of 1.6. A single dashed curve is also plotted for the data of model A, which had an aspect ratio of 1.0. The fact that the data for models A and C do not coincide shows that the inviscid aspect ratio correction does not hold accurately for the viscous flow situation, since if it did the ratio $(C_{N\alpha})_{EXPT}/(C_{N\alpha})_{LT}$ would correlate data for models with different aspect ratios. This problem is discussed in greater detail in the section on Aspect Ratio Data.

It appears from Fig. 7 that there was an influence present which affected the relative order of the data. The relations that the curves for models No. 1, No. 2, and C bear to each other are not consistent with changes in model dimensions; in fact, one might expect the individual curves for models with the same aspect ratio to coincide in their overlapping portions and form a single continuous curve. The relative order of the curves is difficult to explain in terms of errors since the data for any one model are consistent among themselves and were reproducible during the course of the experiments. The deviations of the curves are also greater than can be accounted for by experimental accuracy and the slight Mach Number differences.

One possible explanation for the deviation between the curves is that the sting effects varied with each model. The model-sting combinations were not geometrically similar and, for model No. 1 particularly, it is possible that the sting had an appreciable influence upon the forces. Further experiments are needed to settle this question.

The linearity of the C_N vs. α curves of Fig. 5 indicates that flow separation did not occur near the trailing edge. The pressure ratio $\Delta p/p$ necessary to separate a laminar boundary layer at Reynolds Numbers of the order of 5×10^5 is about 0.20. The pressure ratio $\Delta p/p$ varies as $(Re_x)^{-1/4}$, so at $Re_x = 2{,}500$, $\Delta p/p \approx 0.75$. This pressure ratio corresponds to an oblique shock with flow turning angle of between 10 and 11 degrees, which is greater than the maximum angle of attack used in the experiments. The assumption that flow separation did not occur thus appears justified.

Fig. 8 presents a comparison between the experimental results and weak interaction theory. The agreement is seen to be quite good. It will be recalled that Kendall found induced pressures which were some 15 per cent higher than weak interaction theory, whereas here the theory is, for one model, higher than the data. One factor which may have influenced the normal force measurements is a "trailing-edge effect." Expansion waves are formed at the lower boundary-layer seam, and compression waves at the upper boundary-layer seam, as shown in Fig. 10. The compression waves feed high pressures upstream in the subsonic portion of the boundary layer on the upper surface, and the expansion waves will propagate low pressures upstream on the lower surface. Both effects will tend to decrease the normal force experienced by the plate, with the effect diminishing with increasing Reynolds Number. It seems quite likely that this trailing edge effect might account for part of the differences between the present results and Kendall's data. A decrease in normal force of the order of 10 per cent due to trailing edge influences would be sufficient, since, as will be seen in the discussion which follows, the aspect ratio correction derived from linearized theory which was used to adjust the weak interaction results for finite aspect ratio is in fact too small. The use of the experimentally deduced aspect ratio correction would move the theoretical curves down, on the average, about 5 per cent.

The experimental data can also be compared with the theoretical calculations of Mack. He derived expressions for the normal and tangential force and the moment coefficients for a flat plate at an angle of attack, using an Oseen slip boundary-layer correction. This boundary layer presents a sharp leading edge to the flow; the displacement thickness slope $d\delta^*/dx$ at $x = 0$ in the Oseen slip theory has the value $2/3\ M$. Mack found for the normal force coefficient the result

$$C_N = (4\alpha/\sqrt{M^2 - 1}) \times [1 + (2/3M\sqrt{M^2 - 1}) \exp(J^2) \operatorname{erfc}(J)] \quad (14)$$

where $J = (2/3)(\sqrt{Re}/M)$. At an undisturbed stream Mach Number $M = 4$ and plate Reynolds Number $Re = 400$, which are representative of the present experimental data, Mack's correction to C_N is of the order of magnitude of 1 per cent. It seems reasonable to conclude that in the present tests the effect of slip was negligible, and that the boundary layer presented an essentially blunt leading edge to the flow.

Aspect Ratio Data

The Mach Number and aspect ratio range used in the experiment are such that the maximum difference in normal force coefficients between two models is expected to be about 7 per cent, on the basis of the inviscid correction, for models having aspect ratios of 1.0 and 2.0 at a Mach Number of about 3.70.

Fig. 9 presents a plot of the normal force curve slope for various aspect ratio plates plotted against the hypersonic similarity parameter, $M^2/\sqrt{Re}$. The data for models with aspect ratios of 1.0 and 1.6 enable

reasonably good curves to be drawn. The data for models with aspect ratios of 1.2 and 2.0 appear to be somewhat less reliable and curves were faired through these data so that they were consistent with the curves based on the better data.

The curves show that increasing the aspect ratio has the effect of increasing the normal force curve slope. The difference in the normal force curve slopes for models with aspect ratios of 1.0 and 2.0 at $M = 3.70$, ($M^3/\sqrt{Re} = 2.30$) is approximately 13 per cent, whereas the theoretical difference predicted for these conditions is approximately 7 per cent, as mentioned above. Thus it is seen that the inviscid aspect ratio correction term underestimates the effect of aspect ratio when applied to a viscous flow situation. This is as expected, since the theory confines the influence of the end of the plate to a region lying within the Mach cone originating from the leading-edge wing tip. The flow outside these affected areas is everywhere supersonic according to the theory, so that it remains uninfluenced by disturbances elsewhere in the flow field. In the real case, however, the thick boundary layer over the entire surface of the plate provides a subsonic layer of flow through which disturbances and pressure fields may be transmitted. Because of this, portions of the plate surface well within the region between the tip Mach cones may be affected by pressures at the plate ends, and the aspect ratio influence will be greater than predicted by inviscid theory.

To enable a better comparison of the experimental and theoretical aspect ratio effects, it is convenient to generalize the aspect ratio correction (Eq. 5) by introducing a function of Re,

$$C_N = (4\alpha/\sqrt{M^2-1})\{1 - [f(Re)/\mathrm{R}\sqrt{M^2-1}]\} \tag{15}$$

where $f(Re)$ has the value 0.5 for $Re \to \infty$. Now forming the ratio, $C_{N_{\alpha_1}}/C_{N_{\alpha_2}}$, where the subscripts 1 and 2 denote particular aspect ratios, we have

$$\frac{C_{N_{\alpha_1}}}{C_{N_{\alpha_2}}} = \frac{1 - [f(Re)/\mathrm{R}_1\sqrt{M^2-1}]}{1 - [f(Re)/\mathrm{R}_2\sqrt{M^2-1}]} \tag{16}$$

By rearrangement of the terms there results

$$\mathrm{R}_1\sqrt{M^2-1}[(C_{N_{\alpha_1}}/C_{N_{\alpha_2}}) - 1] = f(Re)[(C_{N_{\alpha_1}}\mathrm{R}_1/C_{N_{\alpha_2}}\mathrm{R}_2) - 1] \tag{17}$$

Now assume that for the range of Reynolds Numbers involved

$$f(Re) = \text{constant} = K$$

This is almost a necessity at this point, since the scatter in the data make it impossible to obtain a check on a more complex, but more accurate expression for $f(Re)$.

From the faired data of Fig. 9 the terms of Eq. (17) were calculated and plotted. The results are shown on Fig. 11, which also shows the theory. For any given pair of aspect ratios, four points are plotted. Each point represents a particular Mach Number and Reynolds Number, but the Reynolds Number variation far exceeds the Mach Number variation. The Mach Number varies about ±5 per cent around mean value, whereas the Reynolds Number increases fourfold as noted on Fig. 11.

A straight line with a slope $K = 0.75$ was drawn through the calculated data. The points for any given pair of aspect ratios scatter about this line showing that in fact a Reynolds Number dependency does exist. However, for these experiments with their limited range of variables, $f(Re) = 0.75$ (approximately) and the aspect ratio correction which multiplies the infinite aspect ratio normal force coefficient to give the normal force coefficient for a finite aspect ratio plate, may be written

$$1 - (0.75/\mathrm{R}\sqrt{M^2-1})$$

The above correction should not be taken as applying accurately for Mach Numbers, aspect ratios, and Reynolds numbers outside the range of these tests.

It is expected that when more aspect ratio data become available, a better aspect ratio correction will have to be devised which will include the effect of Mach Number in the correlation. Possibly, the effective width of the tip Mach cones at the trailing edge could be related to the boundary-layer displacement thickness δ_L^* there. Instead of the inviscid value $L/\sqrt{M^2-1}$, one could write

$$\frac{L}{\sqrt{M^2-1}} + k\delta_L^* = L\left\{\frac{1}{\sqrt{M^2-1}} + \frac{1.73k(1+0.27M^2)}{\sqrt{Re_L}}\right\}$$

where k is an unknown "influence factor." With this formulation, we obtain

$$C_{N_\alpha} = \frac{4}{\sqrt{M^2-1}}\left\{1 - \frac{1}{\mathrm{R}\sqrt{M^2-1}} \times \left[\frac{1}{2} + \frac{1.73k(1+0.27M^2)\sqrt{M^2-1}}{2\sqrt{Re_L}}\right]\right\} \tag{18}$$

The quantity in the brackets replaces the quantity $f(Re)$ introduced in Eq. (15). The limited range of the variables and the scatter in the data make it difficult to reach any conclusions concerning the value of k, in particular, whether it is actually a constant, and therefore Eq. (18) does not offer any advantage over the method used here for determining the aspect ratio correction

Conclusions

Measured normal forces on rectangular flat plates over a Reynolds Number range of 200–2,400 and a Mach Number range of 3.7–4.1 were from 33 to 77 per cent greater than predicted by linearized theory. The experimental normal forces decreased with increasing Reynolds Numbers. First-order weak interaction theory gave a good approximation for both the magni-

tude of the increase in normal force and the trend of the normal force with Reynolds Numbers. No slip effects were discernible.

The decrease in normal force due to a decrease in aspect ratio was found to be from 3 to 7 per cent greater than that predicted by linearized theory. Over the Reynolds Number range of 450–1,700 and Mach Number range of 3.7–4.1 the aspect ratio correction which multiplies the infinite aspect ratio normal force coefficient to give the normal force coefficient for a finite aspect ratio plate can be approximated as $[1 - (0.75/AR\sqrt{M^2 - 1})]$.

References

[1] Busemann, A., *Aerodynamic Lift at Supersonic Speeds*, Luftfahrtforschung, Vol. 12, 1953.

[2] Lighthill, M. J., *The Supersonic Theory of Wings of Finite Span*, British A.R.C., R & M No. 2001, 1944.

[3] Kendall, J. M., Jr., *Experimental Investigation of the Leading Edge Shock Wave - Boundary Layer Interaction at Hypersonic Speeds*, I.A.S. Preprint No. 611, January, 1956.

[4] Talbot, L., *Viscosity Corrections to Cone Probes in Rarefied Supersonic Flow at a Nominal Mach Number of 4*, NACA TN 3219, November, 1954.

[5] Bogdonoff, S. M., and Hammitt, A. G., *A Study of the Flow About Simple Bodies at Mach Numbers from 11 to 15*, Princeton University Aeronautical Engineering Department Report No. 277, September, 1954.

[6] Lees, L., and Probstein, R., *Hypersonic Viscous Flow Over a Flat Plate*, Princeton University Aeronautical Engineering Department Report No. 195, April 20, 1952.

[7] Maslen, S., *Second Approximation to Laminar Compressible Boundary Layer on a Flat Plate in Slip Flow*, NACA TN 2818, November, 1952.

[8] Mack S. F., *Theoretical Aerodynamic Properties for an Inclined Flat Plate in Slip Flow*, University of California Engineering Research Report HE-150-98, March, 1952.

[9] Schaaf, S. A., and Sherman, F. S., *Skin Friction in Slip Flow*, Journal of the Aeronautical Sciences, Vol. 21, No. 2, pp. 85–90, February, 1954.

[10] Kuo, Y. H., *Viscous Flow Along Flat Plate Moving at High Supersonic Speeds*, Journal of the Aeronautical Sciences, Vol. 23, No. 2, February, 1956.

[11] Ferri, A., *Experimental Results with Airfoils Tested in the High Speed Tunnel at Guidonia*, NACA TM 946, 1940.

[12] Owen, J. M., and Sherman, F. S., *Design and Testing of a Mach 4 Axially Symmetric Nozzle for Rarefied Gas Flows*, University of California Engineering Report HE-150-104, July 23, 1952.

[13] Latz, R., *Design of a Two Component Balance for Low Density Flows*, University of California Engineering Report HE-150-124, Aug. 10, 1954.

[14] Hammitt, A. G., and Bogdonoff, S. M., *Hypersonic Studies of the Leading Edge Effect on the Flow Over a Flat Plate*, Paper presented at 25th Meeting of American Rocket Society, November 14–18, 1955, Chicago, Ill.

[15] Bertram, M. H., *Viscous and Leading Edge Thickness Effects on the Pressures on the Surface of a Flat Plate in Hypersonic Flows*, Readers' Forum, Journal of the Aeronautical Sciences, Vol. 21, No. 5, pp. 430–31, June, 1954.

[16] Lees, L., *Hypersonic Flow*, IAS Preprint No. 554, June, 1955.

[17] Hammitt, A. G., Vas, I. E., and Bogdonoff, S. M., *Leading Edge Effects on the Flow Over a Flat Plate at Hypersonic Speeds*, Princeton University Aero. Engineering Dept. Report 326, September, 1955. (Also WADC TN 55-537.)

[18] Lees, L., *Inviscid Hypersonic Flow Over Blunt-Nosed Slender Bodies*, GALCIT Hypersonic Research Project Memorandum No. 31, February 1, 1956.

[19] Bogdonoff, S. M., and Hammitt, A. G., *Fluid Dynamic Effects from M = 11 to 15*, Journal of the Aeronautical Sciences, Vol. 23, No. 2, pp. 108–116, February, 1956.

Influence of Aerodynamic Heating...

(*Continued from page 1093*)

Eq. (B-23) with the factor $p = 1$. Then, the ratio of the actual maximum change in frequency squared to that based on elementary theory is

$$(\Delta\omega^2)_{max}/(\Delta\omega^2_{el})_{max} = [\Lambda(\lambda)p(\lambda)]_{max}/[\Lambda(\lambda)]_{max} \quad \text{(B-24)}$$

where, by way of review,

$$p(\lambda) = 1 - [\pi^2/k(\pi^2 + k^2)] \tanh k$$

$$k^2 = 4[c_1(\lambda)/c_2(\lambda)](G/E)(b/c)^2$$

and $c_1(\lambda)$ and $c_2(\lambda)$ are given by Eqs. (B-14) and (B-15). The function $\Lambda(\lambda)$ is defined by Eq. (9) and $[\Lambda(\lambda)]_{max} = 0.0456$. With $E/G = 2.54$, values of $[\Lambda(\lambda)p(\lambda)]_{max}$ have been calculated for various values of aspect ratio (b/c), and the final results for $(\Delta\omega^2)_{max}/(\Delta\omega^2_{el})_{max}$ are shown in Fig. 14 as a function of aspect ratio.

References

[1] Wagner, H., *Torsion and Buckling of Open Sections*, NACA TM 807, October, 1936.

[2] Goodier, J. N., *Elastic Torsion in the Presence of Initial Axial Stress*, Journal of Applied Mechanics, Volume 17, No. 4, p. 383, 1950.

[3] Jahnke, E., and Emde, F., *Tables of Functions*, 4th Ed., pp. 1–8, Dover Publications, Inc., New York, 1945.

[4] Kaye, J., *The Transient Temperature Distribution in a Wing Flying at Supersonic Speeds*, Journal of the Aeronautical Sciences, Vol. 17, No. 12, p. 787, December, 1950.

[5] Ecker, E. R. G., *Survey on Heat Transfer at High Speeds*, Wright Air Development Center, Technical Report 54-70, April, 1954.

[6] Chu, Chen, *The Effect of Initial Twist on the Torsional Rigidity of Thin Prismatical Bars and Tubular Members*, Proceedings of the First U.S. National Congress of Applied Mechanics, pp. 265–269, June, 1951.

[7] Vosteen, Louis F., and Fuller, Kenneth E., *Behavior of a Cantilever Plate Under Rapid Heating Conditions*, NACA RM L55E20c, July, 1955.

Piston Theory—A New Aerodynamic Tool for the Aeroelastician†

HOLT ASHLEY* AND GARABED ZARTARIAN**

Massachusetts Institute of Technology

SUMMARY

Representative applications are described which illustrate the extent to which simplifications in the solutions of high-speed unsteady aeroelastic problems can be achieved through the use of certain aerodynamic techniques known collectively as "piston theory." Based on a physical model originally proposed by Hayes and Lighthill, piston theory for airfoils and finite wings has been systematically developed by Landahl, utilizing expansions in powers of the thickness ratio δ and the inverse of the flight Mach Number M. When contributions of orders δ/M^3 and δ^2/M^2 are negligible, the theory predicts a point-function relationship between the local pressure on the surface of a wing and the normal component of fluid velocity produced by the wing's motion. The computation of generalized forces in aeroelastic equations, such as the flutter determinant, is then always reduced to elementary integrations of the assumed modes of motion.

Essentially closed-form solutions are given for the bending-torsion and control-surface flutter properties of typical section airfoils at high Mach Numbers. These agree well with results of more exact theories wherever comparisons can be fairly made. Moreover, they demonstrate the increasingly important influence of thickness and profile shape as M grows larger, a discovery that would be almost impossible using other available aerodynamic tools. The complexity of more practical flutter analyses—e.g., on three-dimensional wings and panels—is shown to be substantially reduced by piston theory. An iterative procedure is outlined, by which improved flutter eigenvalues can be found through the successive introduction of higher-order terms in δ and $1/M$.

Other applications to unsteady supersonic problems are reviewed, including gust response and rapid maneuvers of elastic aircraft. Steady-state aeroelastic calculations are also discussed, but for them piston theory amounts only to a slight modification of Ackeret's formulas.

Suggestions are made regarding future research based on the new aerodynamic method, with particular emphasis on areas where computational labor can be reduced with a minimum loss of precision. It is pointed out that a Mach Number zone exists where thermal effects are appreciable but nonlinear viscous interactions may be neglected, and that in this zone piston theory is the logical way of estimating air loads when analyzing aerodynamic-thermoelastic interaction problems.

PRINCIPAL SYMBOLS

a = speed of sound in air

b = reference semichord of wing or half-length of panel

GJ = torsional stiffness of uniform cantilever wing

k = $(\omega b/U)$ reduced frequency of simple harmonic motion

l = span of uniform cantilever wing

$L_1, \ldots, L_{6_0}$

$M_1, \ldots, M_6$ = dimensionless coefficients defining lift and moment on an oscillating airfoil

m = mass of panel or two-dimensional airfoil per unit distance perpendicular to the flow

M = (U/a_∞) free-stream Mach Number

M_α = pitching moment per unit span, about the axis $X = 2bx_0$, on a two-dimensional airfoil (positive nose up)

M_β = hinge moment per unit span on a two-dimensional flap (positive nose up)

p = ambient pressure in air

P = lift per unit span on a two-dimensional airfoil (positive downward)

t = physical time

U = free-stream velocity or flight speed

w = (δw_0) component of fluid velocity in z-direction or normal to wing surface

X, Y, Z = $(2bx, 2by, 2bz)$ rectangular Cartesian coordinates, with X directed parallel to the free stream

Z_u = Z-coordinate of upper wing surface, divided by δ

γ = specific-heat ratio of air ($\gamma \cong 1.4$)

δ = denotes the larger of the wing thickness ratio or the ratio of amplitude of unsteady motion to wing chord

ρ = ambient density of air

ω = circular frequency of simple harmonic motion

Properties of a Two-Dimensional "Typical Section" of a Wing:‡

A_w, A_F = cross-sectional areas of airfoil and flap, respectively

h = bending displacement of axis of rotation (positive downward)

I_α = mass moment of inertia about axis of rotation per unit span

M_w, M_F = static moments of areas of airfoil and flap, respectively, about their leading edges

r_α = $(\sqrt{I_\alpha/mb^2})$ dimensionless radius of gyration about axis of rotation

r_β = dimensionless flap radius of gyration about hingeline

x_0 = dimensionless distance from leading edge to axis of rotation

x_1 = dimensionless distance from leading edge to flap hingeline

x_α = dimensionless static unbalance about axis of rotation (positive for c.g. aft)

x_β = dimensionless static unbalance of flap about its hingeline (positive for c.g. aft)

α = torsional displacement about axis of rotation (positive nose up)

β = angular displacement of flap relative to airfoil chordline (positive nose up)

μ = $(m/4\rho_\infty b^2)$ relative density of typical section

$\tau(x)$ = dimensionless thickness distribution

Presented at the Aeroelasticity Session, Twenty-Fourth Annual Meeting, IAS, New York, January 23–26, 1956.

† This research was supported in part by the United States Air Force under Contract No. AF33(038)-22955.

* Associate Professor of Aeronautical Engineering.

** Research Aeronautical Engineer.

‡ See also Figs. 2 and 3.

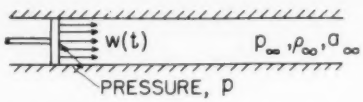

SMALL-DISTURBANCE RELATION:

$$p - p_\infty = \rho_\infty a_\infty w(t)$$

SECOND-ORDER RELATION:

$$p - p_\infty = \rho_\infty a_\infty^2 \left\{ \left(\frac{w}{a_\infty}\right) + \frac{\gamma+1}{4}\left(\frac{w}{a_\infty}\right)^2 \right\}$$

LIGHTHILL'S THIRD-ORDER RELATION:

$$p - p_\infty = \rho_\infty a_\infty^2 \left\{ \left(\frac{w}{a_\infty}\right) + \frac{\gamma+1}{4}\left(\frac{w}{a_\infty}\right)^2 + \frac{\gamma+1}{12}\left(\frac{w}{a_\infty}\right)^3 \right\}$$

FIG. 1. Formulas for the pressure on a piston in a one-dimensional channel.

$\omega_h, \omega_\alpha, \omega_\beta$ = uncoupled natural frequencies of oscillation of spring-restrained typical section in bending, torsion, and flap rotation, respectively

INTRODUCTION

THE TERM "piston theory," as used in this paper, refers to any method for calculating the aerodynamic loads on aircraft in which the local pressure generated by the body's motion is related to the local normal component of fluid velocity in the same way that these quantities are related at the face of a piston moving in a one-dimensional channel. The circumstances under which such an analogy is valid are now well understood and are outlined below. In general, piston theory may be employed for large flight Mach Numbers or high reduced frequencies of unsteady motion, whenever the surface involved is nearly plane and not inclined too sharply to the direction of the free stream. The foregoing shape conditions are fulfilled by all but the immediate tip (and possibily leading-edge) regions of supersonic wings. In most aeronautical applications the normal component of fluid velocity is the given quantity and the surface pressure is the unknown to be determined, so that a point-function relationship between the two is a great convenience. These observations, coupled with the fact that arbitrary small deformations and arbitrarily time-dependent unsteady motions can be taken into account, recommend piston theory to the aeroelastician as a powerful tool for analyzing high-speed problems.

The authors' main purpose is to focus attention on the remarkable simplicity and utility of the method by presenting a selection of new applications and comparisons with previously published results which were originally obtained at the expense of much more laborious computation. The number of different examples which can be given in a single paper is naturally limited, but it is hoped that readers engaged either in the field of aeroelasticity or elsewhere will be encouraged to seek other uses of piston theory on problems of current interest.

Fig. 1 depicts a piston moving with velocity $w(t)$ in the end of a channel containing perfect gas, whose undisturbed pressure, density, and speed of sound are p_∞, ρ_∞, and a_∞. Provided that the piston generates only simple waves and produces no entropy changes, the exact expression for the instantaneous pressure $p(t)$ on its face is

$$p/p_\infty = \left\{1 + [(\gamma - 1)/2](w/a_\infty)\right\}^{2\gamma/(\gamma-1)} \quad (1)$$

Depending on the magnitude of the ratio w/a_∞, Eq. (1) may be approximated by the linear relation,

$$p - p_\infty = \rho_\infty a_\infty w \quad (2)$$

by its second-order binomial expansion,

$$p - p_\infty = \rho_\infty a_\infty^2 \left\{(w/a_\infty) + [(\gamma + 1)/4](w/a_\infty)^2\right\} \quad (3)$$

or by its third-order expansion,

$$p - p_\infty = \rho_\infty a_\infty^2 \left\{(w/a_\infty) + [(\gamma + 1)/4](w/a_\infty)^2 + [(\gamma + 1)/12](w/a_\infty)^3\right\} \quad (4)$$

Eq. (3) resembles Busemann's quadratic formula for steady supersonic flow past an airfoil. Reasoning from a suggestion of Hayes,[1] Lighthill[2] pointed out that Eq. (4) can be used with excellent accuracy even under nonisentropic conditions to calculate the pressure on an airfoil in steady or unsteady motion whenever the flight Mach Number has such an order of magnitude that $M^2 \gg 1$. An additional limitation is that the product $M\delta$ cannot be too large, where for practical purposes δ represents the larger of the thickness ratio of the airfoil or the ratio of maximum amplitude of unsteady motion to airfoil chord length.

It is of historical interest that a theory equivalent to applying the linear relation Eq. (2) to simple harmonic oscillations of a flat plate with hinged flap in two-dimensional flow was given by Collar[3] in 1944. Collar's work consists of an extension by physical reasoning of Ackeret's well-known formula for steady supersonic flight. It was provided a mathematical foundation by Temple and Jahn,[4] who reduced the same results from a series expansion of the exact solution when $M \to \infty$, independent of the frequency of oscillation. (The condition of large Mach Number also implies that the factor $\sqrt{M^2 - 1}$ can be replaced by M, which brings Collar's formulation into exact agreement with linear piston theory.) In 1946 Jordan[5] presented the high Mach Number expansion for two-dimensional sinusoidal motion and noted the point-function relation between p and w which is the characteristic feature of piston theory.

More recently Hjelte[6] and Landahl, Mollø-Christensen, and Ashley[7] have shown that linearized piston theory can be used for arbitrary small motions of thin two-dimensional airfoils whenever any one of the conditions $M^2 \gg 1$, $kM^2 \gg 1$ or $k^2M^2 \gg 1$ is met, k being an appropriate measure of the "unsteadiness" of the flow. The last of these three conditions suggests that certain subsonic flows may be covered, but comparison with more exact solutions indicates that satisfactory accuracy will be attained only in very high-frequency problems such as local skin vibrations.

Landahl's systematic presentation[8] of the circumstances under which linear and second-order piston theory can be deduced from the general theory of unsteady potential flow brings together the various lines of approach outlined above and furnishes a rigorous estimate of the magnitude of errors to be expected when Eq. (2) or Eq. (3) is adapted to practical problems. He treats an upper wing surface close to the X-Y-plane in a uniform stream of velocity U parallel to the X-direction. The instantaneous surface position is given by

$$Z = \delta Z_0(X, Y, t) \tag{5}$$

the parameter δ being factored out so that Z_0 becomes a quantity of order unity when made dimensionless by division with a typical length—i.e., the midspan chord $2b$. The normal fluid velocity produced by the wing's motion is

$$\delta w_0 = [(\partial/\partial t) + U(\partial/\partial X)]\delta Z_0 \tag{6}$$

By means of an iterative procedure Landahl derives a general solution for the pressure coefficient

$$C_p = (p - p_\infty)/[(1/2)\rho_\infty U^2] \tag{7}$$

on the surface. When this is expanded in powers of δ and $1/M^2$, a series develops in the following form:

$$C_p = (\delta/M)C_{p_1}^{(1)} + (\delta/M^3)C_{p_3}^{(1)} + (\delta/M^5)C_{p_5}^{(1)} + O(\delta/M^7) + \delta^2 C_{p_1}^{(2)} + (\delta^2/M^2)C_{p_2}^{(2)} + O(\delta^2/M^4) \tag{8}$$

The various coefficients $C_{p_n}^{(1)}$ and $C_{p_n}^{(2)}$ are of order unity whenever the solution is uniformly convergent, so that the δ and M factors indicate the magnitude of the various terms. Those of importance to the present discussion are listed below.

$$C_{p_1}^{(1)} = 2(w_0/U) \tag{9a}$$

$$C_{p_1}^{(2)} = [(\gamma + 1)/2](w_0/U)^2 \tag{9b}$$

$$C_{p_2}^{(1)} = \left(\frac{\partial^2}{\partial x^2} + \frac{\partial^2}{\partial y^2}\right)\int_{x_l}^{x}(x - \xi) \times \frac{w_0[\xi, y, (Ut/2b) - x + \xi]}{U}\, d\xi \tag{9c}$$

All space coordinates in Eq. (9c) are divided by the typical length $2b$; $x_l(y)$ gives the projection of the wing leading edge on the x-y-plane.

The δ/M and δ^2 terms in Eqs. (8) and (9) are obviously identical to the linear and second-order portions of Eq. (3). Hence, in general, the piston approximation contains absolute errors no greater than the orders of δ/M^3 and δ^2/M^2. There is also a general limitation that neither of the products δM or $k\delta M$ can be too large, which means physically that the surface can nowhere be inclined too sharply to the direction of U and that normal velocities produced by the unsteady motion must be limited in comparison with the speed of sound. Because the mathematical solution is not uniformly convergent in the neighborhood of a cut-off wing tip, as might be expected from the failure of the one-dimensional flow analogy when fluid can spill laterally around the tip, the error estimates are incorrect there. This does not forbid the use of piston theory to account for other three-dimensional effects, however, and the region where inaccuracies may occur is clearly bounded by the inboard Mach line from the tip leading edge. Finally, the third-order term in Eq. (4) cannot be predicted by Landahl's analysis, which is based on a flow assumed free of strong shocks and entropy changes. The justification for including third-order contributions, when they are appreciable, is regarded as excellent but nevertheless empirical.

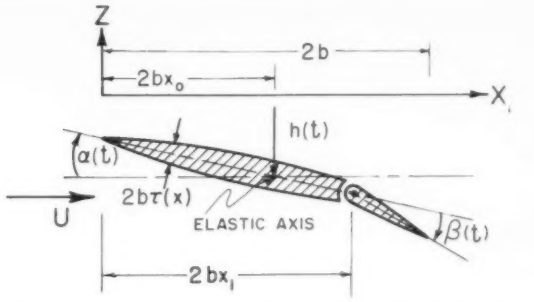

FIG. 2. Geometric properties of an airfoil section with flap.

TWO-DIMENSIONAL FLUTTER PROBLEMS

The aerodynamic derivatives used for predicting the flutter characteristics of a two-dimensional airfoil or "typical section" are calculated by considering sinusoidal motion in the three degrees of freedom h (vertical translation), α (pitching), and β (flap rotation) illustrated in Fig. 2. The axis of pitch and the hingeline of the aerodynamically unbalanced flap are located at distances $2bx_0$ and $2bx_1$, respectively, behind the leading edge. Up to terms of second order, this motion gives rise to normal components of fluid velocity

$$\frac{w}{U} = \begin{cases} \mp\,[(\dot{h}/U) + \alpha + (2b/U)\dot{\alpha}(x - x_0)] + \\ \qquad (1/2)(d\tau/dx), & x < x_1 \\ \mp\,[(\dot{h}/U) + \alpha + (2b/U)\dot{\alpha}(x - x_0) + \\ \quad \beta + (2b/U)\dot{\beta}(x - x_1)] + \\ \qquad (1/2)(d\tau/dx), & x \geq x_1 \end{cases} \tag{10}$$

Here the negative sign refers to the upper surface and the positive to the lower, since w must always be taken in the outward direction from the surface as used in piston formulas like Eqs. (2)–(4).

Although arbitrary time dependence can be handled without additional difficulty, only the case of simple harmonic motion is treated here, because it permits the introduction of the familiar notation of Garrick and Rubinow.[9] For example, the lift and pitching moment about $x = x_0$ per unit span, due to

$$h = \bar{h}e^{i\omega t} \tag{11a}$$

$$\alpha = \bar{\alpha}e^{i\omega t} \tag{11b}$$

$$\beta = \bar{\beta}e^{i\omega t} \tag{11c}$$

can be written in general

$$P = -4\rho_\infty b U^2 k^2 \left[\frac{h}{b}(L_1 + iL_2) + \alpha(L_3 + iL_4) + \beta(L_5 + iL_6)\right] \quad (12)$$

$$M_\alpha = -4\rho_\infty b^2 U^2 k^2 \left[\frac{h}{b}(M_1 + iM_2) + \alpha(M_3 + iM_4) + \beta(M_5 + iM_6)\right] \quad (13)$$

where

$$L_2 = L_3' - 2x_0 L_1 \quad (14a)$$

$$L_4 = L_4' - 2x_0 L_2 \quad (14b)$$

$$M_1 = M_1' - 2x_0 L_1 \quad (14c)$$

$$M_2 = M_2' - 2x_0 L_2 \quad (14d)$$

$$M_3 = M_3' - 2x_0[(M_1' + L_3') - 2x_0 L_1] \quad (14e)$$

$$M_4 = M_4' - 2x_0[(M_2' + L_4') - 2x_0 L_2], \text{ etc. . .} \quad (14f)$$

Note that k now represents the reduced frequency $\omega b/U$ of the oscillation.

When second-order piston theory, according to Eq. (3), is employed to approximate these dimensionless coefficients, the following relatively simple expressions are found:

$$L_1 = 0 \quad (15a)$$

$$L_2 = 1/kM \quad (15b)$$

$$L_3' = 1/k^2 M \quad (15c)$$

$$L_4' = (1/kM) - [(\gamma + 1)/k](A_w/8b^2) \quad (15d)$$

$$L_5 = [(1 - x_1)/k^2 M] - [(\gamma + 1)/k^2][\tau(x_1)/4] \quad (15e)$$

$$L_6 = [(1 - x_1)^2/kM] - [(\gamma + 1)/k](A_F/8b^2) \quad (15f)$$

$$M_1' = 0 \quad (15g)$$

$$M_2' = (1/kM) - [(\gamma + 1)/k](A_w/8b^2) \quad (15h)$$

$$M_3' = (1/k^2 M) - [(\gamma + 1)/k^2](A_w/8b^2) \quad (15i)$$

$$M_4' = (4/3k M) - [(\gamma + 1)/k](M_w/4b^3) \quad (15j)$$

$$M_5 = \left\{[(1 - x_1^2) - 2x_0(1 - x_1)]/k^2 M\right\} - [(\gamma + 1)/k^2]\left\{(x_1 - x_0)[\tau(x_1)/2] + (A_F/8b^2)\right\} \quad (15k)$$

$$M_6 = \frac{(4/3)(1 - x_1^3) - 2(x_1 + x_0)(1 - x_1^2) + 4x_0 x_1(1 - x_1)}{kM} - \frac{(\gamma + 1)}{k}\left[(x_1 - x_0)\frac{A_F}{4b^2} + \frac{M_F}{4b^3}\right] \quad (15l)$$

In each of Eqs. (15) the first term is the linear part, which arises even in the absence of thickness; each contains the Mach Number as a factor M^{-1}, in agreement with Eq. (8). The thickness terms, when not identically zero, are linearly dependent on the thickness distribution function $\tau(x)$. Most of them involve simple geometric properties of the profile, such as A_w and M_w, which are the area and first moment of the area about the leading edge. Similarly the flap derivatives are dependent on flap cross-sectional area A_F and first moment M_F about the hingeline. Certain of these geometrical interpretations have been pointed out by Miles[10] in the discussion of second-order effects in his comprehensive monograph on unsteady flow.

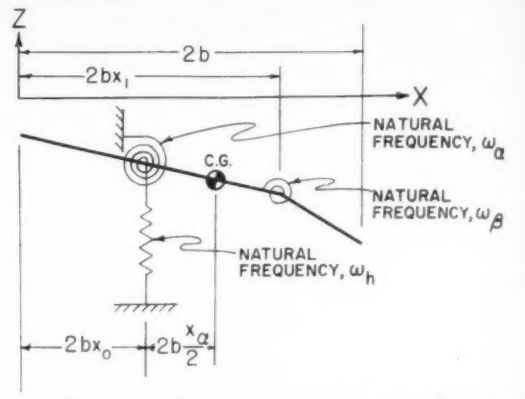

FIG. 3. Elastic and inertial properties of a two-dimensional typical section.

It is of considerable importance to the flutter analyst that, although Eqs. (15) are derived from a nonlinear theory, symmetries between the upper and lower surface motions cause the lift and moments to relate linearly to the oscillations producing them. At the higher Mach Numbers, aerodynamic loads computed from Eqs. (12)–(15) are known to agree closely with calculations by much more complicated second-order theories, such as that of van Dyke.[11] One instructive comparison can be made in the case of single degree of freedom rotational instability of the whole airfoil or the flap: both theories predict the impossibility of such an instability and show the same influence of thickness on the damping moment associated with the rotation. Taking airfoil pitching as an example, stability is dependent on the sign of the coefficient M_4, being positive when M_4 is positive. From Eqs. (15), the piston theory value is

$$M_4 = (1/kM)[(4/3) - 4x_0 + 4x_0^2] - [(\gamma + 1)/k](M_{wx_0}/4b^3) \quad (16)$$

where M_{wx_0} denotes the first moment of the cross-sectional area about $x = x_0$. Eq. (16) is positive for all values of x_0 and all airfoils thin enough to fall within the scope of the theory. If the section has fore-and-aft symmetry (double-wedge, circular-arc, etc.), thickness is seen to make an unstable contribution to M_4 when the axis of rotation is ahead of midchord.

For flutter computations involving more than one degree of freedom, the airfoil is assumed to have the elastic and inertia properties shown in Fig. 3. The flutter equations are not reproduced here, since their derivation and solution have been extensively discussed in the literature—e.g., Garrick and Rubinow.[9] The significant point to be made is that, when the aerodynamic coefficients have forms as simple as Eqs. (15), implicit or explicit algebraic expressions can be worked out for the critical flutter speed U_F and frequency ω_F as functions of M and the other parameters defining the

system. Thus, the trial-and-error process which was formerly characteristic even of two-dimensional flutter analyses is eliminated. Flutter prediction becomes more elementary at high speeds than any other similar calculation—incompressible flow included—in the aeroelastician's experience. The influences of thickness, profile shape and initial angle of attack* can be introduced, for the first time, in a rigorous and routine fashion.

As a first illustration, Fig. 4 shows exact and approximate curves of dimensionless bending-torsion ($h - \alpha$) flutter speed $U_F/b\omega_\alpha$ vs. M for a typical section with a low frequency ratio, elastic axis at mid-chord and center of gravity at 60 per cent chord. The notation is that of Garrick and Rubinow[9] and is reviewed in the list of symbols. Fig. 4 is taken from a previous paper by Heller and the present authors,[12] in which the application of piston theory to two-dimensional bending-torsion flutter is extensively elaborated. A conclusion stated there, to which no exceptions have yet been found, is that the simplified approach yields $U_F/b\omega_\alpha$ values within 10 per cent of their exact counterparts for $M \geqslant 2.5$. Incidentally, third-order terms from Eq. (4) were carried through the original calculations but have since been discovered to have negligible influence within the ranges of variables treated.

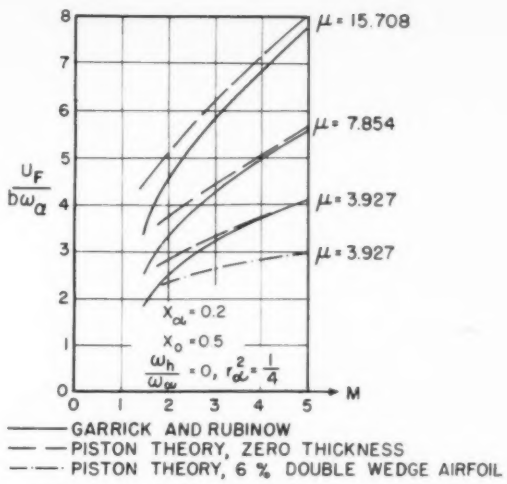

FIG. 4. Bending-torsion flutter of typical section.

All the piston theory curves on Fig. 4, together with similar curves for any other combinations of the bending-torsion parameters, are calculable from the single closed-form solution

$$\frac{U_F}{b\omega_\alpha} = \frac{\mu M}{\sqrt{\chi}} \sqrt{\frac{x_\alpha^2 - [(\omega_h/\omega_\alpha)^2\chi - 1]r_\alpha^2(\chi - 1)}{\mu M\{(1 - 2x_0 + \bar{A})[(\omega_h/\omega_\alpha)^2\chi - 1] + \chi_\alpha\} + (1 - 2x_0 + \bar{A})^2 - [(4/3) - 4x_0 + 4x_0^2 + \bar{B}]}} \tag{17}$$

where

$$\chi = \frac{r_\alpha^2 - 2x_\alpha(1 - 2x_0 + \bar{A}) + [(4/3) - 4x_0 + 4x_0^2 + \bar{B}]}{r_\alpha^2 + (\omega_h/\omega_\alpha)^2[(4/3) - 4x_0 + 4x_0^2 + \bar{B}]} \tag{18a}$$

$$\bar{A} = -M(\gamma + 1)(A_w/8b^2) \tag{18b}$$

$$\bar{B} = -M(\gamma + 1)(M_{wx_3}/4b^3) \tag{18c}$$

Thickness enters only through the constants $\bar{A}$ and $\bar{B}$; its influence may be strongly destabilizing, however, as suggested by the data for a 6 per cent double-wedge airfoil given in Fig. 4. Other interesting implications of Eq. (17) and various reduced forms thereof have been discussed previously.[12]

Figs. 5 and 6 compare piston theory results with exact calculations by Woolston and Huckel[13] for two-dimensional bending-aileron ($h - \beta$) flutter of an airfoil with zero thickness and a 20 per cent chord unbalanced flap. In each case the ordinate, abscissa, and section parameters are chosen to correspond with those given by reference 13. Accordingly, Fig. 5 presents the dimensionless bending stiffness $b\omega_h/a_\infty$ required to produce neutral stability, plotted vs. static unbalance parameter x_β for a system with unrestrained aileron ($\omega_\beta = 0$) and the other parameters stated. Fig. 6 presents the same ordinate, plotted vs. frequency ratio ω_β/ω_h, for two values of static unbalance.

Although the Mach Number is only 2—the highest value included in the exact calculations[13]—the agreement with piston theory seems quite satisfactory. As shown by a few representative points, changes in the critical condition caused by replacing the flat plate with a 6 per cent double-wedge profile are small in this situation. No explicit formulas, comparable to Eqs. (17)–(18), can be written for the critical conditions of bending-aileron, torsion-aileron, or bending-torsion-aileron flutter. From the practical standpoint, however, the implicit formulas that must be solved demand little more computational effort than the bending-torsion case.

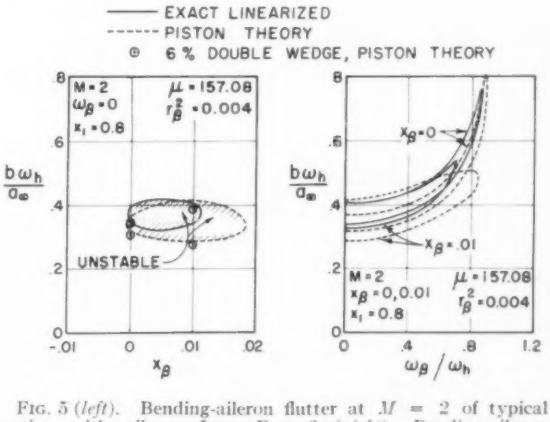

FIG. 5 (*left*). Bending-aileron flutter at $M = 2$ of typical section with aileron free. FIG. 6 (*right*). Bending-aileron flutter at $M = 2$ of typical section for various x_β and ω_β/ω_h.

* Camber and initial angle are accounted for only by Eq. (4).

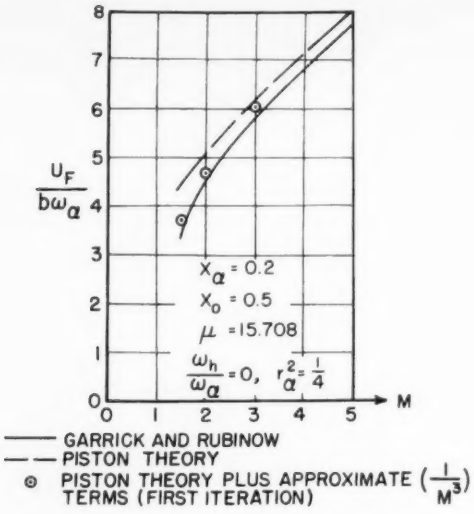

FIG. 7. Bending-torsion flutter of typical section.

In connection with certain of the foregoing conclusions and also with flutter analyses on finite wings in the Mach Number range between 2 and 3, it must be pointed out that a theoretical inconsistency may arise from including thickness effects. Examination of Eq. (8) reveals that, if the δ^2 term is retained while the δ/M^3 term is omitted, it is automatically implied that

$$\delta \gg 1/M^3 \tag{19}$$

This inequality is not fulfilled, for example, by a 6 per cent thick airfoil at $M = 2$. A preliminary study of the influence of the δ/M^3 term on flutter eigenvalues has demonstrated that its omission often produces compensating errors in the elements of the flutter determinant. This would be a fortunate conclusion, if generally valid, because this term is not of the piston theory type.

Following a suggestion by Landahl, it is possible to introduce the higher terms of Eq. (8) into an iterative flutter calculation. For a given M, a first estimate of flutter reduced frequency k_F is taken from piston theory. Corrections based on this k_F are then inserted into the flutter determinant, and a second approximation is computed with relative ease. It appears that a single iteration will normally be sufficient for most purposes, and this involves no especial difficulty. The δ/M^3 corrections to the aerodynamic coefficients for bending-torsion flutter are as follows:

$$\Delta L_1 = \sin 2k/2kM^3 \tag{20a}$$

$$\Delta L_2 = \cos 2k/2kM^3 \tag{20b}$$

$$\Delta L_3' = \sin 2k/4k^3M^3 \tag{20c}$$

$$\Delta L_4' = -(\sin^2 k/2k^3M^3) \tag{20d}$$

$$\Delta M_1' = (\sin 2k/kM^3) + (\cos 2k/2k^2M^3) - (\sin 2k/4k^3M^3) \tag{20e}$$

$$\Delta M_2' = (\cos 2k/kM^3) - (\sin 2k/2k^2M^3) + (\sin^2 k/2k^3M^3) \tag{20f}$$

$$\Delta M_3' = (\sin 2k/2k^3M^3) - (\sin^2 k/2k^4M^3) \tag{20g}$$

$$\Delta M_4' = (\cos 2k/2k^3M^3) - (\sin 2k/4k^4M^3) \tag{20h}$$

Fig. 7 illustrates the improvement in predicted bending-torsion flutter speed that is attained when piston theory is modified by a first iteration in the manner just described. The directions and magnitudes of the changes in $U_F/b\omega_\alpha$ thus found can be expected to turn out about the same, whether or not thickness effects are also introduced into the calculation.

THREE-DIMENSIONAL FLUTTER PROBLEMS

When adapted to flutter calculations for finite lifting surfaces, piston theory is automatically "strip theory," in the sense that the pressure at any point, as well as the loading along any chordwise section, is independent of the motions of other portions of the system. As discussed above, the loads are predicted with the least accuracy near a cut-off tip, but this same criticism can be leveled at any of the other strip theories which have been used so extensively in the past. If the flutter problem is set up in terms of assumed modes and frequencies of vibration, the principal novelty is that the generalized forces acting on the various modes can usually be written down in simple algebraic forms for arbitrary Mach Number and reference reduced frequency. Certain unwieldy trial-and-error procedures common to more conventional methods are thus avoided or minimized, as with the typical section in the foregoing discussion.

The first example presented in this section is selected because unclassified experimental data are available and because it offers startling evidence of the importance of thickness in supersonic flutter. The case is one of

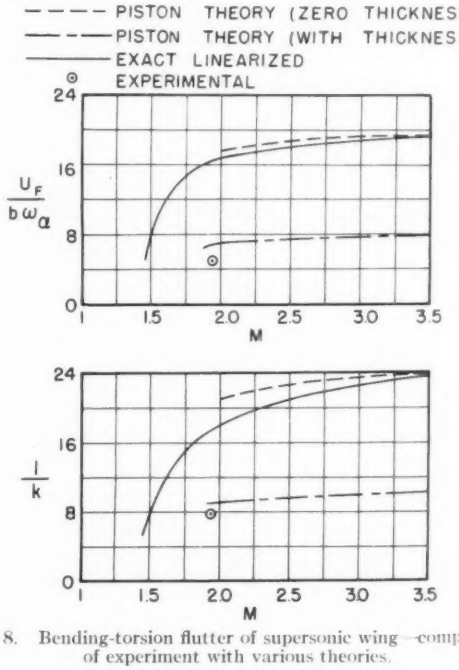

FIG. 8. Bending-torsion flutter of supersonic wing—comparison of experiment with various theories.

bending-torsion flutter of a straight-tapered wing of moderate aspect ratio,* whose other properties are carefully chosen to be representative of lifting surfaces on aircraft designed for appreciable supersonic speeds. The actual properties cannot be revealed for reasons of security.

Fig. 8 presents theoretical curves of the dimensionless flutter characteristics vs. Mach Number. These were obtained from the standard Rayleigh-Ritz equations, including one uncoupled mode of cantilever bending and one of cantilever torsional vibration. The solid curve results from using the two-dimensional linearized aerodynamic theory of Garrick and Rubinow;[9] at higher Mach Numbers it is seen to merge smoothly with the curve based on zero-thickness piston theory, as would be expected. The dot-dashed curve differs only in that the influences of profile shape and thickness have been introduced through Eqs. (15). There is little doubt about which calculation agrees best with the measured data, even though M is less than 2. The linearized prediction is dangerously unconservative, despite the fact that previous experience with lower Mach Numbers suggests that neglecting tip effects should lead to an error in the opposite direction. Introducing terms of the order δ/M^3, as outlined at the end of the preceding section, might be likely to displace the dot-dashed $U_F/b\omega_\alpha$ curve downward by roughly the distance between the two zero-thickness curves, thus giving an even better comparison with experiment.

Quite a different sort of application of piston theory to three-dimensional wings concerns the possibility of finding exact solutions for the damping and frequency of the aeroelastic modes, when the inertia and elastic properties are uniform along the span. A laborious calculation of this type was once made, using incompressible strip techniques, by Goland and Luke.[14] By contrast, the aerodynamic derivatives for arbitrary motion according to piston theory are such that little more difficulty is encountered than when analyzing modes of free vibration in a vacuum.

One simple example which serves to illustrate the method is uncoupled pure torsion in a supersonic stream of a wing having constant chord $2b$, constant torsional stiffness GJ, and constant running moment of inertia I_α about the axis of twist. The differential equation governing the spanwise distribution of twist $\theta(Y, t)$ is

$$I_\alpha(\partial^2\theta/\partial t^2) = GJ(\partial^2\theta/\partial Y^2) - (8\rho_\infty U^2b^2/M) \times \{(2b/U)(\partial\theta/\partial t)[(1/3) - x_0 + x_0^2] + \theta[(1/2) - x_0]\} \quad (21)$$

In Eq. (21) the aerodynamic moment acting about the axis $2bx_0$ behind the leading edge was found directly from Eq. (2), with

$$w = \mp[U\theta + 2b(\partial\theta/\partial t)(x - x_0)] \quad (22)$$

* This wing was flutter tested at M.I.T. as a portion of experimental research conducted for Dynamics Branch, Aircraft Laboratory, Wright Air Development Center, under Contract No. AF33(038)-22955.

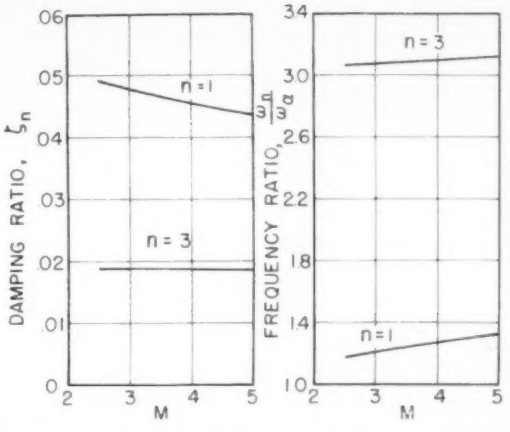

FIG. 9. Frequency and damping ratios of two torsional aeroelastic modes of uniform wing, $\mu r_\alpha^2 = 12$, $x_0 = 0.443$, $k_1 = 0.25/M$.

Thickness effects are omitted, and the minus and plus signs in Eq. (22) refer to the upper and lower wing surfaces, respectively.

Eq. (21) is linear with constant coefficients and is obviously solved by products of exponential functions of Y and t. The boundary conditions of zero twist at the root and zero torque at the tip force the Y-functions to be simple sine curves, as in the case of free vibration. These conditions also yield a characteristic equation, from which can be computed the frequency and the ratio of actual damping to critical damping for the mode of each order. For the nth mode, the damping ratio and the frequency ratio prove to be

$$\zeta_n = \frac{(1/2\mu r_\alpha^2)[(4/3) - 4x_0 + 4x_0^2]}{\sqrt{n^2(Mk_1)^2 + [(1 - 2x_0)/\mu r_\alpha^2]M}} \quad (23a)$$

$$\omega_n/\omega_\alpha = (1/Mk_1)\sqrt{n^2(Mk_1)^2 + [(1 - 2x_0)/\mu r_\alpha^2]M} \times \sqrt{1 - \zeta_n^2}; \qquad n = 1, 3, 5, \ldots \quad (23b)$$

where k_1 is the reduced frequency $\omega_\alpha b/U$ corresponding to the fundamental mode of vibration in vacuum—i.e.,

$$\omega_\alpha = (\pi/2l)\sqrt{GJ/I_\alpha} \quad (23c)$$

All other quantities are defined in the list of symbols. ζ_n is always positive, confirming the previously mentioned stability of pure rotational motions at high Mach Numbers, but, curiously, it turns out to be inversely proportional to n for the modes of larger order. Fig. 9 shows curves of damping ratio and ratio of damped natural frequency in air to the fundamental frequency ω_α, both plotted vs. M for the two lowest orders $n = 1$ and 3. Numerical properties of the particular wing are listed on the Figure.

Panel Flutter

A problem which has caused analytical difficulties out of all proportion to its apparent complexity is the flutter of a flat skin panel exposed on one side to a supersonic air stream. Since most of the trouble stems from inability to construct exact solutions based on available

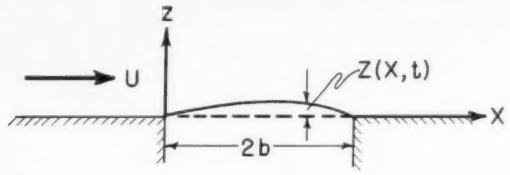

FIG. 10. Two-dimensional panel adjacent to a supersonic air stream.

aerodynamic theories, it is reasonable to expect that piston theory can yield valuable information within the ranges of M and k for which it is valid. This is definitely the case, as will be illustrated here by studying the elementary example of the unbuckled two-dimensional panel.

The panel, pictured in Fig. 10, is embedded in an otherwise rigid, plane surface parallel to the X-axis. The two-dimensional displacement $Z(X, t)$ occurs between supports at $X = 0$ and $X = 2b$. m represents the mass per unit distance perpendicular to the direction of the stream U; EI is the *effective* bending stiffness; and there is a uniform initial tension T per unit span which lies somewhere between the yield strength and the (negative) value which would cause buckling. The differential equation of motion, including air loads by linear piston theory, reads

$$EI(\partial^4 Z/\partial X^4) - T(\partial^2 Z/\partial X^2) + (\rho_\infty U^2/M)(\partial Z/\partial X) + (m/2b)(\partial^2 Z/\partial t^2) + (\rho_\infty U/M)(\partial Z/\partial t) = 0 \quad (24)$$

Pressure variations on the back of the panel are omitted from Eq. (24) because they can usually be expected to increase the stability by removing energy from vibrations. If the panel is simply supported, Z and $\partial^2 Z/\partial X^2$ must vanish at $X = 0$ and $2b$.

The procedure for determining the stability of solutions of Eq. (24) is to assume that $Z(X, t)$ is of the form $\{\bar{Z}(X)e^{i\Omega t}\}$, and to try to find whether, for some combinations of the physical parameter EI, T, etc., it is possible for Ω to have a zero or negative imaginary part. If such is not the case, one is led to the conclusion that all small motions are damped. It will now be proved that for the membrane problem, in which the fourth derivative term of Eq. (24) is assumed to be negligible, Ω can have only positive imaginary part, implying stability.

The equation governing the complex dimensionless amplitude function

$$\bar{z}(x) = (1/2b)\bar{Z}(X/2b)$$

of the membrane can be written in symbolic form

$$[(d^2/dx^2) + a(d/dx) + (c + id)]\bar{z} = 0 \quad (25)$$

where the constants a, c, and d are real numbers. The boundary conditions are

$$\bar{z}(0) = z(1) = 0 \quad (26)$$

If $\bar{z}$ is separated into real and imaginary parts

$$\bar{z}(x) = z_r(x) + iz_i(x) \quad (27)$$

an elimination of z_i leads to the following real differential equation and boundary conditions for z_r:

$$[(d^2/dx^2) + a(d/dx) + c]^2 z_r + d^2 z_r = 0 \qquad d \neq 0 \quad (28)$$

$$\left.\begin{aligned} z_r &= 0 \\ [(d^2/dx^2) + a(d/dx)]z_r &= 0 \end{aligned}\right\} \quad \text{for} \quad x = 0, 1 \quad (29)$$

If the same procedure is used to eliminate z_r, it develops that the differential equation and boundary conditions for z_i are identical with Eqs. (28) and (29). However, it can be shown that Eqs. (28) and (29) have no eigenvalues if $d \neq 0$. If $d = 0$, one obtains a very simple formula for the imaginary part of Ω:

$$\Omega_i = \rho_\infty a_\infty b/m$$

This shows that the membrane panel is always stable, the degree of stability depending on the ratio of the air density to the running mass of the plate. A few calculations of damping ratios have been compared with numerical results from the exact solution of Goland and Luke[15] at $M = \sqrt{8}$; satisfactory agreement is found in all cases.

The foregoing proof holds true only in the case of a membrane.* When the fourth-derivative bending term is included one can demonstrate that, even though the separated differential equations for z_r and z_i are identical with the same boundary conditions, d does not necessarily have to be zero, and the resulting equations will have *two* linearly independent eigensolutions for a given set of eigenvalues (c, $d \neq 0$). In this case, the sign of Ω_i cannot be determined readily.

Recently doubts have been cast on the validity of the Rayleigh-Ritz method as applied to supersonic panel flutter. The relationship between Rayleigh-Ritz and exact solutions is easy to work out at Mach Numbers where piston theory applies. As an illustration, a Rayleigh-Ritz calculation was made on a panel with membrane stiffness only, having $(mM/\rho_\infty b^2) = 40$ (this single parameter fixes the dimensionless stability properties). According to the exact analysis, the panel is absolutely stable, having $(\Omega_i b/U) = 0.025$. However, the assumed-mode procedure yields the dimensionless flutter frequencies and speeds, based on the fundamental frequencies ω_1 of free vibration, which are tabulated below:

Number of Normal Modes Used in the Analysis of a Membrane	$\left(\frac{\omega_F}{\omega_1}\right)$	$\left(\frac{U_F}{b\omega_1}\right)$
2	1.58	4.81
3	2.48	4.82
4	3.43	4.84

It is seen that taking a few modes results in a finite flutter speed, inconsistent with the exact solution. The

* The authors are indebted to J. M. Hedgepeth of NACA and Professor Budiansky of Harvard University for pointing out this fact. The proof given in the original preprint for the plate-type panel is incorrect. (For further discussion, cf. Readers' Forum note by Hedgepeth.[21])

values of $U_F/b\omega_1$ might even seem to be converging toward a real limit, except that reference to the sequence of ω_F/ω_1's and careful examination of the flutter determinant for higher numbers of modes shows that some sort of divergence toward an infinite or imaginary U_F ultimately will take place. Unfortunately, no such careful attention to convergence is observed in routine flutter calculations, so this difficulty could be completely overlooked in the present case. It is interesting to note that if only odd or only even modes are considered, the Rayleigh-Ritz solution will always indicate a damped motion as in the exact solution.

The reader can imagine many other more complicated cases of high-speed panel flutter whose prediction will be expedited by the use of piston theory. Almost-plane plates with finite dimensions normal to the stream direction, and, in fact, with arbitrary shape, fall rigorously within its scope, since they do not have cut-off tips. Nonlinear aerodynamic effects due to initial bucklings are readily included and fit well into an analysis which also involves nonlinear structural properties. No further discussion is presented here on these aspects of the problem, because they are currently under study by Sechler and Fung at California Institute of Technology.

Other Aeroelastic Problems

Equations like (3) and (8) hold for motions with arbitrary time dependence, so that it is natural to consider employing them in unsteady aeroelastic calculations where the displacements are not sinusoidal. Typical cases of this sort are the response of aircraft to gusts or blasts, and high-speed loads due to rapid maneuvers. Certain steady-state analyses may also be simplified because of the point-function character of piston theory, or rendered more accurate through the introduction of thickness effects. A good example of the latter kind is Biot's section on nonlinearities in his study of the chordwise divergence of supersonic wings.[16] To the authors' knowledge, his is the first publication where Lighthill's theory is applied to a practical aeroelastic problem.

Steady-state supersonic calculations with two-dimensional aerodynamics are not facilitated by piston theory, because Ackeret's formula for the supersonic airfoil already exhibits the point-function relationship between pressure and normal velocity. A considerable saving is achieved, on the other hand, when three-dimensional air loads are needed but when some inaccuracy in the treatment of the immediate tip region can be overlooked. Weatherill's recent thesis[17] on the high-speed divergence and loss of aileron control of elastic wings confirms this point very well; his use of piston theory came as a brief afterthought following an elaborate analysis based on three-dimensional aerodynamic influence coefficients.

To demonstrate the utility of piston theory as a tool for dealing with unsteady transients, consider the gust response of a two-dimensional airfoil which can bend or twist but undergoes no elastic chordwise deformation. Bisplinghoff, Ashley, and Halfman[18] discuss how all such problems can be solved by appropriate superposition of six indicial response functions, three lifts and three pitching moments. For example, the piston theory lift and moment following a step change $\dot{h}_0$ in the airfoil's vertical velocity at $t = 0$ assume the following constant values instantaneously:

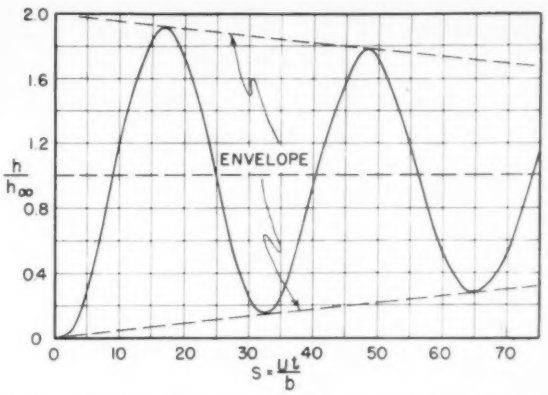

FIG. 11. Bending response of typical section to sharp-edged gust (properties given in text).

$$P = -(4\rho_\infty bU\dot{h}_0/M) \tag{30}$$

$$M_\alpha = -(4\rho_\infty b^2U\dot{h}_0/M)(1 - 2x_0) \tag{31}$$

Thickness effects are omitted from Eqs. (30) and (31), but they can be introduced by means of a single multiplicative factor. Similarly, the lift and moment developed due to an encounter at $t = 0$ with a uniform sharp-edged gust of vertical velocity w_g are

$$P = \begin{cases} -(4\rho_\infty Ubw_g/M)(Ut/2b) & 0 \leq Ut/b \leq 2 \\ -(4\rho_\infty Ubw_g/M) & 2 \leq Ut/b \end{cases} \tag{32}$$

$$M_\alpha = \begin{cases} -(4\rho_\infty Ub^2w_g/M)[(1/4) \times \\ \qquad (Ut/b)^2 - (Ut/b)x_0] & 0 \leq Ut/b \leq 2 \\ -(4\rho_\infty Ub^2w_g/M)\,[1 - 2x_0] & 2 \leq Ut/b \end{cases} \tag{33}$$

At Mach Numbers above 2, Eqs. (30)–(33) check very well with the more exact supersonic indicial functions given by Chang[19] and others. To illustrate the use of these functions, the bending response to a sharp-edged gust has been calculated for the airfoil shown in Fig. 2 with infinite torsional and control-surface stiffnesses ($\omega_\alpha = \omega_\beta = \infty$). The various constants entering the computation are $M = 3$, $\mu = 33^1/_3$, $\omega_h = 100$ rad./sec., $b = 3$ ft., $U \cong 3{,}000$ ft./sec. Fig. 11 presents this response in the form of the ratio of the instantaneous bending displacement $h(t)$ to its final steady-state value. The curve is actually just the transient of a second-order, linear system with constant coefficients. The slow rate of decay indicates that the aerodynamic damping at high Mach Numbers is quite small, so that a large number of cycles of vibration will go by before a significant amplitude reduction occurs.

It should be evident that computations like the above can be performed on three-dimensional wings with other elastic and rigid-body degrees of freedom in-

cluded in the equations of motion. The only increased difficulties are organizational and numerical; the gain in simplicity relative to more exact aerodynamic theories is proportional to the size of the problem.

Concluding Remarks

As was convincingly demonstrated by Bisplinghoff in his 1955 Wright Brothers Lecture,[20] high-temperature structural problems, boundary-layer heat transfer, and a host of related effects are certain to complicate the work of the aeroelastician in the not-too-distant future. It is, therefore, a pleasure to be able to report the practical success of one new element in the picture which represents a significant reduction in labor as compared with corresponding theories appropriate to flight at slower speeds. A Mach Number zone can be defined, lying roughly between 2.5 and the lower limit of hypersonic flow (a boundary determined by the size of the product δM); it is characterized by the fact that thermal effects are usually quite important but that the distinction can still be made between a boundary layer and an external potential flow. Within this zone it seems clear that piston theory is the logical tool to use for estimating aerodynamic forces when analyzing a large majority of all aeroelastic and aerothermoelastic phenomena.

References

[1] Hayes, W. D., *On Hypersonic Similitude*, Quarterly of Applied Mathematics, Vol. 5, No. 1, pp. 105–106, April, 1947.

[2] Lighthill, M. J., *Oscillating Airfoils at High Mach Number*, Journal of the Aeronautical Sciences, Vol. 20, No. 6, pp. 402–406, June, 1953.

[3] Collar, A. R., *Resistance Derivatives of Flutter Theory. Part II: Results for Supersonic Speeds*, Aeronautical Research Council R&M 2139, January, 1944.

[4] Temple, G., and Jahn, H. A., *Flutter at Supersonic Speeds: Derivative Coefficients for a Thin Aerofoil at Zero Incidence*, Aeronautical Research Council R&M 2139, April, 1945.

[5] Jordan, P., *Sections on Supersonic Flutter of Gottingen Monograph G3*, translated at R.T.P. Translation 1014, Aeronautical Research Council No. 11846, 1946.

[6] Hjelte, F., *Methods for Calculating Pressure Distributions on Oscillating Wings of Delta Type at Supersonic and Transonic Flow*, Swedish K.T.H. AERO Technical Note 39, 1955.

[7] Landahl, M., Mollø-Christensen, E. L., and Ashley, H., *Parametric Studies of Viscous and Nonviscous Unsteady Flows*, O.S.R. Technical Report 55-13, April, 1955.

[8] Landahl, M., *Unsteady Flow Around Thin Wings at High Mach Numbers*, O.S.R. Technical Note 55-245, June, 1955.

[9] Garrick, I. E., and Rubinow, S. I., *Flutter and Oscillating Air-Force Calculations for an Airfoil in a Two-Dimensional Supersonic Flow*, NACA Report 846, 1946.

[10] Miles, J. W., *Unsteady Supersonic Flow*, Monograph prepared for Air Research and Development Command under Contract AF18(600)-432, pp. 523–535, March, 1955.

[11] Van Dyke, M. D., *Supersonic Flow Past Oscillating Airfoils Including Nonlinear Thickness Effects*, NACA TN 2982, July, 1953.

[12] Zartarian, G., Heller, A., and Ashley, H., *Application of Piston Theory to Certain Elementary Aeroelastic Problems*, Proceedings of the Second Midwestern Conference on Solid Mechanics and the Fourth Midwestern Conference on Fluid Mechanics, Purdue University, September, 1955 (to be released shortly).

[13] Woolston, D. C., and Huckel, V., *A Calculation Study of Wing-Aileron Flutter in Two Degrees of Freedom for Two-Dimensional Supersonic Flow*, NACA TN 3160, April, 1954.

[14] Goland, M., and Luke, Y. L., *A Study of the Bending-Torsion Aeroelastic Modes for Airplane Wings*, Journal of the Aeronautical Sciences, Vol. 16, No. 7, pp. 389–396, July, 1949.

[15] Goland, M., and Luke, Y. L., *An Exact Solution for Two-Dimensional Linear Panel Flutter at Supersonic Speeds*, Readers' Forum, Journal of the Aeronautical Sciences, Vol. 21, No. 4, pp. 275–276, April, 1954.

[16] Biot, M. A., *The Divergence of Supersonic Wings Including Chordwise Bending*, Preprint No. 502, presented at the Twenty-Third Annual Meeting of the Institute of the Aeronautical Sciences, January, 1955.

[17] Weatherill, W. H., *Steady-State Aeroelastic Properties of Arbitrary-Planform Supersonic Wings Allowing Completely General Deformations*, S.M. Thesis, Department of Aeronautical Engineering, Massachusetts Institute of Technology, May, 1955.

[18] Bisplinghoff, R. L., Halfman, R. L., and Ashley, H., *Aeroelasticity*, 1st Ed., pp. 332–336 and 350; Addison Wesley Publishing Company, Cambridge, 1955.

[19] Chang, C. C., *Transient Aerodynamic Behavior of an Airfoil Due to Different Arbitrary Modes of Nonstationary Motions in a Supersonic Flow*, NACA TN 2333, 1951.

[20] Bisplinghoff, R. L., *Some Structural and Aeroelastic Considerations of High-Speed Flight*, Nineteenth Annual Wright Brothers Lecture, December, 1955, Journal of the Aeronautical Sciences, Vol. 23, No. 4, pp. 289–329, 367, April, 1956.

[21] Hedgepeth, J. M., *On the Flutter of Panels at High Mach Numbers*, Readers' Forum, Journal of the Aeronautical Sciences, Vol. 23, No. 6, p. 609, June, 1956.

Spectral Theory of Buffeting and Gust Response...

(*Continued from page 1077*)

Journal of the Aeronautical Sciences, Vol. 23, No. 10, pp. 917–930, October, 1956.

[4] Batchelor, G. K., *The Theory of Homogeneous Turbulence*, Cambridge University Press, Cambridge, England, 1953.

[5] Ribner, H. S., *Shock-Turbulence Interaction and the Generation of Noise*, NACA Report 1233, 1955.

[6] Tobak, Murray, *On the Use of the Indicial Function Concept In the Analysis of Motions of Wings and Wing-Tail Combinations*, NACA Rep. 1188, 1954.

[7] Houbolt, J. C., and Kordes, E. E., *Structural Response to Discrete and Continuous Gusts of an Airplane Having Wing-Bending Flexibility and a Correlation of Calculated and Flight Results*, NACA Rep. 1181, 1954.

Readers' Forum

BRIEF REPORTS of investigations in the aeronautical sciences and discussions of papers published in the JOURNAL are presented in this special department. Entries must be restricted to a maximum of 1,300 words or the equivalent of one JOURNAL page including formulas and illustrations. Publication is completed as soon as possible after receipt of the material. The Editorial Committee does not hold itself responsible for the opinions expressed by the correspondents.

Contents

Remarks on the Convergence of an Iterative Procedure in Solving Dynamic Response Problems. . TSE-SUN CHOW 1119

Axial Compression Buckling of a Pressurized Cylinder with a Thermally Induced Ring Compression . . . . . LEONARD A. HARRIS 1120

A Study of the Applicability of Rabotnov's Creep Parameter for Aluminum Alloy . . . . . FRED H. TURNER AND KURT E. BLOMQUIST 1121

An Approximate Solution to Supersonic Conical Flow . . . . . HENRY E. FETTIS 1122

Erratum—"Applied Aerodynamics and Flight Mechanics" . . . . . W. BAILEY OSWALD 1123

Nitric Oxide Formation in Hypersonic Flow . . . . . J. G. LOGAN, JR. 1123

On the Initial Vertical Descent of a Helicopter Following Power Failure . . . . . B. W. MCCORMICK, JR. 1125

Comment on the Reliability of the Strength of Stiffened Cylinders in Bending and/or Compression . . . . . BERTRAM KLEIN 1126

The Asymptotic Turbulent Boundary Layer . . . . . R. A. DUTTON 1127

Effects of Free-Steam Vorticity on the Behavior of a Viscous Boundary Layer . . . . . TING YI LI 1128

A Shock-Free Airfoil . . . . . H. C. LEVEY 1129

Remarks on the Convergence of an Iterative Procedure in Solving Dynamic Response Problems

Tse-Sun Chow
Scientific Laboratory, Ford Motor Company, Dearborn, Mich.

July 11, 1956

IN A RECENT research note,[1] Hua Lin examined the rate of convergence of an iterative procedure in solving dynamic response problems by plotting graphically the successive approximations of the following equation:

$$\xi'' + 2\zeta\xi' + \xi = 1 \tag{1}$$

where ξ is the nondimensional displacement, ξ' its derivative with respect to the nondimensional time τ, and ζ the damping ratio, the initial conditions being $\xi(0) = \xi'(0) = 0$. The iterative procedure is defined by

$$\left.\begin{aligned} \xi''_0 + \xi_0 &= 1 \\ \xi_0(0) &= \xi'_0(0) = 0 \end{aligned}\right\} \tag{2}$$

and

$$\left.\begin{aligned} \xi''_n + \xi_n &= 1 - 2\zeta\xi'_{n-1} \\ \xi_n(0) &= \xi'_n(0) = 0 \\ n &= 1, 2, 3, \ldots \end{aligned}\right\} \tag{3}$$

where ξ_n denotes the nth approximation. Lin made the observation that the rate of convergence deteriorates rapidly with high damping ratio ζ and particularly at large values of time, τ. It is a matter of interest to examine further the validity of such a procedure. In this note we shall prove that, for this problem, the successive approximations will converge to the actual solution for all values of ζ and τ. It appears, therefore, for large values of ζ and τ, high order of approximations are required.

By treating the right-hand side of the differential equation of Eq. (3) as known functions of τ, the solution of Eq. (3) can be put in the following form:

$$\xi_n = A \sin \tau + B \cos \tau + \left\{1/[(d^2/d\tau^2) + 1]\right\}\left\{1 - 2\zeta\xi'_{n-1}\right\} \tag{4}$$

and, by applying the boundary conditions $\xi_n(0) = \xi'_n(0) = 0$, Eq. (4) is reduced to

$$\xi_n(\tau) = 1 - \cos \tau - 2\zeta \int_0^\tau \xi_{n-1}(t) \cos (\tau - t)dt \tag{5}$$

Thus,

$$\xi_n(\tau) - \xi_{n-1}(\tau) = -2\zeta\int_0^\tau [\xi_{n-1}(t) - \xi_{n-2}(t)] \cos (\tau - t)\, dt \tag{6}$$

$n = 2, 3, \ldots$

and

$$\xi_n(\tau) - \xi_{n-1}(\tau) = (-2\zeta)^{n-1}\int_0^\tau\int_0^{t_{n-1}}\cdots\int_0^{t_2} [\xi_1(t_1) - \xi_0(t_1)] \times \cos (\tau - t_{n-1}) \ldots \cos (t_2 - t_1)\, dt_1 \ldots dt_{n-1} \tag{7}$$

Hence

$$\left.\begin{aligned} |\xi_n(\tau) - \xi_{n-1}(\tau)| &\leqq (2\zeta)^{n-1} \int_0^\tau \int_0^{t_{n-1}} \cdots \int_0^{t_2} |\xi_1(t_1) - \xi_0(t_1)|\, dt_1 \cdots dt_{n-1} \\ &= \frac{(2\zeta)^{n-1}}{(n-2)!} \int_0^\tau (\tau - t_1)^{n-2} \times |\xi_1(t_1) - \xi_0(t_1)|\, dt_1 \end{aligned}\right\} \quad (8)$$

It is easy to find from Eqs. (2) and (3) that

$$\xi_1(\tau) - \xi_0(\tau) = \zeta(\tau \cos \tau - \sin \tau) \quad (9)$$

so that

$$\left.\begin{aligned} |\xi_1(\tau) - \xi_0(\tau)| &\leqq \zeta \sqrt{1 + \tau^2} \\ &\leqq \zeta (1 + \tau) \end{aligned}\right\} \quad (10)$$

since $\tau > 0$. Substituting Eq. (10) into Eq. (8) we have

$$\left.\begin{aligned} &|\xi_n(\tau) - \xi_{n-1}(\tau)| \\ &\leqq \frac{(2\zeta)^{n-1}\zeta}{(n-2)!} \int_0^\tau (\tau - t_1)^{n-2}(1 + t_1)\, dt_1 \\ &= \frac{2^{n-1}\zeta^n}{(n-2)!} \left\{(1 + \tau) \int_0^\tau (\tau - t_1)^{n-2} dt_1 - \int_0^\tau (\tau - t_1)^{n-1} dt_1\right\} \\ &= 2^{n-1}\zeta^n \tau^{n-1} [(n + \tau)/n!] \end{aligned}\right\} \quad (11)$$

Thus, the series

$$\xi_0(\tau) + \sum_{n=1}^{\infty} \{\xi_n(\tau) - \xi_{n-1}(\tau)\}$$

converges uniformly and absolutely for all given values of ζ and τ and $\lim_{n \to \alpha} \xi_n(\tau) = \xi(\tau)$ is the solution required of Eq. (1).

Reference

[1] Lin, Hua, *On the Convergence of an Iterative Procedure in Solving Dynamic Response Problems*, Readers' Forum, Journal of the Aeronautical Sciences, Vol. 23, No. 4, p. 391, April, 1956.

Axial Compression Buckling of a Pressurized Cylinder with a Thermally Induced Ring Compression

Leonard A. Harris*
Senior Structures Engineer, Missile Development Division, North American Aviation, Inc., Downey, Calif.
July 12, 1956

MODERN, AERODYNAMICALLY HEATED, supersonic aircraft structures must resist thermally induced stresses and deformations in addition to those stresses and deformations caused by external loads. The effect of the thermal stresses superimposed on other stress conditions is not always readily apparent.

The experimental investigation reported herein was performed to establish the effect of one particular thermal condition on the axial compressive buckling strength of a ring-stiffened, pressurized cylinder. The thermal condition investigated is one in which a circumferential line load is induced at the mid-height of the cylinder by refrigerating the ring and heating the skin. The applied load is a uniform axial compression. This combination of thermally and externally applied stresses would simulate a flight condition in which the skin is aerodynamically heated and the ring is kept cool by immersion in fuel.

Axial compressive buckling stresses were obtained from two model cylinders which were rolled from half-hard 18-8 stainless steel ($E = 27.0 \times 10^6$ psi). The cylinders were fabricated with a single longitudinal seam weld and had a radius of 8.75 in., a length of 24 in., and a thickness of 0.0087 in. The length of the cylinder was perpendicular to the direction of rolling.

* The author gratefully acknowledges the assistance of his colleagues of the Stress Design Data and Methods Unit and of the personnel of the Missile Test Laboratory.

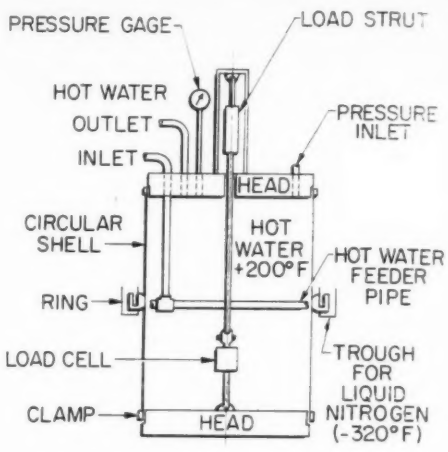

FIG. 1. Schematic view of test specimen.

An aluminum ring was machined to provide a room temperature force fit on the outside of the cylinder. As indicated in Fig. 1, the ring, which was very stiff compared to the thickness of the shell, was not attached to the shell but bore against the shell at mid-height with a moderate force fit pressure. The ends of the cylinders were clamped by straps to the 3-in. thick, circular aluminum head plates of the test jig. When placed in the jig, the weight of the ring was supported by three wires which were connected to the frame of the test jig.

The cylinder was heated internally by circulating hot water inside the tank at a temperature of 200°F. A pipe directed a constant flow of hot water against the skin which was in contact with the ring at the mid-height of the cylinder. When a temperature of approximately 200°F. was attained, liquid nitrogen was poured into the trough around the external ring. Before applying the axial compressive loading, the cylinder and ring were allowed to reach equilibrium temperature. At equilibrium, the skin temperature 1/4 in. from the point of contact of the ring and the shell was about 180°F., and the ring temperature averaged about −200°F. across the section. The thermal de-

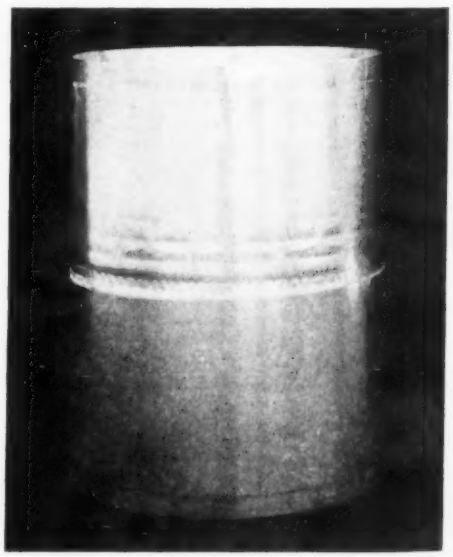

FIG. 2. Buckle pattern on tested cylinder.

formation of the aluminum ring with respect to the steel cylinder was greater than if the ring and cylinder had been made of the same material because of the greater thermal coefficient of contraction of aluminum as compared to steel.

After attaining temperature equilibrium, the internal pressure was increased to 14 psi, and a uniform axial compressive loading was applied by a central internal strut until the cylinder buckled. The critical buckling stresses for the two cylinders were 11,500 psi and 10,050 psi. Fig. 2 shows one of the cylinders after removal from the test jig and after the ring had been pressed off. Two distinct buckle regions are visible. The larger buckles, above the mid-height of the cylinder, are the axial compression buckles which had wave lengths of about 1 in. in the longitudinal direction and about $4^1/_2$ in. in the circumferential direction. Before the load was removed, these buckles were of the diamond shape typical for compression buckles of unstiffened cylinders.

The smaller buckles, which run circumferentially around the tank at mid-height, were caused by the thermal expansion of the skin and contraction of the ring. It is believed that these smaller buckles were present before the axial compression loading had been applied. The circumferential buckles were about $1^1/_4$ in. from crest to crest and about 1 in. wide.

Unstiffened cylinders of the same geometry had previously been tested at room temperature under axial compression with internal pressure. Comparison of the present tests with the unstiffened-cylinder tests indicated that the ring-stiffened cylinders failed at stresses within the lower portion of the scatter band obtained from the tests of the unstiffened cylinders. Therefore, this thermally induced circumferential line load did not appreciably lower the axial compressive buckling strength of these cylinders. A full-scale structure of similar geometrical configuration might likewise be capable of resisting the effects of this type of thermal condition superimposed on an axial compressive load.

A Study of the Applicability of Rabotnov's Creep Parameter for Aluminum Alloy

Fred H. Turner and Kurt E. Blomquist
Stress Office, SAAB Aircraft Company, Linköping, Sweden
July 19, 1956

REFERENCE 1, which is an NACA translation of a paper by Y. N. Rabotnov, has apparently not been observed by creep specialists in Western aeronautical circles. This note is intended to show that at least one expression due to Rabotnov can give useful results for transforming creep curves from one stress level to another. This method is a useful complement to the well-known Larson-Miller parameter which permits transformation of creep data from one temperature level to another.

It has been shown by Rabotnov[1] that it is possible to transform a family of isochronic creep curves to a single master curve by using a suitable parameter. This parameter is

$$\varphi(\epsilon) = \sigma(1 + a \cdot t^{1/3}) \qquad T = \text{const.}$$

where a is a constant which is characteristic for the material and temperature in question, σ is stress, ϵ is strain, t is time, and T is temperature. Thus, for every given value of the strain ϵ, the equation shows the relation between the stresses σ_i and the corresponding times t_i. When $t = 0$, $\varphi = \sigma$—e.g., the master curve coincides with the tensile stress-strain curve at high strain rate, see Fig. 1.

Applications

(A) Given a tensile stress-strain curve and one point on a creep curve at a certain stress, Rabotnov's parameter provides a possibility for predicting creep curves at other stresses. Creep results in reference 2 have been used in order to illustrate this

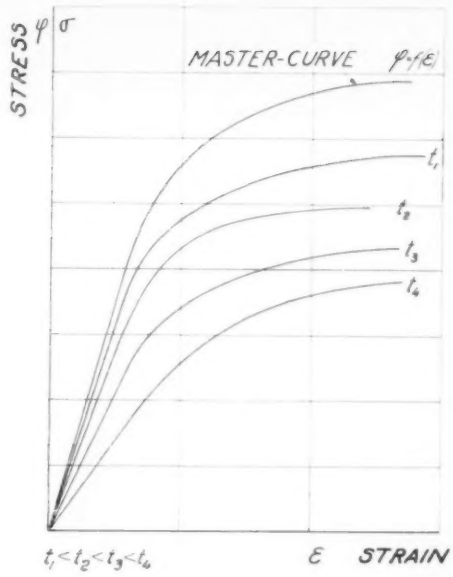

FIG. 1. Family of isochronic stress-strain curves and master curve.

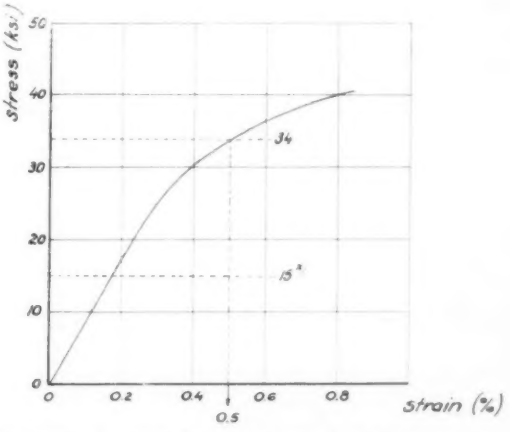

FIG. 2. Stress-strain curve for 24S-T3 Alclad Sheet 450°F.

TABLE 1
24S-T3 Alclad Sheet 450°F.

Data from WADC TR 53-24, Part I		
Stress (psi)	Time to 0.5% Total strain (hours)	Predicted values (hours)
a) 15000	86.0	
17000	37.0	41.1
20000	16.0	14.0
22000	6.0	6.6
25000	3.5	1.9
30000	0.15	0.10

point. The first and second columns in Table 1 have been taken from reference 2, and the third column has been tabulated as follows. The first line in Table 1 gives the time 86 hours for 0.5 per cent total strain when the stress is 15,000 psi. The stress-strain curve in Fig. 2 shows that $\sigma = 34{,}000$ psi gives 0.5 per cent strain in an ordinary tensile test. Using this value of σ as the corresponding φ-value in the equation enables us to determine a as follows:

$$34{,}000 = 15{,}000 \cdot (1 + a \cdot 86^{1/3}) \qquad a = 0.29 \text{ (hours)}^{-1/3}$$

The times for the same total strain at other stresses have been calculated, and a comparison with actual results is shown in Table 1.

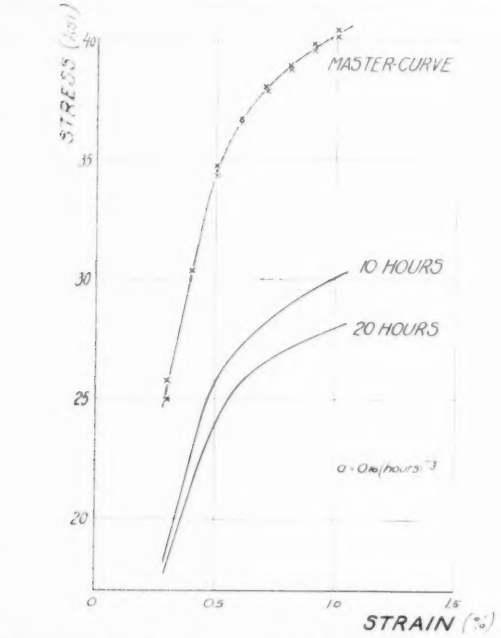

FIG. 3. Evaluation of constant a and construction of master curve for 24S-T3 at 400°F.

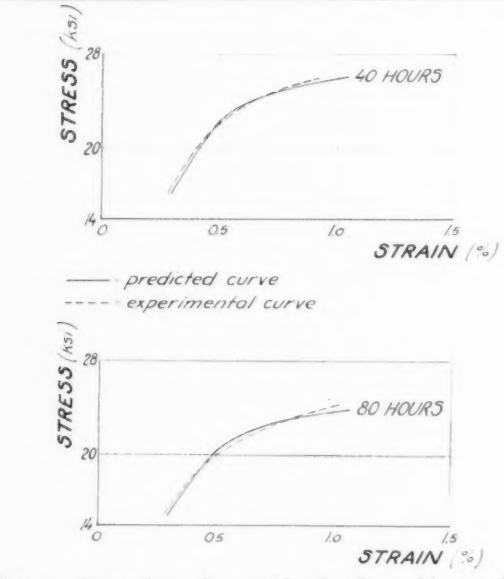

FIG. 4. Comparison of extrapolated values with actual test results for 24S-T3 at 400°F.

TABLE 2
24S-T3 400°F.

Data from ASTM Vol 49			Predicted values (psi)
Total strain (%)	Time (hours)	Stress (psi)	
0.54	100	20000	20400
0.30	100	15000	14600
1.0	200	20000	20800
0.35	200	15000	14400
0.44	400	15000	15000
0.5	600	15000	14700
0.6	800	15000	14700
0.7	1000	15000	14600

(B) A tensile stress-strain curve may not always be obtainable. In this case the master curve can be determined from two isochronic stress-strain curves, where the times can be rather short. At any given value of the strain, corresponding points on the two curves make it possible to calculate the constant a which enables the master curve to be constructed (Fig. 3). Some slight variation in the value of a may be expected at various values of the strain. A mean value has been used for the whole of the master curve in Fig. 3.

It is now possible to predict stress-strain curves for other and longer times. This is shown in Fig. 4 and Table 2 together with the actual test results.[3] The master curve of Fig. 3 is used in this calculation.

These investigations cannot be claimed to prove the universal applicability of Rabotnov's parameter, but the results must be considered satisfactory for aluminum alloy of 24S-T type within the temperature-time-stress region of interest in current aircraft design.

REFERENCES

[1] Rabotnov, Y. N., *Some Problems of the Theory of Creep*, NACA TM 1353, April, 1953.

[2] Guarnieri, G. J., *Intermittent Stressing and Heating Tests of Aircraft Structural Metals*, WADC Technical Report 53-24, May, 1954.

[3] Dorn, J. E., and Tietz, T. E., *Creep and Stress-Rupture Investigations on Some Aluminum Alloy Sheet Metals*, ASTM Proceedings, Vol. 49, 1949.

An Approximate Solution to Supersonic Conical Flow

Henry E. Fettis
Aeronautical Research Laboratory, Wright Air Development Center, ARDC, Wright-Patterson AFB, Ohio

July 23, 1956

THE EQUATIONS which determine the supersonic flow field of an adiabatic gas about an unyawed cone may be written

$$\left.\begin{aligned}(d^2u/d\theta^2) + u &= [a^2(u + v\cot\theta)/(v^2 - a^2)]\\ a^2 &= [(\gamma - 1)/2]\,(c^2 - u^2 - v^2), \quad v = du/d\theta\end{aligned}\right\} \tag{1}$$

In the above equations, u is the velocity component in the radial direction, v the component in the normal direction, θ the angle between the cone axis and the radial direction, a the local speed

of sound, and c a constant which, for any given problem, may be considered as known. (See further, reference 1.) Thus all of the quantities u, v, and a may be regarded as referred to c as unity.

The standard technique for handling the system of Eqs. (1) is to integrate numerically starting with the conditions

$$\left.\begin{aligned} u(\theta_0) &= u_0 \\ v(\theta_0) &= 0 \end{aligned}\right\} \tag{2}$$

where θ_0 is the semiapex angle and u_0 is some number between 0 and unity. The solution is continued until the shock conditions (see reference 1) are satisfied. At this point, a corresponding value is obtained for the Mach Number of the free stream. This procedure has been carried out in reference 1 for numerous values of u_0 and θ_0. The results show that, for small apex angles and Mach Numbers above 2, the shock conditions are met before the component v has become appreciably large. In such cases, it can be seen that if the first equation of Eqs. (1) is rewritten in the form

$$(d^2u/d\theta^2) + \cot\theta(du/d\theta) + 2u = [v^2/(v^2 - a^2)]\,(u + v\cot\theta) \tag{3}$$

and that if v^2 is small compared with a^2 (this is certainly true near the cone wall), then a reasonable approximation can be expected if Eq. (3) is replaced by

$$(d^2u/d\theta^2) + \cot\theta(du/d\theta) + 2u = 0 \tag{4}$$

subject to the conditions

$$\left.\begin{aligned} u(\theta_0) &= u_0 \\ u'(\theta_0) &= 0 \end{aligned}\right\} \tag{5}$$

The general solution of Eq. (4) is

$$u = A\cos\theta + B\{1 + \cos\theta\ln[\sin\theta/(1 + \cos\theta)]\} \tag{6}$$

and, by differentiation,

$$+v = -A\sin\theta + B\{\cot\theta - \sin\theta\ln[\sin\theta/(1 + \cos\theta)]\} \tag{7}$$

The initial conditions of Eqs. (5) give

$$\left.\begin{aligned} A &= u_0\{\cos\theta_0 - \sin^2\theta_0\ln[\sin\theta_0/(1 + \cos\theta_0)]\} \\ B &= u_0\sin^2\theta_0 \end{aligned}\right\} \tag{8}$$

Eq. (4) is the same as would have been obtained if the fluid had been assumed incompressible ($a^2 = \infty$). Nevertheless, the solutions of Eq. (4) do not deviate appreciably from Kopal's values even when v itself is no longer small. In fact, by comparing the solutions of Eq. (4) with the more exact solutions, a maximum error of 1.5 per cent of the total velocity in the u-component and 5.3 per cent in the v-component was found to exist over the complete range of the table. The greatest errors were found when the free-stream Mach Number was close to unity and occurred at the largest value of θ in each case. For Mach Numbers above 3, the maximum error was found to be about 2 per cent.

The approximations given by Eqs. (6) through (8) represent a substantial improvement over that given by the isothermal solution:[1]

$$\begin{aligned} u &= u_0\cos(\theta - \theta_0) \\ -v &= u_0\sin(\theta - \theta_0) \end{aligned}$$

The improvement is greatest in the v-component which, according to the isothermal solution, may be in error by as much as a factor of two. Table 1 gives a comparison of the three solutions for two typical sets of initial values.

TABLE 1

	Numerical Solution[1]		Approximation of Eqs. (6), (7)		Isothermal Solution	
	$\theta_0 = 5°$, $u_0 = 0.4$, $M = 1.01$					
θ	u	$-v$	u	$-v$	u	$-v$
5°	0.40000	0	0.40000	0	0.40000	0
20	0.38144	0.12973	0.38149	0.12939	0.38637	0.10353
35	0.33419	0.22849	0.33437	0.22766	0.34641	0.20000
50	0.26333	0.30961	0.26380	0.30821	0.28284	0.28284
65	0.17395	0.36935	0.17480	0.36711	0.20000	0.34641
80	0.07206	0.40520	0.07379	0.40073	0.10353	0.38637
	$\theta_0 = 20°$, $u_0 = 0.8$, $M = 4.15$					
20°	0.80000	0	0.80000	0	0.80000	0
21	0.79976	0.02733	0.79975	0.02729	0.79988	0.01396
22	0.79905	0.05374	0.79904	0.05341	0.79951	0.02792
23	0.79789	0.07954	0.79789	0.07850	0.79899	0.04187
24	0.79628	0.10504	0.79632	0.10270	0.79805	0.05581
25	0.79422	0.13050	0.79432	0.12608	0.79695	0.06973

REFERENCE

[1] Kopal, Z., *Tables of Supersonic Flow Around Cones*, Massachusetts Institute of Technology, Technical Report No. 1, 1947.

Erratum—"Applied Aerodynamics and Flight Mechanics"*†

W. Bailey Oswald
Chief—Aerodynamics Section, Santa Monica Division, Douglas Aircraft Company, Inc., Santa Monica, Calif.
August 31, 1956

ON PAGE 473* the paragraph including Eq. (4) should be expanded to include both the local and mean coefficients of turbulent skin friction as shown below:

". . . shown approximately in Fig. 2 and given by the relations[1] for turbulent skin-friction coefficients as follows:

Local, c_f:

$$1/c_f^{1/2} = 1.7 + 4.15\log_{10}(R_X c_f) \tag{4}$$

Mean, C_f:

$$0.242/C_f^{1/2} = \log_{10}(R_X C_f) \quad \text{(K. E. Schoenherr)} \tag{4.1}$$

An increment . . ."

* Journal of the Aeronautical Sciences, Vol. 23, No. 5, pp. 469–484, May, 1956.

† See also errata given in the Journal of the Aeronautical Sciences, Vol. 23, No. 9, p. 892, September, 1956.

Nitric Oxide Formation in Hypersonic Flow*

J. G. Logan, Jr.
Head—Theoretical Flow Physics Section, Aerodynamic Research Department, Cornell Aeronautical Laboratory, Inc., Buffalo
July 23, 1956

THE HIGH TEMPERATURES resulting from high-speed flight within the earth's atmosphere are sufficient to cause partial dissociation and ionization of the nitrogen and oxygen molecules as well as the formation of new components. Between flight Mach Numbers of 12 and 20, the high temperatures achieved behind normal shock waves may lead to the formation of NO, NO_2, N_2O, and NO^+ in addition to O_2^- and the atomic species usually associated with the process of dissociation—namely, O, N, O^-, O^+, and N^+ which have been studied by Bethe and Teller[1] and Wood.[2] Also, of course, free electrons are present according to the degree of ionization.

Apart from the thermal excitation of the higher vibrational and rotational states of the air constituents at high temperatures, any variation in chemical composition must obviously influence the aerodynamic characteristics of the flowing medium through changes in molecular weight and specific heat.[3, 4] In assessing the effect of these chemical changes, one must know the equilibrium concentration of the various constituents.[5, 6, 7] However, it is equally important to have knowledge of the rate at which the real gas equilibrium is achieved since understanding of aero-

* The investigations of the NO reaction described were sponsored by the Air Research and Development Command under Contract AF 18(600)-1332.

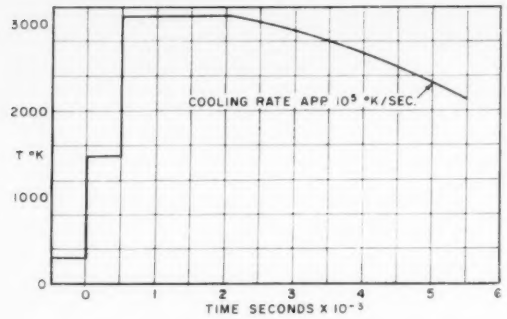

FIG. 1. Chemical shock-tube temperature pulse.

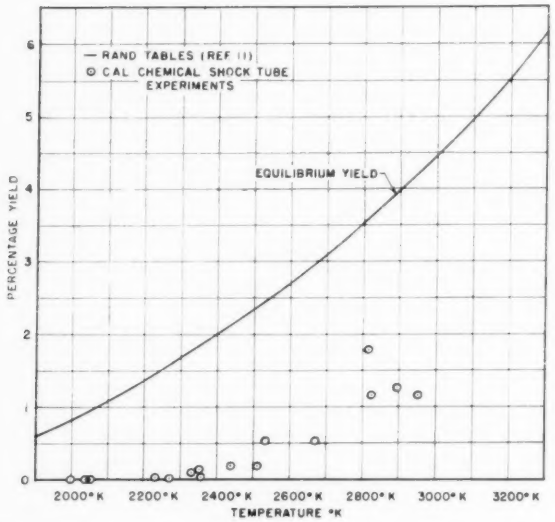
— RAND TABLES (REF 11)
⊙ CAL CHEMICAL SHOCK TUBE EXPERIMENTS
EQUILIBRIUM YIELD
PERCENTAGE YIELD
0 1 2 3 4 5 6
2000°K 2200°K 2400°K 2600°K 2800°K 3000°K 3200°K
TEMPERATURE °K

FIG. 2. Percentage yield of nitric oxide vs. temperature, °K.

dynamic heating effects and boundary-layer phenomena depend to a large extent upon the rates of dissociation and recombination. Relatively small concentrations of components may have large effects, as for example, heating produced by recombination of oxygen atoms at a surface.[8]

From the analyses of Bethe and Teller[1] and Wood,[2] one would conclude that the rates of dissociation of O_2 and N_2 are such that the presence of atomic oxygen may be neglected below 3,000°K. (5,400°R.) and atomic nitrogen below 6,000°K. (10,400°R.) below flight Mach Numbers of 10 and 16, respectively, because of the long relaxation path length required. At these temperatures, free oxygen and nitrogen are present in approximately 1 per cent concentration in thermal equilibrium at pressures greater than 10 atmospheres. Bethe and Teller assume that, when the final equilibrium concentration of the dissociated constituent is small—of the order of 1 per cent—the time required to reach the equilibrium state is large since two molecules must collide with a relative energy at least equal to the dissociation energy. When the final concentration of the dissociated constituent is small, the number of molecules possessing energy sufficient to bring about the dissociation would also be small and effective collisions infrequent. Consequently, they concluded that the relaxation time or corresponding relaxation path length would be large, at least of the order of the projectile or missile length.

Recent experiments at Cornell Aeronautical Laboratory, Inc., suggest that the relaxation time for the formation of free oxygen may be much shorter than one would conclude from these theoretical investigations, and, consequently, it may not be possible to neglect the formation of free oxygen at temperatures of the order of 3,000°K. Nevertheless, even if the conclusions of Bethe and Teller and Wood are correct in regard to formation of free oxygen and nitrogen, additional thermal reactions occur which may have significant aerodynamic effects at 3,000°K. In particular, the reaction $N_2 + O_2 \leftrightarrows 2\,NO$ occurs at temperatures below 3,000°K., and 1 per cent concentrations can be obtained at temperatures of about 2,000°K. Investigations of the reaction rates for the formation and decomposition of NO are being carried out at Cornell Aeronautical Laboratory. These experiments are being conducted in a shock tube designed to yield a single controlled pressure and temperature pulse of several milliseconds' duration (Fig. 1). When the reactant gas, air, is processed by a pulse of this type at the end of the constant temperature heating period, the gas is cooled rapidly by an expansion fan at the rate of about 500,000°K. per sec.

This cooling rate is so rapid that the reverse reaction $2NO \rightarrow O_2 + N_2$ cannot proceed fast enough to achieve the equilibrium concentration of NO at each instant during cooling. Thus, a low temperature is reached with a gas which retains much of the NO corresponding to the high temperature. Because the reverse NO reaction (as well as the forward reaction) is very slow at temperatures below about 1,500°K., the high-temperature NO concentration is, in effect, partially frozen and can be subjected to leisurely chemical analysis at room temperature.

Fig. 2 shows the result of some recent measurements of nitric oxide formation from air. Equilibrium amounts of nitric oxide were not achieved in the low-temperature region of the curve because the reaction rate and heating time were small. At higher temperatures, the reaction rates were large, and, although equilibrium amounts of nitric oxide were apparently formed, the cooling rates were inadequate to freeze the high-temperature equilibrium. From studies of this type, it is possible to determine the reaction rate and the equivalent reaction path length. At 2,000°K. (3,600°R.), the reaction time was calculated to be approximately 70 millisec. decreasing to approximately 1.5 millisec. at 2,800°K. (5,100°R.). At approximately 3,000°K. (5,400°R.), the reaction time becomes sufficiently short—less than one half a millisecond—so that the full equilibrium concentration can be achieved behind a shock wave ahead of a blunt body.

Since the air just outside the boundary layer of a blunt body traveling at hypersonic speeds may be processed by a temperature pulse similar to that employed in the chemical shock tube, it is possible for the full equilibrium concentration of NO attained behind the shock to be frozen as the air particles accelerate away from the stagnation point. Fig. 3 shows the temperature pulse encountered outside the boundary layer of a 1-ft. diameter sphere at a flight Mach Number of 10. The calculated cooling rate is large enough to freeze the equilibrium concentration of NO attained behind the shock. Since the NO reaction is exothermic, it is possible for boundary-layer heating to occur as a result of the breakdown of this nonequilibrium concentration as it enters into and diffuses within the boundary layer. The "freezing" process

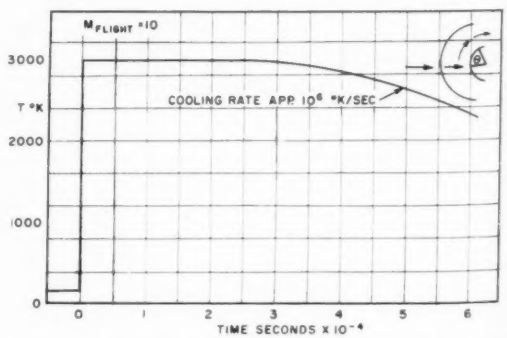

FIG. 3. Typical temperature pulse encountered by fluid particle on a sphere (1-ft. radius).

does not apply strictly to free oxygen and nitrogen atoms since they are not stable at room temperatures. Information is not as yet available as to the recombination rates for these atoms, and it may be possible that the relaxation time is comparable to the times of interest in hypersonic flight problems.

The nitric oxide concentration is also of importance because NO is the first component to ionize, and, at relatively low temperatures, sufficient free electrons may be formed to cause the air behind normal shock waves to become highly conductive. At temperatures of about 5,000°K. (9,000°R.) in thermal equilibrium, there are approximately 10^{13} free electrons per cu.cm. produced almost entirely by thermal ionization of NO. Calculations indicate that, at flight Mach Numbers of 15, the conductivity of the air behind a normal shock wave becomes equivalent to that of sea water, 5 mhos per meter. Knowledge of the electron concentration is also important because electrons may become efficient carriers of heat if sufficient concentrations of electrons are obtained.

At approximately the same temperature conditions at which NO formation occurs, small quantities of NO_2 are formed. Knowledge of this component may be necessary in investigations of radiation phenomena.

In summary, we conclude that, although the dissociation reaction for nitrogen may not have a significant aerodynamic effect below flight Mach Numbers of approximately 16, the breakdown of nitrogen to form other compounds occurs to a significant extent at temperatures as low as 3,000°K., and the resultant aerodynamic effects may not be negligible even at flight Mach Numbers as low as 10.

References

[1] Bethe, H., and Teller, E., *Deviations from Thermal Equilibrium in Shock Waves*, BRL Report No. X-117.

[2] Wood, G. P., *Calculations of the Rate of Thermal Dissociation of Air behind Normal Shock Waves at Mach Numbers of 10, 12, and 14*, NACA TN 3634, April, 1956.

[3] Squire, W., and Logan, J. G., *Real Gas Effects in Hypersonic Flow* (to be published).

[4] Squire, W., Hertzberg, A., and Smith, W. E., *Real Gas Effects in a Hypersonic Shock Tunnel*, AEDC-TN-55-14, March, 1955.

[5] Hilsenrath, J., and Beckett, C. W., *Thermodynamic Properties of Argon Free Air*, NBS Report No. 3991, April, 1955.

[6] Gilmore, L. R., *Equilibrium Composition and Thermodynamic Properties of Air to 24,000°K*, Rand Report No. 1543, August, 1955.

[7] Hirschfelder, J. O., and Curtiss, C. F., *Thermodynamic Properties of Air*, University of Wisconsin Report CM-518, December, 1948.

[8] Hirschfelder, J. O., *Heat Transfer in Chemically Reacting Gas Mixtures*, University of Wisconsin Report WIS-ONR-18, February, 1956.

[9] Hertzberg, A., *The Application of the Shock Tube to the Study of the Problems of Hypersonic Flight*, Jet Propulsion, May, 1956.

[10] Romig, M. F., *The Normal Shock Properties of Air in Dissociation Equilibrium*, Journal of the Aeronautical Sciences, Readers' Forum, Vol. 23, No. 2, pp. 185–186, February, 1956.

[11] Krieger, F. J., and White, W. B., *The Composition and Thermodynamic Properties of Air*, Rand Corp. Report No. R-149, April, 1949.

On the Initial Vertical Descent of a Helicopter Following Power Failure

B. W. McCormick, Jr.
Aero Group Engineer, Vertol Aircraft Corporation, Morton, Pa.

July 26, 1956

RAPID ESTIMATES of the rotor-speed decay and descent velocity of a helicopter following power failure can be made which, for the first 2 or 3 sec., agree closely with more exact calculations.

Consider a single-rotor helicopter. The equation of motion in the vertical direction would be

$$(d^2y/dt^2) = g[1 - (T/W)] \tag{1}$$

where

T = rotor thrust
W = weight of helicopter
y = vertical direction positive downward

The equation of motion of the rotor would be

$$J(d\omega/dt) = Q_s - Q_a \tag{2}$$

where

J = rotor moment of inertia
Q_s = shaft torque tending to increase ω
Q_a = aerodynamic torque tending to decrease ω
ω = angular velocity of rotor

Providing the helicopter does not reach an appreciable velocity of descent or providing the rotor collective pitch angle is not changed, the thrust and aerodynamic torque can be expressed approximately as

$$T = K_T\omega^2 \tag{3}$$

$$Q_a = K_Q\omega^2 \tag{4}$$

Before power failure, the aerodynamic torque and the shaft torque are equal. Also, the thrust of the rotor is equal to the weight of the helicopter. Thus,

$$K_T = W/\omega_0^2 \tag{5}$$

$$K_Q = Q_{s_0}/\omega_0^2 \tag{6}$$

where

ω_0 = rotor angular velocity before power failure
Q_{s_0} = shaft torque before power failure

After power failure, $Q_s = 0$. Substituting Eqs. (3), (4), (5), and (6) into Eqs. (1) and (2) and integrating, the descent velocity and rotor decay can be expressed as

$$\omega/\omega_0 = 1/[1 + (Q_{s_0}t/J\omega_0)] \tag{7}$$

$$dy/dt = gt^{\frac{1}{2}}t/[t + (J\omega_0/Q_{s_0})]^{\frac{1}{2}} \tag{8}$$

It can be seen immediately from these equations that the greater the ratio of rotor angular momentum to shaft torque at the time of power failure, the smaller the rate of decay of rotor speed and, hence, the smaller the vertical acceleration of the helicopter.

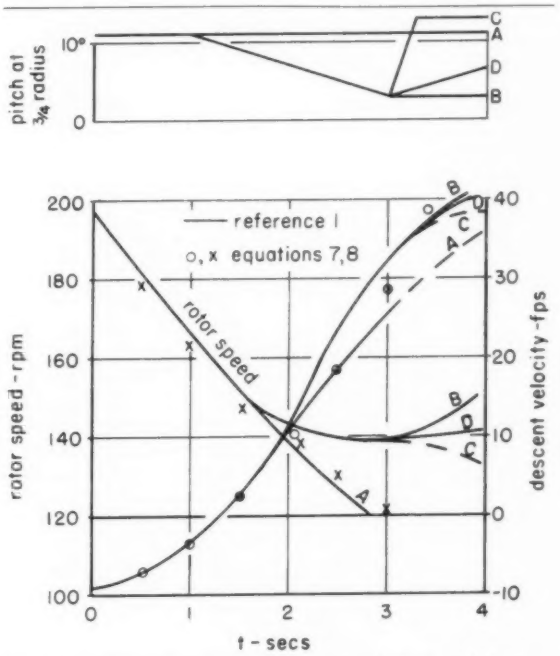

FIG. 1. Comparison of predicted rotor-speed decay and descent velocity with reference 1.

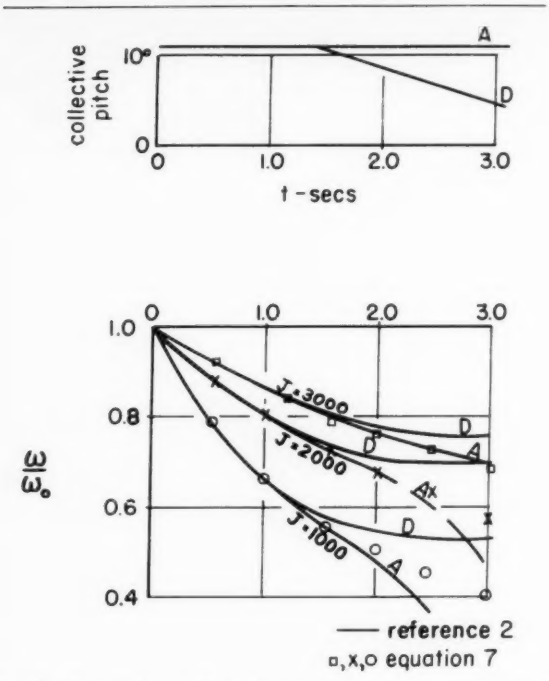

FIG. 2. The predicted effect of moment of inertia on rotor-speed decay as compared with reference 2.

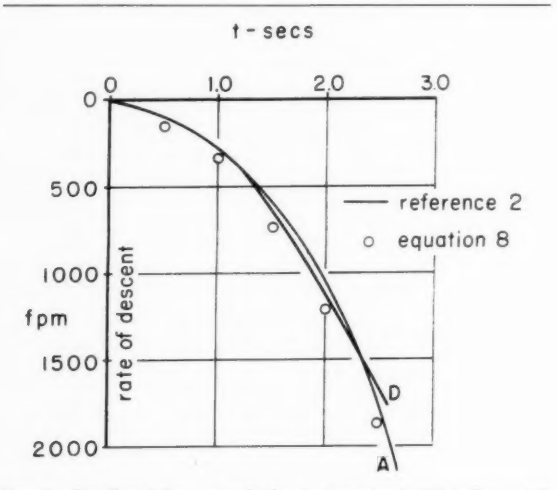

FIG. 3. Predicted descent velocity as compared with reference 2 (J = 1,000).

Eqs. (7) and (8) are compared with the calculated results of reference 1 in Fig. 1 and with the results of reference 2 in Figs. 2 and 3. In the case of reference 2, the information given in the reference was not sufficient to determine the constant Q_{s_0}/ω_0. This was, therefore, chosen to satisfy the ω/ω_0 curve for J = 1,000 slug ft.², and then the rate of descent and ω/ω_0 curves for the other rotor moments of inertia were calculated using this same constant.

The simple approximations of Eqs. (7) and (8) and the more exact calculations of the references are seen to be in substantial agreement.

REFERENCES

[1] Katzenberger, E. F., and Rich, M. J., *An Investigation of Helicopter Descent and Landing Characteristics Following Power Failure*, Journal of the Aeronautical Sciences, Vol. 23, No. 4, pp. 345–356, April, 1956.

[2] Stewart, W., and Sissingh, G. J., *Notes on Helicopter Rotor Behavior after Engine Failure in Hovering Flight*, Gt. Brit. ARC R&M No. 2659, May, 1949.

Comment on the Reliability of the Strength of Stiffened Cylinders in Bending and/or Compression

Bertram Klein

Senior Engineer—Structures, Missile Development Division, North American Aviation, Inc., Downey, Calif.

July 27, 1956

IN A RECENT PAPER,[1] some doubt was expressed concerning the reliability of tests (and presumably calculations) made on stiffened cylinders under axial or bending loading. The contention is that stiffened-cylinder test (and possibly calculation) data exhibit the same large random scatter as unstiffened-cylinder data. It is the purpose of this note to show that in many practical cases this belief is not justified.

For purposes of discussion, stiffened cylinders are divided into two broad types:

(1) *Skin-Buckling Stiffened Cylinders.*—In many practical cases, the skin is made thin and allowed to buckle well below the collapse load of the stiffened cylinder. The structure then is a gridwork of stringers and frames connected by a buckled medium still capable of resisting shearing action. This type is called skin-buckling stiffened cylinders. Let us consider the test data given in Table 1 for such thin-walled skin-buckling cylinders.[2] The specimens were of the same nominal dimensions.

Next, consider the results of calculations for thin-walled skin-buckling cylinders loaded in pure bending[3] shown in Table 2.

All of the cylinders discussed failed in the general instability mode. However, similar degrees of accuracy can be shown for stiffened cylinders that fail in a panel instability mode.

(2) *Orthotropic Cylinders.*—When the skin gage is large enough (or the stiffening elements close enough together) so that no skin buckling occurs prior to failure, the stiffened cylinder may be considered to fall into the orthotropic-cylinder category. In many such practical cases, the test scatter band is still within reasonable limits. For example, consider the test data of Table 3 for stringer-stiffened orthotropic cylinders.[4] Notice that the deeper the stringer compared to the sheet gage t, the less the scatter.

TABLE 1

Test Cylinder No.		Sheet Gage	Type Test	Maximum Compression Load	Maximum Bending Moment	% Deviation in Bending Moment
PIBAL	5	0.02	B	0	308,000	
	6	0.02	B	0	359,000	15
	7	0.02	B&C	13,000	296,000	
	8	0.02	B&C	14,600	302,000	2
	9	0.012	B&C	13,900	227,000	
	10	0.012	B&C	14,200	249,000	10
	12	0.02	B&C	7,400	336,000	
	13	0.02	B&C	7,200	362,000	7

TABLE 2

Cylinder	Maximum Compressive —Strain × 10^3— theory	test	% Deviation
PIBAL 11	22.59	20.86	8.3
PIBAL 54	18.13	16	13.3
GALCIT	17.2	14.0	22.9
GALCIT 30	34.14	29.5	15.8

TABLE 3

Specimen No.	$\frac{l}{r}z^*$	t	Stiffener: Spacing	Stiffener: Width	Stiffener: Depth	Maximum Compressive Load	% Deviation
13	4.45	0.050	3.56	0.255	.090	5,600	
20	1.63	0.050	3.54	0.246	.090	4,460	23
14	4.46	0.052	3.56	0.252	.186	6,650	
21	1.65	0.051	3.49	0.256	.192	5,400	19
15	4.46	0.053	3.56	0.258	.290	8,370	
22	1.64	0.052	3.51	0.248	.294	7,360	8

* When $(1/r)z > 1.5$, the load is practically independent of cylinder length.

In conclusion, let it be stated that this brief note is not intended to cover all aspects of the problem of collapse of stiffened cylinders loaded in bending and/or axial compression. The aim is to illustrate that scatter in the strength of such structures is, in many instances, entirely within the bounds of engineering accuracy.

REFERENCES

[1] Sandorf, P. E., *Design of Structural Models, with Application to Stiffened Panels Under Combined Shear and Compression*, Journal of the Aeronautical Sciences, Vol. 23, No. 7, p. 623–632, July, 1956 (see p. 629).

[2] Hoff, N. J., Fuchs, S. J., and Cirillo, A. J., *The Inward Bulge Type Buckling of Monocoque Cylinders. II—Experimental Investigation of the Buckling in Combined Bending and Compression*, NACA TN 939, 1944.

[3] Hoff, N. J., Klein, B., and Boley, B. A., *The Inward Bulge Type Buckling of Monocoque Cylinders. V—Revised Strain Energy Theory which Assumes more General Shape at Buckling*, NACA TN 1505, 1948.

[4] Kuenzi, E. W., and Norris, C. B., *Longitudinally Stiffened Thin-Walled Plywood Cylinders in Axial Compression*, Forest Products Lab. Report 1562, 1948.

The Asymptotic Turbulent Boundary Layer

R. A. Dutton*

Scientific Officer, Royal Aircraft Establishment, Farnborough, England

July 30, 1956

THE LAMINAR BOUNDARY LAYER on a flat plate with uniform suction develops asymptotically toward the form

$$u/U = 1 - e^{-v_s y/\nu}$$

where the boundary-layer thickness and the velocity profile are independent of x.[1] By analogy, it has been suggested[2, 3] that the turbulent boundary layer with uniform suction should also develop to a common asymptotic form. The present note briefly describes experiments in which the turbulent boundary layer with uniform suction was, in fact, found to achieve an equilibrium condition, with both thickness and velocity profile independent of x. However, the experiments suggest that the measured velocity profile corresponding to this asymptotic condition is not universal, and, in other respects also, the behavior of the turbulent boundary layer with uniform suction evidently differs from that of the corresponding laminar layer.

Experiments were carried out on a flat perforated metal sheet 6-ft. long which replaced the floor of the working section of a wind tunnel. This perforated surface was preceded by a 4-in. solid entry length which formed the upper lip of a bleed through which the tunnel boundary layer was removed. A transition wire was fitted on the front of this solid surface so that the boundary layer at the start of suction was fully turbulent. The subsequent development of the boundary layer was measured for several different suction velocities at a tunnel speed of 60 ft. per sec. For the first series of measurements the perforated surface was left exposed; for the second it was covered with calendered nylon fabric to simulate a continuously porous surface.

* Formerly, Research Student, Engineering Department, University of Cambridge, Cambridge, England.

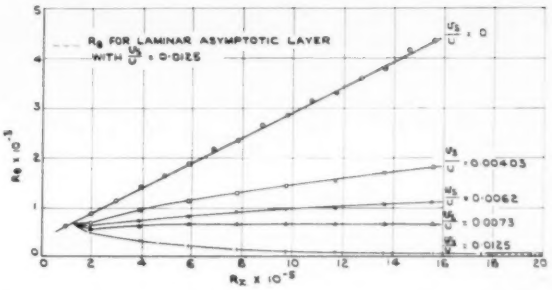

FIG. 1. The development of an initially turbulent boundary layer for various rates of suction through a perforated surface.

The development of the boundary layer on the perforated surface at several different rates of suction is shown in Fig. 1. It will be seen that, for a particular rate of suction ($v_s/U = 0.0073$), the boundary-layer thickness remains substantially constant over virtually the full length of the plate; for greater suction velocities the turbulent boundary layer decays toward the laminar asymptotic form, while for smaller suction velocities it continues to grow. The results obtained with the nylon-covered surface were qualitatively similar, but the suction velocity required to maintain a constant boundary-layer thickness was approximately 40 per cent less. With both surfaces, the velocity profiles of the constant-thickness layer remained substantially unchanged following an initial period of adjustment from the solid-boundary profile at entry. Moreover, in spite of the very different suction velocities required in the two cases, the velocity profiles of the constant-thickness layers were identical except very close to the surface (see Fig. 2).

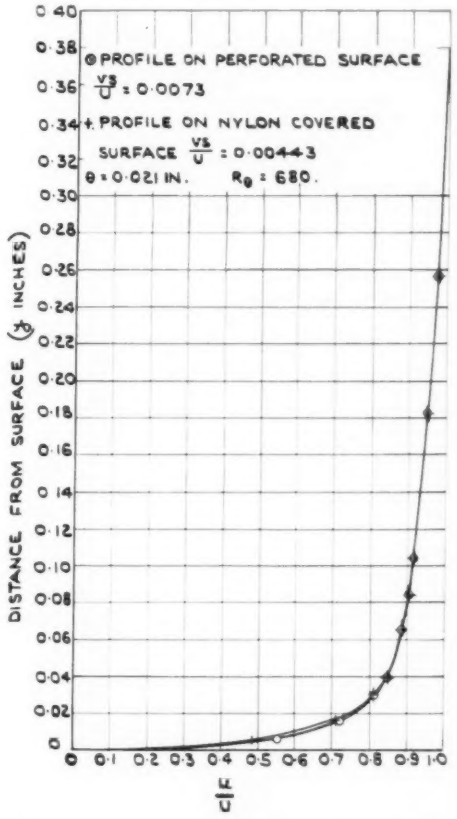
⊙ PROFILE ON PERFORATED SURFACE
$\frac{v_s}{U}$ = 0·0073
+ PROFILE ON NYLON COVERED SURFACE $\frac{v_s}{U}$ = 0·00443
θ = 0·021 IN. R_θ = 680.
DISTANCE FROM SURFACE (y INCHES)
$\frac{u}{U}$

FIG. 2. Asymptotic turbulent velocity profiles on the perforated and nylon-covered surfaces.

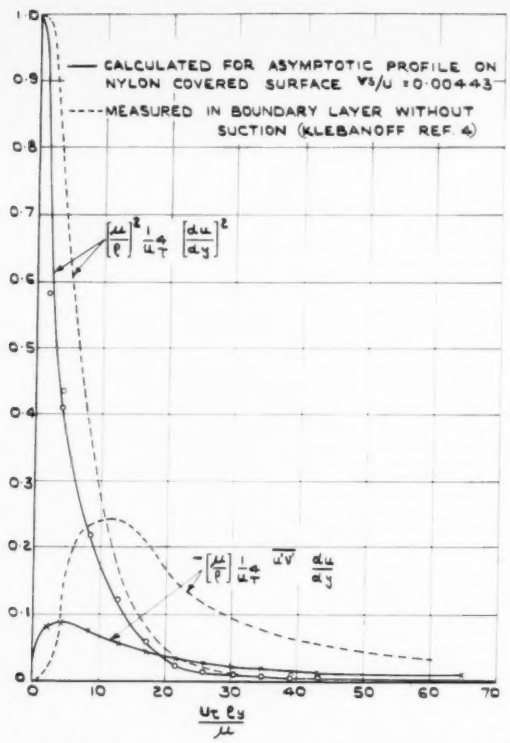
CALCULATED FOR ASYMPTOTIC PROFILE ON NYLON COVERED SURFACE $V_s/U = 0.00443$
MEASURED IN BOUNDARY LAYER WITHOUT SUCTION (KLEBANOFF REF. 4)
$\left[\frac{\mu}{\rho}\right]^2 \frac{1}{u_\tau^4}\left[\frac{du}{dy}\right]^2$
$-\left[\frac{\mu}{\rho}\right]\frac{1}{u_\tau^4}\overline{uv}\,\frac{du}{dy}$
$\frac{u_\tau \rho y}{\mu}$

FIG. 3. Rate of loss of mean-flow energy in turbulent boundary layer with and without distributed suction.

With increased lengths of solid entry and conditions otherwise unchanged, it was possible to maintain a turbulent boundary layer which was substantially constant in momentum thickness, but the velocity profiles now changed continuously along the plate, tending away from rather than toward the equilibrium profiles measured earlier.

It is of interest to note that, when conditions are independent of x, the distribution of turbulent shear stress through the boundary layer can be simply obtained from measurements of the mean velocity profile; the boundary-layer equation reduces to

$$v(\partial u/\partial y) = (1/\rho)(\partial \tau/\partial y)$$

which upon integration gives

$$\rho\overline{u'v'} = \rho v_s U\{[1 - (u/U)] - (\nu/v_s U)(\partial u/\partial y)\}$$

since $\tau = \mu(\partial u/\partial y) - \rho\overline{u'v'}$, and $v = -v_s = \text{const.}$ from continuity.

Distributions through the boundary layer of the turbulence production and direct dissipation terms have been obtained from the mean-flow velocity profiles and are plotted for the nylon surface in Fig. 3, which also shows results obtained by Klebanoff[4] for the solid flat plate. It will be seen that the results are markedly different.

Plotting the asymptotic profile in the form $u/U_\tau = f(U_\tau y/\nu)$ gives a straight-line relation which extends to the edge of the boundary layer, thus suggesting that intermittency is absent.[5]

It is believed that the asymptotic turbulent boundary layer exhibits sufficient features of interest to repay further study. The term asymptotic has been used partly because of the analogy with the laminar case and partly to differentiate this equilibrium layer from the type studied by Clauser[6] and others, where only the velocity defect of the outer part of the layer exhibits longitudinal similarity.

REFERENCES

[1] Griffith, A. A., and Meredith, F. N., *The Possible Improvement in Aircraft Performance Due to the Use of Boundary Layer Suction*, ARC Report No. 2315, 1936.

[2] Schlichting, H., *Die Grenzschicht an der ebenen Platte mit Absaugung und Ausblasen*, Luftfahrtforschung, Vol. 19, p. 293, 1942.

[3] Kay, J. M., *Boundary Layer Flow Along a Flat Plate with Uniform Suction*, ARC, R&M No. 2628, 1948.

[4] Klebanoff, P. S., *Characteristics of Turbulence in a Boundary Layer with Zero Pressure Gradient*, NACA TN 3178, 1954.

[5] Schubauer, G. B., *Turbulent Processes as Observed in Boundary Layer and Pipe*, J. Appl. Phys., Vol. 25, pp. 188–196, 1954.

[6] Clauser, F. H., *Turbulent Boundary Layers in Adverse Pressure Gradients*, Journal of the Aeronautical Sciences, Vol. 21, No. 2, pp. 91–108, 1954.

Effects of Free-Stream Vorticity on the Behavior of a Viscous Boundary Layer*

Ting Yi Li

Associate Professor of Aeronautical Engineering, Rensselaer Polytechnic Institute, Troy, N.Y.

August 2, 1956

THE HYPERSONIC BOUNDARY LAYER on a flat plate is associated with a region of inviscid rotational flow behind a curved shock wave from the plate leading edge. To provide an understanding of the effects of free-stream vorticity on the behavior of a viscous boundary layer, the writer discussed[1, 2] a simple example of a viscous boundary layer in a free stream of constant vorticity. The present note presents a reformulation of the problem wherein the pressure gradient induced by the displacement effect of the boundary layer is taken into account. The highlights of the analysis can be most simply presented in the case of steady incompressible two-dimensional flow. The Navier-Stokes equations can be written in the usual notation as follows:

$$u(\partial\omega/\partial x) + v(\partial\omega/\partial y) = \nu[(\partial^2\omega/\partial x^2) + (\partial^2\omega/\partial y^2)] \quad (1)$$

$$\omega = (\partial u/\partial y) - (\partial v/\partial x) \quad (2)$$

The continuity equation is

$$(\partial u/\partial x) + (\partial v/\partial y) = 0 \quad (3)$$

By examining the order of magnitude of the various terms in these equations, in the same manner that Prandtl originated his famous boundary-layer approximation, it can be shown that in a fluid of small viscosity the variables ω, u, v must vary in accordance with the following boundary-layer equations:

$$u(\partial\omega/\partial x) + v(\partial\omega/\partial y) = \nu(\partial^2\omega/\partial y^2) \quad (1a)$$

$$\omega = \partial u/\partial y \quad (2a)$$

$$(\partial u/\partial x) + (\partial v/\partial y) = 0 \quad (3)$$

in a thin layer $0 \leq y \leq \delta$, $\delta/x \ll 1$. This thin boundary layer adjacent to the surface is a region of strong vorticity. In the simple problem of a uniform shear flow past a flat plate, the free-stream condition is

$$u_\infty = u_0 + \omega_0 y \quad (4a)$$

In reference 1, it was assumed that $v_\infty = 0$—i.e., the boundary-layer displacement effect was neglected. When the boundary-layer displacement effect is taken into account, this condition is expressed more properly as

$$v_\infty = v_\delta \quad (4b)\dagger$$

The usual no-slip conditions on the surface are

$$u = v = 0 \quad (5)$$

Eq. (1a) can be integrated once with respect to y. Thus

$$u(\partial u/\partial x) + v(\partial u/\partial y) = \nu(\partial^2 u/\partial y^2) + f(x) \quad (6)$$

* This research was supported by the United States Air Force through the Air Force Office of Scientific Research, ARDC.

† A more detailed discussion will be given in a forthcoming report.

Applying the conditions of Eqs. (4a) and (4b) on Eq. (6), as $y \to \infty$, yields

$$f(x) = v_\delta \omega_0 \tag{7}$$

which represents the induced pressure gradient due to the displacement effect of the boundary layer. Introduce now the stream function ψ such that

$$\partial\psi/\partial x = -v \qquad \partial\psi/\partial y = u \tag{8}$$

Then the equation of motion and its boundary conditions are

$$(\partial\psi/\partial y)(\partial^2\psi/\partial x\partial y) - (\partial\psi/\partial x)(\partial^2\psi/\partial y^2) = \nu(\partial^3\psi/\partial y^3) - \omega_0(\partial\psi/\partial x)_\infty \tag{9}$$

$$y = 0 \qquad \partial\psi/\partial x = \partial\psi/\partial y = 0 \tag{10}$$

$$y \to \infty \qquad \partial^2\psi/\partial y^2 = \omega_0 \tag{11}$$*

As in reference 1, let

$$\eta = y\sqrt{u_0}/\sqrt{\nu x} \quad \text{(Blasius variable)} \tag{12}$$

$$\xi = (\omega_0/u_0)\sqrt{\nu x/u_0} \quad \text{(vorticity number)} \tag{13}$$

and express ψ in terms of an ascending power series in ξ with functions of η as coefficients:

$$\psi = \sqrt{\nu u_0 x}\,[f_0(\eta) + \xi f_1(\eta) + \ldots] \tag{14}$$

Formal substitution of Eq. (14) into Eqs. (9), (10), and (11) yields the following sequence of equations:

$$2f_0''' + f_0 f_0'' = 0 \tag{15}$$

$$\eta = 0 \qquad f_0 = f_0' = 0 \tag{16}$$

$$\eta \to \infty \qquad f_0'' = 0 \tag{17}$$

$$2f_1''' + f_0 f_1'' - f_0' f_1' + 2f_0'' f_1 = (f_0 - \eta f_0')_{\eta\to\infty} \tag{18}$$

$$\eta = 0 \qquad f_1 = f_1' = 0 \tag{19}$$

$$\eta \to \infty \qquad f_1'' = 1 \tag{20}$$

The f_0 function defined by Eqs. (15)–(17) is the Blasius function. The factor $(f_0 - \eta f_0')_{\eta\to\infty} = -1.73$.[3] Thus, the equation for f_1 can be solved with the boundary conditions as specified.

It can be stated that, to the order of ξ-terms, the induced pressure effects as well as the free-stream vorticity effects are accounted for in the present formulation. As it is demonstrated above, to the zeroth approximation, neither the free-stream vorticity nor the boundary-layer displacement effect contributes any change on the viscous boundary layer. But the free-stream vorticity effects may become significant as soon as the boundary-layer displacement effects become important. In low-speed boundary-layer calculations these effects are both small. In some hypersonic boundary-layer investigations, however, both effects are expected to be significant. As a matter of fact, the induced pressure effects on a hypersonic boundary layer cannot be accurately studied without a full knowledge of the free-stream vorticity conditions. Thus, the study of the inviscid flow field around a body at hypersonic speeds becomes a necessary condition for successfully carrying out hypersonic viscous-flow calculations. In general, it can be argued that one of the effects of free-stream vorticity is to introduce a modified pressure field. Consequently, the skin friction, heat transfer, boundary-layer separation, and laminar stability characteristics are all affected. These effects are important as soon as the displacement effects become significant.

References

[1] Li, T. Y., *Simple Shear Flow Past a Flat Plate in an Incompressible Fluid of Small Viscosity*, Journal of the Aeronautical Sciences, Readers' Forum, Vol. 22, No. 9, pp. 651, 652, September, 1955.

[2] Li, T. Y., *Simple Shear Flow Past a Flat Plate in a Compressible Viscous Fluid*, Journal of the Aeronautical Sciences, Readers' Forum, Vol 22, No. 10, pp. 724, 725, October, 1955.

[3] Schlichting, H., *Boundary Layer Theory*, p. 106; McGraw-Hill Book Company, Inc., 1955.

* It is required that the inviscid free stream have constant vorticity. When v_δ is considered here, this condition is, strictly speaking,

$$[(\partial^2\psi/\partial x^2) + (\partial^2\psi/\partial y^2)]_\infty = \omega_0$$

but $$[(\partial^2\psi/\partial x^2)/(\partial^2\psi/\partial y^2)]_\infty = 0(\nu/u_0 x) = 0(1/R_x) \ll 1$$

Thus, in the present calculations, Eq. (11) is consistent with the boundary-layer approximation.

A Shock-Free Airfoil

H. C. Levey*

Aeronautical Research Laboratories, Department of Supply, Australia

July 30, 1956

Introduction

The equations which govern the steady two-dimensional flow of an inviscid ideal gas admit solutions which have the property of transonic isentropic recompression. In particular, it is possible to find profiles which theoretically give rise to shock-free supersonic regions which placed in an appropriate subsonic stream. The fact that this phenomenon does not seem to be observed experimentally is a matter of some controversy although evidence is accumulating to show that the reason may be "the non-existence of neighbouring flows."[1] Before any experimental investigations can be made, it is necessary to have a profile for which the exact solution exhibits a comparatively large shock-free supersonic region, and such a profile is given in this note.

The hodograph method is used, in which the profile shape can only be specified in advance in fairly general terms. It was judged that typical conditions would be met by a symmetrical profile with a thickness ratio of about 10 per cent in a free stream of Mach Number 0.8. Since the method of expansion in eigenfunctions and analytical continuation throughout the hodograph plane[2, 3] leads to slowly convergent series, it was decided to use more complex solutions developed by Cherry[4] because of the rapid convergence of the series involved. These solutions lead to a profile pointed at both ends (despite a number of attempts at modification), but this was not thought to be a serious limitation since the solutions are only valid for zero incidence.

It was found that two solutions of the type given by Cherry were necessary, the first (with subscript A) to give the basic shape and the second (with subscript 2) to modify the thickness ratio. In addition, a particular elementary solution was added to avoid the occurrence of a limit line in the flow field.

Formulas

At the point x, y, let q, θ be the polar velocity components with q normalized so that $q = 1$ is the vacuum speed, and denote the sonic speed by $q_s[=(\gamma - 1)/(\gamma + 1)]$. The positive constants α, β, λ are now defined by

$$\left.\begin{aligned} 2\alpha(1+\alpha) &= \beta = 1/(\gamma - 1) \\ \lambda &= (2\alpha)^{-1} \end{aligned}\right\} \tag{1}$$

and a transformation is made to the variables q, φ through

$$\theta + i\kappa = \varphi - 2\alpha \arctan\,[q \sin\varphi/(1 - q\cos\varphi)] \tag{2}$$

where κ is defined in terms of the free-stream speed q_∞ by

$$\kappa = \operatorname{arctanh}\left\{[1 - (q_\infty^2/q_s^2)]^{1/2}(1 - q_\infty^2)^{-1/2}\right\} - q_s^{-1}\arctanh\,[(q_s^2 - q_\infty^2)^{1/2}(1 - q_\infty^2)^{-1/2}] \tag{3}$$

The solutions used are then given (with real parts understood) by

$$\left.\begin{aligned} \Psi_A &= i(1-q^2)^\nu(qX_2 - \Omega_0) \\ qX_A &= (q\partial\Omega_A/\partial q) + [2i\alpha q \sin\varphi\,\Omega_0/(1 - 2q\cos\varphi + q^2)] \\ qY_A &= i\Omega_0 \end{aligned}\right\} \tag{4}$$

*Acknowledgment is made to the Chief Scientist, Department of Supply, Australia, for permission to publish this article.

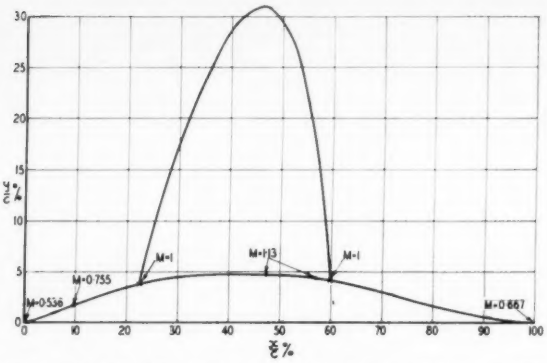

FIG. 1. Airfoil with shock-free supersonic region at $M_\infty = 0.8$; upper surface and sonic line.

$$\left.\begin{aligned}
\Psi_2 = i\Big\{ &- \sum_{n=1}^{\infty} n^{-2} q^n e^{-in\varphi} + \\
&\frac{1}{2}\alpha\left(\log[(1 - qe^{-i\varphi})(1 - qe^{i\varphi})^{-1}]\right)^2 - \\
&\sum_{n=0}^{\infty} q^n e^{in\varphi} \sum_{r=0}^{\infty} \bar{b}_{nr} q^{2r} - \Big[1 + \frac{1}{2}\beta \sum_{r=1}^{\infty} r^{-2} \times \\
&(1 - \beta) \ldots . (r - 1 - \beta) q^{2r}/(r - 1)!\Big] \times \\
&\log(1 - 2q\cos\varphi + q^2)\Big\} \\
qX_2 = (1 - q^2)^{-\beta}\Big\{ &-\log(1 - qe^{-i\varphi}) + \\
&\sum_{n=0}^{\infty} q^n e^{in\varphi} \sum_{r=0}^{\infty} \bar{a}_{nr} q^{2r}\Big\} \\
qY_2 = i\Big\{ &\log(1 - qe^{-i\varphi}) - \sum_{n=0}^{\infty} q^n e^{in\varphi} \sum_{r=0}^{\infty} b_{nr} q^{2r}\Big\}
\end{aligned}\right\} \quad (5)$$

$$x = X\cos\theta - Y\sin\theta, \quad y = X\sin\theta + Y\cos\theta \quad (6)$$

where

$$\Omega_0 = \sum_{n=1}^{\infty} q^n e^{in\varphi} \sum_{r=0}^{\infty} a_{nr} q^{2r} - (1 + \alpha)^{-1} \times \left[1 - \frac{(1 - q^2)^{1-(1/2)\beta}}{1 - 2(1 + \alpha)q\cos\varphi + (1 + 2\alpha)q^2}\right] \quad (7)$$

$$q\partial\Omega_A/\partial q = qe^{-i\varphi}(1 - qe^{-i\varphi})^{-1} + (1 - q^2)^{-2} \times \left\{\sum_{n=0}^{\infty} q^n e^{in\varphi} \sum_{r=0}^{\infty} \bar{c}_{nr} q^{2r} + \left(\frac{1}{2} - \frac{1}{3}q^2 - \frac{1}{3}q^4\right) qe^{i\varphi}(1 - qe^{i\varphi})^{-1}\right\} \quad (8)$$

The coefficients a_{nr}, b_{nr} are tabulated by Cherry[4] and the $\bar{a}_{nr}$, $\bar{b}_{nr}$, $\bar{c}_{nr}$ are privately tabulated by the same author. Elementary solutions are given by

$$\left.\begin{aligned}
\Psi^{(n)} &= (n - 1)q^{n-1}\sin n\theta \bar{F}_n(q^2) \\
X^{(n)} &= n(1 - q^2)^{-\beta} q^{n-1}\cos n\theta \left\{\bar{F}_n(q^2) + [2q^2\bar{F}_n'(q^2)]/(n + 1)\right\} \\
Y^{(n)} &= -(1 - q^2)^{-\beta} q^{n-1}\sin n\theta \left\{n\bar{F}_n(q^2) + [2q^2\bar{F}_n'(q^2)]/(n + 1)\right\}
\end{aligned}\right\} \quad (9)$$

where the $\bar{F}_n(q^2)$ are the standard hypergeometric functions occurring in hodograph theory.[2, 3]

Discussion

The final solution used was of the form

$$\Psi = \Psi_A + A_2\Psi_2 - \Sigma B_n\Psi^n \quad (10)$$

where A_2 and B_n were adjusted so that $\Psi = 0$ gave the desired profile. The occurrence of a limit line was avoided by adjusting the profile streamline in the hodograph plane to avoid tangency with the characteristics, and it was found that, within the limitations of the initial requirements, the greatest supersonic Mach Number—circa 1.13—was attained with $A_2 = 1.4$ and $14B_{15} = 10^7$ with the other B_n zero. The field points have been computed to five significant figures, and the upper surface of the profile and the sonic line are shown in Fig. 1. There is a flattening near the downstream sonic point, which is not discernable on the figure, but otherwise the profile exhibits no marked peculiarities.

References

[1] Morawetz, C. S., *On the Non-existence of Transonic Flows, I*, Commun. on Pure & Appl. Math., Vol. 9, No. 1, p. 45, February, 1956.

[2] Cherry, T. M., *Flow of a Compressible Fluid about a Cylinder*, Proc. Royal Soc., Series A, Vol. 192, No. 1,028, p. 45, December, 1947.

[3] Levey, H. C., *Exact Solutions for Transonic Flow Past Cusped Aerofoils*, A.R.L. Report A.87, March, 1954.

[4] Cherry, T. M., *A Transformation of the Hodograph Equation*, Philos. Trans. Royal Soc. of London, Series A, Vol. 245, No. 905, p. 583, April, 1953.

Notice to Contributors

Manuscripts submitted for publication *must* be double- or triple-spaced originals. There should be wide margins on all sides of the sheets and triple spacing around formulas to allow for the marking of directions for the printer.

Original drawings (jet black India ink on white paper or tracing cloth) should accompany the manuscript. *(Blueprints are not acceptable.)* Photographs *must* be on glossy white paper. The smallest lettering on 8- by 10-in. figures should be no less than 1/4 in. high.

Only the simplest formulas should be typewritten; all others should be carefully written in pen and ink. The difference between capital and lower-case letters and Greek symbols should be clearly distinguished.

See Inside Back Cover of this issue for further details

Index to Volume 23

Journal of the Aeronautical Sciences

Numbers 1–12, January–December, 1956

No. 1, January, 1956, pages 1– 96
No. 2, February, 1956, pages 97–192
No. 3, March, 1956, pages 193–288
No. 4, April, 1955, pages 289–400
No. 5, May, 1956, pages 401–516
No. 6, June, 1956, pages 517–612
No. 7, July, 1956, pages 613–708
No. 8, August, 1956, pages 709–804
No. 9, September, 1956, pages 805–900
No. 10, October, 1956, pages 901–980
No. 11, November, 1956, pages 981–1060
No. 12, December, 1956, pages 1061–1140

The material has been indexed under a subject heading and by author.

*—An asterisk following an item identifies it as having appeared in the Readers' Forum section.

ABZUG, MALCOLM J. Applications of Matrix Operators to the Kinematics of Airplane Motion 679

Aerodynamics

Applied Aerodynamics and Flight Mechanics, W. Bailey Oswald 469
Errata—"Applied Aerodynamics and Flight Mechanics," W. Bailey Oswald* 892, 1123
An Approximate Solution to Supersonic Conical Flow, Henry E. Fettis* 1122
Aspects of the Problem of Turbulent Motion, C. C. Lin 453
Conical Techniques for Incompressible Nonviscous Flow, Homer J. Stewart and Allen I. Ormsbee 1029
The Decay of Turbulence Near the Critical Reynolds Number, A. F. Charwat* 799
Double and Triple Correlations Behind a Heated Grid, A. L. Kistler, V. O'Brien, and S. Corrsin* 96
Effect of Wind-Tunnel Contraction on Free-Stream Turbulence, Mahinder S. Uberoi 754
The Effects of Prandtl Number on High-Speed Viscous Flows over a Flat Plate, Y. H. Kuo* 1058
An Experimental Study of the One-Dimensional Refraction of a Rarefaction Wave at a Contact Surface, I. J. Billington 997
An Experimental Study of One-Dimensional Shock-Wave Refraction, C. A. Ford and I. I. Glass* 189
Fluid Dynamic Effects at Speeds from $M = 11$ to 15, Seymour M. Bogdonoff and Andrew G. Hammitt 108
Forced Convection of Heat from Cylinders at Low Reynolds Numbers, D. C. Collis* 697
Heat Transfer in Turbulent Shear Flow, W. D. Rannie 485
The Hydraulic Analogy as a Distorted Dissimilar Model, R. A. A. Bryant* 282
Hydrodynamics—A Review of von Karman's Contributions, Arthur T. Ippen 438
An Investigation of the Noise Produced by a Subsonic Air Jet, J. H. Gerrard 855
The Laminar Free-Convective Heat Transfer from the Surfaces of a Vertical Circular Cylinder, Knox Millsaps and Karl Pohlhausen* 381
Linearized Theory of Water Drop Impingement, Theodore R. Goodman* 399
A Method for Predicting Lift Effectiveness of Spoilers at Subsonic Speeds, Arthur L. Jones, Owen P. Lamb, and Alfred E. Cronk 330
The Normal Shock Properties for Air in Dissociation Equilibrium, Mary F. Romig* 185
Note on "On the Stability Theory of Flow with Finite Disturbances," J. T. Stuart* 894
A Numerical Method for Laminar Heat Transfer on Cylinders in Plane Compressible Flow, Kwang-Tzu Yang and Harold H. Sogin* 277
On Equation of Motion for a Compressible Viscous Gas, E. V. Laitone 846
On the Method of Averaging Stagnation Pressures, Raymond L. Chuan* 378
Erratum—"On the Method of Averaging Stagnation Pressures," Raymond L. Chuan* 797
On the Role of Reynolds Stresses in Stability Theory, J. T. Stuart* 86
On the Stability Theory of Flow with Finite Disturbances, S. I. Pai* 274
On the Supersonic Flow of a Viscous Fluid Past a Flat Plate, Stephen H. Maslen* 801
A Principle of Maximum Power for Real Fluids in Steady Motion, Carlo Riparbelli* 971
Reduction of Drag Due to Lift in Supersonic Flight by Distributing Lift Along a Fuselage, R. M. Licher 1037
Remarks on Chaplygin Functions, Vivian O'Brien* 894
The Rotational Field Behind a Curved Shock Wave Calculated by the Method of Flux Analysis, Shigeo Uchida and Michiru Yasuhara 830
Similar Solutions in Compressible Laminar Free Mixing Problems, Luigi G. Napolitano* 389
The Skewness Factor According to Obukhoff's Transfer Theory, W. H. Reid* 379
Some Comments on Surface Contamination in Hydraulic Analogy Research, R. A. A. Bryant* 1056
Some Recent Aerodynamic Techniques in Design of Fin-Stabilized Free-Flight Missiles for Minimum Dispersion, M. W. Hunter, A. Shef, and D. V. Black 571
Supplementary Note on Turbulent Velocity Fluctuations, Heinrich B. Helmbold* 702
The Transonic Flow Hydraulic Analogy, R. A. A. Bryant* 90
Viscous Flow Along a Flat Plate Moving at High Supersonic Speeds, Y. H. Kuo 125
Viscous Flow Along a Flat Plate Moving at High Supersonic Speeds, Y. H. Kuo* 977

Aerodynamics—Bodies

Aerodynamic Cross-Coupling Between Side Force and Normal Force on Bodies and Wing-Body Combinations, Martin Zlotnick* 192
Application of Second-Order Shock-Expansion Theory to Several Types of Bodies of Revolution, Robert E. Lavender and Raymond A. Deep* 1052
Base Pressure Studies in Rarefied Supersonic Flows, L. L. Kavanau 193

Aerodynamics—Bodies (*Continued*)

An Experimental Investigation of Flow About Simple Blunt Bodies at a Nominal Mach Number of 5.8, Robert Earl Oliver* ... 177
An Experimental Investigation of Flow over Blunt Nosed Cones at a Mach Number of 5.8, William T. O'Bryant and Reginald M. Machell* ... 1054
Experiments on Circular Cones at Yaw in Supersonic Flow, Maurice Holt and John Blackie ... 931
The Flow over a Body in a Choked Wind Tunnel and in a Sonic Free Jet, Bernard W. Marschner ... 368
The Forces on the General Slender Body of Elliptic Cross Section in Supersonic Flow, H. Portnoy* ... 91
Low-Wave-Drag Bodies of Revolution as Determined by Linearized Theory, G. C. Grogan* ... 612
The Magnus Effect at High Reynolds Numbers, Howard R. Kelly and Ray W. Van Aken* ... 1053
Measurements of Turbulent Heat Transfer on Bodies of Revolution at Supersonic Speeds, W. S. Bradfield and D. G. DeCoursin* ... 272
Negative Magnus Force, E. Krahn* ... 377
On Inviscid Flow Near an Airfoil Leading Edge or an Ogive Tip at High Supersonic Mach Numbers, Abraham Kogan* ... 794
On Linearized Transonic Flow Theory for Slender Bodies, John W. Miles* ... 704
On the Sonic Drag of a Slender Body, John W. Miles ... 146
Recent Developments in the Theory of Wing-Body Wave Drag, Harvard Lomax and Max. A. Heaslet ... 1061
Similarity-Rule Estimation Methods for Cones and Parabolic Noses, Richard D. Linnell and Jerry Z. Bailey* ... 796
Some Effects of Viscosity on Wing-Body Interference at $M = 1.9$, T. R. Rhees and W. P. Crenshaw ... 43
Some Integrated Volume Properties in Linearized Flow and Their Connection with Drag Reduction at Supersonic Speeds, Z. O. Bleviss ... 1078
Some Results of Linearized Transonic Flow About Slender Airfoils and Bodies of Revolution, P. F. Maeder and H. U. Thommen* ... 187
Tip-Bluntness Effects on Cone Pressures at $M = 6.85$, Mitchel H. Bertram* ... 898

Aerodynamics—Boundary Layer & Skin Friction

The Asymptotic Behavior of the Boundary Layer to Transverse Curvature, H. G. Lew* ... 276
Asymptotic Suction Characteristics of the Boundary Layer over a Circular Cylinder, H. G. Lew* ... 895
The Asymptotic Turbulent Boundary Layer, R. A. Dutton* ... 1127
Boundary-Layer Effect on Local Mach Number Measurements on a Circular Arc Half Profile, James B. Carroll and Gordon F. Anderson* ... 604
Boundary-Layer Measurements in Hypersonic Flow, F. K. Hill ... 35
Comments on Viscous Heating, H. M. DeGroff* ... 978
The Correction of Hot-Wire Readings in a Boundary Layer for Proximity to the Solid Boundary, E. G. Richardson* ... 970
The Development of Turbulent Boundary Layers, D. A. Spence ... 3
The Downstream Effect of a Thickening of the Laminar Boundary Layer, D. G. Hurley* ... 383
Effect of Diffusion in an Isothermal Boundary Layer, E. R. G. Eckert and P. J. Schneider* ... 384
The Effect of Heating and Cooling on the Stability of the Boundary-Layer Flow of a Liquid over a Curved Surface, R. C. Di Prima and D. W. Dunn ... 913
The Effect of Mass Transfer on the Compressible Turbulent Boundary-Layer Skin Friction and Heat Transfer—An Addendum, William H. Dorrance* ... 283
Effects of Free-Stream Vorticity on the Behavior of a Viscous Boundary Layer, Ting Yi Li* ... 1128
Effects of Pressure Gradient and Heat Transfer on the Stability of the Compressible Laminar Boundary Layer, Norman M. Shapiro* ... 81
Energy Dissipation in Turbulent Boundary Layers, Itiro Tani* ... 606
An Experimental Investigation of the Boundary-Layer Flow on a Rotating Flat Plate, Jerome Persh and A. Wiley Sherwood* ... 703
Experimental Observation of Laminar Boundary-Layer Oscillations in Supersonic Flow, John Laufer* ... 184
Free-Flight Measurements of Skin Friction of Turbulent Boundary Layers with High Rates of Heat Transfer at High Supersonic Speeds, Simon C. Sommer and Barbara J. Short ... 536
Heat Transfer to an Incompressible Turbulent Boundary Layer and Estimation of Heat-Transfer Coefficients at Supersonic Nozzle Throats, Merwin Sibulkin ... 162
Influence of the Leading-Edge Shock Wave on the Laminar Boundary Layer at Hypersonic Speeds, Lester Lees ... 594
Interaction of a Shock Wave with a Thermal Boundary Layer, Wayland C. Griffith ... 16
The Limiting Wall Temperature Ratios Required for Complete Stabilization of Laminar Boundary Layers with Blowing, Shan-fu Shen and Jerome Persh* ... 286
Nitric Oxide Formation in Hypersonic Flow, J. G. Logan, Jr.* ... 1123
A Note on the Effects of Gas Dissociation on Boundary-Layer Heat Transfer, Robert Bromberg* ... 976
A Note on Transient Aerodynamic Heating, Eugene Covert and Frank Durgin* ... 699
On the Boundary-Layer Equations of a Very Slender Body of Revolution, S. I. Pai* ... 795
On the Energy Balance in a Compressible Boundary Layer, K. T. Yen* ... 274
On Heat Transfer in Laminar Boundary Layers at High Prandtl Number, George W. Morgan and W. H. Warner ... 937
On the Model of the Free, Shock-Separated, Turbulent Boundary Layer, Artur Mager* ... 181
On Viscous Heating, H. M. DeGroff* ... 395
Rapid Laminar Boundary-Layer Calculations by Piecewise Application of Similar Solutions, A. M. O. Smith ... 901
A Simple Theory for Interactions Between Shock Waves and Entirely Laminar Boundary Layers, G. E. Gadd ... 225
Some Examples of Laminar Boundary-Layer Flow on Rotating Blades, Nicholas Rott and William E. Smith ... 991
Some Features of Boundary Layers and Transition to Turbulent Flow, Arnold M. Kuethe ... 444
Transition Studies and Skin-Friction Measurements on an Insulated Flat Plate at a Mach Number of 5.8, Robert H. Korkegi ... 97
Transpiration Cooling Experiments in a Turbulent Boundary Layer at $M = 3$, B. M. Leadon and C. J. Scott* ... 798
The Transverse Curvature Effect in Compressible Axially Symmetric Laminar Boundary-Layer Flow, Ronald F. Probstein and David Elliott ... 208

Aerodynamics—Internal Flow

Comments on Supersonic Diffuser Instability, W. C. Randels* ... 390
Comments on "Supersonic Diffuser Instability," Robert L. Trimpi* ... 611
Further Comments on the Decay of a Nonuniform Velocity Distribution, William J. Guman* ... 979

Aerodynamics—Internal Flow *(Continued)*

Heat Flow in a Fluid with Eddying Flow, William H. Durfee* ... 188
Heat Transfer to an Incompressible Turbulent Boundary Layer and Estimation of Heat-Transfer Coefficients at Supersonic Nozzle Throats, Merwin Sibulkin ... 162
An Investigation on Fully Developed Turbulent Flows in a Curved Channel, Salamon Eskinazi and Hsuan Yeh ... 23
Laminar Jet Mixing of Two Compressible Fluids with Heat Release, S. I. Pai ... 1012
On Strong Transverse Waves Without Shocks in a Circular Cylinder, Stephen H. Maslen and Franklin K. Moore ... 583
On Turbulent Flow Near a Wall, E. R. van Driest ... 1007
The Oscillations of a Supersonic Gas Jet Embedded in a Supersonic Stream, D. C. Pack ... 747
Simple Wave Solutions of the Transonic Equation, L. J. F. Broer* ... 287
Vortex Structures in Pipe Flow, W. H. Webb and R. P. Harrington* ... 792

Aerodynamics—Turbines & Compressors

An Analysis of the Performance of an Axial-Flow Compressor at Low Reynolds Number, Robert L. Sohn ... 741
An Approximate Method of Calculating Three-Dimensional Compressible Flow in Axial Turbomachines, Comdr. Carl O. Holmquist and W. Duncan Rannie ... 543
Compressibility Effects on Secondary Flows, H. G. Loos ... 76
Determination of the Stationary Flow Field in Front of a Supersonic Cascade, P. Schwaar* ... 888
An Investigation of the Flutter Characteristics of Compressor and Turbine Blade Systems, Chi-Teh Wang, Frank Lane, and Robert J. Vaccaro ... 335
Stall Propagation in a Cascade of Airfoils, Anthony R. Kriebel* ... 897
System Mode Shapes in the Flutter of Compressor Blade Rows, Frank Lane ... 54
Variational Method in the Theory of Axisymmetric Rotational Flow of a Compressible Fluid, Bohdan Krajewski* ... 891

Aerodynamics—Wings & Airfoils

Aspect Ratio Influence at High Subsonic Speeds, Gordon F. Anderson ... 874
Conical Techniques for Incompressible Nonviscous Flow, Homer J. Stewart and Allen I. Ormsbee ... 1029
Dynamic Derivatives in Yaw and Sideslip of Thin Wings at Supersonic Speeds, Theodore R. Goodman ... 357
Exact and Approximate Solutions for the Supersonic Delta Wing, L. R. Fowell ... 709
Interpolation Formulas for Supersonic-Hypersonic Airfoils, Richard D. Linnell and Jerry Z. Bailey* ... 398
Inviscid Leading-Edge Effect in Hypersonic Flow, H. K. Cheng and A. J. Pallone* ... 700
The Lift of a Blowing Wing in a Parallel Stream, D. A. Spence* ... 92
Normal Forces on Flat Plates in Low-Density Supersonic Flow, D. M. Tellep and L. Talbot ... 1099
Notes on the Calculation of the Subsonic Downwash and Sidewash Angles Near Wings, Raymond F. Anderson* ... 707
On Inviscid Flow Near an Airfoil Leading Edge or an Ogive Tip at High Supersonic Mach Numbers, Abraham Kogan* ... 794
On Transonic Airfoil Theory, Gottfried Guderley ... 961
The Optimum Distribution of Lift in Certain Prismatic Regions at Supersonic Speed, William W. Willmarth* ... 800
A Review of Source Superposition and Conical Flow Methods in Supersonic Wing Theory, H. J. Stewart ... 507
A Shock-Free Airfoil, H. C. Levey* ... 1129
Some Recent Developments in Airfoil Theory, W. R. Sears ... 490
Some Results of Linearized Transonic Flow About Slender Airfoils and Bodies of Revolution, P. F. Maeder and H. U. Thommen* ... 187
Subsonic Influence of Compressibility on the Pressure Distribution of a Profile, F. S. Weinig* ... 279
Erratum—"Subsonic Influence of Compressibility on the Pressure Distribution of a Profile," F. S. Weinig* ... 705

Aeroelasticity

The Aerodynamic Force on an Airfoil in a Moving Gust, John W. Miles ... 1044
Aerodynamic Influence Coefficients for an Oscillating Finite Thin Wing in Supersonic Flow, Ta Li ... 613
An Aeroelastic Parameter for Estimation of the Effects of Flexibility on the Lateral Stability and Control of Aircraft, William P. Rodden ... 660
Comments on "Computation of Vibration Modes and Frequencies," David Feign* ... 603
The Compressible Flow Past an Oscillating Airfoil in a Wind Tunnel, John W. Miles ... 671
The Design and Testing of Supersonic Flutter Models, John F. McCarthy, Jr., and Robert L. Halfman ... 530
The Divergence of Supersonic Wings Including Chordwise Bending, M. A. Biot ... 237
The Dynamic Response of a Large Airplane to Continuous Random Atmospheric Disturbances, Franklin W. Diederich ... 917
The Effect of Shape on the Orthotropic Characteristics of a Rectangular Plate, Wasfi A. Hijab* ... 696
Equations for the Loading, Section Pitching-Moment Coefficient, and Center-of-Pressure Distributions on Triangular Wings Having Supersonic Leading and Trailing Edges for Various Basic Camber Distributions, Julian H. Kainer ... 137
Experimental Pressure Distributions on Oscillating Low Aspect Ratio Wings, William R. Laidlaw and Robert L. Halfman ... 117
A First-Order Formulation of the Unsteady Supersonic Flow Problem for Finite Wings, John W. Miles ... 578
Forced Responses of Two Elastic Beams Interconnected by Spring-Damper Systems, Michael Dublin and Hans R. Friedrich ... 824
The Integrated Use of Analog and Digital Computing Machines for Aircraft Dynamic Load Problems, Bernard Mazelsky and Robert F. O'Connell ... 721
Iteration in Semidefinite Eigenvalue Problems, Samuel Pines* ... 380
A Least Squares Matrix Interpolation of Flexibility Influence Coefficients, Alfred F. Schmitt* ... 980
A Note on the Fatigue of Wings, A. O. Payne* ... 797
On the Aerodynamic Instability of Thin Panels, John W. Miles ... 771
On the Convergence of an Iterative Procedure in Solving Dynamic Response Problems, Hua Lin* ... 391
On the Evaluation of the Schwarz Function, Yudell L. Luke and Henry E. Fettis* ... 975
On the Flutter of Panels at High Mach Numbers, John M. Hedgepeth* ... 609
On a Matrix Characteristic Value Problem, A. P. Hillman* ... 286
Piston Theory—A New Aerodynamic Tool for the Aeroelastician, Holt Ashley and Garabed Zartarian ... 1109
Remarks on the Convergence of an Iterative Procedure in Solving Dynamic Response Problems, Tse-Sun Chow* ... 1119
Some Structural and Aeroelastic Considerations of High-Speed Flight (Nineteenth Wright Brothers Lecture), R. L. Bisplinghoff ... 289
Spectral Theory of Buffeting and Gust Response: Unification and Extension, H. S. Ribner ... 1075

Aeroelasticity *(Continued)*
Stiffness and Deflection Analysis of Complex Structures, M. J. Turner, R. W. Clough, H. C. Martin, and L. J. Topp ... 805
Stress Distribution, Instability, and Free Vibration of Beam Grid-Works on Elastic Foundations, Hugh L. Cox and Paul H. Denke ... 173
Theoretical Aerodynamic Properties of Vanishing Aspect Ratio Harmonically Oscillating Rigid Airfoils in a Compressible Medium, Bernard Mazelsky ... 639
Torsional Vibration of Rotating Twisted Bars, J. L. Bogdanoff and J. T. Horner* ... 393

AMBA RAO, C. L. Note on Photoelastic Study of Swept Wings* ... 889
ANDERSON, GORDON F. Aspect Ratio Influence at High Subsonic Speeds ... 874
ANDERSON, GORDON F., AND JAMES B. CARROLL. Boundary-Layer Effect on Local Mach Number Measurements on a Circular Arc Half Profile* ... 604
ANDERSON, RAYMOND F. Notes on the Calculation of the Subsonic Downwash and Sidewash Angles Near Wings* ... 707
ASHLEY, HOLT, AND GARABED ZARTARIAN. Piston Theory—A New Aerodynamic Tool for the Aeroelastician ... 1109

BAILEY, JERRY Z., AND RICHARD D. LINNELL. Interpolation Formulas for Supersonic-Hypersonic Airfoils* ... 398
BAILEY, JERRY Z., AND RICHARD D. LINNELL. Similarity-Rule Estimation Methods for Cones and Parabolic Noses* ... 796
BERMAN, ALEX. Response Matrix Method of Rotor Blade Analysis ... 155
BERTRAM, MITCHEL H. Tip-Bluntness Effects on Cone Pressures at $M = 6.85$* ... 898
BESSELING, J. F. Analysis of the Plastic Collapse of a Cruciform Column with Initial Twist, Loaded in Compression ... 49
BILLINGTON, I. J. An Experimental Study of the One-Dimensional Refraction of a Rarefaction Wave at a Contact Surface ... 997

Biographical
Introduction. The Institute of the Aeronautical Sciences Extends Congratulations to Dr. Theodore von Kármán on the Occasion of His Seventy-Fifth Birthday May 11, 1956 ... 403
A Salute to Hugh L. Dryden ... 1
Theodore von Kármán, Clark B. Millikan ... 404

BIOT, M. A. Applied Mathematics—An Art and a Science ... 406
BIOT, M. A. The Divergence of Supersonic Wings Including Chordwise Bending ... 237
BISPLINGHOFF, R. L. Some Structural and Aeroelastic Considerations of High-Speed Flight (Nineteenth Wright Brothers Lecture) ... 289
BLACK, D. V., A. SHEF, AND M. W. HUNTER. Some Recent Aerodynamic Techniques in Design of Fin-Stabilized Free-Flight Missiles for Minimum Dispersion ... 571
BLACKIE, JOHN, AND MAURICE HOLT. Experiments on Circular Cones at Yaw in Supersonic Flow ... 931
BLEVISS, Z. O. Some Integrated Volume Properties in Linearized Flow and Their Connection with Drag Reduction at Supersonic Speeds ... 1078
BLOMQUIST, KURT E., AND FRED H. TURNER. A Study of the Applicability of Rabotnov's Creep Parameter for Aluminum Alloy* ... 1121
BODNER, S. R., AND M. J. FORRAY. Bending Moments in an Initially Bent, Spring Restrained Column* ... 387
BOGDANOFF, J. L., AND J. T. HORNER. Torsional Vibration of Rotating Twisted Bars* ... 393
BOGDONOFF, SEYMOUR M., AND ANDREW G. HAMMITT. Fluid Dynamic Effects at Speeds from $M = 11$ to 15 ... 108
BOLEY, BRUNO A. The Determination of Temperature, Stresses, and Deflections in Two-Dimensional Thermoelastic Problems ... 67
BOLEY, BRUNO A. On Thin-Ring Analysis* ... 802
BOLEY, BRUNO A. Thermally Induced Vibrations of Beams* ... 179
BRADFIELD, W. S., AND D. G. DECOURSIN. Measurements of Turbulent Heat Transfer on Bodies of Revolution at Supersonic Speeds* ... 272
BROER, L. J. F. Simple Wave Solutions of the Transonic Equation* ... 287
BROMBERG, ROBERT. A Note on the Effects of Gas Dissociation on Boundary-Layer Heat Transfer* ... 976
BRYANT, R. A. A. The Hydraulic Analogy as a Distorted Dissimilar Model* ... 282
BRYANT, R. A. A. Some Comments on Surface Contamination in Hydraulic Analogy Research* ... 1056
BRYANT, R. A. A. The Transonic Flow Hydraulic Analogy* ... 90
BUDIANSKY, BERNARD, AND J. MAYERS. Influence of Aerodynamic Heating on the Effective Torsional Stiffness of Thin Wings ... 1081

CALLIGEROS, J. M., T. H. H. PIAN, AND J. W. MAR. A Note on Methods for the Determination of Transient Stresses* ... 94
CARROLL, JAMES B., AND GORDON F. ANDERSON. Boundary-Layer Effect on Local Mach Number Measurements on a Circular Arc Half Profile* ... 604
CHARWAT, A. F. The Decay of Turbulence Near the Critical Reynolds Number* ... 799
CHENG, H. K., AND A. J. PALLONE. Inviscid Leading-Edge Effect in Hypersonic Flow* ... 700
CHOW, TSE-SUN. Remarks on the Convergence of an Iterative Procedure in Solving Dynamic Response Problems* ... 1119
CHUAN, RAYMOND L. On the Method of Averaging Stagnation Pressures* ... 378
CHUAN, RAYMOND L. Erratum—"On the Method of Averaging Stagnation Pressures"* ... 797
CLAUSER, FRANCIS H. The Behavior of Nonlinear Systems ... 411
CLOUGH, R. W., M. J. TURNER, H. C. MARTIN, AND L. J. TOPP. Stiffness and Deflection Analysis of Complex Structures ... 805
COLLIS, D. C. Forced Convection of Heat from Cylinders at Low Reynolds Numbers* ... 697
CORRSIN, S., A. L. KISTLER, AND V. O'BRIEN. Double and Triple Correlations Behind a Heated Grid* ... 96
COVERT, EUGENE, AND FRANK DURGIN. A Note on Transient Aerodynamic Heating* ... 699
COX, HUGH L. The Buckling of Isosceles Triangular Plates Subjected to Combined Compression and Shear* ... 287
COX, HUGH L., AND PAUL H. DENKE. Stress Distribution, Instability, and Free Vibration of Beam Grid-Works on Elastic Foundations ... 173
CRENSHAW, W. P., AND T. R. RHEES. Some Effects of Viscosity on Wing-Body Interference at $M = 1.9$ ... 43
CRONK, ALFRED E., OWEN P. LAMB, AND ARTHUR L. JONES. A Method for Predicting Lift Effectiveness of Spoilers at Subsonic Speeds ... 330

DECKER, JAMES L. The Human Pilot and the High-Speed Airplane ... 765
DECOURSIN, D. G., AND W. S. BRADFIELD. Measurements of Turbulent Heat Transfer on Bodies of Revolution at Supersonic Speeds* ... 272

DEEP, RAYMOND A., AND ROBERT E. LAVENDER. Application of Second-Order Shock-Expansion Theory to Several Types of Bodies of Revolution* ... 1052
DEGROFF, H. M. Comments on Viscous Heating* ... 978
DEGROFF, H. M. On Viscous Heating* ... 395
DENKE, PAUL H. The Matric Solution of Certain Nonlinear Problems in Structural Analysis ... 231
DENKE, PAUL H., AND HUGH L. COX. Stress Distribution, Instability, and Free Vibration of Beam Grid-Works on Elastic Foundations ... 173
DIEDERICH, FRANKLIN W. The Dynamic Response of a Large Airplane to Continuous Random Atmospheric Disturbances ... 917
DI PRIMA, R. C., AND D. W. DUNN. The Effect of Heating and Cooling on the Stability of the Boundary-Layer Flow of a Liquid over a Curved Surface ... 913
DORRANCE, WILLIAM H. The Effect of Mass Transfer on the Compressible Turbulent Boundary-Layer Skin Friction and Heat Transfer—An Addendum* ... 283
DUBLIN, MICHAEL, AND HANS R. FRIEDRICH. Forced Responses of Two Elastic Beams Interconnected by Spring-Damper Systems ... 824
DUNN, D. W., AND R. C. DI PRIMA. The Effect of Heating and Cooling on the Stability of the Boundary-Layer Flow of a Liquid over a Curved Surface ... 913
DURFEE, WILLIAM H. Heat Flow in a Fluid with Eddying Flow* ... 188
DURGIN, FRANK, AND EUGENE COVERT. A Note on Transient Aerodynamic Heating* ... 699
DUTTON, R. A. The Asymptotic Turbulent Boundary Layer* ... 1127
DUWEZ, POL. Physics of Solids—Plastic Flow ... 435

ECKERT, E. R. G., AND P. J. SCHNEIDER. Effect of Diffusion in an Isothermal Boundary Layer* ... 384
ECKHARDT, HOMER D. Graphical Aids for Frequency Response Analysis* ... 83
ELLIOTT, DAVID, AND RONALD F. PROBSTEIN. The Transverse Curvature Effect in Compressible Axially Symmetric Laminar Boundary-Layer Flow ... 208
ESKINAZI, SALAMON, AND HSUAN YEH. An Investigation on Fully Developed Turbulent Flows in a Curved Channel ... 23

FEIGN, DAVID. Comments on "Computation of Vibration Modes and Frequencies"* ... 603
FETTIS, HENRY E. An Approximate Solution to Supersonic Conical Flow* ... 1122
FETTIS, HENRY E., AND YUDELL L. LUKE. On the Evaluation of the Schwarz Function* ... 975

Flight Propulsion
Approximative Determination of the Ceiling of Turbojet Engines, Karl L. Sanders* ... 804
Effect of Radioactivity and Corona Discharge on Flame Stabilization, Morton Mitchner and Robert A. Gross*. 607
An Extension of "Effect of a Turbojet Engine on the Dynamic Stability of an Aircraft," W. P. Rodden, T. E. Surber, and J. H. Wykes* ... 284
Flame Theory and Combustion Technology, Frank E. Marble ... 462
Propulsive Ducts at the Tips of Rotor Blades, J. V. Foa, A. Gail, and T. R. Goodman* ... 381
Propulsive Ducts at the Tips of Rotor Blades, P. R. Payne* ... 1057

FOA, J. V., A. GAIL, AND T. R. GOODMAN. Propulsive Ducts at the Tips of Rotor Blades* ... 381
FORD, C. A., AND I. I. GLASS. An Experimental Study of One-Dimensional Shock-Wave Refraction* ... 189
FORRAY, M. J. Buckling Loads of Pin-Ended Fluid Columns* ... 972
FORRAY, M. J., AND S. R. BODNER. Bending Moments in an Initially Bent, Spring Restrained Column* ... 387
FOWELL L. R. Exact and Approximate Solutions for the Supersonic Delta Wing ... 709
FRIEDRICH, HANS R., AND MICHAEL DUBLIN. Forced Responses of Two Elastic Beams Interconnected by Spring-Damper Systems ... 824

GADD, G. E. A Simple Theory for Interactions Between Shock Waves and Entirely Laminar Boundary Layers ... 225
GAIL, A., J. V. FOA, AND T. R. GOODMAN. Propulsive Ducts at the Tips of Rotor Blades* ... 381
GATEWOOD, B. E., AND J. P. HONAKER. On *S-N* Curves for Fatigue Analysis* ... 276
GEBHARD, DAVID F., AND LEONARD GOLAND. On the Damping in Pitch of a Helicopter Rotor in Forward Flight* ... 1051
GERARD, GEORGE. A Creep Buckling Hypothesis ... 879
GERARD, GEORGE. Generalized Crippling Analysis of Formed Sections* ... 88
GERARD, GEORGE, AND ARTHUR C. GILBERT. Note on Photothermoelasticity* ... 702
GERRARD, J. H. An Investigation of the Noise Produced by a Subsonic Air Jet ... 855
GILBERT, ARTHUR C., AND GEORGE GERARD. Note on Photothermoelasticity* ... 702
GLASS, I. I., AND C. A. FORD. An Experimental Study of One-Dimensional Shock-Wave Refraction* ... 189
GOLAND, LEONARD, AND DAVID F. GEBHARD. On the Damping in Pitch of a Helicopter Rotor in Forward Flight* ... 1051
GOLDBERG, MARTIN A. Investigation of the Temperature Distribution and Thermal Stresses in a Hypersonic Wing Structure ... 981
GOODMAN, THEODORE R. Dynamic Derivatives in Yaw and Sideslip of Thin Wings at Supersonic Speeds ... 357
GOODMAN, THEODORE R. Linearized Theory of Water Drop Impingement* ... 399
GOODMAN, THEODORE R. The Tip Correction for Wind-Tunnel Tests of Propellers ... 1094
GOODMAN, T. R., A. GAIL, AND J. V. FOA. Propulsive Ducts at the Tips of Rotor Blades* ... 381
GRIFFITH, WAYLAND C. Interaction of a Shock Wave with a Thermal Boundary Layer ... 16
GROGAN, G. C. Low-Wave-Drag Bodies of Revolution as Determined by Linearized Theory* ... 612
GROSS, ROBERT A., AND MORTON MITCHNER. Effect of Radioactivity and Corona Discharge on Flame Stabilization* ... 607
GRZEDZIELSKI, ALEXANDER. Eccentric Landing with Heavy Masses at the Wing Tips ... 653
GUDERLEY, GOTTFRIED. On Transonic Airfoil Theory ... 961
GUMAN, WILLIAM J. Further Comments on the Decay of a Nonuniform Velocity Distribution* ... 979

HALFMAN, ROBERT L., AND WILLIAM R. LAIDLAW. Experimental Pressure Distributions on Oscillating Low Aspect Ratio Wings ... 117
HALFMAN, ROBERT L., AND JOHN F. MCCARTHY, JR. The Design and Testing of Supersonic Flutter Models ... 530
HAMMITT, ANDREW G., AND SEYMOUR M. BOGDONOFF. Fluid Dynamic Effects at Speeds from $M = 11$ to 15 ... 108
HARRINGTON, R. P., AND W. H. WEBB. Vortex Structures in Pipe Flow* ... 792
HARRIS, LEONARD A. Axial Compression Buckling of a Pressurized Cylinder with a Thermally Induced Ring Compression* ... 1120
HAZONY (HASANOVITSH), DOV. Deflection of Inelastic Columns* ... 390

HEASLET, MAX. A., AND HARVARD LOMAX. Recent Developments in the Theory of Wing-Body Wave Drag.... 1061
HEDGEPETH, JOHN M. On the Flutter of Panels at High Mach Numbers*.... 609
HELMBOLD, HEINRICH B. Supplementary Note on Turbulent Velocity Fluctuations*.... 702
HIJAB, WASFI A. The Effect of Shape on the Orthotropic Characteristics of a Rectangular Plate*.... 696
HILL, F. K. Boundary-Layer Measurements in Hypersonic Flow.... 35
HILLMAN, A. P. On a Matrix Characteristic Value Problem*.... 286
HOFF, N. J. Approximate Analysis of the Reduction in Torsional Rigidity and of the Torsional Buckling of Solid Wings Under Thermal Stresses*.... 603
HOFF, N. J. Comparison of Radiant and Conductive Heat Transfer in a Supersonic Wing*.... 694
HOFF, N. J. Thermal Buckling of Supersonic Wing Panels 1019
HOLLIDAY, P. T., AND W. J. OAKES, JR. Analysis of a Rolling Pull-Out Maneuver.... 517
HOLMQUIST, COMDR. CARL O., AND W. DUNCAN RANNIE. An Approximate Method of Calculating Three-Dimensional Compressible Flow in Axial Turbomachines.... 543
HOLT, MAURICE, AND JOHN BLACKIE. Experiments on Circular Cones at Yaw in Supersonic Flow.... 931
HONAKER, J. P., AND B. E. GATEWOOD. On *S-N* Curves for Fatigue Analysis*.... 276
HOPKINS, EDWARD J., AND NORMAN E. SORENSEN. A Device for Vortex-Core Measurements*.... 396
HORNER, J. T., AND J. L. BOGDANOFF. Torsional Vibration of Rotating Twisted Bars*.... 393
HUBBARD, P. G., AND S. C. LING. The Hot-Film Anemometer: A New Device for Fluid Mechanics Research*.... 890
HUNTER, M. W., A. SHEF, AND D. V. BLACK. Some Recent Aerodynamic Techniques in Design of Fin-Stabilized Free-Flight Missiles for Minimum Dispersion.... 571
HURLEY, D. G. The Downstream Effect of a Thickening of the Laminar Boundary Layer*.... 383

Hydraulic Equipment

Buckling Loads of Pin-Ended Fluid Columns, M. J. Forray*.... 972

Instruments

Rotational Vibration Response of Inertial Instruments, Bernard H. Wallach*.... 605

IPPEN, ARTHUR T. Hydrodynamics—A Review of von Kármán's Contributions.... 438

JONES, ARTHUR L., OWEN P. LAMB, AND ALFRED E. CRONK. A Method for Predicting Lift Effectiveness of Spoilers at Subsonic Speeds.... 330
JONES, E. EDRYD. On the Flexure of a Stepped Cantilever Beam*.... 1057

KAINER, JULIAN H. Equations for the Loading, Section Pitching-Moment Coefficient, and Center-of-Pressure Distributions on Triangular Wings Having Supersonic Leading and Trailing Edges for Various Basic Camber Distributions.... 137
KATZENBERGER, E. F., AND M. J. RICH. An Investigation of Helicopter Descent and Landing Characteristics Following Power Failure.... 345
KAUFMAN, LAWRENCE, AND KENNETH PERESS. A Review of Methods for Predicting Helicopter Longitudinal Response.... 259
KAVANAU, L. L. Base Pressure Studies in Rarefied Supersonic Flows.... 193
KELLY, HOWARD R., AND RAY W. VAN AKEN. The Magnus Effect at High Reynolds Numbers*.... 1053
KISTLER, A. L., V. O'BRIEN, AND S. CORRSIN. Double and Triple Correlations Behind a Heated Grid*.... 96
KLEIN, BERTRAM. Comment on the Reliability of the Strength of Stiffened Cylinders in Bending and/or Compression*.... 1126
KOGAN, ABRAHAM. On Inviscid Flow Near an Airfoil Leading Edge or an Ogive Tip at High Supersonic Mach Numbers*.... 794
KORKEGI, ROBERT H. Transition Studies and Skin-Friction Measurements on an Insulated Flat Plate at a Mach Number of 5.8.... 97
KRAHN, E. Negative Magnus Force*.... 377
KRAJEWSKI, BOHDAN. Variational Method in the Theory of Axisymmetric Rotational Flow of a Compressible Fluid*.... 891
KRIEBEL, ANTHONY R. Stall Propagation in a Cascade of Airfoils*.... 897
KRON, GABRIEL. Solution of Complex Nonlinear Plastic Structures by the Method of Tearing.... 557
KUETHE, ARNOLD M. Some Features of Boundary Layers and Transition to Turbulent Flow.... 444
KUO, Y. H. The Effects of Prandtl Number on High-Speed Viscous Flows over a Flat Plate*.... 1058
KUO, Y. H. Viscous Flow Along a Flat Plate Moving at High Supersonic Speeds.... 125
KUO, Y. H. Viscous Flow Along a Flat Plate Moving at High Supersonic Speeds*.... 977

LAIDLAW, WILLIAM R., AND ROBERT L. HALFMAN. Experimental Pressure Distributions on Oscillating Low Aspect Ratio Wings.... 117
LAITONE, E. V. On Equations of Motion for a Compressible Viscous Gas.... 846
LAMB, OWEN P., ARTHUR L. JONES, AND ALFRED E. CRONK. A Method for Predicting Lift Effectiveness of Spoilers at Subsonic Speeds.... 330
LANE, FRANK. System Mode Shapes in the Flutter of Compressor Blade Rows.... 54
LANE, FRANK, CHI-TEH WANG, AND ROBERT J. VACCARO. An Investigation of the Flutter Characteristics of Compressor and Turbine Blade Systems.... 335
LARSSON, L. HANNES. Inelastic Column Buckling.... 867
LAUFER, JOHN. Experimental Observation of Laminar Boundary-Layer Oscillations in Supersonic Flow*.... 184
LAVENDER, ROBERT E., AND RAYMOND A. DEEP. Application of Second-Order Shock-Expansion Theory to Several Types of Bodies of Revolution*.... 1052
LEADON, B. M., AND C. J. SCOTT. Transpiration Cooling Experiments in a Turbulent Boundary Layer at $M = 3$*. 798
LEES, LESTER. Influence of the Leading-Edge Shock Wave on the Laminar Boundary Layer at Hypersonic Speeds.... 594
LEONE, PETER F. Mechanical Stability of a Two-Bladed Cantilever Helicopter Rotor.... 633
LEVEY, H. C. A Shock-Free Airfoil*.... 1129
LEW, H. G. The Asymptotic Behavior of the Boundary Layer to Transverse Curvature*.... 276
LEW, H. G. Asymptotic Suction Characteristics of the Boundary Layer over a Circular Cylinder*.... 895
LI, TA. Aerodynamic Influence Coefficients for an Oscillating Finite Thin Wing in Supersonic Flow.... 613
LI, TA. A Method for the Solution of an Eigenvalue Problem with a Complex Matrix*.... 705
LI, TING YI. Effects of Free-Stream Vorticity on the Behavior of a Viscous Boundary Layer*.... 1128
LICHER, R. M. Reduction of Drag Due to Lift in Supersonic Flight by Distributing Lift Along a Fuselage.... 1037
LIN, C. C. Aspects of the Problem of Turbulent Motion.. 453

LIN, HUA. On the Convergence of an Iterative Procedure in Solving Dynamic Response Problems* ... 391
LIN, T. H. Creep Deflection of Viscoelastic Plate Under Uniform Edge Compression ... 883
LING, S. C., AND P. G. HUBBARD. The Hot-Film Anemometer: A New Device for Fluid Mechanics Research ... 890
LINNELL, RICHARD D., AND JERRY Z. BAILEY. Interpolation Formulas for Supersonic-Hypersonic Airfoils* ... 398
LINNELL, RICHARD D., AND JERRY Z. BAILEY. Similarity-Rule Estimation Methods for Cones and Parabolic Noses* ... 796
LIVESEY, J. L. The Behavior of Transverse Cylindrical and Forward Facing Total Pressure Probes in Transverse Total Pressure Gradients ... 949
LOGAN, J. G., JR. Nitric Oxide Formation in Hypersonic Flow* ... 1123
LOMAX, HARVARD, AND MAX. A. HEASLET. Recent Developments in the Theory of Wing-Body Wave Drag ... 1061
LOOS, H. G. Compressibility Effects on Secondary Flows ... 76
LUKE, YUDELL L., AND HENRY E. FETTIS. On the Evaluation of the Schwarz Function* ... 975

MACHELL, REGINALD M., AND WILLIAM T. O'BRYANT. An Experimental Investigation of Flow over Blunt Nosed Cones at a Mach Number of 5.8* ... 1054
MAEDER, P. F., AND H. U. THOMMEN. Some Results of Linearized Transonic Flow About Slender Airfoils and Bodies of Revolution* ... 187
MAGER, ARTUR. On the Model of the Free, Shock-Separated, Turbulent Boundary Layer* ... 181
MAR, J. W., T. H. H. PIAN, AND J. M. CALLIGEROS. A Note on Methods for the Determination of Transient Stresses* ... 94
MARBLE, FRANK E. Flame Theory and Combustion Technology ... 462
MARSCHNER, BERNARD W. The Flow over a Body in a Choked Wind Tunnel and in a Sonic Free Jet ... 368
MARTIN, H. C., M. J. TURNER, R. W. CLOUGH, AND L. J. TOPP. Stiffness and Deflection Analysis of Complex Structures ... 805
MASLEN, STEPHEN H. On the Supersonic Flow of a Viscous Fluid Past a Flat Plate* ... 801
MASLEN, STEPHEN H., AND FRANKLIN K. MOORE. On Strong Transverse Waves Without Shocks in a Circular Cylinder ... 583

Materials

Physics of Solids—Plastic Flow, Pol Duwez ... 435
A Study of the Applicability of Rabotnov's Creep Parameter for Aluminum Alloy, Fred H. Turner and Kurt E. Blomquist* ... 1121

Mathematics

Applied Mathematics—An Art and a Science, M. A. Biot ... 406
The Integrated Use of Analog and Digital Computing Machines for Aircraft Dynamic Load Problems, Bernard Mazelsky and Robert F. O'Connell ... 721
A Method for the Solution of an Eigenvaue Problem with a Complex Matrix, Ta Li* ... 705

MAYERS, J., AND BERNARD BUDIANSKY. Influence of Aerodynamic Heating on the Effective Torsional Stiffness of Thin Wings ... 1081
MAZELSKY, BERNARD. Theoretical Aerodynamic Properties of Vanishing Aspect Ratio Harmonically Oscillating Rigid Airfoils in a Compressible Medium ... 639
MAZELSKY, BERNARD, AND ROBERT F. O'CONNELL. The Integrated Use of Analog and Digital Computing Machines for Aircraft Dynamic Load Problems ... 721
MCCARTHY, JOHN F., JR., AND ROBERT L. HALFMAN. The Design and Testing of Supersonic Flutter Models ... 530
MCCORMICK, B. W., JR. On the Initial Vertical Descent of a Helicopter Following Power Failure* ... 1125

Mechanics

The Behavior of Nonlinear Systems, Francis H. Clauser ... 411

MILES, JOHN W. The Aerodynamic Force on an Airfoil in a Moving Gust ... 1044
MILES, JOHN W. The Compressible Flow Past an Oscillating Airfoil in a Wind Tunnel ... 671
MILES, JOHN W. A First-Order Formulation of the Unsteady Supersonic Flow Problem for Finite Wings ... 578
MILES, JOHN W. On the Aerodynamic Instability of Thin Panels ... 771
MILES, JOHN W. On Linearized Transonic Flow Theory for Slender Bodies* ... 704
MILES, JOHN W. On the Sonic Drag of a Slender Body ... 146
MILLIKAN, CLARK B. Theodore von Kármán ... 404
MILLSAPS, KNOX, AND KARL POHLHAUSEN. The Laminar Free-Convective Heat Transfer from the Surfaces of a Vertical Circular Cylinder* ... 381
MITCHNER, MORTON, AND ROBERT A. GROSS. Effect of Radioactivity and Corona Discharge on Flame Stabilization* ... 607
MOORE, FRANKLIN K., AND STEPHEN H. MASLEN. On Strong Transverse Waves Without Shocks in a Circular Cylinder ... 583
MORGAN, GEORGE W., AND W. H. WARNER. On Heat Transfer in Laminar Boundary Layers at High Prandtl Number ... 937

NAGEL, FELIX E. Column Instability of Pressurized Tubes* ... 608
NAPOLITANO, LUIGI G. Similar Solutions in Compressible Laminar Free Mixing Problems* ... 389

OAKES, W. J., JR., AND P. T. HOLLIDAY. Analysis of a Rolling Pull-Out Maneuver ... 517
O'BRIEN, VIVIAN. Remarks on Chaplygin Functions* ... 894
O'BRIEN, V., A. L. KISTLER, AND S. CORRSIN. Double and Triple Correlations Behind a Heated Grid* ... 96
O'BRYANT, WILLIAM T., AND REGINALD M. MACHELL. An Experimental Investigation of Flow over Blunt Nosed Cones at a Mach Number of 5.8* ... 1054
O'CONNELL, ROBERT F., AND BERNARD MAZELSKY. The Integrated Use of Analog and Digital Computing Machines for Aircraft Dynamic Load Problems ... 721
OLIVER, ROBERT EARL. An Experimental Investigation of Flow About Simple Blunt Bodies at a Nominal Mach Number of 5.8* ... 177
ORDWAY, DONALD EARL, AND CARLO RIPARBELLI. An Application of the Method of Equivalence to the Deflection of a Triangular Plate ... 252
ORMSBEE, ALLEN I., AND HOMER J. STEWART. Conical Techniques for Incompressible Nonviscous Flow ... 1029
OSWALD, TELFORD W. Dynamic Behavior During Accelerated Flight with Particular Application to Missile Launching ... 781
OSWALD, W. BAILEY. Applied Aerodynamics and Flight Mechanics ... 469
OSWALD, W. BAILEY. Errata—"Applied Aerodynamics and Flight Mechanics"* ... 892, 1123

PACK, D. C. The Oscillations of a Supersonic Gas Jet Embedded in a Supersonic Stream ... 747
PAI, S. I. Laminar Jet Mixing of Two Compressible Fluids with Heat Release ... 1012
PAI, S. I. On the Boundary-Layer Equations of a Very Slender Body of Revolution* ... 795

PAI, S. I. On the Stability Theory of Flow with Finite Disturbances* 274
PALLONE, A. J., AND H. K. CHENG. Inviscid Leading-Edge Effect in Hypersonic Flow* 700
PAYNE, A. O. A Note on the Fatigue of Wings* 797
PAYNE, P. R. Propulsive Ducts at the Tips of Rotor Blades* 1057
PERESS, KENNETH, AND LAWRENCE KAUFMAN. A Review of Methods for Predicting Helicopter Longitudinal Response 259

Performance

Analysis of a Rolling Pull-Out Maneuver, W. J. Oakes, Jr., and P. T. Holliday 517
Applications of Matrix Operators to the Kinematics of Airplane Motion, Malcolm J. Abzug 679
Dynamic Behavior During Accelerated Flight with Particular Application to Missile Launching, Telford W. Oswald 781
Eccentric Landing with Heavy Masses at the Wing Tips, Alexander Grzedzielski 653

PERSH, JEROME, AND SHAN-FU SHEN. The Limiting Wall Temperature Ratios Required for Complete Stabilization of Laminar Boundary Layers with Blowing* 286
PERSH, JEROME, AND A. WILEY SHERWOOD. An Experimental Investigation of the Boundary-Layer Flow on a Rotating Flat Plate* 703
PIAN, T. H. H., J. W. MAR, AND J. M. CALLIGEROS. A Note on Methods for the Determination of Transient Stresses* 94
PINES, SAMUEL. Iteration in Semidefinite Eigenvalue Problems* 380
POHLHAUSEN, KARL, AND KNOX MILLSAPS. The Laminar Free-Convective Heat Transfer from the Surfaces of a Vertical Circular Cylinder* 381
PORTNOY, H. The Forces on the General Slender Body of Elliptic Cross Section in Supersonic Flow* 91
PRIDE, RICHARD A. Comments on "The Ultimate Strength of Multiweb Box Beams in Pure Bending"* 1059
PROBSTEIN, RONALD F., AND DAVID ELLIOTT. The Transverse Curvature Effect in Compressible Axially Symmetric Laminar Boundary-Layer Flow 208

Propellers

The Tip Correction for Wind-Tunnel Tests of Propellers, Theodore R. Goodman 1094

RADHAKRISHNAN, S. Plastic Buckling of Circular Cylinders* 892
RANDELS, W. C. Comments on Supersonic Diffuser Instability* 390
RANNIE, W. D. Heat Transfer in Turbulent Shear Flow 485
RANNIE, W. DUNCAN, AND COMDR. CARL O. HOLMQUIST. An Approximate Method of Calculating Three-Dimensional Compressible Flow in Axial Turbomachines 543
REID, W. H. The Skewness Factor According to Obukhoff's Transfer Theory* 379
REISS, EDWARD L. On the Nonlinear Buckling of Shallow Spherical Domes* 973
RHEES, T. R., AND W. P. CRENSHAW. Some Effects of Viscosity on Wing-Body Interference at $M = 1.9$ 43
RIBNER, H. S. Spectral Theory of Buffeting and Gust Response: Unification and Extension 1075
RICH, M. J., AND E. F. KATZENBERGER. An Investigation of Helicopter Descent and Landing Characteristics Following Power Failure 345
RICHARDSON, E. G. The Correction of Hot-Wire Readings in a Boundary Layer for Proximity to the Solid Boundary* 970
RIPARBELLI, CARLO. A Principle of Maximum Power for Real Fluids in Steady Motion* 971
RIPARBELLI, CARLO, AND DONALD EARL ORDWAY. An Application of the Method of Equivalence to the Deflection of a Triangular Plate 252
RODDEN, WILLIAM P. An Aeroelastic Parameter for Estimation of the Effects of Flexibility on the Lateral Stability and Control of Aircraft 660
RODDEN, W. P., T. E. SURBER, AND J. H. WYKES. An Extension of "Effect of a Turbojet Engine on the Dynamic Stability of an Aircraft"* 284
ROMIG, MARY F. The Normal Shock Properties for Air in Dissociation Equilibrium* 185

Rotating Wing Aircraft

An Investigation of Helicopter Descent and Landing Characteristics Following Power Failure, E. F. Katzenberger and M. J. Rich 345
Mechanical Stability of a Two-Bladed Cantilever Helicopter Rotor, Peter F. Leone 633
On the Damping in Pitch of a Helicopter Rotor in Forward Flight, David F. Gebhard and Leonard Goland* 1051
On the Initial Vertical Descent of a Helicopter Following Power Failure, B. W. McCormick, Jr.* 1125
Propulsive Ducts at the Tips of Rotor Blades, J. V. Foa, A. Gail, and T. R. Goodman* 381
Propulsive Ducts at the Tips of Rotor Blades, P. R. Payne* 1057
Response Matrix Method of Rotor Blade Analysis, Alex Berman 155
A Review of Methods for Predicting Helicopter Longitudinal Response, Lawrence Kaufman and Kenneth Peress 259
Stability of a Flexible Helicopter Rotor Blade in Forward Flight, Yechiel Shulman 663

ROTT, NICHOLAS, AND WILLIAM E. SMITH. Some Examples of Laminar Boundary-Layer Flow on Rotating Blades 991

SANDERS, KARL L. Approximative Determination of the Ceiling of Turbojet Engines* 804
SANDORFF, P. E. Design of Structural Models, with Application to Stiffened Panels Under Combined Shear and Compression 623
SCHMITT, ALFRED F. A Least Squares Matrix Interpolation of Flexibility Influence Coefficients* 980
SCHNEIDER, P. J., AND E. R. G. ECKERT. Effect of Diffusion in an Isothermal Boundary Layer* 384
SCHWAAR, P. Determination of the Stationary Flow Field in Front of a Supersonic Cascade* 888
SCOTT, C. J., AND B. M. LEADON. Transpiration Cooling Experiments in a Turbulent Boundary Layer at $M = 3$*. 798
SEARS, W. R. Some Recent Developments in Airfoil Theory 490
SECHLER, E. E. Inelastic Buckling—From a Designer's Viewpoint 500
SEIDE, PAUL. Elasto-Plastic Bending of Beams on Elastic Foundations 563
SHAPIRO, NORMAN M. Effects of Pressure Gradient and Heat Transfer on the Stability of the Compressible Laminar Boundary Layer* 81
SHEF, A., M. W. HUNTER, AND D. V. BLACK. Some Recent Aerodynamic Techniques in Design of Fin-Stabilized Free-Flight Missiles for Minimum Dispersion 571
SHEN, SHAN-FU, AND JEROME PERSH. The Limiting Wall Temperature Ratios Required for Complete Stabilization of Laminar Boundary Layers with Blowing* 286
SHERWOOD, A. WILEY, AND JEROME PERSH. An Experimental Investigation of the Boundary-Layer Flow on a Rotating Flat Plate* 703
SHORT, BARBARA J., AND SIMON C. SOMMER. Free-Flight Measurements of Skin Friction of Turbulent Boundary

Layers with High Rates of Heat Transfer at High Supersonic Speeds ... 536
SHULMAN, YECHIEL. Stability of a Flexible Helicopter Rotor Blade in Forward Flight ... 663
SIBULKIN, MERWIN. Heat Transfer to an Incompressible Turbulent Boundary Layer and Estimation of Heat-Transfer Coefficients at Supersonic Nozzle Throats ... 162
SMITH, A. M. O. Rapid Laminar Boundary-Layer Calculations by Piecewise Application of Similar Solutions ... 901
SMITH, WILLIAM E., AND NICHOLAS ROTT. Some Examples of Laminar Boundary-Layer Flow on Rotating Blades ... 991
SOGIN, HAROLD H., AND KWANG-TZU YANG. A Numerical Method for Laminar Heat Transfer on Cylinders in Plane Compressible Flow* ... 277
SOHN, ROBERT L. An Analysis of the Performance of an Axial-Flow Compressor at Low Reynolds Number ... 741
SOMMER, SIMON C., AND BARBARA J. SHORT. Free-Flight Measurements of Skin Friction of Turbulent Boundary Layers with High Rates of Heat Transfer at High Supersonic Speeds ... 536
SORENSEN, NORMAN E., AND EDWARD J. HOPKINS. A Device for Vortex-Core Measurements* ... 396
SPENCE, D. A. The Development of Turbulent Boundary Layers ... 3
SPENCE, D. A. The Lift of a Blowing Wing in a Parallel Stream* ... 92

Stability & Control

An Aeroelastic Parameter for Estimation of the Effects of Flexibility on the Lateral Stability and Control of Aircraft, William P. Rodden ... 660
An Extension of "Effect of a Turbojet Engine on the Dynamic Stability on an Aircraft," W. P. Rodden, T. E. Surber, and J. H. Wykes* ... 284
Graphical Aids for Frequency Response Analysis, Homer D. Eckhardt* ... 83
The Human Pilot and the High-Speed Airplane, James L. Decker ... 765

STEWART, H. J. A Review of Source Superposition and Conical Flow Methods in Supersonic Wing Theory ... 507
STEWART, HOMER J., AND ALLEN I. ORMSBEE. Conical Techniques for Incompressible Nonviscous Flow ... 1029

Stress Analysis & Structures

Analysis of the Plastic Collapse of a Cruciform Column with Initial Twist, Loaded in Compression, J. F. Besseling ... 49
An Application of the Method of Equivalence to the Deflection of a Triangular Plate, Donald Earl Ordway and Carlo Riparbelli ... 252
Bending Moments in an Initially Bent, Spring Restrained Column, M. J. Forray and S. R. Bodner* ... 387
Bending of Rectangular Plate with Clamped Edges, Ching-Sheng Wu* ... 601
The Buckling of Isosceles Triangular Plates Subjected to Combined Compression and Shear, Hugh L. Cox* ... 287
Buckling Loads of Pin-Ended Fluid Columns, M. J. Forray* ... 972
Column Instability of Pressurized Tubes, Felix E. Nagel* ... 608
Comment on the Reliability of the Strength of Stiffened Cylinders in Bending and/or Compression, Bertram Klein* ... 1126
Comments on "The Ultimate Strength of Multiweb Box Beams in Pure Bending," Richard A. Pride* ... 1059
A Creep Buckling Hypothesis, George Gerard ... 879
Creep Deflection of Viscoelastic Plate Under Uniform Edge Compression, T. H. Lin ... 883
Deflection of Inelastic Columns, Dov Hazony (Hasanovitsh)* ... 390
Design of Structural Models, with Application to Stiffened Panels Under Combined Shear and Compression, P. E. Sandorff ... 623
Elasto-Plastic Bending of Beams on Elastic Foundations, Paul Seide ... 563
Generalized Crippling Analysis of Formed Sections, George Gerard* ... 88
Inelastic Buckling—From a Designer's Viewpoint, E. E. Sechler ... 500
Inelastic Column Buckling, L. Hannes Larsson ... 867
The Matric Solution of Certain Nonlinear Problems in Structural Analysis, Paul H. Denke ... 231
Minimum Weight Design of a Simply Supported Transversely Stiffened Plate Loaded in Shear, Malcolm F. Symonds ... 685
Errata—"Minimum Weight Design of a Simply Supported Transversely Stiffened Plate Loaded in Shear," Malcolm F. Symonds* ... 1057
Nonlinear Minimum-Weight Design of Planar Structures, Louis G. Vargo ... 956
A Note on Methods for the Determination of Transient Stresses, J. W. Mar. T. H. H. Pian, and J. M. Calligeros* ... 94
Note on Photoelastic Study of Swept Wings, C. L. Amba Rao* ... 889
On the Flexure of a Stepped Cantilever Beam, E. Edryd Jones* ... 1057
On the Nonlinear Buckling of Shallow Spherical Domes, Edward L. Reiss* ... 973
On *S-N* Curves for Fatigue Analysis, B. E. Gatewood and J. P. Honaker* ... 276
On Thin-Ring Analysis, Bruno A. Boley* ... 802
Plastic Buckling of Circular Cylinders, S. Radhakrishnan* ... 892
Solution of Complex Nonlinear Plastic Structures by the Method of Tearing, Gabriel Kron ... 557
Some Structural and Aeroelastic Considerations of High-Speed Flight (Nineteenth Wright Brothers Lecture), R. L. Bisplinghoff ... 289

Stress Analysis & Structures—Thermal Stresses

Approximate Analysis of the Reduction in Torsional Rigidity and of the Torsional Buckling of Solid Wings Under Thermal Stresses, N. J. Hoff* ... 603
Axial Compression Buckling of a Pressurized Cylinder with a Thermally Induced Ring Compression, Leonard A. Harris* ... 1120
Comparison of Radiant and Conductive Heat Transfer in a Supersonic Wing, N. J. Hoff* ... 694
Creep Buckling of Plates at Elevated Temperatures, William Zuk* ... 610
The Determination of Temperature, Stresses, and Deflections in Two-Dimensional Thermoelastic Problems, Bruno A. Boley ... 67
Influence of Aerodynamic Heating on the Effective Torsional Stiffness of Thin Wings, Bernard Budiansky and J. Mayers ... 1081
Investigation of the Temperature Distribution and Thermal Stresses in a Hypersonic Wing Structure, Martin A. Goldberg ... 981
Note on Photothermoelasticity, George Gerard and Arthur C. Gilbert* ... 702
Thermal Buckling of Supersonic Wing Panels, N. J. Hoff 1019
Thermally Induced Vibrations of Beams, Bruno A. Boley* ... 179

STUART, J. T. Note on "On the Stability Theory of Flow with Finite Disturbances"* ... 894
STUART, J. T. On the Role of Reynolds Stresses in Stability Theory* ... 86

SURBER, T. E., W. P. RODDEN, AND J. H. WYKES. An Extension of "Effect of a Turbojet Engine on the Dynamic Stability of an Aircraft"* 284
SYMONDS, MALCOLM F. Minimum Weight Design of a Simply Supported Transversely Stiffened Plate Loaded in Shear 685
SYMONDS, MALCOLM F. Errata—"Minimum Weight Design of a Simply Supported Transversely Stiffened Plate Loaded in Shear"* 1057

TALBOT, L., AND D. M. TELLEP. Normal Forces on Flat Plates in Low-Density Supersonic Flow 1099
TANI, ITIRO. Energy Dissipation in Turbulent Boundary Layers* 606
TELLEP, D. M., AND L. TALBOT. Normal Forces on Flat Plates in Low-Density Supersonic Flow 1099
THOMMEN, H. U., AND P. F. MAEDER. Some Results of Linearized Transonic Flow About Slender Airfoils and Bodies of Revolution* 187
TOPP, L. J., M. J. TURNER, R. W. CLOUGH, AND H. C. MARTIN. Stiffness and Deflection Analysis of Complex Structures 805
TRIMPI, ROBERT L. Comments on "Supersonic Diffuser Instability"* 611
TRUITT, ROBERT W. Comments on Vortex-Core Measurements* 889
TURNER, FRED H., AND KURT E. BLOMQUIST. A Study of the Applicability of Rabotnov's Creep Parameter for Aluminum Alloy* 1121
TURNER, M. J., R. W. CLOUGH, H. C. MARTIN, AND L. J. TOPP. Stiffness and Deflection Analysis of Complex Structures 805

UBEROI, MAHINDER S. Effect of Wind-Tunnel Contraction on Free-Stream Turbulence 754
UCHIDA, SHIGEO, AND MICHIRU YASUHARA. The Rotational Field Behind a Curved Shock Wave Calculated by the Method of Flux Analysis 830

VACCARO, ROBERT J., FRANK LANE, AND CHI-TEH WANG. An Investigation of the Flutter Characteristics of Compressor and Turbine Blade Systems 335
VAN AKEN, RAY W., AND HOWARD R. KELLY. The Magnus Effect at High Reynolds Numbers* 1053
VAN DRIEST, E. R. On Turbulent Flow Near a Wall 1007
VARGO, LOUIS G. Nonlinear Minimum-Weight Design of Planar Structures 956

WALLACH, BERNARD H. Rotational Vibration Response of Inertial Instruments* 605
WANG, CHI-TEH, FRANK LANE, AND ROBERT J. VACCARO. An Investigation of the Flutter Characteristics of Compressor and Turbine Blade Systems 335
WARNER, W. H., AND GEORGE W. MORGAN. On Heat Transfer in Laminar Boundary Layers at High Prandtl Number 937
WEBB, W. H., AND R. P. HARRINGTON. Vortex Structures in Pipe Flow* 792
WEINIG, F. S. Subsonic Influence of Compressibility on the Pressure Distribution of a Profile* 279
WEINIG, F. S. Erratum—"Subsonic Influence of Compressibility on the Pressure Distribution of a Profile"* 705
WILLMARTH, WILLIAM W. The Optimum Distribution of Lift in Certain Prismatic Regions at Supersonic Speed* 809

Wind Tunnels
The Behavior of Transverse Cylindrical and Forward Facing Total Pressure Probes in Transverse Total Pressure Gradients, J. L. Livesey 949
Comments on Vortex-Core Measurements, Robert W. Truitt* 889
The Correction of Hot-Wire Readings in a Boundary Layer for Proximity to the Solid Boundary, E. G. Richardson* 970
The Design and Testing of Supersonic Flutter Models, John F. McCarthy, Jr., and Robert L. Halfman 530
A Device for Vortex-Core Measurements, Edward J. Hopkins and Norman E. Sorensen* 396
Effect of Wind-Tunnel Contraction on Free-Stream Turbulence, Mahinder S. Uberoi 754
An Experimental Investigation of the Boundary-Layer Flow on a Rotating Flat Plate, Jerome Persh and A. Wiley Sherwood* 703
An Experimental Study of the One-Dimensional Refraction of a Rarefaction Wave at a Contact Surface, I. J. Billington 997
An Experimental Study of One-Dimensional Shock-Wave Refraction, C. A. Ford and I. I. Glass* 189
Fluid Dynamic Effects at Speeds from $M = 11$ to 15, Seymour M. Bogdonoff and Andrew G. Hammitt 108
The Hot-Film Anemometer: A New Device for Fluid Mechanics Research, S. C. Ling and P. G. Hubbard* 890
Normal Forces on Flat Plates in Low-Density Supersonic Flow, D. M. Tellep and L. Talbot 1099
The Tip Correction for Wind-Tunnel Tests of Propellers, Theodore R. Goodman 1094

WU, CHING-SHENG. Bending of Rectangular Plate with Clamped Edges* 601
WYKES, J. H., T. E. SURBER, AND W. P. RODDEN. An Extension of "Effect of a Turbojet Engine on the Dynamic Stability of an Aircraft"* 284

YANG, KWANG-TZU, AND HAROLD H. SOGIN. A Numerical Method for Laminar Heat Transfer on Cylinders in Plane Compressible Flow* 277
YASUHARA, MICHIRU, AND SHIGEO UCHIDA. The Rotational Field Behind a Curved Shock Wave Calculated by the Method of Flux Analysis 830
YEH, HSUAN, AND SALAMON ESKINAZI. An Investigation on Fully Developed Turbulent Flows in a Curved Channel 23
YEN, K. T. On the Energy Balance in a Compressible Boundary Layer* 274

ZARTARIAN, GARABED, AND HOLT ASHLEY. Piston Theory—A New Aerodynamic Tool for the Aeroelastician 1109
ZLOTNICK, MARTIN. Aerodynamic Cross-Coupling Between Side Force and Normal Force on Bodies and Wing-Body Combinations* 192
ZUK, WILLIAM. Creep Buckling of Plates at Elevated Temperatures* 610

ST. LOUIS PUBLIC LIBRARY SEP 27 1957